UNIVERSITY OF SOUTHAMPTON

FINITE ELEMENT MODELLING OF BIOLOGICAL CONNECTIVE SOFT TISSUES APPLICATION TO THE LIGAMENTS OF THE HUMAN KNEE

Georges Limbert

A thesis submitted in partial fulfilment of the requirements for the degree of

Doctor of Philosophy

FACULTY OF ENGINEERING AND APPLIED SCIENCE
SCHOOL OF ENGINEERING SCIENCES
Bioengineering Science Research Group

November 2001

UNIVERSITY OF SOUTHAMPTON

ABSTRACT

FACULTY OF ENGINEERING AND APPLIED SCIENCE
DEPARTMENTS OF MECHANICAL ENGINEERING & ENGINEERING MATERIALS

Doctor of Philosophy

Finite Element Modelling of Biological Connective Soft Tissues.
Application to the Ligaments of the Human Knee.

By Georges Limbert

The research presented in this thesis addresses the issue of analytical and numerical aspects of the constitutive modelling of biological soft connective tissues. A general theoretical framework for the modelling of strongly anisotropic continuum fibre-reinforced composites at finite strain was first developed in order to provide solid theoretical bases for the formulation of a structurally-justified constitutive law describing the mechanical behaviour of ligaments. Then, a three-dimensional (3D) incompressible transversely isotropic hyperelastic law accounting for the key features of ligaments (incompressibility, anisotropy, nonlinear material, large deformations and rotations, very small bending stiffness, presence of residual stresses) was implemented into a commercial explicit finite element (FE) code. As applications of the material model, finite element analyses using experimental material data, were performed for simulating the behaviour of a human Anterior Cruciate Ligament (ACL) when the knee is subjected to a passive flexion. A second set of FE analyses was carried out in order to simulate the mechanical response of a 3D knee joint model (including the two collateral and the two cruciate ligaments) under anterior-posterior drawer forces.

The originality of the theoretical framework for strongly anisotropic continuum fibre-reinforced composite at finite strain lie in the fact that the first and second derivatives of the strain energy function was performed without assuming any particular material symmetry or any kinematic constraints such as incompressibility. This provided the advantage of capturing all the possible mutual interactions of the matrix and the two families of fibres and encompassing all types of material symmetry. Describing material with particular symmetries or kinematic constraints or accounting for specific mechanical interactions is just a question of degenerating the equations involved.

The incompressible transversely isotropic hyperelastic material implemented in the finite element code was properly validated against analytical solutions for homogeneous states of deformation and demonstrated robust and very good performance in the sensitivity analyses phase.

The present research was motivated by the hypothesis that 3D isotropic models are not valid to represent the natural behaviour of ligaments. In fact, it was shown in a finite element model of the ACL, that highly unphysiological compressive and flexural stresses were generated as soon as a ligament undergoes compression in what should be the natural direction of the extended collagen fibres. The new anisotropic material model for the ACL was able to address successfully these severe limitations and by accounting for residual stress provided excellent agreement with quantitative experimental data such as the resultant force developed in the ligament.

The FE material model for soft tissue was also used to develop a global 3D model of the knee joint. For the first time, full 3D contact interactions between ligaments and bony structures was accounted for in simulated anterior-posterior drawer tests giving new insights in to the FE modelling of the knee. The FE model was sensitive enough to differentiate the mechanical response of an intact knee and that of an ACL-deficient knee. The primary restraining role of the ACL in anterior tibial drawer tests was also confirmed.

I have waited for this moment for a long time and have now finally reach the end. I would like to dedicate this work to various people who provided the support and encouragement which allowed me to reach this point. They also provided a few laughs along the way when the going got tough!

To

Michelle, for the love we share, her never ending support, for having been my best friend during all these years and for providing that listening ear on a Sunday afternoon when knee ligaments seemed to be a major topic of conversation !

My parents, for having endlessly shown me the right way and having always encouraged and supported me in all of my interests. This degree is due as much as their efforts over the last 29 years as to my own.

The Nicolaï family for their generosity, support and especially for all the good times we had in Toulouse.

Pauline and Dennis, my English family, for all the happy moments we have shared and the support that they showed me during my stay in Southampton.

All my family and friends, particularly Suzanne, Victoria, Véronique, Laurence, Jean-François, Phillipe, Bertrand and Sandrine.

Finally to an individual that sparked an interest in me at a very early age to look at the world of Biomechanics -he may have been a fictitious character on our screens but thanks Colonel Steve Austin as for me you certainly are worth six million dollars ...

"heavier-than-air flying machines are impossible"

Lord Kelvin (William Thomson), 1824-1907
President of the Royal Society

(in 1895 at the Australian Institute of Physics)

TABLE OF CONTENTS

LIST OF FIGURES

LIST OF TABLES

PREFACE

The aim of this preface is to highlight the author's original contributions to the vast domain that is the constitutive modelling of connective soft tissues. The main efforts of this research were concentrated on the theoretical developments (Chapter V) and the finite element implementation of the incompressible transversely isotropic material law. The contributions presented in this thesis arose variously from the author, from skilled and imaginative supervision and through valuable interaction with researchers from a range of disciplines.

The research presented in Chapter V has been accepted for publication as an original article in the *International Journal of Solids and Structures*. The initial concept and theoretical developments are all original personal contributions. However, there was input from Dr. Mark Taylor at the article submission stage, in the drafting of the manuscript. The full reference is given below (1).

The research presented in Chapter VI has been published as a private communication within ESI Group Company (Paris, France). Since the developed finite element anisotropic hyperelastic material model will be integrated in the next commercial release of the software suite PAM-CRASH™/PAM-SAFE™ (2002), it was also the author's task to write relevant sections within the PAM-CRASH™/PAM-SAFE™ user manuals. This includes "Solver Reference Manual", "Solver Notes Manual" and "Theory Notes Manual". With the exception of supervisory guidance, the programming, testing and integration of the finite element material model within the global explicit code represent all personal contributions. For obvious reasons, the developed Fortran subroutines are not reported in this thesis. The full and provisional references are given below (2, 3).

The research material presented in Chapter VIII and related studies not presented in the present thesis have been presented at various conferences and some of them have been published as referred book sections. The concept of residual stress and the relevance of their integration was suggested by Dr. Taylor. Otherwise, the concepts, finite element methodology and results represent an original personal contribution. Full references are given below (4-7).

Results from Chapter IX have been submitted and accepted as oral presentations and referred book section at the *Sixth US Congress on Computational Mechanics, August 1-3, 2001, Dearborn, MI, USA* and at the *Fifth International Symposium on Computer Methods in Biomechanics and Biomedical Engineering, October 31 – November 3, 2001, Rome, Italy.* The idea of simulating the mechanical behaviour of the human knee under drawer tests was partly suggested by Dr. Taylor. Otherwise, the finite element techniques developed and results represent all an original personal contribution. Full and provisional references are given below (8-9).

1. Limbert, G. and Taylor, M. (2002). On the constitutive modelling of biological soft connective tissues. A general theoretical framework and tensors of elasticity for strongly anisotropic fiber-reinforced composites at finite strain. *International Journal of Solids and Structures*, 39(8), 2343-2358.

2. Limbert, G. (2000). An incompressible transversely isotropic hyperelastic material for modelling the mechanical behaviour of ligaments and tendons. Theory and finite element implementation. *ESI Group private communication.*

3. Limbert, G. (2002). PAM-CRASH™/PAM-SAFE™ Version 2002. Theory Notes Manual / Solver Reference Manual / Solver Notes Manual, PAM Systems International, ESI Group (to be published).

4. Limbert, G. and Taylor, M. (2001). Three-dimensional finite element modelling of the anterior cruciate ligament: influence of the initial stress field. *Computer Methods in Biomechanics & Biomedical Engineering - 3, October 13-16, Lisbon, Portugal, Edited by J. Middleton, M.L. Jones and G.N. Pande, Gordon and Breach Science Publishers, 355-360.* (referred book section)

5. Limbert, G. and Taylor, M. (2001). An explicit three-dimensional finite element model of an incompressible transversely isotropic hyperelastic material. Application to the study of the human anterior cruciate ligament. *First M.I.T. Conference on Computational Fluid and Solid Mechanics, June 12-15, 2001, Cambridge, MA, USA, K.J. Bathe Editor, Elsevier Science, vol. 1, 319-322.* (referred book section).

[A conference and travel fellowships were awarded by the M.I.T. for this work].

6. Limbert, G., Taylor, M. and Freeman, M. A. R. (2001). Three-dimensional finite element model of the human ACL. Simulation of a passive knee flexion cycle. Analysis of deformations and stresses. *47th Annual Meeting of the Orthopaedic Research Society, February 25-28, 2001, San Francisco, CA, USA, 794.*

7. Limbert, G. and Taylor, M. (2001). An explicit three-dimensional finite element model of the human ACL. Influence of a residual stress on a passive knee flexion. *Ninth Annual Symposium on Computational Methods in Orthopaedic Biomechanics, February 24, 2001, San Francisco, CA, USA.*

8. Limbert, G. and Taylor, M. (2001). An explicit anisotropic hyperelastic finite element material model. Application to the ligaments of the human knee. *Sixth US National Congress on Computational Mechanics, August 1-3, Dearborn, MI, USA, 506.*

9. Limbert, G. and Taylor, M. (2002). Three-dimensional finite element modelling of the knee joint under anterior-posterior forces. *Computer Methods in Biomechanics & Biomedical Engineering - 4, Edited by J. Middleton, M.L. Jones and G.N. Pande, Gordon and Breach Science Publishers,* (in press)

Publication manuscripts related to Chapters VIII and IX are currently in preparation.

ACKNOWLEDGEMENTS

I am extremely grateful to my supervisor Dr. Mark Taylor for his exceptional scientific guidance, his support, encouragement and for being a friend during the course of my PhD. I am sure that this is the beginning of a long lasting friendship. By placing trust in my judgements, encouraging and supporting me in going further in the investigation of my ideas, Dr. Taylor has helped me to develop qualities necessary for an independent researcher. His outstanding knowledge of biomechanics and rigourousness have always been very helpful to provide an objective evaluation of my work and to point out relevant directions for research.

I am also especially grateful to Dr. Eberhard Haug, from ESI Group, for his interest in my work and without whom part of the project might never have happened. I would also like to thank Dr. Salim Bouabdallah, Dr. Diane Dan and Dr. Argiris Kamoulakos for their kind help, advice and willingness to engage in protracted conversations during my stay at ESI Group/ESI Software in Rungis, France.

My thanks also go to Professor Michael Freeman for the time he spent with me to discuss clinical and engineering issues related to my project. His broad experience as a consultant orthopaedic surgeon and his exceptional human qualities made these moments not only fascinating but also very enjoyable.

Special thanks are due to Dr. Sandra Martelli and Dr. Vera Pinskerova for providing some of the experimental data used in Chapter VIII (knee kinematics and geometry of the ACL).

I am also endebted to Professor Andy Keane for the early stages of my PhD during which he kindly assured the role of temporary supervisor and helped me to settle down in my new environment at the Computational Engineering and Design Centre within the Mechanical Engineering Department.

I would also like to warmly thank all my colleagues and the staff from the Mechanical Engineering and Engineering Materials Departments for their various help, support and friendship.

I am very grateful to Mr. John Middleton who has shown great understanding and support in the final stages of completion of my PhD and who is currently providing me with exciting opportunities to put my new skills and experience into practice.

Lastly, but my no means least, I would like to extend thanks to the University of Southampton and ESI Group Company. Not only have they placed great faith in my ability but provided me with the support that I needed. As a result of their financial backing I have been able to study in the best possible conditions and they have assisted me in realising my goal of completing my PhD study in the United Kingdom.

Conventions

Cartesian coordinates are always assumed for vectors, matrices and tensors whose components are designated by numerical indices ranging from 1 to 3. A repeated index denotes summation over the range of the index. Vectors, vector fields, matrices and tensors are defined by boldface characters. Material quantities are defined by upper case letters while spatial quantities are defined by lower case letters. Components of a tensor are written in italic fonts.

If a colon is set before an equally sign, as in :=, the right hand-side defines the left-hand side.

The symbols $\Rightarrow$ and $\Leftrightarrow$ mean respectively "implies" and "is equivalent to".

Differentiation with respect to time is denoted by an over dotted symbol. Superscripts and subscripts added to symbols provide additional information, the meaning of which should be clear from the context. A bar symbol placed over a symbol generally means "prescribed". A superscript "e" concerns a quantity defined at the (finite) element level whereas a superscript "n" means that the quantity is defined at the instant corresponding to the time step number n.

Vectors, matrices, tensors and indices

$\mathbf{v}$	vector $\mathbf{v}$	v_i	Cartesian components of $\mathbf{v}$
$\mathbf{M}$	matrix $\mathbf{M}$	M_{ij}	Cartesian components of $\mathbf{M}$
$\mathbf{T}$	tensor $\mathbf{T}$	T_{ij}	Cartesian components of $\mathbf{T}$

Operators

$\rightarrow$	a mapping; *example:* $\chi : \mathrm{B} \rightarrow \mathscr{E}$ reads "χ maps B into $\mathscr{E}$"
.	scalar product of two vectors (i.e., $\mathbf{u}.\mathbf{v} = u_i v_i$) or inner product of a second-order tensor with a vector [i.e., $(\mathbf{A}.\mathbf{v})_i = A_{ij} v_j$)]
:	inner product of two second-order (or higher) tensors [i.e., $(\mathbf{D}:\mathbf{C})_{ij} = D_{ijkl} C_{kl}$)].
$\otimes$	dyadic product or outer product of two second-order tensors [i.e., $(\mathbf{A} \otimes \mathbf{B})_{ijkl} = A_{ij} B_{kl}$] or dyadic product of two vectors [i.e., $(\mathbf{u} \otimes \mathbf{v})_{ij} = u_i v_j$]
$\mathbf{A}^{\mathrm{T}}$, $\mathbf{T}^{\mathrm{T}}$	transpose of a matrix $\mathbf{A}$ or a tensor $\mathbf{T}$
$\mathbf{A}^{-1}$, $\mathbf{T}^{-1}$	inverse of a matrix $\mathbf{A}$ or a tensor $\mathbf{T}$
trace $(\mathbf{A})$	trace of $\mathbf{A}$ [i.e., *trace* $(\mathbf{A}) = A_{11} + A_{22} + A_{33}$]
$\mathbf{A}^2$	square of $\mathbf{A}$ [i.e., $(\mathbf{A}^2)_{ij} = A_{ik} A_{kj}$]
cof $(\mathbf{A})$	cofactor of $\mathbf{A}$ [i.e., cof $(\mathbf{A})$ = det $(\mathrm{A})\mathbf{A}^{-\mathrm{T}}$]

$\det(\mathbf{A})$	determinant of $\mathbf{A}$
$\mathbf{D}_{\varphi}, \nabla\varphi$	gradient of φ, referred to the reference configuration
$\nabla.\varphi$	divergence of φ, referred to the reference configuration
φ_*	push-forward operator
φ^*	pull-back operator

Greek symbols

α	material parameter, angle between fibre vectors $\mathbf{n}_0$ and $\mathbf{m}_0$
$\alpha_1, \alpha_2, \alpha_3, \alpha_4, \alpha_5$	dimensionless ratios
β	material parameter
χ	configuration of B, dimensionless ratio
χ_0	reference configuration of B
$\boldsymbol{\delta}$	Kronecker tensor
δ	dimensionless ratio
$\boldsymbol{\varepsilon}$	Lagrangean strain tensor
ε_V	volumetric strain ($\varepsilon_V = \varepsilon_{11} + \varepsilon_{22} + \varepsilon_{33}$)
ε_0	transitional strain
ε_C	ultimate strain
φ	deformation from the reference to the current configuration
γ	shear strain
κ	bulk modulus, stiffness parameter in hourglass control
$\kappa_{\mathbf{n}_0}$	extension modulus in the direction $\mathbf{n}_0$
$\kappa_{\mathbf{m}_0}$	extension modulus in the direction $\mathbf{m}_0$
λ	stretch in the fibre direction
λ_i (i = 1..3)	principal stretches
λ_1	initial stretch in the fibre direction
$\lambda_{\mathbf{n}_0}$	stretch in the direction $\mathbf{n}_0$
$\lambda_{\mathbf{m}_0}$	stretch in the direction $\mathbf{m}_0$
ν	Poisson's ratio
θ_x , θ_y , θ_z	rotational degrees of freedom around the axes X, Y and Z
Π	represents the assembly of elementary matrices
ρ	density in the current configuration
ρ_0	density in the reference configuration
$\boldsymbol{\sigma}$	Cauchy stress tensor
$\boldsymbol{\sigma}_{dev}$	deviatoric Cauchy stress tensor defined as $\boldsymbol{\sigma}_{dev} = \boldsymbol{\sigma} - p\mathbf{1}$
$\boldsymbol{\sigma}^{\mathcal{L}}$	stress tensor of the linear elasticity theory

σ_{vM}	von Mises Cauchy stress defined as $\sigma_{vM} = \sqrt{\frac{3}{2}(\boldsymbol{\sigma}_{dev} : \boldsymbol{\sigma}_{dev})}$
$\overset{\nabla}{\boldsymbol{\sigma}}$	objective rate of Cauchy stress
σ_{i} (i = 1..3)	principal Cauchy stresses
σ_{C}	ultimate stress
$\boldsymbol{\omega}$	spin tensor
Ψ	Helmholtz free energy function, strain energy function, strain energy density
Ψ_I	strain energy function of an isotropic material
Ψ_{m}	strain energy function for the matrix
Ψ_{TI}	strain energy function of a transversely isotropic material
Ψ_{λ}	strain energy function for the fibres
Ψ_{i} (i = 1..8)	short-hand notation for $\frac{\partial \Psi}{\partial I_{\mathrm{i}}}$
Ψ_{ij} (i, j = 1..8)	short-hand notation for $\frac{\partial^2 \Psi}{\partial I_{\mathrm{i}} \partial I_{\mathrm{j}}}$

Latin symbols

A	material parameter for the incompressibility penalty function g
$\mathbf{A}^{\mathscr{L}}$	elasticity tensor of the linear elasticity theory
$\mathbf{A}^{\mathscr{m}}$	elasticity tensor in the material configuration
$\overline{\mathbf{A}}^{\mathscr{m}}_{m}, \tilde{\mathbf{A}}^{\mathscr{m}}_{m}$	components of the material elasticity tensors related only to the matrix
$\tilde{\mathbf{A}}^{\mathscr{m}}_{F_1 m}, \overline{\mathbf{A}}^{\mathscr{m}}_{F_1 m}$	components of the material elasticity tensors related only to the mechanical interactions between the matrix and the family of fibres F_1
$\overline{\mathbf{A}}^{\mathscr{m}}_{F_2 m}, \tilde{\mathbf{A}}^{\mathscr{m}}_{F_2 m}$	components of the material elasticity tensors related only to the mechanical interactions between the matrix and the family of fibres F_2
$\overline{\mathbf{A}}^{\mathscr{m}}_{F_1 F_2 m}, \tilde{\mathbf{A}}^{\mathscr{m}}_{F_1 F_2 m}$	components of the material elasticity tensors related to the mechanical interactions between the matrix and the family of fibres F_1 and F_2
$\mathbf{A}^{\mathscr{m}}_{F_1 F_2}$	components of the material elasticity tensors related only to the mutual mechanical interactions between the two family of fibres F_1 and F_2
$\mathbf{A}^{\mathscr{s}}$	elasticity tensor in the spatial configuration
B	material parameter for the incompressibility penalty function g
B	continuum medium (physical body)
$\mathbf{b}$	left Cauchy-Green deformation tensor
$\mathscr{B}$	mapping representing B in the current configuration
$\mathscr{B}_0$	mapping representing B in the reference configuration
$\partial\mathscr{B}_0$	frontier of $\mathscr{B}_0$

$\partial_{\varphi}\mathcal{B}_0$	boundary of $\mathcal{B}_0$ where displacements are prescribed
$\partial_{t}\mathcal{B}_0$	boundary of $\mathcal{B}_0$ where forces are prescribed
$\mathbf{C}$	right Cauchy-Green deformation tensor
C_i (i = 1..6)	material parameters
c_e	sound wave speed within element e
e	base of natural logarithms
E	Young's modulus
$\mathcal{E}$	Euclidean space
$\mathbf{E}$	Green-Lagrange strain tensor
$(\mathbf{e}_1, \mathbf{e}_2, \mathbf{e}_3)$	orthonormal basis in the current configuration
$(\mathbf{E}_1, \mathbf{E}_2, \mathbf{E}_3)$	orthonormal basis in the reference configuration
f	function of the stretch in the fibre direction
ℓ	scalar function of the right Cauchy-Green deformation tensor $\mathbf{C}$
$\tilde{\ell}$	isotropic scalar function of the invariants of $\mathbf{C}$
$\mathbf{f}^{n}$	residual forces vector
$\mathbf{f}^{int}$	internal forces vector
$\mathbf{f}^{ext}$	external forces vector
$\mathcal{F}$	function of symmetric tensors
$\mathbf{F}$	deformation gradient tensor, assembled nodal forces vector
$\mathbf{F}_{c0}$	deformation gradient tensor from stress-free to current configuration
$\mathbf{F}_{cI}$	deformation gradient tensor from pre-stressed to current configuration
$\mathbf{F}_{I0}$	deformation gradient tensor from stress-free to pre-stressed configuration
$\hat{\mathbf{F}}_{I0}$	deformation gradient tensor from stress-free to pre-stressed configuration in an orthonormal basis aligned with the fibre direction
F_i (i = 1..3)	principal forces
F_C	tensile strength
F_{12}	function of the invariants I_1 and I_2
g	penalty function [g = g(I_3)],
$\mathbf{g}_i$	$\mathbf{g}_i(\mathbf{u}^n) = 0$, i = 1 to n_c (boundary conditions and constraints)
$\mathbf{g}$	prescribed displacement vector
G	shear modulus
$\mathcal{G}_{IX}$	symmetry group characterising isotropy in the reference configuration
$\mathcal{G}_{TI}$	symmetry group characterising transversely isotropy

I_i (i = 1..11)	invariants of the tensor **C** and its structural tensor agencies
$\mathbf{I}$	fourth-order identity tensor
$\mathbf{I}_{b^{-1}}$	fourth-order tensor defined as $\left(\mathbf{I}_{b^{-1}}\right)_{ijkl} := \left(\varphi_* \mathbf{I}\right)_{ijkl} = -\frac{1}{2}\left(b^{-1}_{ik} b^{-1}_{jl} + b^{-1}_{il} b^{-1}_{jk}\right)$
$\mathbf{I}_{C^{-1}}$	fourth-order tensor defined as $(\mathbf{I}_{C^{-1}})_{IJKL} := \frac{\partial C^{-1}_{IJ}}{\partial C_{KL}} = -\frac{1}{2}\left(C^{-1}_{IK} C^{-1}_{JL} + C^{-1}_{IL} C^{-1}_{JK}\right)$
J	Jacobian of the deformation = determinant of **F**
K	stiffness matrix
l_e	characteristic length of a finite element e
$\mathscr{L}$	vector space of all linear transformations from $\Re^3$ into $\Re^3$
$\mathscr{L}^+$	$\mathscr{L}^+ := \left\{ \mathbf{F} \in \mathscr{L}(\Re^3, \Re^3) / \ det(\mathbf{F}) > 0 \right\}$
m	current unit vector field characterising the direction of the fibre family F_2
$\mathbf{m}_0$	reference unit vector field characterising the direction of the fibre family F_2
M	structural tensor in the current configuration [$\mathbf{M} := \mathbf{m} \otimes \mathbf{m}$]
	mass matrix
$\mathbf{M}_0$	structural tensor in the reference configuration [$\mathbf{M}_0 := \mathbf{m}_0 \otimes \mathbf{m}_0$]
$\mathbf{M}_{0C}$	second-order tensor defined as $\mathbf{M}_{0C} := \mathbf{M}_0.\mathbf{C} + \mathbf{C}.\mathbf{M}_0$ (reference configuration)
$\mathbf{M}_b$	second-order tensor defined as $\mathbf{M}_b := \mathbf{M}.\mathbf{b} + \mathbf{M}.\mathbf{b}$ (current configuration)
n_c	number of constraints in the boundary value problem
n_{TS}	number of time steps
n	current unit vector field characterising the direction of the fibre family F_1
$\mathbf{n}_0$	reference unit vector field characterising the direction of the fibre family F_1
N	outward normal field perpendicular to the boundary of B in χ_0
	structural tensor in the current configuration [$\mathbf{N} := \mathbf{n} \otimes \mathbf{n}$]
$\mathbf{N}_0$	structural tensor in the reference configuration [$\mathbf{N}_0 := \mathbf{n}_0 \otimes \mathbf{n}_0$]
$\mathbf{N}_{0C}$	second-order tensor defined as $\mathbf{N}_{0C} := \mathbf{N}_0.\mathbf{C} + \mathbf{C}.\mathbf{N}_0$ (reference configuration)
$\mathbf{N}_b$	second-order tensor defined as $\mathbf{N}_b := \mathbf{N}.\mathbf{b} + \mathbf{N}.\mathbf{b}$ (current configuration)
$\mathscr{O}^+$	$\mathscr{O}^+ := \left\{ \mathbf{T} \in \mathscr{L}^+ / \ \mathbf{T}^T.\mathbf{T} = \mathbf{1} \right\}$
p	hydrostatic pressure, Lagrange multiplier
P	material point of B occupying the position **X**
P	First Piola-Kirchhoff stress tensor
P′(x)	transform of P upon the deformation φ, occupying the position **x**
q	reaction stress to the inextensibility constraint in the direction **n**

$\mathbf{Q}$	orthogonal transformation
r	reaction stress to the inextensibility constraint in the direction $\mathbf{m}$
R	resultant force
$R_{xy}^{\max}$	maximum resultant force developed on the XY plane
$R_{xz}^{\max}$	maximum resultant force developed on the XZ plane
$\mathbf{R}$	orthogonal transformation, rotation matrix
$\mathbf{S}$	Second Piola-Kirchhoff stress tensor
$\mathcal{S}^+$	$\mathcal{S}^+ := \left\{ \mathbf{T} \in \mathcal{L}^+ \,/\, \mathbf{T}^{\mathrm{T}} = \mathbf{T} \right\}$
t	time, instant
$\mathbf{t}$	traction vector
$\mathbf{T}_{\mathrm{nm}}$	second-order tensor defined as $\mathbf{T}_{\mathrm{nm}} := \frac{1}{2}(\mathbf{n}_0.\mathbf{m}_0)(\mathbf{n} \otimes \mathbf{m} + \mathbf{m} \otimes \mathbf{n})$
$\mathbf{T}_{\mathrm{n_0m_0}}$	second-order tensor defined as $\mathbf{T}_{\mathrm{n_0m_0}} := \frac{1}{2}(\mathbf{n}_0.\mathbf{m}_0)(\mathbf{n}_0 \otimes \mathbf{m}_0 + \mathbf{m}_0 \otimes \mathbf{n}_0)$
$\mathbf{u}$	displacement vector
$\mathrm{u_x}$, $\Delta \mathrm{u_x}$	displacement along the positive X direction
$\mathrm{u_y}$, $\Delta \mathrm{u_y}$	displacement along the positive Y direction
$\mathrm{u_z}$, $\Delta \mathrm{u_z}$	displacement along the positive Z direction
$\mathbf{U}$	right stretch tensor
$\mathbf{V}$	left stretch tensor
W	work
$\mathbf{x}$	position of the particle P of B in the current configuration
$\mathbf{X}$	position of the particle P of B in the reference configuration
$\mathbf{Y}_{\mathrm{n_0m_0}}$	second-order tensor defined as $\mathbf{Y}_{\mathrm{n_0m_0}} := I_6\mathbf{N}_0 + I_4\mathbf{M}_0$
$\mathbf{Z}_0$	second-order tensor defined as $\mathbf{Z}_0 := \mathbf{N}_0 + \mathbf{M}_0$
$\mathbf{Z}_{0\mathrm{C}}$	second-order tensor defined as $\mathbf{Z}_{0\mathrm{C}} := \mathbf{N}_{0\mathrm{C}} + \mathbf{M}_{0\mathrm{C}}$

Other symbols

$\subset$	subset	$\Re^n$	Euclidean n-space
$\in$	"is a member of"	$\varnothing$	empty set
$\cup$	union	o	composition of linear maps
$\cap$	intersection	$\mathbf{1}$	second-order identity tensor

Abbreviations

3D	Three-dimensional
ACL	Anterior cruciate ligament
AMB	Anteromedial band
ANT	Anterior
AP	Anterior-posterior
CAD	Computer Aided Design
FE	Finite element
FEA	Finite element analysis
FEM	Finite element method
FEM	Femur, femoral
GSRI	Generalised selective reduced integration
HA	Hyaluronic acid
IS	Initial stretch
LCL	Lateral collateral ligament
MCL	Medial collateral ligament
PA	Posterior-anterior
PCL	Posterior cruciate ligament
PG	Proteoglycan
PLB	Posterolateral band
POST	Posterior
SRI	Selective reduced integration
TIB	Tibia, tibial
TKA	Total knee arthroplasty
TKR	Total knee replacement
URI	Uniform reduced integration
vM	von Mises stress

Chapter I

Introduction, motivations and objectives

I.1 The human knee joint: generalities

The knee joint is one of the most heavily loaded joints in the body and this can be attributed to various mechanical factors. The knee is located below the centre of gravity of the body and its large range of flexion can generate significant lever arms. Due to this, the knee can be subjected to very high loads. The knee's functions and its position between some of the longest bones in the body, i.e. femur and tibia, subject it to high forces and torques, making it prone to injury. Also, the knee is a nonconforming joint, which accounts for its large range of mobility. With nonconforming surfaces, the load is distributed over relatively small areas and hence the stresses can be large. The stability of the knee joint depends upon: the congruency or fit of its articular surfaces, the ligaments that cross the joint, and the muscles that cross the joint. The knee joint is a relatively mobile joint stabilised primarily by ligaments. Understanding the mechanical behaviour of the ligaments is therefore pivotal in understanding the mechanics of the whole knee. Damage to ligaments can lead to various orthopaedics problems that need to be managed using either non operative or surgical means. Obtaining a good understanding of the interactions between the bony structures and the ligaments can allow the investigation of pathological effects when certain components of the system lose their normal function.

I.1.1 Role of ligaments in knee stability (clinical sense)

An unstable knee joint (after ligament or joint capsule rupture) leads to abnormally high stresses on the articular cartilage and may lead to early osteoarthritis. Knee joint instability, as frequently seen in the knee following anterior cruciate ligament (ACL) injury, can lead to progressive changes in the articular cartilage, in the menisci, and in other ligaments attempting to restraint the increased joint mobility (Noyes *et al.*, 1985; Tamea and Henning, 1981). After menisco-ligamentous injury the kinematics of the knee is disturbed and the medial femoro- tibial compartment is overloaded especially when the meniscus has been resected and when the patient has a morphology in genu varum. Long-term follow up has shown that 15-20 % of patients go on to suffer arthritis of the knee following knee joint injuries (Aubriot, 1998).

I.1.2 Role of ligaments in total knee joint replacement

During the design process of total knee joint replacement, the kinematics and kinetic requirements of the joint must to be taken into account to restore normal function after prosthetic replacement. Furthermore, the estimated joint loading magnitude and its frequency applied to test the implant and its fixation to bone must be assessed to assure long term performance of the surgical implant under *in vivo* conditions. More and more studies emphasize the importance of the ligament imbalance on the success of total knee replacement and particularly for "condylar-type" knee prostheses (Sambatakakis *et al.*, 1993). Soft tissue imbalance, defined in both flexion and extension, can be described as the resultant trapezoidal geometry, after the bony cuts have been made, and when the knee is tensed by equal medial and lateral forces. The imbalance is quantified by measuring the difference in length between the medial and the lateral sides of the trapezoid or by measuring the rotary deflection away from the parallel, or zero, position. Ligaments of the knee play a significant role in the success or the failure of knee replacement. In a TKA, the geometry of the prosthetic components is essential (Delp *et al.*, 1995; Kocmond *et al.*, 1995) but a better understanding of the ligament functions and their mechanical interaction with the surgical prostheses could offer insight into clinical performance.

I.2 Computational models in biomechanics

Today, it is almost a tautology to say that numerical models in biomechanics are of great importance for understanding biomechanical concepts and bring solutions to orthopaedic clinical problems. Biological tissues, are by essence, highly complex systems that host chemical, cellular, electrical and mechanical processes. Computational models have the ability to allow investigation into the complexity of diarthrodial joint mechanics by decomposing the physical reality into a collection of simpler problems for which solutions are achievable. Models of this nature can answer some of the essential questions orthopaedics surgeons face during their practice:

In the management of the intact and injured knee:

- *What is the magnitude of forces in a ligament during a particular physiological motion ?*
- *How are ligaments damaged ?*
- *How does an injured ligament affects the kinematics of the knee joint during a gait cycle ?*
- *Is it necessary to apply a pretension to a graft for ligament reconstruction ?*
- *Can other operative procedures restore normal function ?*

In the management of a replaced knee:

- *What is the optimal medial / lateral ligament balance ?*
- *Retention or resection of the PCL ?*
- *What is the optimal way to constrain articular surfaces ?*

Due to the broad availability of computer workstations and their capacities, biomechanical computational models are a cheap way to perform studies in biomechanics, avoiding costly experiments and/or harmful experimental studies on animals or humans.

It is worthy to note that experiments are necessary to obtain kinematic and material data as input into computational models. In fact, the material constitutive laws (mathematical laws relating stress and strain) used in finite element codes rely on parameters derived from experimental tests performed on cadaveric tissue specimens. These test are therefore essential for implementing a finite element constitutive law. Kinematic tests can be used for two distinct purposes. The first one is to obtain information regarding the physiological kinematic conditions a knee can be subjected to. These will constitute boundary conditions for the finite element model (boundary conditions prescribed in displacement).

The second purpose is to validate the finite element model by comparison of numerical results with experimental results. The displacements of the various knee structures (tibia, femur and ligaments) calculated in a finite element simulation must match (or, at least, get as close as possible to) the displacements obtained experimentally. In this particular case, the boundary conditions are not prescribed in displacement but in terms of force or stress. Once a numerical model is operational, any set of conditions (boundary, kinematics) can be simulated.

Unlike "traditional" engineering materials, biological materials, especially soft tissues, exhibit mechanical behaviour extremely complex to characterise. Indeed, they are living, highly heterogeneous, anisotropic and strain rate dependent, have a very nonlinear behaviour, sustain very large deformations and have generally irregular geometries. Perhaps mainly due to the difficulties associated with these tissues, they have received minor attention on the constitutive modelling side and on the practical numerical implementation of their mechanical behaviour into finite element codes. Robust and realistic finite element material models for soft connective tissues are seriously lacking. A literature survey has shown that indeed very few three-dimensional nonlinear finite element models have been developed. Weiss (1994) and Weiss *et al.* (1996) formulated a three-dimensional incompressible transversely isotropic hyperelastic constitutive law for soft tissues and implemented the model into a research finite element code. The time dependence on the mechanical properties of soft tissue was further incorporated into a transversely isotropic hyperviscoelastic finite element model (Puso and Weiss, 1998). Material data fitting this model were later extracted for the human medial collateral ligament (Quapp and Weiss, 1998). Pioletti (1997, 1998a) formulated a three-dimensional isotropic hyperviscoelastic constitutive law, derived material data from experiments and implemented the purely elastic part of the law into a commercial implicit finite element code. The approach adopted by Pioletti, (1997, 1998a) considers ligaments and tendons as isotropic materials and as will be shown this hypothesis is clearly untrue. Although Weiss (1994) implemented an anisotropic constitutive law for biological soft tissues, this was done within the framework of an *implicit* finite element code. No similar model was ever implemented into an *explicit* finite element code where the term *explicit* refers to the time integration numerical scheme used to solve the elastodynamic boundary value problem. This latter type of numerical code is particularly well suited to the study of dynamic mechanical systems involving highly nonlinear phenomena (material, geometric, boundary and contact-impact nonlinearities) such as those occurring in human diarthrodial joints.

Besides this, car manufacturers and other transport industries devote more and more means into research concerning occupant safety and crash impact simulations. Indeed, to have a better understanding of the injury mechanisms occurring during these crash events, it is essential to represent as accurately as possible not only the three-dimensional interactions between the occupants and the vehicle structure but also the biomechanical interactions within the human body. For example, the mechanical interaction between the bony and ligamentous structures are fundamental aspects in scenarios involving the so-called *dash-board injury* which accounts for rupture of the PCL within the knee joint. Computational biomechanical models are used more and more to carry out finite element analyses simulating impact scenarios. As these numerical simulations are performed within explicit finite element codes, it is essential to develop adequate three-dimensional material models which take into account the key features of soft tissues and provide a much better alternative to the existing simplified unidimensional models currently in use. These models have the major disadvantage of not being able to capture the three-dimensional states of stress and strain within ligaments and tendons.

I.3 Aim and objectives of the thesis

The aim of the present work is to contribute to the field of constitutive modelling of biological soft connective tissues from an analytical and numerical point of view. This will be achieved by developing a general theoretical framework for the constitutive formulation of anisotropic biological materials. The task will be then to identify and implement a suitable constitutive law for ligaments into a commercial finite element code. Availability of experimental material data in literature will condition the choice of the mathematical formulation adopted. The implementation of a fully three-dimensional incompressible transversely isotropic hyperlastic material model for ligaments will extend the current possibilities of realistic numerical simulations in soft tissue mechanics. This will overcome a significant shortage of reliable finite element models for modelling the mechanical behaviour of ligaments and particularly, the collateral and cruciate ligaments of the human knee joint. Finite element analyses will be performed and in the light of the results this will lead to the view that current isotropic models of ligaments are not valid and should not be used for particular simulated physiological conditions such as passive flexion of the knee. A fully dynamic model of the knee ligaments integrated into a knee joint model will also permit the simulation of physiological dynamic and static conditions.

The aim of this research work will be achieved in the context of the existing body of knowledge in the field –at times building on this knowledge but also sometimes offering fundamental criticism of current opinion.

The first specific objective is proposed in the context of a continuum theory of fibre-reinforced composites at finite strains to justify the theoretical bases adopted in this work for the constitutive modelling of biological soft connective tissues. An extension of the theory proposed by Spencer (1992) is developed in order to describe a more *general* theoretical framework suitable for the constitutive modelling of ligaments and tendons. Particular attention is paid to the symmetry groups because mechanical anisotropy is one of the essential characteristics of ligaments and tendons.

Entirely new explicit expressions, not previously reported in literature, for the elasticity tensors in the spatial and material descriptions are established. These expressions are developed and discussed in connection with their biological significance. The various terms of the elasticity tensors can be helpful in exploring and incorporating into the constitutive formulation complex interactions between the components of the fibre-reinforced composite material that can be missed otherwise. Moreover, elasticity tensors are essential in investigating mathematical properties of the constitutive laws and their knowledge is fundamental in any finite element method. It is shown how typical mechanical features of soft connective tissues can be taken into account at the mathematical formulation stage.

The second specific objective is to identify and implement a suitable three-dimensional constitutive law to represent the mechanical behaviour of ligaments into a commercial explicit finite element code. As the model will be used to simulate ligaments operating in physiological conditions, the numerical implementation must be extremely robust to track accurately all the nonlinear phenomena involved. Since ligamentous structures are in a state of residual stress *in vivo*, it is essential to implement numerically the capacity to pre-stretch the finite element soft tissue models. This will constitute another objective of the numerical developments done in the context of an explicit finite element code.

The fourth specific objective is proposed in response to the view that isotropic constitutive laws can predict the natural mechanical behaviour of ligaments.

It is believed that at least the simplest class of anisotropic symmetry (transverse isotropy) is crucial in the definition of a constitutive law in order to accurately represent and predict the natural behaviour of ligaments. By performing finite element analyses of the mechanical behaviour of a human ACL (for passive knee flexion) the severe deficiencies of isotropic models are highlighted and overcome by the significant advantages offered by transversely isotropic models. Essentially an objective aimed at evaluating an important concept, the residual stress hypothesis will also be tested in the same finite element model of the ACL and for the same boundary conditions.

The sixth specific objective is to test the transversely isotropic hyperelastic model of the ligaments in the context of diarthrodial joint biomechanics. The new three-dimensional constitutive model will allow us to integrate the complex geometrical and mechanical properties of the four main knee ligaments into a full three-dimensional anatomical model of this joint. The complex mutual contact interactions occurring between the ligaments and the bones will extend the current possibilities in biomechanical finite element analyses by providing more realistic boundary conditions. In fact, this will permit the capture of mechanical interactions that are absent in the existing finite element models of the knee joint and this will establish the possible role that they play in the kinematics of a knee subjected to drawer tests.

I.4 Outline of the thesis

As the thesis objectives are concerned with the finite element analyses of the ligaments of the knee in simulated physiological conditions, anatomy and mechanical characteristics of this joint (bony and ligamentous structures) will be reviewed as a preliminary step. This will be accomplished in Chapter II.

Chapter III reviews the structural and mechanical properties of ligaments. The knowledge of these features is fundamental in the formulation of a constitutive law and so will be essential to structurally justify the mechanical formulation that is adopted in this work.

In addition to these physiological aspects, a critical review of previous material modelling approaches will be presented in Chapter IV.

In Chapter V, the theoretical basis of the constitutive modelling of soft connective tissues will be laid down. The theory of fibre-reinforced composites at finite strain developed by Spencer (1992) will be further extended and discussed in relation with soft tissue mechanics.

The numerical implementation of an incompressible transversely isotropic hyperelastic law into an explicit finite element code will be presented in Chapter VI. The correct implementation of the material model will be demonstrated by showing excellent agreement between numerical and analytical solutions for states of homogeneous deformations.

Chapter VII will concentrate on the essential practical aspects related to the finite element analyses of ligamentous structures. Sensitivity finite element analyses will be performed in order to test the accuracy of the implemented material model with regards to the choice of the hourglass mode stabilisation methods for 8-noded hexahedral solid elements, the validity of the quasi-static process, mesh density and boundary conditions.

In Chapter VIII, it is proposed to demonstrate the relevance and usefulness of the numerical implementation of the anisotropic constitutive law for biological soft connective tissues. The capacity to apply a residual stress to a FE model of a soft tissue structure will also be shown to be essential. The incompressible transversely isotropic hyperelastic FE model will be used to model the mechanical behaviour of the human ACL when the knee is subjected to passive flexion.

Chapter IX is another illustration of the very promising potential brought by the Finite Element Method in the field of joint biomechanics. The mechanical response of an anatomical human knee joint model subjected to anterior-posterior drawer tests will be evaluated. The novelty of the proposed model consists in the simultaneous integration of realistic three-dimensional constitutive law for ligaments, anatomically accurate description of bones and ligaments and above all, accounting of all the potential three-dimensional contact interactions between bony and ligamentous structures.

Finally, Chapter X will end with concluding remarks about the present research work and will offer recommendations for future work.

Chapter II

Anatomy and physiology of the human knee joint

The primary function of the knee is to provide locomotion and in doing so to support the weight of the body, to aid in the conservation of momentum of the lower extremity and to transmit loads through the lower limbs. The knee joint consists of three joints: the femoral-tibial joint, the femoral-patellar joint and the tibio-fibular joint, and four bones: *the femur*, *the tibia, the fibula* and *the patella.*

The knee joint is a synovial joint which means that the opposite surfaces are covered by hyaline articular cartilage and are enclosed in a joint cavity containing a highly viscous synovial fluid formed from an inner synovial membrane, and the outer fibrous capsule. The additional fibrous bands both outside the joint capsule, and inside the joint cavity are known as the ligaments. Although the knee joint possesses six degrees of freedom, the dominant motions are: *flexion / extension, internal / external rotation, anterior / posterior translations.*

The following smaller motions are also allowed (although constrained by ligaments): *varus / valgus rotations*, *medial / lateral translations* and *inferior / superior translations.*

The mechanical complexity of the knee is outstanding in the sense that this joint must satisfy two antagonistic conditions:

1. *to have an excellent stability in full extension, when the knee is subjected to high stresses generated by the body weight and the muscle forces*;
2. *to have a good mobility after a certain degree of flexion has been achieved, this feature being essential for running and the optimal orientation of the foot relative to the ground, particularly on uneven surfaces.*

The stability of this highly complex engineering problem is achieved by the way of ingenious mechanical linkages, namely the ligaments (Kapandji, 1987). The knee joint has four main ligaments: *the two collateral* and *the two cruciate ligaments* (Figure II.1).

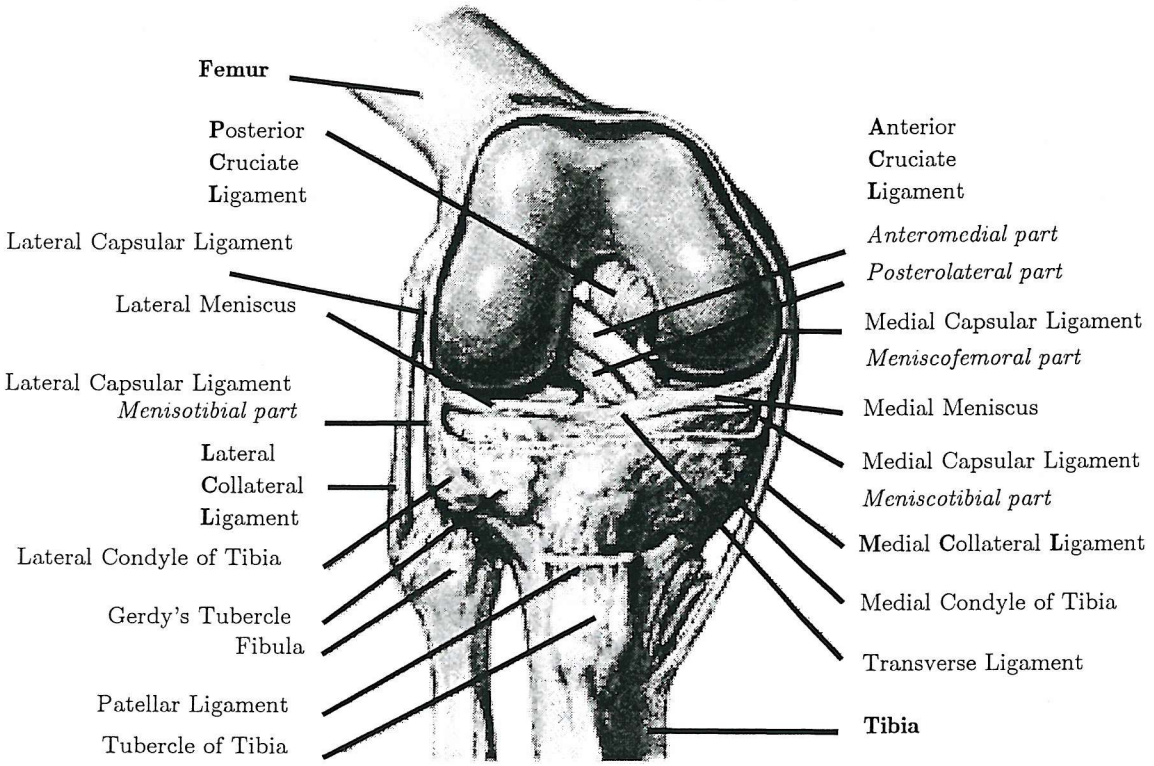

Figure II.1 – Anatomy of a right knee in flexion (frontal view). The patella is not represented. The anterior part of the capsule has been removed in order to show the intracapsular components (*Anonymous picture found on the Internet*).

At this stage, it is also important to mention the menisci which are two dense fibrous semi-circular soft structures with a wedge-shaped cross section. They are interposed on the tibial plateaux between tibia and femur, one medially and the other laterally. The *medial meniscus*, which is the larger of the two, is attached to the tibia at its anterior and posterior horns by fibrous tissues. Its outer circumference is connected through the capsule of the joint to the femur and tibia. Thus its capsular attachments to the tibia are lax whereas those to the femur are strong on the medial side and form the deep capsular ligament. The *lateral meniscus* is fixed to the tibia at both its horns and in addition, its posterior convexity is secured to the femur by the menisco-femoral ligaments. The anterior convex margin of the lateral meniscus is connected to the anterior horn of the medial meniscus by the transverse ligament (Kapandji, 1987).

The main role of the menisci is to enhance the stability of the knee and to protect the articular cartilage from excessive concentration of force. Most of the direct tibiofemoral contact is eliminated while the surface contact of the joint is increased thus reducing contact stress. Menisci are also considered as shock-absorbing structures that protect the articular surfaces of the bone.

II.1 The collateral ligaments

The medial collateral ligaments stiffen the articular capsule on its medial and lateral aspects (Kapandji, 1987). They are therefore responsible for the transverse stability of the knee during extension by preventing side to side movements of the tibia and the femur relative to one another. The stability of the knee is achieved when the external forces acting on the knee joint are correctly balanced by the internal forces provided by the capsular structures, ligaments, muscles and joint contact geometryThey also prevent lift off of the femur in varus-valgus tilt. The two ligaments allow more movement during knee flexion than extension because of their more posterior locations on the sides of the knee joint. Both ligaments are tight during extension and relatively loose during flexion.

II.1.1 The medial (or tibial) collateral ligament (MCL)

The MCL is a 8-10 cm long, broad, flat ligament that blends with the postero-medial aspect of the joint capsule (Pope, 1996). The ligament lies somewhat posteriorly on the medial side of the joint and is attached to the medial epicondyle of the femur superiorly and the medial tibial condyle, and medial surface of the tibial shaft. The MCL is composed of two parts: the superficial and the deep portions. The superficial MCL is attached proximally to the posterior aspect of the medial femoral condyle and distally to the metaphyseal region of the tibia, up to 4-5 cm distal to the joint, lying beneath the pes anserinus (Hughston *et al.*, 1976a; Hughston *et al.*, 1976b; Pope, 1996). The superficial ligament can be further subdivided into anterior and posterior portions. The posterior fibres form the posterior oblique ligament. The anterior fibres of the ligament are separated from the joint capsule, often by one or more bursa, while the posterior fibres blend with the medial meniscus and the joint capsule. The deep MCL is anatomically the third (deep) layer of the medial compartment, which in many cases will be separated from the superficial MCL by a bursa (which allows sliding of the tissues during flexion). Essentially, the MCL resists valgus stresses across the knee joint, being especially effective in the extended knee when the ligament is taut.

Grood *et al.* (1981) showed that the MCL carried 57% of the valgus stress when the knee was at 5 degrees of flexion but 78 % when the knee was flexed to 25 degrees. Harfe *et al.* (1998), Nielsen (1987) and Nielsen *et al.* (1984) found that the MCL made a major contribution throughout the knee joint range of motion to checking lateral rotation of the tibia combined with either anterior or posterior tibial displacement. A 3 degrees valgus rotation significantly increases the strain in the MCL for flexion angles ranging between 15 and 20 degrees. A 10 degrees external tibial axial rotation significantly reduces the strain in the MCL for flexion angles varying between 30 and 120 degrees (Harfe *et al.*, 1998).

II.1.2 The lateral (or fibular) collateral ligament (LCL)

The fibular collateral ligament is a strong, rounded cord-like ligament on the lateral side of the knee joint. This ligament is very distinct from the joint capsule and does not attach to it or to the lateral meniscus. The entire lateral collateral ligament is about 5 cm long. At full extension, the LCL is at 35 degrees relative to the MCL on a sagittal plane projection (Zuppinger, 1904). The LCL resists varus stresses across the knee. Given its alignment, it also appears to limit lateral rotation of the tibia, making its most substantial contribution at about 35 degrees of flexion, in conjonction with the posterolateral capsule (Nielsen and Helming, 1985; Nielsen *et al.*, 1984). The LCL also resists combined lateral rotation with posterior displacement of the tibia in conjunction with the tendon of the popliteus muscle (Nicholas and Hershman, 1986). As shown by Harfe *et al.* (1998), a 3 degrees varus rotation significantly increases the strain in the LCL for flexion angles of 15-120 degrees. As opposed to the case of the MCL, internal or external tibial axial rotation does not seem to affect the strain response of the LCL.

II.2 The cruciate ligaments

These ligaments lie inside the joint capsule and for this reason are called intracapsular ligaments (like the transverse ligament, the anterior and posterior meniscofemoral ligaments). It is worth noting that they are intracapsular but extrasynovial. The cruciate ligaments are essential ligaments that prevent anterior-posterior displacement of the tibia relative to the femur. They cross one another and form an "X" when viewed from the anterior-posterior and medial-lateral aspects of the knee joint. The ACL is attached to the *anterior* intercondylar fossa and the PCL is attached to the *posterior* intercondylar fossa on the tibia. The two cruciate ligaments are separated by a cul-de-sac of synovial membrane where they cross one another.

They are both relatively tight in all movements of the knee and serve to limit translational sliding movements between the tibia and femur, the ACL limiting anterior sliding and the PCL preventing posterior sliding (Haines, 1941). They help to prevent lateral rotation of the femur on the tibia and tighten during lateral rotation (Haines, 1941). There is a controversy between various authors concerning this issue. According to Haines, the cruciate ligaments unwind to some extent during medial rotation of the femur upon the tibia and therefore allow this rotation to occur during the last few degrees of extension. Williams and Warwick (1980) consider that the two ligaments are most tense during extension of the knee when this medial rotation occurs and tightens the cruciate as they cross one another. Others authors like Hollinshead (1982) hold that the ACL is most tense during full extension, while the PCL is most tense during hyperextension of the knee. However, most anatomists agree that both cruciate ligaments are tense during hyperextension of the knee (Brantigan and Voshell, 1941).

II.2.1 The anterior cruciate ligament (ACL)

This ligament is made of multiple collagen fascicles and its length ranges from 25 to 41 mm (mean: 38 mm) with a width varying between 7 and 12 mm (mean: 10 mm). The ACL is attached to the medial aspect of the anterior intercondylar area of the tibia, between the attachment sites of the anterior horns of the lateral and medial menisci. It passes posterosuperiorly and laterally attaches to the lateral condyle of the femur on its posteromedial surface. The ACL is composed of two principal fibre bundles: a small anteromedial band (AMB) and a larger bulky posterolateral band (PLB). An intermediate bundle can also be identified (Amis and Dawkins, 1991). The different bundles of the ACL contribute to resisting anterior subluxation in flexion and extension. The AMB is tight in flexion (maximumly tensed at 70 degrees of flexion) and the PLB is tight in extension (Jeffreys, 1963). This correlates with increased contributions to knee stability and the likehood of partial ruptures in these positions. At 5 degrees of hyperextension, the anterior cruciate ligament forces range between 50 and 240 N (mean: 118 N) (Markolf *et al.*, 1990). Markolf *et al.* (1990) found that ACL load was maximum during internal tibial rotation and was negligible during external tibial rotation. Hyperextension of the knee develops much higher forces in ACL than in PCL. During isometric quadriceps contraction, ACL strains at 30 degrees of knee flexion are significantly higher than at 90 degrees of flexion where the ligament remains unstrained with isometric quadriceps activity. The ACL is the predominant restraint to anterior tibial displacement and accepts 75 % of anterior force at full extension and approximately 85 % at 30 and 90 degrees of flexion (Cabaud, 1983).

Piziali *et al.* (1980a, 1980b) performed cadaveric studies and showed that the ACL carried 87% of the total load when an anterior translational force was applied to an extended knee. Nicholas and Hershman (1986) and Torzilli *et al.* (1981) have found that the stresses on the ACL produced by an anterior translational force on the tibia create an internal rotation of the tibia. The ACL may also appear to make at least a minor contribution to restraining both varus and valgus stresses across the knee joint (Grood *et al.*, 1981). During gait the ACL is taut at knee extension, and tends to externally rotate the tibia. Tension is minimal at 40 to 50 degrees of knee flexion. As the knee moves from flexion to extension, posterior displacement of the lateral condyle of the femur is checked by ACL. The larger and less curved medial femoral condyle continues to forward roll and skids backward, assisted by tightening of PCL (Feagin and Lambert, 1985). Towards full extension there is lateral rotation of tibia and the joint is "screwed home".

II.2.2 The posterior cruciate ligament (PCL)

The PCL is shorter and stronger than the ACL. This ligament is approximately 38 mm long with a width of 13 mm (Pope, 1996). It is attached to the posterior intercondylar fossa of the tibia posterior to the attachments of the posterior horns of both of the menisci. The PCL passes anterosuperiorly and medially to attach to the anterior aspect of the lateral surface of the medial femoral condyle. The PCL is less oblique in its course than the ACL and it broadens considerably as it nears its femoral attachment. Generally, as with the ACL, the PCL is separated into an AMB and a PLB named by the tibial origin. At 80 to 90 degrees of flexion the AMB is maximumly taut and the PLB is relaxed (France *et al.*, 1983). The PCL is the primary restraint to posterior displacement of the tibia relative to the femur, with little or no displacement possible in full extension. The secondary restraints to posterior displacement of the tibia include posterolateral capsule, popliteus tendon and MCL. It appears that the PCL plays a role in restraining varus and valgus forces (Fukubayashi *et al.*, 1982; Grood *et al.*, 1981; Nielsen *et al.*, 1984) and, like the ACL, plays a role in both restraining and producing rotation of the tibia, with little or no rotation produced at the femur (Torzilli *et al.*, 1981). The PCL provides 93% of total restraining force to straight posterior translation of the tibia relative to the femur in the extended knee (Piziali *et al.*, 1980b). At 75 to 80 degrees of flexion, the displacement of the tibia, accompanied with a posterior translational force, is maximum. However sectioning of the PCL increases posterior translation at all angles of flexion (Fukubayashi *et al.*, 1982).

II.3 The kinematics of the normal knee joint

The primary motions of the knee joint are flexion/extension, anterior-posterior displacements and, to a lesser extent, internal-external rotation. These motions occur about changing but definable axes and serve the weight-bearing functions of the lower extremity (Kapandji, 1987). An essential feature of the knee joint kinematics is represented by the complex combination of rotational gliding and rolling of the bony structures. It is now largely recognised that the basic kinematics of the knee joint can be represented by the mechanism of a crossed four-bar linkage defined by the cruciate ligaments. In early flexion (0 to 25 degrees), rolling predominates while in deep flexion, most of the femoral motion is sliding on the tibia. The anterior glide of the femoral condyles results in part from the tension exerted by the ACL as the femur rolls posteriorly on the tibial condyle. The shape of the menisci constrains the femoral condyle to roll as the knee flexes. There is a progressive posterior translational displacement of femoral-tibial contact which allows for the range of motion in deep flexion (Müller, 1983). In the normal knee, there is an initial internal tibial rotation during flexion and a constantly shifting centre of rotation which can be explained by femoral-tibial adduction and proximal tibial medial translation with increasing flexion. Also there is a proximal tibial migration towards the femur during flexion explained by rollback onto the posterior proximal tibial slope. The most significant translation occurs in the sagital axis and is characterized in the normal knee by posterior translation or rollback. Extension of the knee from flexion occurs initially as a rolling of the femoral condyles on the tibial condyles, displacing the femoral condyles back to neutral position. After the initial forward rolling, the femoral condyles glide posteriorly just enough to continue extension of the femur as an almost pure spin (roll plus posterior glide) of the femoral condyles on the tibial condyles. The intra-articular movement of the femoral condyles is partly facilitated by the tension present in the PCL. The other contribution comes from the shape of the menisci. The asymmetry in the size of the medial and lateral condyles leads to a complex intra-articular motion pattern. As the femur extends to about 30 degrees of flexion, the shorter lateral femoral condyles completes its rolling-gliding motion. As extension continues, the longer medial femoral condyle has checked. This continued motion of the medial femoral condyle results in medial rotation of the femur on the tibia, pivoting about the fixed lateral condyle. Increasing tension in the knee joint ligaments as the knee approaches full extension may also contribute to the rotation within the joint. To initiate flexion, the knee must first be unlocked. That is, the medially rotated femur cannot flex in the sagittal plane, but must laterally rotate before flexion can proceed.

II.3.1 Flexion / Extension

The basic human gait pattern requires approximately 60 degrees of knee flexion whereas stair climbing increases the necessary angle of flexion to 80 degrees (Inman *et al.*, 1981). Sitting down into a chair and rising from it require at least 90 degrees of flexion (Nicholas and Hershman, 1986). For activities beyond simple mobility tasks, the requirement can increase to 115 degrees of knee flexion or more. Knee joint extension (or hyperexetension) of 5 to 10 degrees is considered within normal limits. During squatting knee flexion can reach 160 degrees (Kapandji, 1987) and this limit is due to the contact of soft tissues of the leg and thigh.

II.3.2 Internal / External Rotation

The range of knee joint rotation varies according to the degree of knee flexion. At full extension, when the knee is in the closed-packed (locked) position and the ligaments are taut (state of maximum congruency of the knee joint), no rotation can occur. At 90 degrees of flexion, ligaments are lax, 60 to 70 degrees (30 degrees of internal rotation and 40 degrees of external rotation) of either active or passive rotation were considered to be possible (Kapandji, 1987) although this has been proven to be not correct. The range for lateral rotation (0 to 40 degrees) is slightly greater than the range for medial rotation (0 to 30 degrees) (Kapandji, 1987). With maximum rotation available at 90 degrees of knee flexion, rotation diminishes as the knee approaches both full extension and full flexion.

II.3.3 Anterior / Posterior translations

During knee extension, the tibia glides anteriorly on the femur. During the last 20 degrees of knee extension, anterior tibial glide persists on the tibia's medial condyle because its articular surface is longer in that dimension than that of the lateral condyle.

When the knee begins to flex from a position of full extension, posterior tibial glide begins first on the longer medial condyle. Between 0 and 20 degrees of flexion, posterior glide on the medial side produces relative tibial internal rotation, a reversal of the screw-home mechanism (Kapandji, 1987).

During external rotation of the tibia the lateral femoral condyle moves forward over the lateral tibial condyle while the medial femoral condyle moves backward over the medial tibial condyle. During internal rotation the reverse mechanism takes place (Kapandji, 1987).

Chapter III

Structural and mechanical properties of ligaments

III.1 Introduction

Ligaments are dense connective soft tissues possessing a fibrous structure made of parallel arrangements of collagenous fibres. These tissues are composed largely of *collagen*, a fibrous protein constituting approximately one third of the total protein mass in the body (White *et al.*, 1964). Also, collagen is not only found in bone and cartilage where it constitutes a large portion of the organic matrix but also in soft tissues such as blood vessels, muscle, ureters, intestines, the kidneys, skin and the liver where it provides a significant mechanical supportive function.

III.2 Structure and chemical composition of ligaments

Like other connective tissues, ligaments consist of relatively few cells (fibroblasts) and an abundant extracellular matrix. In general, the cellular material occupies about 20% of the total tissue volume, while the extracellular matrix accounts for the remaining 80%. About 70% of the matrix, also known as *ground substance* consists of water and approximately 30% as solids. These solids are *collagen*, *proteoglycans*, a small amount of *elastin* and other *glycoproteins* such as *actin* and *fibronectin* (Frank and Shrive, 1999). Roughly, 70 to 80% of the dry weight of normal tendon or ligament is composed of Type I collagen, also found in skin and bone (Fung, 1981). The structure and chemical composition of ligaments (and tendons as well) are identical in humans and in other mammal species such as rats, rabbits, dogs and monkeys (Fung, 1981). Results of experimental studies on these animals can therefore be directly related to the physiology of human ligaments and tendons.

An essential feature of the ligaments (as well as tendons) is that, when observed under polarised light microscopy, a periodic arrangement of wavy collagen appears (Figure III.1). This wavy pattern is known as the *crimp pattern* with a typical geometrical period of about 50 μm (Frank and Shrive, 1999). The progressive uncrimping of the collagen fibres is the source of the increasing stiffness in the first phase of the uniaxial stress-strain curve.

Figure III.1 – Photograph exhibiting the crimped pattern of collagen in ligament, from (Frank and Shrive, 1999). The typical wavy pattern of the collagen fibres is clearly visible.

III.2.1 Collagen

Collagen is a fibrous protein possessing a structural hierarchy. The basic constituent of collagen is the *tropocollagen* molecule which is composed of three polypeptide chains (α chains), each coiled in a right-handed helix (Rich and Crick, 1955) giving to the collagen molecule a rod-like shape (Figure III.2). The length of the molecule is about 280 nm, and its diameter is about 1.5 nm (Diamant *et al.*, 1972; Rich and Crick, 1955; White *et al.*, 1964). Five collagen molecules wrap one another to form a superhelix called a *microfibril*. Groups of collagen molecules, aggregated in a quaternary structure are called collagen *fibrils*. These structures, in which each molecule overlaps the other, are responsible for the repeating bands observed on the fibrils under the electron microscope. Their diameters range from 20 to 40 nm depending on the animal species and the tissue. The fibrils aggregate further to form *collagen fibres*, which are visible under the light microscope. These fibres ranging from 0.2 to 20 μm in diameter, do not branch and may be many centimetres long.

They reflect a 64 nm (in native fibrils) or 68 nm (in moistened fibrils) periodicity of the fibrils and have a characteristic undulated form. The fibres aggregate further into *primary bundles* or *fasciculi* (Fung, 1981). *Fibroblasts* (cells synthesising the collagen molecule) are aligned in rows between these bundles and are elongated along the axis in the direction of ligament or tendon function.

The arrangement of the collagen fibres differs somewhat in the tendons and ligaments and is suited to the function of each structure. The fibres composing the tendons have an orderly, parallel arrangement, which allows the tendons to handle the high unidirectional tensile loads to which they are subjected during activity. The ligaments generally sustain tensile loads in one preferred direction but may also bear smaller tensile loads in other directions; their fibres may not be completely parallel but are closely interlaced with one another. The specific orientation of the fibre bundles varies to some extent among the ligaments and is dependent on the function of the ligament (Amiel *et al.*, 1984; Kennedy *et al.*, 1976). It is worth noting that ligaments are also subjected to shear loading and compressive forces over bony structures allowing them to transfer load to the bone surface far from the insertion sites. A typical example concerns the warping of the collateral ligaments on the medial and the lateral sides of the knee joint.

An important contribution to the collagenous tissue integrity and mechanical properties is provided by the existence of cross-links between collagen molecules. This also plays an essential role in the aggregation at the fibril level. Collagen has the ability to form covalent intramolecular (*aldol*) and intermolecular (Schiff base) cross-links which are the keys to its tensile stiffness and resistance to chemical or enzymatic breakdown (Bailey, 1968; Mechanic, 1974; Tanzer, 1973). Within the fibrils, cross-links are characterised by "head-to-tail" interactions between the molecules. At the next superior level in the structural hierarchy, interfibrillar cross-linking of a more complex nature may occur.

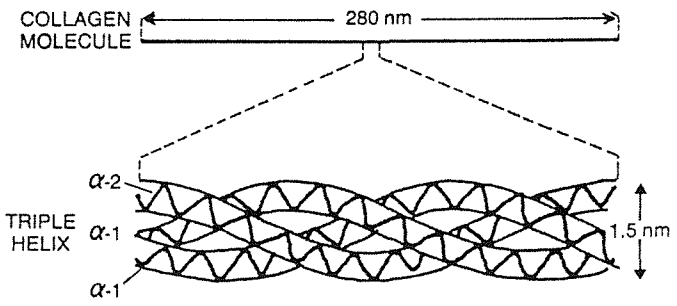

Figure III.2 – Structure of the collagen molecule. From Carlstedt and Nordin (1989).

III.2.2 Elastin

This protein is a major constituent of the extracellular matrix of soft connective tissues but does not have a pronounced hierarchical organisation like collagen. Its highly elastic properties (up to 250 % deformation) are believed to be responsible for the elastic recovery properties that it provides to connective tissues. The elastin is scarcely present in tendons and extremity ligaments, but in elastic ligaments such as the ligamentum flavum (ligament which connects the laminae of adjacent vertebrae) the proportion of elastic fibres is substantial.

III.2.3 Ground substance

Basically, the ground substance is a hydrophilic gel-like substance consisting of water, acid mucopolysaccharides, chondroitin sulfates A, B and C, keratosulfate and the heparins (Minns and Soden, 1973). The acid mucopolysaccharides are made of macromolecules, the *proteoglycans* (PGs), which bind to a long hyaluronic acid (HA) chain to form an extremely high-molecular weight PG aggregate. These PG aggregates bind most of the extracellular water of the ligament and tendon.

The ground substance of tendons or ligaments make up only a small percentage of the total dry tissue weight but are nevertheless quite significant because of their association with water, which represent 60 to 80% of the total wet weight. The water content of the human ACL varies between 65 and 70% (Woo *et al.*, 1986). The amount of ground substance depends on the tissue considered, as dense connective tissues possess a very small quantity of it as compared to loose connective tissues. The movement of water in the ground substance is of a very complex nature due to the numerous mechanical, biochemical and electrical interactions taking place. The study of these phenomena is a very challenging issue that requires the mobilisation of various disciplines such as biochemistry, cell biology and biomechanics.

The PG aggregates are essential in providing matrix-like cohesion between the collagen microfibrils and, as composite structures, ligaments and tendons are strengthened by these satbilising structural arrangements. They therefore contribute important features to the collagen fibre-ground substance interaction. The water and PGs provide lubrication and spacing crucial to the gliding function at intercept points where fibres cross in the tissue matrix. The PG molecules are highly negatively charged and possess a large number of hydroxyl groups which attract water through hydrogen bonding.

III.3 Physiological functions of ligaments

Tendons and ligaments are well suited to the physiological functions they perform. Multiple tendons and ligaments serve a single joint, providing a mechanism for both locomotion and the maintenance of static and dynamic protection through a wide range of movement. In addition to their purely mechanical function, ligaments of the knee are innervated and play an important proprioceptive role during the various kinematic and kinetic conditions the joint can be subjected to (Brand, 1986). Ligaments and tendons assure the transmission of loads between, respectively, bony structures and bony structures and muscles and, in doing so, maintain the proper alignment of the skeleton and guide joint motions.

III.4 Insertion of ligaments into bone

Tendon and ligament insertions to bone are functionally adapted to dissipate forces by passing through fibrocartilage to bone. As documented by Matyas *et al.* (1995), it appears that there is a correlation between the shape of the cells in the ligament-bone insertion zone and the mechanical stresses. The study, performed on rabbit MCLs, showed that the cells are the most rounded at the place where the highest compressive stresses occur and that the areas with the flattest cells correspond to the areas with the lowest compressive stresses.

The insertions of tendons and ligaments into bone are classified as either *direct* or *indirect.*

The structure of the *direct insertion* consists of four zones. At its extremity, the tendon has its collagen fibres (zone 1) intermeshing with fibrocartilage (zone 2). Then a gradual mineralisation of this fibrocartilage appears (zone 3) as the tissue merge more deeply into cortical bone (zone 4). The gradual alteration of the mechanical properties of the tissue is optimised in some way to distribute the stresses in the soft connective tissue. Indeed, as the tendon or ligaments inserts into bone, its stiffness progressively increases with the effect of reducing the stress concentration effect at the insertion into the stiffer bone.

The *indirect insertion* consists of a superficial layer, which connects directly with the periosteum, with deeper layers that anchor to the bone via Sharpey's fibres. The medial collateral ligament is particular in the sense that it has a direct femoral insertion and an indirect tibial insertion (Matyas *et al.*, 1995; Woo *et al.*, 1999). As noted by Frank and Shrive (1999), *indirect insertion* occurs also during growth when the ligament inserts into the periosteum.

III.5 Mechanical behaviour of ligaments

Ligaments display time- and history-dependent viscoelastic properties that reflect the complex interactions of collagen and the surrounding proteins and the ground substance mechanical properties. The ligaments are capable of sustaining finite strains and rotations without causing damage to their structure and by doing so, provide important restraining and cohesive functions in various joints. An important feature of these soft tissues is that their loading, unloading curves do not follow the same path, thereby forming an hysteresis loop. This is due to the fact that there are internal energy losses. As viscoelastic tissues, ligaments are also subject to creep (an increase of deformation over time under a constant load) and stress relaxation (a decline in stress over a time under a constant deformation). Soft connective tissues are therefore sensitive to strain rate (rate at which a load is applied).

III.5.1 The stress-strain relationship

A typical strain-stress curve for a tensile test of the ligament highlights several key characteristics of the soft tissues (Figure III.3).

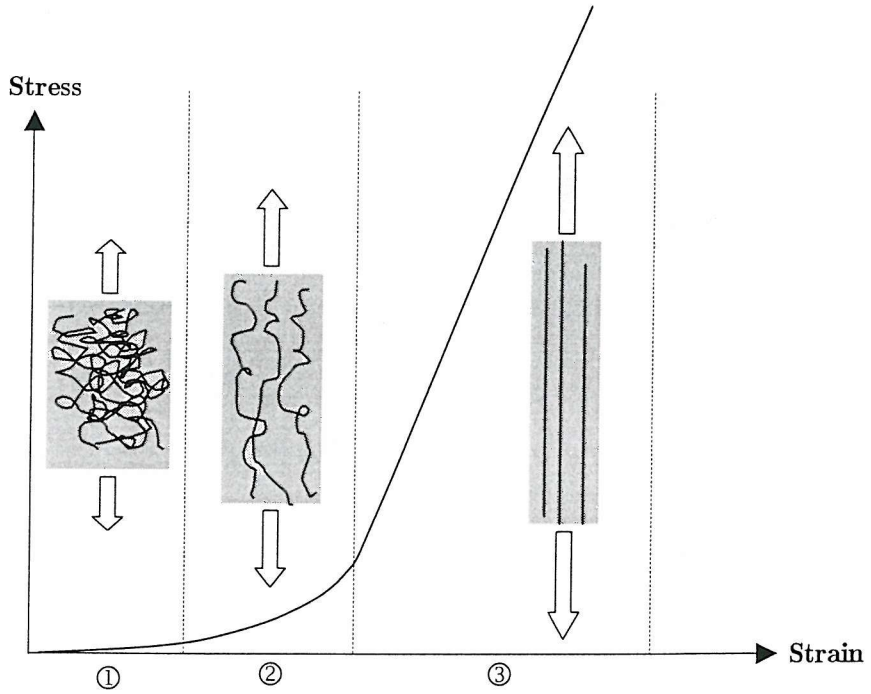

Figure III.3 – Stress-strain curve showing the pattern of deformation observed during a uniaxial tensile test on a ligament and the progressive modifications of the structural arrangement of the collgan fibres within the solid matrix of the tissue sample. Three principal regions are identified: ①, ② and ③.

In the relaxed state of the ligament, collagen fibres are also stress-free and are arranged in wavy and crimped-shaped patterns.

In the first region of the elongation curve (① on Figure III.3), a very low force is required to achieve finite deformations of the individual fibres without stretching them. The collagen fibres are simply unfolded and this translates into an approximately linear stress-strain relationship for the soft tissue sample tested.

The second region (② on Figure III.3), generally called *the toe region*, of the load-elongation curve is upwardly concave. In this part of the curve, the tissue is elongated with a small increase in loads as the wavy collagen fibres are straightened out and align with the loading direction. The collagen fibres start to carry loads as they elongate and interact with the surrounding solid matrix. As loading continues, the stiffness of the tissue increases, and progressively greater force is required to produce equivalent amounts of elongation. The end of the toe region has been reported to have a strain value of between 1.5 and 4 % (Abrahams, 1967; Rigby *et al.*, 1959; Viidik, 1973).

The third region (③ on Figure III.3), which is more or less linear, corresponds to a phase where the collagen fibres are straightened and the stiffness of the tissue is roughly constant.

Then if the elongation of the tissue sample is pursued until a critical value, sequential failure of the most stressed fibre bundles initiates (Butler *et al.*, 1978). This phenomenon is accompanied by small force reductions that can sometimes be observed in the loading curves for both tendons and ligaments. When the ultimate tensile strength of the specimen is reached, complete failure occurs rapidly, and the tissue can carry less load until full failure

Chapter IV

Constitutive models of ligaments

Equation Section 4

The constitutive modelling of soft tissues like ligaments or tendons can be described using three main approaches:

1. *Structural models.*
2. *Phenomenologicalmodels*
3. *Continuum models.*

The structural models can, generally speaking, be subdivided in two categories: *structural and microstructural models.* These types of model take into account respectively the structure (observable under light microscopy) and the microstructure (observable under electronic microscopy) of the tissue to predict the mechanical behaviour of the tissue at the macroscopic level. Generally the distinction between microstructural and structural models is not made.

The phenomenological models (often referred as *empirical* or *rheological*) are developed to describe the gross mechanical response of the tissue in the simplest possible terms.

The continuum models are not supported by structural considerations but are described by purely mathematical parameters (Woo *et al.*, 1993) which are directly related to the macroscopic behaviour of the whole structure. The coefficients are derived from experimental stress-strain curves during a process called identification (Lin *et al.*, 1978), but do not have necessarily a physical interpretation.

These models can allow for a broader generalisation of the formulation of the mechanical response of soft tissues and are more suitable for independent tests. These can then be the basis for analytical models or finite element models exploiting the developed mathematical formulations. It is noteworthy that, in literature, phenomenological and continuum based models are very often confused. In fact, the difference between the two concepts is vague and lies at the scale where the phenomena are described and is linked to the mathematical formulation used. A continuum model is generally based on a more rigorous mechanical formulation which finds its roots in thermodynamic considerations and is described by the Continuum Mechanics. Continuum models can therefore be considered as a subcategory of phenomenological models.

IV.1 Structural models

The general idea behind microstructural or structural models is to take into account the known (or assumed) structural geometry, the mechanical properties of the elemental constituents of the tissue (collagen, fibril, microfibril) and the way the constituents interact together to describe the gross continuum material behaviour. Once the scale upon the formulation is based is chosen (either microstructural or structural), an important assumption needs to be made: it must be assumed the existence of a representative unit volume inside which the material is supposed to be homogeneous. The structural models aim to assess the influence of the structural geometry on the global mechanical properties of the soft tissue. There are two different organisational scales: for example, the wavyness pattern of the fibres (or crimp) is considered as a *structural* feature of the tissue while fibril organisation of the fibres is considered as a *microstructural* feature.

IV.1.1 Mechanical properties of the constituents of ligaments and tendons

Morgan (1960) investigated the properties of the collagen fibres and found that those of the cowhide have nonlinear load-strain relations which can be represented by a power law. Kato *et al.* (1989) made direct measurements of fibre stiffness of rat tail tendon. Bovine Achilles tendon fibres were tested in tension by Sasaki and Odajima (1996a, 1996b). The aim was to investigate the elongation mechanisms of tendon collagen on the basis of the hierarchical structure of the tissue and the Hodge-Petruska model (model describing the arrangement of collagen molecules in a collagen fibril) of the arrangement of collagen molecules in the collagenous tissue. Based on the triple helix of the collagen molecule, Nestler *et al.* (1983) estimated the modulus of the collagen fibril.

IV.1.2 Structural organisation of the collagenous tissues (2 levels)

At the structural level, polarizing light microscopy have been used to observe changes in crimp patterns with deformation (Diamant *et al.*, 1972; Rigby *et al.*, 1959; Viidik and Ekholm, 1968b). *At the microstructural level*, scanning electron microscopy and transmission electron microscopy have been used to characterize the fibril orientation, size, and volume fraction as well as fibre organisation in healing rat MCLs (Frank *et al.*, 1991; Frank *et al.*, 1992; Padgett and Dahners, 1992).

X-ray diffraction methods have bee used to quantify fibril orientation in tendons and ligaments (Kastelic *et al.*, 1978; Sasaki and Odajima, 1996a; Sasaki and Odajima, 1996b). The organisation of the fibrils inside the collagen fibre is as important as the mechanical properties to describe the global mechanical behaviour of the tissue and, Frank *et al.* (1991) described the orientation of the fibrils in various planes of the tissue. The type of wavyness pattern of the collagen fibres is subject to discussion. An helical shape was described by Cruise (1958) and Comninou and Yannas (1976), whereas other authors (Diamant *et al.*, 1972; Lanir, 1978) found that the structure of the collagen fibre is planar and sinusoidal or planar zig-zag. However, to the best of our knowledge, no data is available concerning the full three-dimensional arrangement of the fibril. Another point raised in the literature concerns the shape of the isolated fibres. It was shown (Diamant *et al.*, 1972; Lanir, 1978) that the collagen fibres conserve their wavy appearance when extracted from the matrix but Kastelic *et al.* (1978) found that the zig-zag configuration is no longer kept when the fibres are isolated. An important aspect of the structural models is the understanding of the crosslinks that exist between different fibres and between the fibres and the matrix (Minns and Soden, 1973). The latter authors found that the ground substance has a significant role in the global mechanical properties of the tissue while Partington and Wood (1963) found that elastin (non collagenous fibre present in the ground substance) has a more significant contribution than that of the ground substance. According to Yannas (1972), the ground substance would have no effect. These crosslinks can take various forms such as covalent, ionic or hydrogen bonding and play a significant role in the mechanical properties.

IV.1.3 Integration of the nonlinear behaviour of ligament into structural models

According to the general ideas developed in literature (Rigby *et al.*, 1959), the wavy pattern of the collagen fibres is responsible for the nonlinear behaviour observed during a typical uniaxial tensile test. The toe region is a manifestation of the progressive recruitment of the collagen fibres (or *uncrimping*) that is accompanied by an increase in the overall stiffness of the ligament sample. This feature is often integrated into the structural models by considering that during the recruitment of the collagen fibres they have a small linear modulus of elasticity and that when they reach a certain length, their modulus then increases (Kwan and Woo, 1989; Soong and Huang, 1973) leading to the observed toe-region. In their study, Hurschler *et al.* (1997) used the microstructural hierarchy described by Kastelic *et al.* (1978) to build a mathematical model which reproduces the features of the collagen fibres which are aggregated collagen fibrils (structural scale) embedded in an hydrated proteoglycan matrix. The collagen fibres (structural scale) further aggregate to form fascicles and finally, ligaments or tendons. In addition to this structural considerations the authors used a probabilistic distribution to model the various states of crimp in the undeformed configuration. Some models incorporate microstructural and structural features at the same time (Ault and Hoffman, 1992b; Hurschler *et al.*, 1997). The later authors' include the nonlinear behaviour of ligaments, including toe-in, the linear region, damage and finally failure. The last two criteria are related to the stretch and are fibre and fibril based. The model was capable of representing the nonlinear toe-in and failure response of healing ligaments even if the constitutive law for the collagen fibres was assumed to be linear elastic. The microstructural (Frank *et al.*, 1991; Frank *et al.*, 1992) and structural models (Frank *et al.*, 1991; Frank *et al.*, 1992; Padgett and Dahners, 1992) of ligaments have been investigated in order to understand the differences in mechanical properties between immobilised (fixed for a period of time) and non-immobilised medial collateral ligaments. Review of this aspect of the mechanical properties of ligaments is out of the scope of the present study. However, fibril organisation is found to be superior in immobilised MCLs (Frank *et al.*, 1991; 1992) in early healing but non immobilised MCLs are generally found to have superior mechanical and structural properties (Woo *et al.*, 1987). There is a spatial variation in the crimp pattern as suggested by experimental observations (Noyes *et al.*, 1984). In fact, during failure tests on the bone-patellar tendon-bone units, local strains in the proximity of the bone-attachment sites were much larger than in the central region of the specimen. The physical properties of the crimp are also known to change systematically with development and age. With increasing age the wave length increases while the wave crimping angle decreases (Diamant *et al.*, 1972).

IV.1.4 Discussion concerning microstructural and structural models

Structural models are generally aimed at describing the gross mechanical behaviour of soft tissue (ligament or tendon) by considering structural and mechanical properties of the constituents of the tissue. Their main weakness is that they rely on assumed structural geometry (for example, the way the collagen fibres are organised inside the ground substance), consider basic loading conditions (uniaxial tension) and are only applicable to idealised geometry of tendons or ligaments. However, this kind of model should be seen as a complementary approach to phenomenological models. In fact, structural models allow for the appreciation of the contribution of the structural geometry of the ligament to the global stress-strain curve obtained during tensile tests. Therefore, they give a clue to the interpretation and the understanding of the macroscopic mechanical behaviour of ligaments. The particular features observed can then be included in the mathematical formulation of continuum based models. In addition to the assumption of a particular microstructural or structural geometry chosen for a structural formulation, the mechanical properties of the elemental constituents of the tissue need to be known. This is intimately linked to very delicate experimental processes that can go down to the molecular level (Sasaki and Odajima, 1996a). In structural models, in addition to the hypothesis concerning the structural properties, numerous assumptions usually need to be applied for the derivations of the equilibrium equations [state of stress, state of strain (uniformity, orientation)...]. Due to their structural hierarchy, structural models can easily become intractable and their implementation into a finite element code is very often the only way to solve the equilibrium equations when no reductive assumptions are made (idealised geometry and idealised loading conditions). Moreover, it is believed that, in the context of a macroscopic knee joint model, such a degree of structural hierarchy description is not necessary, difficult to integrate into a whole ligament model, and that phenomenological or continuum based models of soft tissue are more appropriate. Continuum based models, when coupled with the Finite Element Method, can cope more easily with spatial variations in the mechanical properties at the macroscopic level.

In Appendix A, Table A1 summarises the published structural and microstructural models of connective soft tissues encountered in literature.

IV.2 Phenomenological and continuum based models

The accuracy of phenomenological models used to represent the mechanical behaviour of the soft tissue (by identification with the experimental stress-strain curves) is dictated by several assumptions. The mechanical behaviour can be considered as elastic or viscoelastic and linear or nonlinear. Table A2 (Appendix A) presents some phenomenological models encountered in literature.

IV.2.1 Linear Elasticity

When the identification of the experimental stress-strain curve (uniaxial tensile test) is done with a linear elastic law, only the linear part of the stress-strain curve is considered. The toe region is therefore not taken into account and this is a serious limitation. Indeed, Fung (1981) believes that this region usually includes the physiological range of normal tissue function. The linear elastic models overestimate the modulus of elasticity in the toe region.

For sake of illustration, Table IV.1 presents some values reported in literature regarding the mechanical properties of various knee ligaments. The large variabiliy of the values reported can be explained by the experimental protocols which affect significantly the results and it is well known that ligaments are of tissues very sensitive to the age of donors from which the specimens are extracted (Hollis *et al.*, 1988; Noyes and Grood, 1976). Figure IV.1 illustrates results from a typical tensile test performed on bone-fascicle-bone units of several ligaments (Butler *et al.*, 1986).

Authors	Human Tissues	E_T (MPa)	σ_C (MPa)	ε_C (%)	F_C (N)
(Hollis *et al.*, 1988) (Noyes and Grood, 1976)	**ACL**				1725 ± 269
(Trent *et al.*, 1976)	**PCL**				739 ± 368
(Kennedy *et al.*, 1976)	**PCL**			24.2 ± 6.3	1051 ± 237
	MCL				467.46 ±33.32
(Marinozzi *et al.*, 1983)	**PCL**			20 ± 5	855 ± 225
(Prietto *et al.*, 1988)	**PCL**	109 ± 50	26.8 ± 9.1	28.5 ± 9.1	1627 ± 491
(Butler *et al.*, 1986)	**ACL, PCL, LCL** fascicle-bone units	345 ± 22.4	36.4 ± 2.5	15.0 ± 0.8	
	PT	643.1 ± 53.0	68.5 ± 6.0	13.5 ± 0.7	
(Butler *et al.*, 1992)	**ACL** (AMB)	283.1 ± 114.4	45.7 ± 19.5	19.1 ± 2.8	
	ACL (ALB)	285.9 ±140.6	30.6 ± 11.0	16.1 ± 3.9	
	ACL (PB)	154.9 ± 119.5	15.4 ± 9.5	15.2 ± 5.2	
(Race and Amis, 1994)	**PCL** (ALB)	248 ± 119	35.9 ± 15.2	18.0 ± 5.3	258 ± 83
	PCL (PMB)	145 ± 69	24.4 ± 10.0	19.5 ± 5.4	1620 ± 500
(Quapp and Weiss, 1998)	**MCL** (long. test)	332.15 ± 58.27	38.56 ± 4.76	17.11 ± 1.53	
	MCL (trans. test)	11.02 ± 3.57	1.69 ± 0.53	11.7 ± 0.93	

Table IV.1 – Sample of the mechanical properties for various knee ligaments reported in literature .*AMB*: Anteromedial Band; *ALB*: Anterolateral Band; *PB*: Posterior Band; *PMB*: Posteromedial Band ; *PT*: Patellar Tendon. E: Young's modulus; σ_C : ultimate stress; ε_C : ultimate strain; F_C : tensile strength.

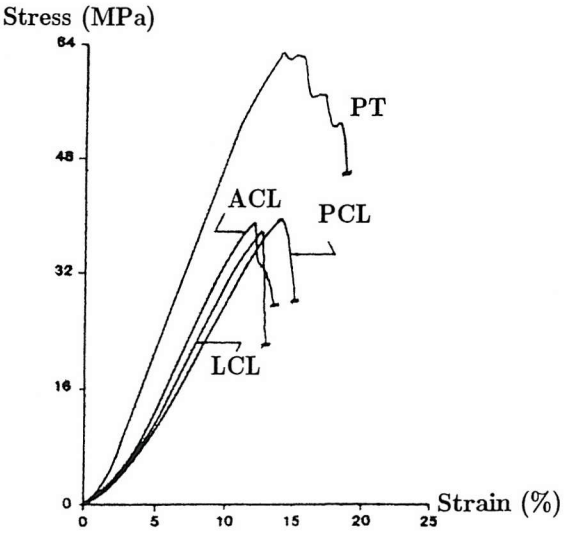

Figure IV.1 – Stress-strain curves obtained for for bone-fascicle-bone units of human knee ligaments tested in uniaxial tension until failure. From Butler *et al.* (1986). For sake of clarity the portion sof the curves beyond maximum stress are not shown.

IV.2.2 Nonlinear Elasticity

In the context of nonlinear elasticity, the elastic modulus is not longer a unique scalar but is a function of the strain. A general approach successfully used by various authors (Demiray, 1972; Fung, 1967; Haut and Little, 1972; Jenkins and Little, 1974; Veronda and Westmann, 1970) consists in postulating the existence of an elastic potential (usually taken as the strain energy function) which depends on the three strain invariants of the strain tensor. When the material is assumed to be incompressible, the third invariant is not integrated into the potential. Once the form of the elastic potential is chosen, a process of identification is performed between the parameters of the coefficients of the strain energy function and the characteristics of the experimental stress-strain tensile curve. The authors cited above made the assumption that the material possessed an isotropic symmetry and this is not true as tendons or ligaments have a preferred direction dictated by the orientation of the collagen fibres. These tissues are primarily orientated to resist tensile loads. Veronda and Westmann (1970) proposed the following form for the strain energy function:

$$\Psi = \alpha\, e^{\beta(I_1-3)} - \frac{\alpha\beta}{2}\left(I_2 - 3\right) + g\left(I_3\right) \qquad \text{[IV.1]}$$

C_1, C_2, β are material parameters, I_1, I_2 and I_3 are the first three invariants of the Cauchy-Green deformation tensor, and g is a function which characterizes the degree of incompressibility (g is null when the material is fully incompressible, i.e. $I_3 = 1$).

If the dependence on the second invariant is removed, the potential reduces to that of a neo-Hookean material, similar to that proposed by Demiray (1972):

$$\Psi = \frac{\alpha}{2\beta}\left(e^{\beta(I_1-3)} - 1\right) \qquad \text{[IV.2]}$$

The form chosen showed a good agreement with the experimental curve.

Using the strain energy function presented by Valanis and Landel (1967), Blatz *et al.* (1969) presented the following elastic potential Ψ:

$$\Psi\left(\ln\lambda_i\right) = C\left(\lambda_i^{\alpha} - 1\right) \qquad \text{[IV.3]}$$

where λ_i represents the principal stretch in the i-th principal direction. The authors applied this function to the mechanical behaviour of the rabbit's mesentery and rubber.

For further expressions see Fung (1981). Fung (1973) modelled the mechanical behaviour of soft tissue by assuming a linear form for the modulus of elasticity. In this case the stress-strain relation is given by an exponential law.

Weiss (1994) developed an incompressible transversely isotropic hyperelastic model for the characterization of the mechanical behaviour of soft connective tissues. It is worth noting that this model was fully three-dimensional and was implemented into an implicit finite element code. In addition to the three classic strain invariants, a fourth strain invariant was introduced in order to capture the dependence of the fibre direction on the strain energy function (Spencer, 1992).

IV.2.3 Viscoelasticity

Viscoelasticity is an important feature of ligaments that is clearly exhibited during cyclic testing (hysteresis loop appearing on the classic tensile stress-strain curve). The stress-relaxation phenomenon is another significant aspect of the mechanical properties of soft tissues (Johnson *et al.*, 1994). Therefore, the rheological behaviour of soft tissue is more accurately described by the form of the stress-strain-time relationships when the loading rates justify it. During mechanical testing of the specimen considered, the preconditioning of the sample is fundamental in order to achieve a reproducible pattern of loading (Rigby *et al.*, 1959). The quasi-linear viscoelastic (QLV) theory developed by Fung (1981) has been largely used in the study of soft tissues and more especially for tendons and ligaments (Woo *et al.*, 1981; Woo *et al.*, 1982). The basic idea of the QLV is to assume that the stress at a fixed time can be represented by a convolution integral, separating the elastic response and the relaxation function. Moreover this latest function is supposed to have a continuous spectrum. This theory can represent accurately the long term memory effects (determined by stress relaxation or creep tests) but is unable to account for short term memory effects (related to the strain rate dependence on strain). Pioletti and co-workers (1997, 1998a) developed a general theoretical framework to encompass short term and long term memory effects in order to describe the mechanical behaviour of ligaments and tendons. The material parameters were identified with experimental coefficients and a very good agreement was found between the theoretical and experimental tests. This theory can easily accommodate small or high strain rates to predict the mechanical response of the tissue. The study of the influence of the strain rate on the stress-strain relations showed a general trend for an increase in stress with a corresponding increasing in the strain rate (Haut and Little, 1972).

Johnson *et al.* (1996) proposed a constitutive model of soft tissue which can be applied to ligaments and tendons in a full three-dimensional and finite deformation context. It is based on a nonlinear viscoelastic integral representation. By linearisation, this constitutive law reduces to classic viscoelasticity and the QLV can be recovered with few assumptions. Material parameters were fitted from experimental curves of uniaxial tests for human patellar tendons and curve fit to the QLV model previously tested for canine medial collateral ligaments (Woo *et al.*, 1981). The fading memory effects (this concept is based on the fact that events in the recent past have more influence on the current state of stress than those of the more distant past) were incorporated into the model.

IV.3 Mathematical and geometrical models

At this stage of this review, it is necessary to bring some clarification to avoid unnecessary confusion regarding the terms "mathematical and geometrical models". This paragraph encompasses models describing the ligaments, generally integrated in a whole knee joint model, as a collection of linear or nonlinear springs and/or dashpots. A ligament can be represented by a set of several springs or dashpots representing a fibre bundle. These analytical models can be dynamic or quasi-static but generally include basic mechanical properties under the form of a one-dimensional stress-strain relation and simplified geometry for ligaments and bony structures. Numerous authors have developed mathematical models of the knee and ligaments (Abdel-Rahman and Hefzy, 1998; Andriacchi *et al.*, 1983; Blankevoort and Huiskes, 1991b; Imran and O'Connor, 1997; Loch *et al.*, 1992; Martelli *et al.*, 1998; Shelburne and Pandy, 1997; Toutoungi *et al.*, 1997) and a complete literature review of these biomechanical studies is beyond the scope of the present work. For the region of the strain-stress curve corresponding to the uncrimping of the collagen fibres (the strain is supposed to be bounded superiorly by a transitional strain ε_0) the stress is generally chosen as a quadratic function of the strain and as a linear function of the strain when the strain goes over ε_0 (Toutoungi *et al.*, 1997). A similar class of models describe the knee ligaments by a system of geometrical components [inextensible strings (isometric fibres), bar linkage] (Chan and Seedhom, 1995; O'Connor and Zavatsky, 1993). The resultant equations encountered in both types of models can be solved numerically but, according to our own nomenclature, this type of model is not categorised as "numerical". Generally, these models intend to obtain information regarding the forces (intensity, line of action) developed in a knee joint in order to have a better understanding of the constraint interactions that occur.

Given the complexity of the knee joint, *in-vivo* and *in-vitro* experimental measurements are a delicate process and mathematical models can therefore bring an interesting approach to give a first estimate of various mechanical and geometrical quantities. The aim of these models is also to study the influence of the position and the stiffness of ligaments on the kinematics of the joint.

IV.4 Finite Element models

This class of models refer to continuum mechanics based models whose the resultant equations (static or dynamic) are solved by the ***Finite Element Method*** (FEM).

IV.4.1 The Finite Element Method

Basically, the FEM consists in decomposing a (possibly very complex) continuous mechanical problem into a set of simpler discrete problems by defining a finite number of state variables. In case of a static problem the discretisation (process of decomposing a domain into several simplier ones) is applied to the geometry of the body which can be one-, bi- or three-dimensional. For dynamic problems the time domain is introduced as an additional region of interest that undergoes a discretisation and is associated with dynamical quantities such as velocities, accelerations and inertial forces. The space domain is decomposed into elemental subdomains (finite elements) which have an assumed simple geometry. The elements are connected to each other at points called *nodes*. Over each element, it is assumed that the functions appearing in the equations describing the phenomenon (in mechanics, these equations are the equilibrium equations), vary in a specific manner. These approximation functions are derived using the basic idea that any continuous function can be represented by a linear combination of algebraic polynomials. The algebraic relations among the undetermined coefficients (nodal values) are obtaining by satisfying the governing equations for each element. The approximation functions are often taken to be algebraic polynomials, and the undetermined parameters represent the values of the solution at a finite number of preselected points, the nodes, on the boundary and within the interior of the element. A set of algebraic equations is obtained for each element and the finite element technique requires that these sets be combined (this process is called *assembly of the system*) into a single set of equations which describe completely the governing equations of the whole discretised system. These equations, especially in the context of the modelling of soft tissues, are often nonlinear.

Solving these algebraic equations will determine the values of all the state variables at equilibrium and therefore achieve the resolution of the initial complex continuous problem. The displacements of each element are found, from which strain values are derived. The stresses are computed thanks to the material constitutive equations that relate them to strains. The FEM has several significant advantages with respect to the other numerical methods. It allows the description of problems with complex geometry and complex boundary conditions. The technique is able to accommodate heterogeneous materials and arbitrary complex constitutive laws. It is not hard to realise why this method has been so commonplace in the field of biomechanics. Biological structures and tissues are the perfect candidates to give a " raison d'être " to the FEM.

IV.4.2 Finite Element models of ligaments

Despite the fact that the FEM has been extensively used in the field of bone mechanics and related problems, such as arthroplasty and surgical prosthesis design, ligaments have received less attention regarding the implementation of their material behaviour into finite element codes. This lack of attention is partly due to the fact that load transmission in the joint operates through the bony structures and the articular cartilage and therefore the state of stress in these regions is of particular relevance (Schreppers *et al.*, 1990). This is also due to the difficulty to extract material data from experimental testing. Indeed, the mechanical behaviour of soft tissues is far from fully understood and due to the variety of components (chemical composition and structure) and their interaction between each other, an accurate constitutive representation is difficult to obtain. The FEM is very promising in this matter as it allows to study stress distribution in ligaments for arbitrarily complex geometries but the existing models should be assessed in all simulated physiological conditions to check their validity. A literature survey showed that few authors have developed and implemented suitable constitutive laws for the knee ligaments within three-dimensional finite element models. Pioletti, (1997, 1998a) developed a full thermodynamic formulation of a constitutive law, based on an incompressible isotropic hyperelastic formulation, for the ACL and derived material data from experiments and implemented it into a commercial finite element code. Weiss (1994) and Weiss *et al.* (1996) developed a general finite element framework for soft tissue modelling. Weiss formulated an incompressible transversely isotropic hyperelastic constitutive law and performed a parametric analysis to derive the material constants from experiments performed on fascia lata tendons.

Further experiments were later done in order to extract mechanical properties of human medial collateral ligaments (Quapp and Weiss, 1998) for identification with the hyperelastic potential proposed by Weiss (1994). The formulation used captures the key-features of soft tissues (uncrimping, large deformations and rotations, incompressible behaviour, preferred fibre direction accounting for the orthotropy of the material). The time dependence of the mechanical properties of soft tissue was further incorporated into a transversely isotropic hyperviscoelastic finite element model (Puso and Weiss, 1998). Hirokawa and Tsuruno (1997) developed a finite element model of the ACL in order to analyse the stress distribution and changes in shapes at the surface of the ACL when subjected to physiological kinematic conditions. This bi-dimensional mechanical model (the geometry of the ACL is idealised) is based on the Theory of Membranes made of a hyperelastic Mooney-Rivlin material and assumes that the material is incompressible. This latter assumption is often made in the context of soft tissue modelling because it allows the calculation of out-of-plane deformations which are extremely difficult to measure experimentally. Moreover, it simplifies the identification process established in the context of homogeneous deformations. The hypothesis of incompressibility is largely justified by the fact that soft tissues have a high water content. However, it has been shown that tissue volume may change with deformation due to the exudation of water (Thielke *et al.*, 1995). The incompressibility constraint leads to numerical difficulties in the context of finite element analyses and this aspect will be discussed in detail in section VI.1. Simbeya *et al.* (1996) performed a parameter sensitivity analysis on a bi-dimensional FE model of the rabbit medial collateral ligament and showed that, indeed, the experimental conditions and alignment of specimen are an important factor for the stress distribution. The ligament was modelled as a composite material where cable elements (supporting only tension) were embedded between isotropic homogeneous quadrilateral elements. This micromechanical formulation was first described by Simbeya *et al.* (1992) who implemented it into a FE model and was the basis of other models such as the one of Wilson *et al.* (1996) who studied the stress distribution within a three-dimensional FE model of rabbit medial collateral ligament. This model was validated against experimental data. The mechanical formulation includes the main features of ligaments: water, matrix and fibres. The interfibrillar matrix was modelled using 8-noded-hexahedral solid elements, collagen fibres were represented by nonlinear spring elements and the water content of the tissue was incorpoorated by means of poroelastic solid elements. A good fitting of the FE model with the experimental data was possible and the numerical model reproduced closely enough the mechanical characteristics of ligaments under simulated tests.

A similar model was used by Grassmann *et al.* (1998) to simulate a lapine MCL reconstruction with the semitendinosus tendon as graft tissue. Recently, Daniel (1999) developed and implemented a three-dimensional orthotropic viscoelastic finite element model of a human ligament. This composite approach considers the ligament as made of elastic fibres embedded in an elastic matrix undergoing finite strain deformation. Under 2% of strain the fibre modulus increases exponentially from zero with an invariant that provides a measure of the stretch in the fibre direction. After 2% of strain the modulus of fibres is made constant. The strain rate dependence is included in the constitutive behaviour. The coding of the material was performed in an explicit finite element code. More recently, Hirokawa and Tsuruno (2000) proposed a structurally-based phenomenological model that encompasses the full three-dimensional and finite strain regimes. The model was implemented into an implicit finite element code and used to simulate the mechanical behaviour of the ACL during a passive flexion of the knee and a drawer test. This model, defined by means of a strain energy function, assumes that the ACL is a composite reinforced by two families of collagen fibres. Instead of identifying the constitutive law with experimental tensile tests on the ACL, the authors have mixed structural considerations to the phenomenological approach. In fact, they considered the tensile properties of collagen fibres and the elastic properties of the ground substance to define the hyperelastic strain energy function. The study of Hirokawa and Tsuruno (2000) was the first published attempt to develop a continuum anisotropic constitutive law for the ACL.

In the context of the present research project, a preliminary study was performed to investigate the influence of the initial stress field present in the ACL (at full extension) on the stress distribution during a simulated passive knee flexion (see Appendix D). The model proposed by Pioletti (1997) was implemented into the commercial FE code ABAQUS Standard 5.8 (® Hibbit, Karlsson & Sorensen Inc., Pawtucket, RI, USA) using a customised internal subroutine (UMAT). This study was used to highlight essential results concerning the formulation of an isotropic hyperelastic model. It has appeared that the model performs badly when the ligament is loaded in compression or flexion. In fact, the calculated resultant force within the ACL was in disagreement with experimental data for passive neutral knee flexions (Roberts *et al.*, 1994; Wascher *et al.*, 1993) as soon as the ligament undergoes compression or flexion in the direction of its orientated fibres. This severe restriction was not mentioned by Pioletti (1997) and Pioletti *et al.* (1998a, 1998b) and this has called in to question the validity of an isotropic hyperelastic model of ligament for representing the physiological mechanical behaviour of ligaments.

Commercial FE codes offer only continuum isotropic hyperelastic materials. Ligaments have a preferred mechanical direction that corresponds roughly to the orientation of the collagen fibres. The mechanical behaviour of connective soft tissue is largely conditioned by their anisotropic properties. For this reason, isotropic models of ligaments exclude such key features. Moreover, collagen fibres do not support a significant compressive load along their longitudinal direction and structures that are composed of mostly collagen are prone to buckle under very small compressive forces. This specific characteristic can be integrated when formulating a particular constitutive law. For example, when compressive stresses appear in the fibre direction within the soft tissue, no mechanical contribution of the collagen fibres is provided to the strain energy density.

With regards to the advantages offered by continuum anisotropic hyperelastic model of ligaments over isotropic hyperelastic models which exhibit severe physical limitations, it appears fundamental to represent ligaments as anisotropic structures. Continuum mechanics of fibre-reinforced composites (Spencer, 1992) is a promising theoretical tool that can describe accurately and account for the fundamental mechanical features of soft connective tissues. Theoretical soft tissue mechanics is a branch of continuum mechanics that still provides numerous opportunities for research developments.

Chapter V

Constitutive modelling of biological connective soft tissues. A general theoretical framework for strongly anisotropic fibre-reinforced composites at finite strain.

Equation Section 5

In this chapter, a general theoretical framework for the constitutive modelling of biological soft connective tissues is developed. The approach is based on the theory of *continuum* fibre-reinforced composites at finite strain. Biological soft connective tissues are assumed to be made of an isotropic hyperelastic matrix reinforced by up to two families of fibres acting in the finite strain regime. Expressions of the stress tensors in the material and spatial configurations are established *in the general case*, without precluding any assumption regarding possible kinematics constraints or any particular mechanical symmetry of the material. Original expressions of the elasticity tensors in the material and spatial configurations are derived and new coupling terms, characterising the interactions between the constituents of the continuum composite material, are isolated and their biological significance is highlighted. This constitutes one of the important scientific contributions of the present research work to nonlinear elasticity. Conditions of existence of the hyperelastic potential and constitutive requirements are briefly discussed. To illustrate the theoretical developments on the constitutive modelling of soft connective tissues, a particular strain energy function is described. Later on, this strain energy function and the associated constitutive equations will be the object of a finite element implementation as detailed in the next chapter. Finally, the mechanical formulation of the constitutive equations is discussed with regards to its relevance and applicability.

V.1 Structure of Chapter V

The next section details the physiological and structural motivations behind the use of a continuum theory of fibre-reinforced composites at finite strain to model the mechanical behaviour of biological soft connective tissues. Objectives of the Chapter V are presented in the third section. The fourth section summarises the essential results of continuum mechanics with regards to the kinematics of a solid body at finite strain, material frame indifference and the characterisation of material symmetry groups. The fifth section presents the theorems and definitions relative to a continuum theory of fibre–reinforced composites. Invariants of the right Cauchy-Green deformation tensor and structural tensors agencies are defined in order to postulate the existence of a strain energy function from which stress and elasticity tensors are derived. The expressions of these tensors are established in the material and spatial descriptions for an isotropic material reinforced by two families of fibres, i.e. a strongly anisotropic material. In section V.6, these results will serve as a basis to particularise expressions for special classes of material symmetries: *orthotropy*, *local orthotropy*, *transversely isotropy* and *isotropy*. In the seventh section, kinematics constraints are briefly discussed and also constitutive inequalities in section V.8. The ninth section provides an example of a strain energy function likely to represent the mechanical behaviour of biological connective soft tissues whereas section V.10 ends with concluding remarks.

V.2 Physiological and structural motivations

Ligaments and tendons are dense connective tissues consisting primarily of parallel-fibred collagenous tissues embedded in a highly compliant solid matrix. The arrangement of the collagen fibres dictates the directional mechanical properties of tendons or ligaments and is suited to the particular mechanical function of each of these connective tissues. Tendons are subjected to high unidirectional tensile loads and therefore their (large) collagen fibres are aligned in an orderly parallel arrangement. Ligaments are mainly subjected to uniaxial tensile loads but can also undergo mechanical actions in other non-preferred directions and more complex loading conditions (shear at the insertion sites, contact interactions with bony structures). In consequence, and according to their physiological role, their fibres are not necessarily completely parallel but can form a complex network of interlaced fibres leading to strongly anisotropic mechanical properties (Amiel *et al.*, 1984; Kennedy *et al.*, 1976).

The collateral ligaments of the knee are made of collagen fibres mostly parallel whereas the cruciate ligaments are composed of more interwoven fibres. The fibrous architecture and properties are also dependent on the specific location within a ligament or a tendon, namely when one looks at the insertion into bone (Woo *et al.*, 1988).
Ligaments display time- and history-dependent viscoelastic properties that reflect the complex interactions between the mechanical properties of the collagen, the surrounding proteins and the ground substance. However, the inclusion of such features in a constitutive law are only relevant when the tissue is submitted to strain rates greater than those in a quasi-static state.

In summary, due to their structural properties ligaments can be considered as composite materials where one or several families of fibres, namely collagen fibres, are embedded in a highly compliant solid matrix (i.e. the ground substance made of proteoglycans, water, collagen and glycoproteins). As mentioned previously, the structural arrangement of the collagen fibres characterise the macroscopic mechanical and directional properties of ligaments. Anisotropic mechanical properties arise directly from the presence of the collagen fibres and their orientation.

The simplest case of anisotropic material is represented by an isotropic solid matrix containing one family of fibres possessing a single preferred principal direction (at least, locally). This represents *transversely isotropic* symmetry. This formulation is suitable to describe the constitutive behaviour of tendons and ligaments possessing mostly parallel collagen fibres. Weiss *et al.* (1996) successfully used this approach to describe and simulate the behaviour of fascia lata tendons and the medial collateral ligament. However, when the soft connective tissue considered is made with branching and interwoven collagen fibres (like the cruciate ligaments) that give rise to strongly anisotropic mechanical properties, it can prove relevant to consider two distinct families of fibres (Hirokawa and Tsuruno, 2000). However, this approach is limited by the lack of relevant experimental data. When two distinct families of fibres are arranged in a way such that their principal directions are mutually orthogonal, the material is said to be *orthotropic*.

V.3 Objectives of Chapter V

- *The first objective* of this chapter is to describe a general theoretical framework suitable for the constitutive modeling of biological soft connective tissues such as ligaments and tendons and presenting it in the most self-contained format as possible.

This is achieved by looking at the necessary definitions, theorems and constitutive requirements used in the formulation of an objective constitutive law. The approach adopted here is based on the seminal work of Spencer (1992) who developed a continuum theory for fibre-reinforced composites. The basic idea is to provide a global description of the composite structure at the continuum level by postulating the existence of a strain energy function dependent on strain invariants and structural tensors from which the stress and elasticity tensors are derived. This approach has been successfully used by various authors, namely Hirokawa and Tsuruno (2000), Weiss *et al.* (1996) for finite element modelling of ligaments and tendons, by Holzapfel *et al.* (1996), Humphrey (1990a, 1990b), Humphrey and Yin (1987) for finite element modeling of cardiac tissue mechanics and by Klisch and Lotz (1999) in an experimental and analytical model of the annulus fibrosus.

- *The second objective* of our research is to extend the developments of Spencer (1992) by providing entirely new explicit expressions for the elasticity tensors in the spatial and material descriptions in the most general case, that is, when no assumption is made regarding the particular orientation of any of the two families of fibres or regarding any simplifying kinematics hypothesis such as incompressibility or inextensibility.

To the best of our knowledge, this aspect is missing in the relevant literature. The full generality attached to the terms of the elasticity tensor can be helpful in exploring and incorporating into the constitutive formulation complex interactions between the components of the fibre-reinforced composite material that can be missed otherwise. Moreover, elasticity tensors are essential in investigating mathematical properties of the constitutive laws and are a prerequisite in any incremental type nonlinear finite element method.

V.4 Basic results in continuum mechanics

Before developing the constitutive model the basic notations and results relevant to the formulation of anisotropic hyperelasticity are given below. For further details please refer to Ogden (1984), Mardsen and Hughes (1994) and Spencer (1992).

V.4.1 Kinematics

Let B be a continum body which is a set of points, referred to as particles. Let us assume that there exists a one-to-one-mapping, called a *configuration* of B, $\chi : \mathsf{B} \rightarrow \mathscr{E} = \Re^3$, twice continuously differentiable (as its inverse χ^{-1}) which puts into correspondence B with some region, referred as $\mathscr{B}$, of the Euclidean point space $\mathscr{E} = \Re^3$. The *reference configuration* denoted by $\chi_o : \mathsf{B} \rightarrow \mathscr{E} = \Re^3$ is assumed to be given. Let be: $\mathscr{B}_0 = \chi_0(\mathsf{B}) \subset \Re^3$ and $\mathscr{B} = \chi(\mathsf{B}) \subset \Re^3$, respectively the *reference* and *current* positions of B. A point P of B is labeled $\mathbf{X} = \chi_0(\mathsf{B})$ in $\mathscr{B}_0$ and $\mathbf{x} = \chi(\mathsf{B})$ in $\mathscr{B}$. Let $\partial\mathscr{B}_0$ be the boundary of $\mathscr{B}_0$. Lets make the assumption that $\partial\mathscr{B}_0 = \overline{\partial_\varphi\mathscr{B}_0 \cup \partial_t\mathscr{B}_0}$ and $\partial_\varphi\mathscr{B}_0 \cap \partial_t\mathscr{B}_0 = \varnothing$, where $\partial_\varphi\mathscr{B}_0$ is the part of $\partial\mathscr{B}_0$ where configuration χ_0 is assumed prescribed as $\varphi\big|_{\partial_\varphi\mathscr{B}_0} = \bar{\mathbf{g}}$ and $\partial_t\mathscr{B}_0$ is the part of $\partial\mathscr{B}_0$ where the traction vector is prescribed as $\mathbf{PN} = \mathbf{t}$. In the above, $\mathbf{P}$ is the first Piola-Kirchhoff stress tensor and $\mathbf{N}$ is the outward normal field perpendicular to the boundary of the body in the reference configuration. The one-to-one mapping $\varphi = \chi_0\chi^{-1} \subset \Re^3$ is the deformation from $\mathscr{B}_0$ to $\mathscr{B}$ (Figure V.1). Upon deformation, the material point $\mathrm{P}(\mathbf{X})$ is mapped into a spatial position $\mathrm{P}'(\mathbf{x})$ by means of φ:

$$\mathbf{x} = \varphi(\mathbf{X}) = \mathbf{X} + \mathbf{u}(\mathbf{X}) \qquad [V.1]$$

$\mathbf{u}$ is the displacement field and $\varphi \in \mathscr{U}$, $\mathscr{U}$ being the space of admissible motions defined as:

$$\mathscr{U} := \left\{ \varphi : \mathscr{B} \rightarrow \Re^3 \,/\, \varphi = \bar{\mathbf{g}} \text{ on } \partial\mathscr{B}_0 \right\} \qquad [V.2]$$

The deformation gradient $\mathbf{F}$ is the derivative of the deformation, using the notation:

$$\mathbf{F}(\mathbf{X}) = \frac{d\mathbf{x}}{d\mathbf{X}} = \mathbf{D}_\varphi = \frac{\partial\varphi}{\partial\mathbf{X}} = \sum_{i,I=1}^{3} \frac{\partial\varphi_i}{\partial \mathrm{X}_I}\mathbf{e}_i \otimes \mathbf{E}_I \qquad [V.3]$$

where "⊗" denotes the *outer tensor product*. $\{\mathbf{E}_I\}_{I=1,2,3}$ and $\{\mathbf{e}_i\}_{i=1,2,3}$ are fixed orthonormal bases in $\mathscr{B}_0$ and $\mathscr{B}$ respectively. These bases are assumed to be coincident with the standard bases in $\Re^3$. However, for sake of clarity, the notation has been kept different between both bases.

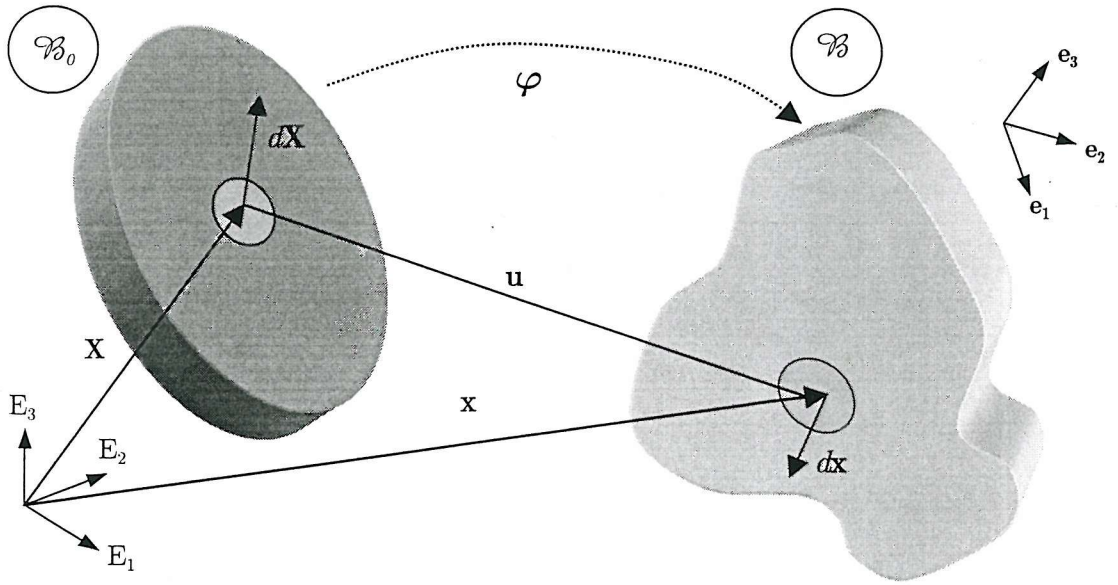

Figure V.1 - Deformation mapping between reference and current configuration. Upon the deformation φ , the point P is mapped into $P'(\mathbf{x})$ and the ratio of any infinitesimal variation around their respective positions is represented by the deformation gradient $\mathbf{F}$ according to the following expression : $\mathbf{F}(\mathbf{X}) = d\mathbf{x} / d\mathbf{X}$.

The uppercase and lowercase letters used in indicial notation refer to the reference and the deformed (current) configuration respectively. For further developments, we also define " . " and " : ", respectively as the *scalar product* or *contracted tensor product* and the *inner tensor product* or *double contracted tensor product*. The local condition of impenetrability of matter requires that $J(\mathbf{X}) = det[\mathbf{F}(\mathbf{X})] = \rho(\mathbf{x}) / \rho_0(\mathbf{X}) > 0$ where " *det* "represents the determinant of the linear transformation [**F**] and, ρ_0 and ρ, are the density of the material, respectively in the reference and deformed configurations. Following standard usage, one denotes $\mathcal{L}$ ($\Re^3$,$\Re^3$) the vector space of linear transformations in $\Re^3$. Then $\mathcal{L}^+$ is defined as:

$$\mathcal{L}^+ := \left\{ \mathbf{F} \in \mathcal{L}(\Re^3,\Re^3) / \; det(\mathbf{F}) > 0 \right\} \qquad [V.4]$$

For fixed $\mathbf{X} \in \mathcal{B}_0$, $\mathbf{D}_\varphi(\mathbf{X}) \subset \mathcal{L}^+$, one also defines $\mathcal{S}^+$ and $\mathcal{O}^+$:

$$\mathcal{S}^+ := \left\{ \mathbf{T} \in \mathcal{L}^+ / \; \mathbf{T}^T = \mathbf{T} \right\} \qquad [V.5]$$

$$\mathcal{O}^+ := \left\{ \mathbf{T} \in \mathcal{L}^+ / \; \mathbf{T}^T.\mathbf{T} = \mathbf{1} \right\}, \qquad [V.6]$$

where the superscript " T " denotes the transpose of the linear transformation, and **1** is the second-order identity tensor.

The right and left Cauchy-Green deformation tensors are respectively defined as:

$$\mathbf{C} = \mathbf{F}^{\mathrm{T}}.\mathbf{F} \text{ and } \mathbf{b} = \mathbf{F}.\mathbf{F}^{\mathrm{T}} \qquad [V.7]$$

C and **b**, respectively *material* and *spatial* quantities, possess the same eigenvalues. Under conditions of regularity for **C** and **b**, **U** and **V**, the right and left stretch tensors, can be defined as unique, symmetric, positive-definite square roots of **C** and **b**, respectively. From the *Polar Decomposition Theorem* (Mardsen and Hughes, 1994), if φ is regular enough, it can be stated that: for each $\mathbf{X} \in \mathcal{B}_0$ there exists an orthogonal transformation $\mathbf{R}(\mathbf{X})$: $\mathcal{C}^+ \rightarrow \Re^3$ such that:

$$\mathbf{F} = \mathbf{R}.\mathbf{U} = \mathbf{V}.\mathbf{R} \qquad [V.8]$$

Each of these decompositions is unique. The deformation gradient includes the effects of both stretching and rotation. It is relevant to note that **U** and **V** operate on different spaces.

V.4.2 Finite elasticity

Materials for which the constitutive behaviour depends only on the current state of deformation are called *elastic* (Ogden, 1984). The current state of deformation at a particle **X** being fully defined by the deformation gradient **F** associated with this particle and the fact that the first Piola-Kirchhoff stress tensor **P** is the conjugate of $\dot{\mathbf{F}}$ (where an overdotted symbol means its material derivative with respect to the time), allows to define *elasticity* in the simple following form:

$$\mathbf{P} = \mathbf{P}[\mathbf{X},\mathbf{F}(\mathbf{X})] \qquad [V.9]$$

Hyperelasticity extends this definition by requiring that the work done by the stresses during a deformation process be path-independent. As a consequence of the path-independent behaviour and the fact that **P** is work conjugate with the rate of deformation gradient $\dot{\mathbf{F}}$, a *stored strain energy function* or *elastic potential per unit undeformed volume* W, $W : \mathcal{B}_0 \times \mathcal{L}^+ \rightarrow \Re$, can be established as the work done by the stresses from the initial to the current position (time t_0 to time t). This stored strain energy function is only a function of the initial position of the particle and the local deformation gradient, that is $W = W(\mathbf{X},\mathbf{F}(\mathbf{X}))$. In the case of a non dissipative process (which corresponds to the hypothesis of the present developments), W correspond to a *Helmholtz free energy of deformation function* $\bar{\Psi}$. The work defined above is expressed as:

$$[\mathbf{X},\mathbf{F}(\mathbf{X})] = \bar{\Psi}[\mathbf{X},\mathbf{F}(\mathbf{X})] = \int_{t_0}^{t} \mathbf{P}[(\mathbf{X},\mathbf{F}(\mathbf{X})] : \dot{\mathbf{F}}\,\mathrm{d}t \qquad [V.10]$$

which implies:

$$\dot{\bar{\Psi}} = \mathbf{P} : \dot{\mathbf{F}} \qquad [V.11]$$

In the subsequent developments *strain energy function*, *free energy function*, *reduced stored energy function* will be employed as synonyms. The rate of change of the potential $\bar{\Psi}$ can be expressed as:

$$\dot{\bar{\Psi}} = \sum_{i,I=1}^{3} \frac{\partial \bar{\Psi}}{\partial F_{iI}} \dot{F}_{iI} \qquad [V.12]$$

To define an objective constitutive law, $\bar{\Psi}$ must satisfy the *Principle of Objectivity* or *Material Frame Indifference* (Mardsen and Hughes, 1994). The *Principle of Objectivity* states that if we view the same configuration from a rotated point of view, then the stress transforms by the same rotation. In mathematical terms this condition is expressed as follows:

$$\bar{\Psi}(\mathbf{X}, \mathbf{F}) = \bar{\Psi}(\mathbf{X}, \mathbf{Q}.\mathbf{F}) \;\; \forall \; (\mathbf{F}, \mathbf{Q}) \in \mathcal{L}^{+} \times \mathcal{O}^{+} \qquad [V.13]$$

This means that the dependence of constitutive relations on $\mathbf{F}$ must only come through the part of $\mathbf{F}$ causing stretching, that is $\mathbf{U}$. Thus, frame indifference is equivalent to the assertion that $\bar{\Psi}$ depends on $\mathbf{F}$ trough $\mathbf{C}$. In summary, it exists a function $\Psi : \mathcal{B}_0 \times \mathcal{S}^{+} \rightarrow \Re$ such that:

$$\bar{\Psi}(\mathbf{X}, \mathbf{F}) = \Psi(\mathbf{X}, \mathbf{F}^{\mathrm{T}}.\mathbf{F}) \equiv \Psi(\mathbf{X}, \mathbf{C}) \;\; \forall \; \mathbf{C} \in \mathcal{S}^{+} \qquad [V.14]$$

V.4.3 Material symmetry

Extensive work has been done on the subject of material symmetry (Cohen and Wang, 1987; Coleman and Noll, 1964; Ericksen, 1978, 1979; Ericksen and Rivlin, 1954; Negahban and Wineman, 1989a, 1989b; Wineman and Pipkin, 1964; Zheng and Boehler, 1994). Before going further it is relevant to refer to an important principle, namely the *Neumann's Principle* (Hahn, 1987), which states that:

The symmetry group of a given material must be included in the symmetry group of any tensor function in any constitutive laws of the material.

Boehler (1978) demonstrated that any scalar-, vector-, and second-order tensor-valued functions of vectors and second-order tensors relative to any anisotropy characterised in terms of vectors and second-order tensors can be expressed as an isotropic function of the original tensor agencies and the structural tensors as additional agencies.

This means that the strain energy function of an anisotropic material can be expressed as an isotropic function of its classical three principal strain invariants (as in the isotropic case) plus invariants relating the right Cauchy-Green deformation tensor and any combination of structural tensors characterising the anisotropy.

Material symmetries are characterised by symmetry groups that impose restrictions on the form of the strain energy function (Ogden, 1984). Any orthogonal transformation member of the symmetry group of the material will leave the strain energy function unchanged when applied to the material in the natural state (prior to deformation).
Lets call $\mathcal{G}_{\mathbf{X}}$, the symmetry group of a material at $\mathbf{X} \in \mathcal{B}_0$.

The *isotropy group at* $\mathbf{X} \in \mathcal{B}_0$, $\mathcal{G}_{I\mathbf{X}}$, is the set of proper orthogonal transformations that have the stored energy function unchanged and is defined as follows:

$$\mathcal{G}_{I\mathbf{X}} := \left\{ \mathbf{Q} \in \mid \mathcal{O}^+ \,/\, \overline{\Psi}(\mathbf{X}, \mathbf{Q}.\mathbf{C}.\mathbf{Q}^{\mathrm{T}}) = \overline{\Psi}(\mathbf{X}, \mathbf{C}) \quad \forall\, \mathbf{X} \in \mathcal{B}_0 \right\} \qquad [\mathrm{V}.15]$$

If $\mathcal{G}_{I\mathbf{X}} \equiv \mathcal{O}^+$ in the configuration $\mathcal{B}_0$, the material is said to be *isotropic* (relative to $\mathcal{B}_0$ and $\mathbf{X} \in \mathcal{B}_0$), otherwise, the material is said to be *anisotropic.*

V.4.3.1 Isotropy

A function $\mathcal{F} : \mathcal{S}^+ \rightarrow \Re$ of symmetric tensors $\mathbf{T} \in \mathcal{S}^+$ is *isotropic* if and only if:

$$\mathcal{F}(\mathbf{Q}.\mathbf{T}.\mathbf{Q}^{\mathrm{T}}) = \mathcal{F}(\mathbf{T}) \;\; \forall\, (\mathbf{T}, \mathbf{Q}) \in \mathcal{S}^+ \times \mathcal{O}^+ \qquad [\mathrm{V}.16]$$

In the present context, $\mathbf{T}$, the symmetric tensor, is the right Cauchy-Green tensor $\mathbf{C}$. Then, if the strain energy function is an isotropic function of $\mathbf{C}$ and material frame indifference has already been satisfied, the following equality holds:

$$\Psi(\mathbf{X}, \mathbf{C}) \equiv \Psi(\mathbf{X}, \mathbf{Q}\mathbf{C}\mathbf{Q}^{\mathrm{T}}) \;\; \forall\, (\mathbf{C}, \mathbf{Q}) \in \mathcal{S}^+ \times \mathcal{O}^+ \quad \forall\, \mathbf{X} \in \mathcal{B}_0 \qquad [\mathrm{V}.17]$$

V.4.3.2 Transversely isotropy

A material is *transversely isotropic* if there exists a plane such that every plane perpendicular to it is a plane of material symmetry (Ogden, 1984). Transverse isotropy with respect to a preferred direction $\mathbf{n}$, is characterised by a symmetry group, $\mathcal{G}_{TI}$, such that:

$$\mathcal{G}_{TI} := \left\{ \mathbf{Q} \in \mathcal{O}^{+} \,/\, \mathbf{Q}.\mathbf{n} = \mathbf{n} \right\} \qquad [V.18]$$

The *Representation Theorem* for transversely isotropic scalar functions, states that a scalar function $\phi(\mathbf{C})$ is transversely isotropic if and only if there exists a function $\tilde{\phi}$ such that:

$$\phi(\mathbf{C}) = \tilde{\phi}(I_1, I_2, I_3, I_4, I_5) \qquad [V.19]$$

where I_1, I_2, I_3 are the principal invariants of $\mathbf{C}$. The invariants I_4 and I_5 were first introduced by Ericksen and Rivlin (1954). They will be described in more detail in the next section, but basically they relate $\mathbf{C}$ and a unit vector $\mathbf{n}$ which corresponds to a preferred mechanical direction of the material. Then $\tilde{\phi}$ becomes an isotropic function of the five invariants considered above. This implies that $\tilde{\phi}$ is invariant under any proper orthogonal transformation and if $\tilde{\phi}$ is identified with the strain energy function Ψ, then Ψ is an objective quantity.

V.5 Fibre-reinforced continuum

To describe the constitutive behaviour of biological soft connective tissue in the most general case, we consider a material constructed from two families of fibres continuously distributed in a (highly) compliant solid isotropic matrix (Figure V.2). The result of the geometrical and mechanical interactions of the three constituents gives the material strongly anisotropic macroscopic properties (Spencer, 1992).

The two family of fibres F_1 and F_2 are characterised by, respectively a unit vector $\mathbf{n}_0(\mathbf{X})$ and a unit vector $\mathbf{m}_0(\mathbf{X})$, both defined in the reference configuration $\mathcal{B}_0$. These two vectors define locally the preferred directions from which the anisotropy directly arises and then the fibre directions can vary within the material. For sake of clarity, the possible dependence on $\mathbf{X}$ of $\mathbf{n}_0$ and $\mathbf{m}_0$ will be omitted in the next developments.

The obvious way to ensure satisfaction of frame indifference without precluding anisotropic response is to formulate the constitutive response function in terms of objects associated with the reference state. For nonlinear elasticity this amounts to formulating response in terms of the right Cauchy-Green deformation tensor $\mathbf{C}$ and the second Piola-Kirchhoff stress tensor $\mathbf{S}$. Given that the fibre directions are dependent on the position within the continuum body it is more convenient to formulate the constitutive law in a coordinate free system. This leads to the direct inclusion of the unit vectors $\mathbf{n}_0$ and $\mathbf{m}_0$ in the constitutive equations. The existence of a strain energy function $\overline{\Psi}$, isotropic function of its arguments, is postulated. The strain energy function $\overline{\Psi}$ is only a function of $\mathbf{X}$, $\mathbf{C}$, $\mathbf{n}_0$ and $\mathbf{m}_0$ and is therefore written as $\overline{\Psi} = \overline{\Psi}(\mathbf{X}, \mathbf{C}, \mathbf{n}_0, \mathbf{m}_0)$. It is relevant to note that the sense of the two unit vectors has no physical meaning and, in consequence, the strain energy function $\overline{\Psi}$ must be an even function of these two vectors.

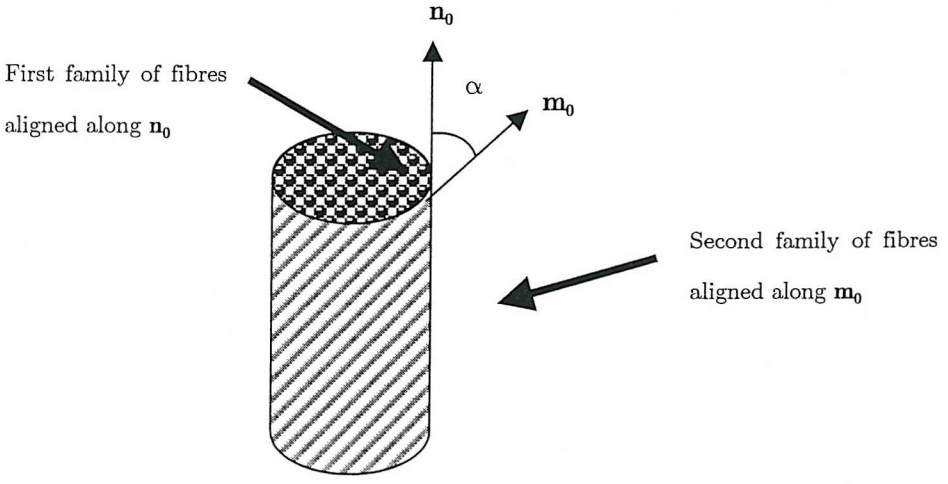

Figure V.2 – Simplified representation of a continuum material made of an isotropic matrix reinforced by two families of fibres respectively associated with directions $\mathbf{n}_0$ and $\mathbf{m}_0$ in the reference configuration. The particular arrangement of the fibres is defined locally and therefore depends on the position $\mathbf{X}$ of the material point. The angle α between the two vectors $\mathbf{n}_0$ and $\mathbf{m}_0$ characterises the local degree of anisotropy.

The two structural tensors $\mathbf{n}_0 \otimes \mathbf{n}_0$ and $\mathbf{m}_0 \otimes \mathbf{m}_0$ have to be introduced. The invariance requirement of the strain energy function with respect to the material symmetry group can be stated as follows: $\forall\ (\mathbf{X}, \mathbf{Q}, \mathbf{C}) \in \mathcal{B}_0 \times \mathcal{Q}^+ \times \mathcal{S}^+$

$$\overline{\Psi}(\mathbf{X}, \mathbf{C}, \mathbf{n}_0 \otimes \mathbf{n}_0, \mathbf{m}_0 \otimes \mathbf{m}_0) = \overline{\Psi}(\mathbf{X}, \mathbf{Q}.\mathbf{C}.\mathbf{Q}^T, \mathbf{Q}.\mathbf{n}_0 \otimes \mathbf{n}_0.\mathbf{Q}^T, \mathbf{Q}.\mathbf{m}_0 \otimes \mathbf{m}_0.\mathbf{Q}^T) \qquad [V.20]$$

A set of eight invariants ($I_{\alpha,\ \alpha=1..8}$) are necessary to form the *irreducible integrity bases* of the tensors $\mathbf{C}$, $\mathbf{n}_0 \otimes \mathbf{n}_0$ and $\mathbf{m}_0 \otimes \mathbf{m}_0$ (Spencer, 1992). In other words, it must exist a strain energy function Ψ, $\Psi : \Re^+ \times \Re^+ \times \Re^+ \times \Re^+ \times \Re^+ \times \Re^+ \times \Re^+ \times \Re^+ \to \Re$ such that $\overline{\Psi}$ can be written in the following form:

$$\overline{\Psi}(\mathbf{X}, \mathbf{C}, \mathbf{n}_0, \mathbf{m}_0) = \Psi\left[\mathbf{X}, I_1(\mathbf{C}), I_2(\mathbf{C}), I_3(\mathbf{C}), I_4(\mathbf{C}, \mathbf{n}_0), I_5(\mathbf{C}, \mathbf{n}_0), I_6(\mathbf{C}, \mathbf{m}_0), I_7(\mathbf{C}, \mathbf{m}_0), I_8(\mathbf{C}, \mathbf{n}_0, \mathbf{m}_0)\right] \quad [V.21]$$

The latest form of the strain energy function satisfies the *Principle of frame indifference* and the material symmetry arising from the anisotropy. The invariants defining Ψ are the following:

$$I_1 = trace(\mathbf{C}), \quad I_2 = \frac{1}{2}[I_1^2 - trace(\mathbf{C}^2)], \quad I_3 = det(\mathbf{C}), \quad [V.22]$$

These latter invariants characterise the isotropic response of the material.

The invariants characterising the anisotropic mechanical response of the material are given below:

$$I_4 = \mathbf{N}_o : \mathbf{C}, \quad I_5 = \mathbf{N}_o : \mathbf{C}^2 \quad [V.23]$$

$$I_6 = \mathbf{M}_o : \mathbf{C}, \quad I_7 = \mathbf{M}_o : \mathbf{C}^2 \quad [V.24]$$

$$I_8 = (\mathbf{n}_0.\mathbf{m}_0)\mathbf{n}_0.(\mathbf{C}.\mathbf{m}_0), \quad [V.25]$$

where $\mathbf{N_0}$ and $\mathbf{M_0}$ (equation [V.26]) denote structural tensors in the reference configuration. They reflect the local structural arrangement of the fibres and thus define local directional properties of the composite material. This theoretical aspect connects to the fact that connective tissues have different structural properties according to the location (Frank and Shrive, 1999) and shows that the theory presented can take into account this feature.

$$\mathbf{N}_0 := \mathbf{n}_0 \otimes \mathbf{n}_0, \quad \mathbf{M}_0 := \mathbf{m}_0 \otimes \mathbf{m}_0 \quad [V.26]$$

Observing that:

$$I_4 = \mathbf{n}_0.(\mathbf{C}.\mathbf{n}_0) = (\lambda_{\mathbf{n}_0})^2 \quad [V.27]$$

$$I_6 = \mathbf{m}_0.(\mathbf{C}.\mathbf{m}_0) = (\lambda_{\mathbf{m}_0})^2, \quad [V.28]$$

where $\lambda_{\mathbf{n}_0}$ and $\lambda_{\mathbf{m}_0}$ denote respectively the stretch associated with the direction $\mathbf{n_0}$ and the stretch associated with the direction $\mathbf{m_0}$, allows an easy physical interpretation of the invariants I_4 and I_6 as shown on Equations [V.27] and [V.28]. These two invariants are directly related to the type of data one can obtain experimentally when performing tensile tests on a soft tissue specimen.

This makes straightforward the parameter identification for any constitutive law using I_4 and/or I_6. Upon deformation, the unit vectors $\mathbf{n}_0$ and $\mathbf{m}_0$ (from the reference configuration) are transformed into a vector $\lambda_{\mathbf{n}_0}\mathbf{n}$ and $\lambda_{\mathbf{m}_0}\mathbf{m}$ (Equations [V.29] and [V.30])respectively where $\mathbf{n}$ and $\mathbf{m}$ represent the unit vectors associated with each family of fibres in the distorted configuration.

$$\lambda_{\mathbf{n}_0}\mathbf{n} = \sqrt{I_4}\mathbf{n} = \mathbf{F}.\mathbf{n}_0 \qquad [V.29]$$

$$\lambda_{\mathbf{m}_0}\mathbf{m} = \sqrt{I_6}\mathbf{m} = \mathbf{F}.\mathbf{m}_0\,, \qquad [V.30]$$

V.5.1 Definition of stress tensors

Given that the Green-Lagrange strain tensor $\mathbf{E}$ and $\mathbf{C}$ have proportional material derivatives and that $\mathbf{E}$ is work conjugate to the second Piola-Kirchhoff stress tensor $\mathbf{S}$, it is straightforward to construct a totally Lagrangean constitutive equation as follows:

$$\dot{\Psi} = \frac{\partial \Psi}{\partial \mathbf{C}} : \dot{\mathbf{C}} = \frac{1}{2}\mathbf{S} : \dot{\mathbf{C}} \qquad [V.31]$$

In a convective representation of elasticity, and more especially for a hyperelastic material, the second Piola-Kirchhoff stress tensor is derived from the strain energy as:

$$\mathbf{S}\left[\mathbf{X}, \mathbf{C}(\mathbf{X}), \mathbf{n}_0, \mathbf{m}_0\right] = 2\frac{\partial \Psi}{\partial \mathbf{C}} = \frac{\partial \Psi}{\partial \mathbf{E}} \qquad [V.32]$$

It is worth noting that this equality is valid only in the case of a non dissipative process (which corresponds to the hypothesis of the present developments). Since Ψ is a function of the invariants $I_{\alpha,\ \alpha = 1,..,8}$, $\mathbf{S}$ is expressed as follows:

$$\mathbf{S} = 2\sum_{\alpha=1}^{8}\left(\frac{\partial \Psi}{\partial I_\alpha}\frac{\partial I_\alpha}{\partial \mathbf{C}}\right) \qquad [V.33]$$

The first derivatives of the tensorial invariants with respect to $\mathbf{C}$ (Spencer, 1992) are:

$$\frac{\partial I_1}{\partial \mathbf{C}} = \mathbf{1}, \quad \frac{\partial I_2}{\partial \mathbf{C}} = I_1\mathbf{1} - \mathbf{C}, \quad \frac{\partial I_3}{\partial \mathbf{C}} = I_2\mathbf{1} - I_1\mathbf{C} + \mathbf{C}^2 = I_3\mathbf{C}^{-1} \qquad [V.34]$$

$$\frac{\partial I_4}{\partial \mathbf{C}} = \mathbf{N}_0, \quad \frac{\partial I_5}{\partial \mathbf{C}} = \mathbf{N}_0\mathbf{C} + \mathbf{C}\mathbf{N}_0 := \mathbf{N}_{0\mathbf{C}} \qquad [V.35]$$

$$\frac{\partial I_6}{\partial \mathbf{C}} = \mathbf{M}_0, \quad \frac{\partial I_7}{\partial \mathbf{C}} = \mathbf{M}_0.\mathbf{C} + \mathbf{C}.\mathbf{M}_0 := \mathbf{M}_{0\mathbf{C}} \qquad [V.36]$$

$$\frac{\partial I_8}{\partial \mathbf{C}} = \frac{1}{2}(\mathbf{n}_0.\mathbf{m}_0)(\mathbf{n}_0 \otimes \mathbf{m}_0 + \mathbf{m}_0 \otimes \mathbf{n}_0) := \mathbf{T}_{\mathbf{n}_0\mathbf{m}_0} \qquad [V.37]$$

From Equations [V.33], [V.34], [V.35], [V.36] and [V.37], the expression of the second Piola-Kirchhoff stress tensor **S** is established:

$$\begin{aligned}\mathbf{S} = 2\Big[&(\Psi_1 + I_1\Psi_2 + I_2\Psi_3)\mathbf{1} - (\Psi_2 + I_1\Psi_3)\mathbf{C} + \Psi_3\,\mathbf{C}^2\Big] \\ &+2\Big[\Psi_4\,\mathbf{N}_0 + \Psi_5\,\mathbf{N}_{0\mathrm{C}} + \Psi_6\,\mathbf{M}_0 + \Psi_7\,\mathbf{M}_{0\mathrm{C}} + \Psi_8\mathbf{T}_{\mathbf{n}_0\mathbf{m}_0}\Big]\end{aligned} \qquad [V.38]$$

or, in a more reduced form, using the inverse of **C**:

$$\mathbf{S} = 2\Big[(\Psi_1 + I_1\Psi_2)\mathbf{1} - \Psi_2\,\mathbf{C} + I_3\Psi_3\,\mathbf{C}^{-1} + \Psi_4\,\mathbf{N}_0 + \Psi_5\,\mathbf{N}_{0\mathrm{C}} + \Psi_6\,\mathbf{M}_0 + \Psi_7\,\mathbf{M}_{0\mathrm{C}} + \Psi_8\mathbf{T}_{\mathbf{n}_0\mathbf{m}_0}\Big] \qquad [V.39]$$

where the following notation has been introduced: $\Psi_\alpha := \partial\Psi / \partial I_\alpha,\ _{\alpha=1..8}$.

At this stage, it is convenient to introduce the notion of *push-forward* and *pull-back* of a tensor (Mardsen and Hughes, 1994).

The *push-forward* of an arbitrary tensor **T** that is referred to the reference configuration to one that is referred to the spatial, or deformed, configuration can be generalised as:

$$\left(\varphi_*\mathbf{T}\right)^{a..d}_{e..h} = F_{aA}..F_{dD}\,(T^{A..D}_{E..F})\,F^{-1}_{Ee}..F^{-1}_{Fh} \qquad [V.40]$$

The left hand-side of the above equation is the "push-forward of **T** by the deformation φ". In the same manner, the *pull-back* of an arbitrary tensor **t** that is referred to the deformed configuration to one that is referred to the reference configuration can be defined as:

$$\left(\varphi^*\mathbf{t}\right)^{A..D}_{E..H} = F^{-1}_{Aa}..F^{-1}_{Dd}\,(t^{a..d}_{e..h})\,F_{eE}..F_{hH} \qquad [V.41]$$

S can be interpreted as the force per unit area in the undeformed configuration (if one considers a rigid motion) and $\boldsymbol{\sigma}$ as the force per unit area in the deformed configuration. In hyperelasticity, the Cauchy stress tensor is typically calculated from the second Piola-Kirchhoff stress tensor by means of the *Piola transformation*, another name for the *push-forward* operation with or without the factor $1/J$:

$$\boldsymbol{\sigma} = \frac{1}{J}(\varphi_*\,\mathbf{S}) \qquad [V.42]$$

$$\Rightarrow \boldsymbol{\sigma} = \frac{1}{J}\mathbf{F}.\mathbf{S}.\mathbf{F}^{\mathrm{T}} = \frac{2}{J}\mathbf{F}.\frac{\partial\Psi}{\partial\mathbf{C}}.\mathbf{F}^{\mathrm{T}} \qquad [V.43]$$

The Cauchy stress tensor $\boldsymbol{\sigma}$ is expressed as follows:

$$\boldsymbol{\sigma} = \frac{2}{J}\Big[(\Psi_1 + I_1\Psi_2)\,\mathbf{b} - \Psi_2\,\mathbf{b}^2 + I_3\Psi_3\,\mathbf{1} + I_4\Psi_4\,\mathbf{N} + I_4\Psi_5\,\mathbf{N}_b + I_6\Psi_6\,\mathbf{M} + I_6\Psi_7\,\mathbf{M}_b + \sqrt{I_4 I_6}\Psi_8\,\mathbf{T}_{nm}\Big] \quad [V.44]$$

where:

$$\mathbf{N}_b := \mathbf{N}.\mathbf{b} + \mathbf{N}.\mathbf{b}, \quad \mathbf{M}_b := \mathbf{M}.\mathbf{b} + \mathbf{b}.\mathbf{M}, \quad \mathbf{T}_{nm} := \frac{1}{2}\mathbf{n}_0.\mathbf{m}_0(\mathbf{n}\otimes\mathbf{m} + \mathbf{m}\otimes\mathbf{n}) \quad [V.45]$$

$\mathbf{N}$ and $\mathbf{M}$ are the spatial counterparts of $\mathbf{N_0}$ and $\mathbf{M_0}$ according to the following definition:

$$\mathbf{N} := \mathbf{n}\otimes\mathbf{n}, \quad \mathbf{M} := \mathbf{m}\otimes\mathbf{m} \quad [V.46]$$

Having reviewed the necessary theoretical background for strongly anisotropic fibre-reinforced composites (Spencer, 1992), I am now going to develop new *general explicit* expression of the tensors of elasticity (material and spatial versions) by considering *all* the possible mutual interactions between the matrix and the two families of fibres.

V.5.2 Definition of the elasticity tensors

In his work, Spencer (1992) did not develop general closed form expressions for the elasticity tensors of fibre-reinforced composites at finite strain. Weiss (1994) established closed form expressions of the elasticity tensors (material and spatial configurations) for a continuum composite but reinforced by a single family of fibres and by making the hypothesis of incompressible behaviour. This latest assumption excludes all the terms of the strain energy function involving the third invariant I_3 of the Cauchy-Green deformation tensors. In this section, the expressions of the elasticity tensors in the material and the spatial configurations are derived. Not only does the elastic tensor specify the response of a material to applied stresses, but it also gives criteria about the actual stability of the structure. However, the discussion of the later concept is out of the scope of this work.

V.5.2.1 Elasticity tensor in the material configuration

The material elasticity tensor is obtained by differentiation of the second Piola Kirchhoff stress tensor **S** with respect to the deformation tensor **C**, as given in equation [V.47]:

$$\mathbf{A}^{m} = 4\frac{\partial^2 \Psi}{\partial \mathbf{C} \partial \mathbf{C}} = 2\frac{\partial \mathbf{S}}{\partial \mathbf{C}} = 2\frac{\partial S_{IJ}}{\partial C_{KL}} \mathbf{E}_{\mathrm{I}} \otimes \mathbf{E}_{\mathrm{J}} \otimes \mathbf{E}_{\mathrm{K}} \otimes \mathbf{E}_{\mathrm{L}} \qquad [V.47]$$

Combining equation [V.47] and the fact that **S** and **C** are symmetric tensors proves that $\mathbf{A}^{m}$ possesses the so-called *minor symmetries*:

$$A^{m}_{IJKL} = A^{m}_{IJLK} = A^{m}_{JILK} \qquad [V.48]$$

The definition of the elasticity tensor given in equation [V.47] ($\mathbf{A}^{m}$ is the second derivative of Ψ with respect to **C**), implies the so-called *major symmetry* expressed as follows:

$$A^{m}_{IJKL} = A^{m}_{KLIJ} \qquad [V.49]$$

In summary, $\mathbf{A}^{m}$ possesses the following symmetries:

$$A^{m}_{IJKL} = A^{m}_{KLIJ} = A^{m}_{IJLK} = A^{m}_{JILK} \qquad [V.50]$$

In order to obtain a convenient form for $\mathbf{A}^{m}$, the following notations are introduced (Mardsen and Hughes, 1994):

$$\frac{\partial C_{IJ}}{\partial C_{KL}} = \frac{1}{2}\frac{\partial (C_{IJ} + C_{JI})}{\partial C_{KL}} = \frac{1}{2}\left(\delta_{IK}\delta_{JL} + \delta_{IL}\delta_{JK}\right) := (\mathbf{I})_{IJKL} \qquad [V.51]$$

$$\frac{\partial C^{-1}_{IJ}}{\partial C_{KL}} = -\frac{1}{2}\left(C^{-1}_{IK}C^{-1}_{JL} + C^{-1}_{IL}C^{-1}_{JK}\right) := (\mathbf{I}_{\mathbf{C}^{-1}})_{IJKL} \qquad [V.52]$$

I is the identity mapping on the six-dimensional space of symmetric second-order tensors and δ is the Kronecker tensor ($\delta_{IJ} = 1$ if $I = J$, 0 otherwise). Differentiating [V.39] with respect to **C** leads to the following non-reduced form for $\mathbf{A}^{m}$:

$$\begin{aligned}\mathbf{A}^{m} = 4\left[\mathbf{1}\otimes\frac{\partial\Psi_1}{\partial\mathbf{C}} + \Psi_2\mathbf{1}\otimes\frac{\partial I_1}{\partial\mathbf{C}} + I_1\mathbf{1}\otimes\frac{\partial\Psi_2}{\partial\mathbf{C}} - \mathbf{C}\otimes\frac{\partial\Psi_2}{\partial\mathbf{C}} - \Psi_2\frac{\partial\mathbf{C}}{\partial\mathbf{C}}\right] \\ +4\left[\Psi_3\mathbf{C}^{-1}\otimes\frac{\partial I_3}{\partial\mathbf{C}} + I_3\mathbf{C}^{-1}\otimes\frac{\partial\Psi_3}{\partial\mathbf{C}} + I_3\Psi_3\frac{\partial\mathbf{C}^{-1}}{\partial\mathbf{C}}\right] \\ +4\left[\mathbf{N}_0\otimes\frac{\partial\Psi_4}{\partial\mathbf{C}} + \mathbf{N}_{0\mathbf{C}}\otimes\frac{\partial\Psi_5}{\partial\mathbf{C}} + \Psi_5(\mathbf{N}_0\otimes\mathbf{1}+\mathbf{1}\otimes\mathbf{N}_0)\right] \\ +4\left[\mathbf{M}_0\otimes\frac{\partial\Psi_6}{\partial\mathbf{C}} + \mathbf{M}_{0\mathbf{C}}\otimes\frac{\partial\Psi_7}{\partial\mathbf{C}} + \Psi_7(\mathbf{M}_0\otimes\mathbf{1}+\mathbf{1}\otimes\mathbf{M}_0)\right] \\ +4\left[\mathbf{T}_{\mathbf{n}_0\mathbf{m}_0}\otimes\frac{\partial\Psi_8}{\partial\mathbf{C}}\right]\end{aligned} \qquad [V.53]$$

For further developments, let us establish the following generic differential expression for $\partial\Psi_\alpha/\partial\mathbf{C}$:

$$\begin{aligned}\frac{\partial\Psi_\alpha}{\partial\mathbf{C}} = (\Psi_{\alpha1} + I_1\Psi_{\alpha2})\mathbf{1} - \Psi_{\alpha2}\mathbf{C} + I_3\Psi_{\alpha3}\mathbf{C}^{-1} \\ + \Psi_{\alpha4}\mathbf{N}_0 + \Psi_{\alpha5}\mathbf{N}_{0\mathbf{C}} + \Psi_{\alpha6}\mathbf{M}_0 + \Psi_{\alpha7}\mathbf{M}_{0\mathbf{C}} + \Psi_{\alpha8}\mathbf{T}_{\mathbf{n}_0\mathbf{m}_0}\end{aligned} \qquad [V.54]$$

After introducing the following notation: $\Psi_{\alpha\beta} := \partial^2\Psi/\partial I_\alpha\partial I_\beta,\ _{\beta=1..8}$, development of the second derivatives of Ψ, application of the chain rule and lengthily algebraic manipulations, the material elasticity tensor is obtained in the following form:

$$\mathbf{A}^{m} := \bar{\mathbf{A}}^{m}_{m} + \tilde{\mathbf{A}}^{m}_{m} + \bar{\mathbf{A}}^{m}_{F_1m} + \tilde{\mathbf{A}}^{m}_{F_1m} + \bar{\mathbf{A}}^{m}_{F_2m} + \tilde{\mathbf{A}}^{m}_{F_2m} + \bar{\mathbf{A}}^{m}_{F_1F_2m} + \tilde{\mathbf{A}}^{m}_{F_1F_2m} + \mathbf{A}^{m}_{F_1F_2}, \qquad [V.55]$$

where $\mathbf{A}^{m}$ has been split into several contributions which characterise specific interactions between the matrix and the fibres and between the two families of fibres (Equations [V.56], [V.57], [V.58], [V.59], [V.60], [V.61], [V.62], [V.63] and [V.64]) and highlights the crossed contributions of the differential terms of the strain energy function with respect to the three constituents of the material (Table IV.1).

Interactions	***Matrix***		***Family of fibres F_1***		***Family of fibres F_2***	
Matrix	$\partial(I_1, I_2)$	$\partial(I_1, I_2, I_3)$	$\partial(I_1, I_2, I_4, I_5)$	$\partial(I_3, I_4, I_5)$	$\partial(I_1, I_2, I_6, I_7)$	$\partial(I_3, I_6, I_7)$
	$\bar{\mathbf{A}}^{\mathcal{M}}_{m}$	$\tilde{\mathbf{A}}^{\mathcal{M}}_{m}$	$\bar{\mathbf{A}}^{\mathcal{M}}_{F_1 m}$	$\tilde{\mathbf{A}}^{\mathcal{M}}_{F_1 m}$	$\bar{\mathbf{A}}^{\mathcal{M}}_{F_2 m}$	$\tilde{\mathbf{A}}^{\mathcal{M}}_{F_2 m}$
			$\partial(I_2, I_8)$	$\partial(I_3, I_8)$	$\partial(I_2, I_8)$	$\partial(I_3, I_8)$
			$\bar{\mathbf{A}}^{\mathcal{M}}_{F_1 F_2 m}$	$\tilde{\mathbf{A}}^{\mathcal{M}}_{F_1 F_2 m}$	$\bar{\mathbf{A}}^{\mathcal{M}}_{F_1 F_2 m}$	$\tilde{\mathbf{A}}^{\mathcal{M}}_{F_1 F_2 m}$
Family of fibres F_1	$\partial(I_1, I_2, I_4, I_5)$	$\partial(I_3, I_4, I_5)$	$\partial(I_4, I_5)$		$\partial(I_4, I_5, I_6, I_7, I_8)$	
	$\bar{\mathbf{A}}^{\mathcal{M}}_{F_1 m}$	$\tilde{\mathbf{A}}^{\mathcal{M}}_{F_1 m}$	$\bar{\mathbf{A}}^{\mathcal{M}}_{F_1 m}$		$\mathbf{A}^{\mathcal{M}}_{F_1 F_2}$	
Family of fibres F_2	$\partial(I_1, I_2, I_6, I_7)$	$\partial(I_3, I_6, I_7)$	$\partial(I_4, I_5, I_6, I_7, I_8)$		$\partial(I_6, I_7)$	
	$\bar{\mathbf{A}}^{\mathcal{M}}_{F_2 m}$	$\tilde{\mathbf{A}}^{\mathcal{M}}_{F_2 m}$	$\mathbf{A}^{\mathcal{M}}_{F_1 F_2}$		$\bar{\mathbf{A}}^{\mathcal{M}}_{F_2 m}$	

Table V.1 - Table summarizing the various contributions to the material elasticity tensor by separating the various differential terms of the strain energy function. The symbol "∂", placed before a bracket containing invariants I_α, means that the corresponding term of the elasticity tensor contains partial derivatives of the strain energy function Ψ with respect to the invariant(s) considered.

$$\begin{aligned}\bar{\mathbf{A}}^{\mathcal{M}}_{\mathrm{m}} := {} & 4\Big[(\Psi_{11} + 2I_1\Psi_{12} + \Psi_2 + I_1^2\Psi_{22})\mathbf{1}\otimes\mathbf{1} - (\Psi_{12} + I_1\Psi_{22})(\mathbf{1}\otimes\mathbf{C} + \mathbf{C}\otimes\mathbf{1})\Big] \\ & + 4\Big[\Psi_{22}(\mathbf{C}\otimes\mathbf{C}) - \Psi_2\mathbf{I}\Big]\end{aligned} \qquad [V.56]$$

The term $\bar{\mathbf{A}}^{\mathcal{M}}_{\mathrm{m}}$ is made of the isotropic components of the derivatives of the strain energy function with respect to the two first invariants, I_1 and I_2, of the Cauchy-Green deformation tensors. I_1 has an easy physical interpretation as it corresponds to the sum of the square of the principal stretches. Uniaxial, shear, biaxial and equibiaxial tension are examples of tests that are performed on a soft tissue sample in order to obtain this information.

Compression tests may be required to compute out-of-plane stress if the material is not assumed to be incompressible or simply because different behaviours in compression and tension of the matrix are considered. If Ψ_2 is null, the matrix has a constant shear modulus. Thus if a variable shear modulus is to be accounted for in the constitutive law, one must define at least function of I_2 of degree one.

Terms containing the derivatives of Ψ with respect to I_3 are isolated (Equation [V.57]) in order to highlight the terms of the elasticity tensor that are directly related to change of volume.

It is relevant to emphasize that this does not constitute the classic decomposition resulting from the split of the deformation gradient **F** into a volumetric and a deviatoric part, as often used in incompressible finite element analyses (Flory, 1961). Our decomposition concerns only the terms of the strain energy function and not those involving **C**. By examining the expression of $\tilde{\mathbf{A}}_m^m$, it appears that the hypothesis of incompressibility ($I_3 = 1 \Rightarrow \tilde{\mathbf{A}}_m^m = \mathbf{0}$) provides a significant simplification at least at the constitutive formulation level, not the numerical one. Soft tissues are very often assumed to have an isochoric behaviour because of their high water content. However, due to the improvement of experimental methods it appears that a fluid exudation can be observed when a ligament is subjected to a mechanical loading as reported by Thielke *et al.* (1995). In consequence, it seems relevant to consider this aspect by using either using a porohyperelastic formulation or the present formulation that takes into account the corresponding volumetric terms that may generate non negligible coupled actions between the various constituents of the composite material. The compressibility can be dependent on the state of deformation within the matrix [$\left(\partial^2\Psi / \partial I_\alpha \partial I_3\right)_{\alpha=1,2} \neq \mathbf{0}$] and this could be captured by coupled terms of Ψ including the invariants I_1, I_2 and I_3.

$$\begin{aligned}\tilde{\mathbf{A}}_m^m := 4\Big[&\left(I_3\Psi_3 + I_3^2\Psi_{33}\right)\mathbf{C}^{-1}\otimes\mathbf{C}^{-1} + I_3\Psi_3\mathbf{I}_{\mathbf{C}^{-1}} + I_3\left(\Psi_{13} + I_1\Psi_{23}\right)\left(\mathbf{1}\otimes\mathbf{C}^{-1} + \mathbf{C}^{-1}\otimes\mathbf{1}\right)\Big] \\ &+4\Big[-I_3\Psi_{23}\left(\mathbf{C}\otimes\mathbf{C}^{-1} + \mathbf{C}^{-1}\otimes\mathbf{C}\right)\Big]\end{aligned} \qquad [V.57]$$

Terms $\bar{\mathbf{A}}_{F_1 m}^m$ and $\bar{\mathbf{A}}_{F_2 m}^m$ (Equations [V.58] and [V.59]) of the elasticity tensor characterise the interactions between the isotropic matrix and, respectively, the families of fibres F_1 and F_2. Some of the effects governed by I_4 and I_5 are probably indentical despite the relative independence of I_4 and I_5 as tensorial invariants. Naturally, similar remarks apply to I_6 and I_7. The most obvious kind of interactions between matrix and fibres in soft connective tissues is probably shear but one can imagine more complex interactions by using appropriate coupling functions. The experimental characterisation of these combined interactions is probably one of the biggest challenges when developing constitutive laws. Moreover, I_5 and I_7 do not have an immediate physical interpretation and this can be subject to further investigation. Deformation of the matrix can produce elongation of the fibres and the reverse effect can also be envisaged. As suggested by Minns and Soden (1973), an important function of the collagen fibres is to ensure a uniform distribution of deformation and thus avoiding excessive local deformations which are likely to induce early failure of the soft tissue.

$$\begin{aligned}\bar{\mathbf{A}}^{m}_{F_1 m} := {} & 4\left[(\Psi_{14}+I_1\Psi_{24}+\Psi_5)\left(\mathbf{1}\otimes\mathbf{N}_0+\mathbf{N}_0\otimes\mathbf{1}\right)+(\Psi_{15}+I_1\Psi_{25})\left(\mathbf{1}\otimes\mathbf{N}_{0C}+\mathbf{N}_{0C}\otimes\mathbf{1}\right)\right] \\ & +4\left[-\Psi_{24}\left(\mathbf{C}\otimes\mathbf{N}_0+\mathbf{N}_0\otimes\mathbf{C}\right)-\Psi_{25}\left(\mathbf{C}\otimes\mathbf{N}_{0C}+\mathbf{N}_{0C}\otimes\mathbf{C}\right)\right] \\ & +4\left[\Psi_{44}\left(\mathbf{N}_0\otimes\mathbf{N}_0\right)+\Psi_{45}\left(\mathbf{N}_0\otimes\mathbf{N}_{0C}+\mathbf{N}_{0C}\otimes\mathbf{N}_0\right)+\Psi_{55}\mathbf{N}_{0C}\otimes\mathbf{N}_{0C}\right]\end{aligned} \qquad [V.58]$$

$$\begin{aligned}\bar{\mathbf{A}}^{m}_{F_2 m} := {} & 4\left[(\Psi_{16}+I_1\Psi_{26}+\Psi_7)\left(\mathbf{1}\otimes\mathbf{M}_0+\mathbf{M}_0\otimes\mathbf{1}\right)+(\Psi_{17}+I_1\Psi_{27})\left(\mathbf{1}\otimes\mathbf{M}_{0C}+\mathbf{M}_{0C}\otimes\mathbf{1}\right)\right] \\ & +4\left[-\Psi_{26}\left(\mathbf{C}\otimes\mathbf{M}_0+\mathbf{M}_0\otimes\mathbf{C}\right)-\Psi_{27}\left(\mathbf{C}\otimes\mathbf{M}_{0C}+\mathbf{M}_{0C}\otimes\mathbf{C}\right)\right] \\ & +4\left[\Psi_{66}\left(\mathbf{M}_0\otimes\mathbf{M}_0\right)+\Psi_{67}\left(\mathbf{M}_0\otimes\mathbf{M}_{0C}+\mathbf{M}_{0C}\otimes\mathbf{M}_0\right)+\Psi_{77}\mathbf{M}_{0C}\otimes\mathbf{M}_{0C}\right]\end{aligned} \qquad [V.59]$$

By forming a complex network surrounded by and, at the same time, entrapping water, proteoglycans, glycoproteins and elastin, collagen fibres can play a central role in the overall compressibility of the material by interacting with the isotropic matrix. When stretched, collagen fibres squeeze the surrounding interfibrillar matrix and have their diameters reduced. These coupled interactions can be included in the formulation by defining bilinear functions of I_3 and I_4, or I_3 and I_5, or I_3 and I_6, or I_3 and I_7, exhibiting the possibility to have non zero second derivatives appearing in the elasticity tensor (Equations [V.60] and [V.61]):

$$\tilde{\mathbf{A}}^{m}_{F_1 m} := 4\left[I_3\Psi_{43}\left(\mathbf{C}^{-1}\otimes\mathbf{N}_0+\mathbf{N}_0\otimes\mathbf{C}^{-1}\right)+I_3\Psi_{53}\left(\mathbf{C}^{-1}\otimes\mathbf{N}_{0C}+\mathbf{N}_{0C}\otimes\mathbf{C}^{-1}\right)\right] \qquad [V.60]$$

$$\tilde{\mathbf{A}}^{m}_{F_2 m} := 4\left[I_3\Psi_{63}\left(\mathbf{C}^{-1}\otimes\mathbf{M}_0+\mathbf{M}_0\otimes\mathbf{C}^{-1}\right)+I_3\Psi_{73}\left(\mathbf{C}^{-1}\otimes\mathbf{M}_{0C}+\mathbf{M}_{0C}\otimes\mathbf{C}^{-1}\right)\right] \qquad [V.61]$$

The possible coupling between the tensorial invariants related to the fibres and that related to the volume ratio ($J=\sqrt{I_3}$) can help to characterise typical behaviours such as the fact that fluid exudation in soft tissues can be observed in particular directions (Armstrong *et al.*, 1984). The fluid exudation that affects the global compressibility is probably (this remains to be proven) channeled by the fibre network. It was shown that water contributes significantly to the nonlinear viscoelastic behaviour of ligaments (Chimich *et al.*, 1992). The water content may play a role in conditioning the distance at which collagen fibres can interact mechanically or biochemically. As proteoglycans are highly hydrophilic molecules, significant pressure gradients are likely to be generated within the tissue and hence producing redistribution of the water.

Several experimental studies have reported very interesting observations, namely the fact that the stiffness of connective soft tissues is much higher than that of a single collagen fibre (Hayashi *et al.*, 2000; Minns and Soden, 1973). In addition to evident size effects as mentioned by the previous authors, obvious explanations could be put forward by considering that mechanical interactions between the ground substance and the collagen fibres play a major role in the significant difference of stiffness observed (Hayashi *et al.*, 2000). At the atomic level, covalent liaisons between the components of the ground substance and the collagen fibres are certainly responsible for a strengthening of the whole structure. Collagen fibres, bonded together by an interfibrillar matrix, are arranged in bundles which in turn are structured in fascicles. This arrangement is likely to produce shear between the collagen fibres and the matrix when a ligament or a tendon is loaded in tension. This effect can explain the stronger stiffness of the connective tissue over a single collagen fibre. Others reasons include the presence of elastin fibres that provide the elastic recovery capabilities (storage of elastic energy) of a ligament and that are responsible for bringing back collagen fibres in their crimped state. Their actions could be viewed as a resisting factor in the elongation of the collagen fibres. In connection with this, non-uniform pre-stretch of the collagen fibres is probably present in an apparent relaxed soft connective tissue due to its strain and stress history. Rate effects such as viscoelasticity may be accountable for the experimental observations mentioned above (although they are supposed to be performed on conditioned specimens) because in an isolated collagen fibre, viscosity interactions provided by the presence of the ground substance (water, glycoproteins, elastin) are missing and thus alter the apparent stiffness. Some ligaments are encapsulated in a membrane, called the epiligament (Frank and Shrive, 1999), which contains randomly orientated collagen fibrils and a network of blood vessels branching and penetrating the intrasubstance of the ligament, running along and between the collagen fascicles. This is the kind of structural arrangement that can add significant stiffness to a connective tissue even thought its structural components have lower stiffnesses.

The combined interactions of the two families of fibres with the isotropic matrix are governed by $\bar{\mathbf{A}}^{m}_{F_1F_2m}$ and $\tilde{\mathbf{A}}^{m}_{F_1F_2m}$ (Equations [V.62] and [V.63]). $\mathbf{T}_{\mathbf{n}_0\mathbf{m}_0}$ is a second-order tensor that reflects the relative orientation of the two family of fibres and disappears if the orientation is orthogonal. It is well known that fibres orient themselves according to the load they carry. If we consider a ligament in a relaxed state, at each local continuum location considered, $\mathbf{T}_{\mathbf{n}_0\mathbf{m}_0}$ is probably nonzero, but as the ligament is submitted to multiaxial loading, fibres may align in a way such that $\mathbf{T}_{\mathbf{n}_0\mathbf{m}_0}$ becomes zero and thus modifying locally the stiffness and producing singularities in the stress distribution.

These phenomena could account partly for injuries when, in addition to high strain rates, ligaments are loaded in abnormal directions.

$$\bar{\mathbf{A}}^{\mathcal{M}}_{F_1F_2m} := 4\Big[(\Psi_1 + I_1\Psi_{28})\big(\mathbf{1}\otimes\mathbf{T}_{\mathbf{n}_0\mathbf{m}_0} + \mathbf{T}_{\mathbf{n}_0\mathbf{m}_0}\otimes\mathbf{1}\big) - \Psi_{28}\big(\mathbf{C}\otimes\mathbf{T}_{\mathbf{n}_0\mathbf{m}_0} + \mathbf{T}_{\mathbf{n}_0\mathbf{m}_0}\otimes\mathbf{C}\big)\Big] \qquad [V.62]$$

$$\tilde{\mathbf{A}}^{\mathcal{M}}_{F_1F_2m} := 4\,I_3\Psi_{38}\big(\mathbf{C}^{-1}\otimes\mathbf{T}_{\mathbf{n}_0\mathbf{m}_0} + \mathbf{T}_{\mathbf{n}_0\mathbf{m}_0}\otimes\mathbf{C}^{-1}\big) \qquad [V.63]$$

$\mathbf{A}^{\mathcal{M}}_{F_1F_2}$ (Equation [V.64]) exhibits the pure mutual interaction between the two families of fibres. Stretch of one family of fibres can produce stress in the other family of fibres under various forms such as shear, compression or tension if they are intermeshed with each other. However, the difficulty of the experimental measurement of these effects is a real practical limitation for now, in addition to the very demanding requirements of testing of biological tissues.

$$\begin{aligned}\mathbf{A}^{\mathcal{M}}_{F_1F_2} :=\ & 4\Big[\Psi_{46}\big(\mathbf{N}_0\otimes\mathbf{M}_0 + \mathbf{M}_0\otimes\mathbf{N}_0\big) - \Psi_{47}\big(\mathbf{N}_0\otimes\mathbf{M}_{0C} + \mathbf{M}_{0C}\otimes\mathbf{N}_0\big)\Big]\\ & + 4\Big[\Psi_{56}\big(\mathbf{N}_{0C}\otimes\mathbf{M}_0 + \mathbf{M}_0\otimes\mathbf{N}_{0C}\big) - \Psi_{57}\big(\mathbf{N}_{0C}\otimes\mathbf{M}_{0C} + \mathbf{M}_{0C}\otimes\mathbf{N}_{0C}\big)\Big]\\ & + 4\Big[\Psi_{48}\big(\mathbf{N}_0\otimes\mathbf{T}_{\mathbf{n}_0\mathbf{m}_0} + \mathbf{T}_{\mathbf{n}_0\mathbf{m}_0}\otimes\mathbf{N}_0\big) + \Psi_{58}\big(\mathbf{N}_{0C}\otimes\mathbf{T}_{\mathbf{n}_0\mathbf{m}_0} + \mathbf{T}_{\mathbf{n}_0\mathbf{m}_0}\otimes\mathbf{N}_{0C}\big)\Big]\\ & + 4\Big[\Psi_{68}\big(\mathbf{M}_0\otimes\mathbf{T}_{\mathbf{n}_0\mathbf{m}_0} + \mathbf{T}_{\mathbf{n}_0\mathbf{m}_0}\otimes\mathbf{M}_0\big) + \Psi_{78}\big(\mathbf{M}_{0C}\otimes\mathbf{T}_{\mathbf{n}_0\mathbf{m}_0} + \mathbf{T}_{\mathbf{n}_0\mathbf{m}_0}\otimes\mathbf{M}_{0C}\big)\Big]\\ & + 4\Big[\Psi_{88}\mathbf{T}_{\mathbf{n}_0\mathbf{m}_0}\otimes\mathbf{T}_{\mathbf{n}_0\mathbf{m}_0}\Big]\end{aligned} \qquad [V.64]$$

To the best of my knowledge, the expressions of the various terms of the elasticity tensor, containing coupling contributions between the matrix and the two families of fibres, have not been previously reported in the literature. The explicit dependence of the elasticity tensor on the partial derivatives of the strain energy function can serve as a basis to derive in a straightforward manner the elasticity tensor for a particular strain energy function. This is helpful to investigate particular mechanical effects determined by carefully chosen strain energy functions.

V.5.2.2 Elongation moduli in the material description

From the expression of the elasticity tensor one can define elongation moduli $\kappa_{\mathbf{n}_0}$ and $\kappa_{\mathbf{m}_0}$, respectively associated with the fibre directions $\mathbf{n}_0$ and $\mathbf{m}_0$. They characterise the stress response associated with the deformations in the fibre directions and are therefore directly related to the appropriate structural tensors by the following relationships:

$$\kappa_{\mathbf{n}_0} = \mathbf{N}_0 : (\mathbf{A}^{\mathcal{M}}.\mathbf{N}_0), \quad \kappa_{\mathbf{m}_0} = \mathbf{M}_0 : (\mathbf{A}^{\mathcal{M}}.\mathbf{M}_0) \qquad [V.65]$$

It is worthy to note that these extension moduli, particularly κ_{n_0}, when assessed in the linear phase (after recruitment of the collagen fibres) of the stress-strain curve (typically over 4 % of strain) represent the classical Young's modulus reported in experimental studies considering ligament as simple elastic material (Butler *et al.*, 1986).

V.5.2.3 Bulk modulus in the material description

The bulk modulus κ of the material can be defined as follows:

$$\kappa = \frac{1}{9}\mathbf{1} : (\mathbf{A}^{m}.\mathbf{1}) \qquad [V.66]$$

κ characterises the volumetric stresses associated with volumetric deformations of the material. From Equations [V.65] and [V.66], it is straightforward to derive the elastic moduli of the linear elasticity theory by assuming a state of vanishing strains. If the hypothesis of small perturbations is made and if it is assumed that fibres have no mechanical contribution in this strain regime, an equivalent isotropic bulk modulus can be deduced and used as a coefficient characterising the initial compressibility of the material.

V.5.2.4 Elasticity tensor in the spatial configuration

The spatial counterpart of the material elasticity tensor, $\mathbf{A}^{s}$, is defined by the push-forward relation:

$$\mathbf{A}^{s} = \frac{1}{J}(\mathbf{C}.\mathbf{A}^{m}.\mathbf{C}^{\mathrm{T}}) \Leftrightarrow A^{s}_{ijkl} = \frac{1}{J}F_{iI}F_{jJ}F_{kK}F_{lL}A^{m}_{IJKL} \qquad [V.67]$$

To avoid redundancy, the spatial elasticity tensor has not been split into various contributions as performed for the material elasticity tensor. The full general expression of $\mathbf{A}^{s}$ is given in Equation [V.68]. It appears that such a closed-form expression of the spatial version of the elasticity has never been reported in literature.

$$\begin{aligned}
\mathbf{A}^{s} = {} & 4\left[(\Psi_{11}+2I_1\Psi_{12}+\Psi_2+I_1^2\Psi_{22})\mathbf{b}\otimes\mathbf{b}+\Psi_{22}\left(\mathbf{b}^2\otimes\mathbf{b}^2\right)\right] \\
& +4\left[-(\Psi_{12}+I_1\Psi_{22})\left(\mathbf{b}\otimes\mathbf{b}^2+\mathbf{b}^2\otimes\mathbf{b}\right)-\Psi_2\mathbf{I}_{\mathbf{b}^{-1}}\right] \\
& +4\left[\left(I_3\Psi_3+I_3^2\Psi_{33}\right)\mathbf{1}\otimes\mathbf{1}+I_3\Psi_3\mathbf{I}+I_3\left(\Psi_{13}+I_1\Psi_{23}\right)(\mathbf{b}\otimes\mathbf{1}+\mathbf{1}\otimes\mathbf{b})\right] \\
& +4\left[-I_3\Psi_{23}\left(\mathbf{b}^2\otimes\mathbf{1}+\mathbf{1}\otimes\mathbf{b}^2\right)\right] \\
& +4\left[I_3I_4\Psi_{43}(\mathbf{1}\otimes\mathbf{N}+\mathbf{N}\otimes\mathbf{1})+I_3I_4\Psi_{53}\left(\mathbf{1}\otimes\mathbf{N}_{\mathrm{b}}+\mathbf{N}_{\mathrm{b}}\otimes\mathbf{1}\right)\right] \\
& +4\left[I_3I_6\Psi_{63}(\mathbf{1}\otimes\mathbf{M}+\mathbf{M}\otimes\mathbf{1})+I_3I_6\Psi_{73}\left(\mathbf{1}\otimes\mathbf{M}_{\mathrm{b}}+\mathbf{M}_{\mathrm{b}}\otimes\mathbf{1}\right)\right] \\
& +4\left[I_4(\Psi_{14}+I_1\Psi_{24}+\Psi_5)(\mathbf{b}\otimes\mathbf{N}+\mathbf{N}\otimes\mathbf{b})+I_4(\Psi_{15}+I_1\Psi_{25})\left(\mathbf{b}\otimes\mathbf{N}_{\mathrm{b}}+\mathbf{N}_{\mathrm{b}}\otimes\mathbf{b}\right)\right] \\
& +4\left[-I_4\Psi_{24}\left(\mathbf{b}^2\otimes\mathbf{N}+\mathbf{N}\otimes\mathbf{b}^2\right)-I_4\Psi_{25}\left(\mathbf{b}^2\otimes\mathbf{N}_{\mathrm{b}}+\mathbf{N}_{\mathrm{b}}\otimes\mathbf{b}^2\right)\right] \\
& +4\left[I_4^2\Psi_{44}(\mathbf{N}\otimes\mathbf{N})-I_4^2\Psi_{45}\left(\mathbf{N}\otimes\mathbf{N}_{\mathrm{b}}+\mathbf{N}_{\mathrm{b}}\otimes\mathbf{N}\right)+I_4^2\Psi_{55}\mathbf{N}_{\mathrm{b}}\otimes\mathbf{N}_{\mathrm{b}}\right] \\
& +4\left[I_6(\Psi_{16}+I_1\Psi_{26}+\Psi_7)(\mathbf{b}\otimes\mathbf{M}+\mathbf{M}\otimes\mathbf{b})+I_6(\Psi_{17}+I_1\Psi_{27})\left(\mathbf{b}\otimes\mathbf{M}_{\mathrm{b}}+\mathbf{M}_{\mathrm{b}}\otimes\mathbf{b}\right)\right] \\
& +4\left[-I_6\Psi_{26}\left(\mathbf{b}^2\otimes\mathbf{M}+\mathbf{M}\otimes\mathbf{b}^2\right)-I_6\Psi_{27}\left(\mathbf{b}^2\otimes\mathbf{M}_{\mathrm{b}}+\mathbf{M}_{\mathrm{b}}\otimes\mathbf{b}^2\right)\right] \\
& +4\left[\mathrm{I}_6^2\Psi_{66}(\mathbf{M}\otimes\mathbf{M})-\mathrm{I}_6^2\Psi_{67}\left(\mathbf{M}\otimes\mathbf{M}_{\mathrm{b}}+\mathbf{M}_{\mathrm{b}}\otimes\mathbf{M}\right)+\mathrm{I}_6^2\Psi_{77}\mathbf{M}_{\mathrm{b}}\otimes\mathbf{M}_{\mathrm{b}}\right] \\
& +4\left[I_4I_6\Psi_{46}(\mathbf{N}\otimes\mathbf{M}+\mathbf{M}\otimes\mathbf{N})-I_4I_6\Psi_{47}\left(\mathbf{N}\otimes\mathbf{M}_{\mathrm{b}}+\mathbf{M}_{\mathrm{b}}\otimes\mathbf{N}\right)\right] \\
& +4\left[I_4I_6\Psi_{56}\left(\mathbf{N}_{\mathrm{b}}\otimes\mathbf{M}+\mathbf{M}\otimes\mathbf{N}_{\mathrm{b}}\right)-I_4I_6\Psi_{57}\left(\mathbf{N}_{\mathrm{b}}\otimes\mathbf{M}_{\mathrm{b}}+\mathbf{M}_{\mathrm{b}}\otimes\mathbf{N}_{\mathrm{b}}\right)\right] \\
& +4\left[\sqrt{I_4I_6}(\Psi_1+I_1\Psi_{28})(\mathbf{b}\otimes\mathbf{T}_{\mathrm{nm}}+\mathbf{T}_{\mathrm{nm}}\otimes\mathbf{b})-\sqrt{I_4I_6}\Psi_{28}\left(\mathbf{b}^2\otimes\mathbf{T}_{\mathrm{nm}}+\mathbf{T}_{\mathrm{nm}}\otimes\mathbf{b}^2\right)\right] \\
& +4\left[\sqrt{I_4I_6}I_3\Psi_{38}(\mathbf{1}\otimes\mathbf{T}_{\mathrm{nm}}+\mathbf{1}\otimes\mathbf{T}_{\mathrm{nm}})\right] \\
& +4\left[\Psi_{48}\sqrt{I_4I_6}I_4(\mathbf{N}\otimes\mathbf{T}_{\mathrm{nm}}+\mathbf{T}_{\mathrm{nm}}\otimes\mathbf{N})+\Psi_{58}\sqrt{I_4I_6}I_4\left(\mathbf{N}_{\mathrm{b}}\otimes\mathbf{T}_{\mathrm{nm}}+\mathbf{T}_{\mathrm{nm}}\otimes\mathbf{N}_{\mathrm{b}}\right)\right] \\
& +4\left[\Psi_{68}\sqrt{I_4I_6}I_6(\mathbf{M}\otimes\mathbf{T}_{\mathrm{nm}}+\mathbf{T}_{\mathrm{nm}}\otimes\mathbf{M})+\Psi_{78}\sqrt{I_4I_6}I_6\left(\mathbf{M}_{\mathrm{b}}\otimes\mathbf{T}_{\mathrm{nm}}+\mathbf{T}_{\mathrm{nm}}\otimes\mathbf{M}_{\mathrm{b}}\right)\right] \\
& +4\left[\Psi_{88}I_4I_6\mathbf{T}_{\mathrm{nm}}\otimes\mathbf{T}_{\mathrm{nm}}\right]
\end{aligned} \qquad [V.68]$$

where:

$$\left(\mathbf{I}_{\mathbf{b}^{-1}}\right)_{ijkl} := \left(\varphi_{*}\,\mathbf{I}\right)_{ijkl} = -\frac{1}{2}\left(b^{-1}_{ik}b^{-1}_{jl}+b^{-1}_{il}b^{-1}_{jk}\right) \qquad [V.69]$$

V.6 Mechanical symmetries for fibre-reinforced composites

The previous expressions of the stress and elasticity tensors have been established in the general case of a fibre-reinforced composite material containing two distinct families of fibres F_1 and F_2. No assumption was made regarding the mutual orientation of the two families of fibres. Orthotropic, transversely isotropic and isotropic symmetries are special cases that will be derived, in the next section, in a straightforward manner from the general anisotropic formulation. For sake of illustration, the degenerated expressions of the spatial elasticity tensors and the second Piola-Kirchhoff stress tensors are presented for each material symmetry.

V.6.1 Orthotropic symmetry and locally orthotropic symmetry

When the principal preferred directions of the two families of fibres are mutually orthogonal in the reference configuration, the composite material possesses an *orthotropic symmetry* because there exist three orthogonal planes of symmetry: two normal to the fibre directions and one parallel to the surface where the fibres lie. This symmetry group requires nine independent scalar coefficients to fully characterise the material. The scalar product of the two unit vector $\mathbf{n}_0$ and $\mathbf{m}_0$ is zero, as the eighth invariant I_8 and its derivative with respect to $\mathbf{C}$. $\mathbf{A}^{\mathcal{m}}$ and $\mathbf{S}$ are expressed by means of Equations [V.70] and [V.71] respectively.

$$\mathbf{A}^{\mathcal{m}} := \bar{\mathbf{A}}^{\mathcal{m}}_{m} + \tilde{\mathbf{A}}^{\mathcal{m}}_{m} + \bar{\mathbf{A}}^{\mathcal{m}}_{F_1 m} + \tilde{\mathbf{A}}^{\mathcal{m}}_{F_1 m} + \bar{\mathbf{A}}^{\mathcal{m}}_{F_2 m} + \tilde{\mathbf{A}}^{\mathcal{m}}_{F_2 m} + \mathbf{A}^{\mathcal{m}}_{F_1 F_2} \qquad [V.70]$$

$$\mathbf{S} = 2\Big[(\Psi_1 + I_1\Psi_2)\mathbf{1} - \Psi_2\,\mathbf{C} + I_3\Psi_3\,\mathbf{C}^{-1} + \Psi_4\,\mathbf{N}_0 + \Psi_5\,\mathbf{N}_{0\mathrm{C}} + \Psi_6\,\mathbf{M}_0 + \Psi_7\,\mathbf{M}_{0\mathrm{C}}\Big] \qquad [V.71]$$

One can define a *local orthotropy* when the two families of fibres are mechanically equivalent, i.e. it is possible to interchange $\mathbf{n}_0$ and $\mathbf{m}_0$ without affecting the properties of symmetry. In this case, the material is said to be *locally orthotropic* with respect to the mutually orthogonal planes which bisect the two families of fibres (with direction $\mathbf{n}_0$ and $\mathbf{m}_0$) and the plane in which the fibres lie. The dependence of $\mathbf{n}_0$ and $\mathbf{m}_0$ on Ψ is symmetric with respect to swap between $\mathbf{n}_0$ and $\mathbf{m}_0$. In this case, Ψ can be defined by means of I_1, I_2, I_3, I_8 and three additional invariants I_9, I_{10} and I_{11} defined as follows (Spencer, 1992):

$$I_9 = I_4 + I_6, \quad I_{10} = I_4 I_6, \quad I_{11} = I_5 + I_7 \qquad [V.72]$$

The second Piola-Kirchhoff stress tensor is defined as:

$$\mathbf{S} = 2\Big[(\Psi_1 + I_1\Psi_2)\mathbf{1} - \Psi_2\mathbf{C} + I_3\Psi_3\,\mathbf{C}^{-1} + \Psi_8\mathbf{T}_{\mathbf{n}_0\mathbf{m}_0} + \Psi_9\mathbf{Z}_0 + \Psi_{10}\mathbf{Y}_{\mathbf{n}_0\mathbf{m}_0} + \Psi_{11}\mathbf{Z}_{0\mathrm{C}}\Big], \qquad [V.73]$$

where:

$$\mathbf{Z}_0 := \mathbf{N}_0 + \mathbf{M}_0, \quad \mathbf{Z}_{0C} := \mathbf{N}_{0C} + \mathbf{M}_{0C}, \quad \mathbf{Y}_{\mathbf{n}_0\mathbf{m}_0} := I_6\mathbf{N}_0 + I_4\mathbf{M}_0 \qquad [V.74]$$

To keep the present developments concise, the expression of the material elasticity tensor corresponding to local orthotropy is not presented.

V.6.2 Transversely isotropic symmetry

In this case, the material is assumed to be a solid isotropic matrix reinforced by a single family of fibres characterised by a fibre direction given by $\mathbf{n}_0$ (Figure V.3).

Five independent scalar coefficients are needed to define the constitutive law. Of course, I_6, I_7 and I_8 are no longer arguments of the strain energy function and the spatial elasticity and stress tensor reduces to:

$$\mathbf{A}^{m} := \bar{\mathbf{A}}^{m}_{m} + \tilde{\mathbf{A}}^{m}_{m} + \bar{\mathbf{A}}^{m}_{F_1 m} + \tilde{\mathbf{A}}^{m}_{F_1 m} \qquad [V.75]$$

$$\mathbf{S} = 2\left[(\Psi_1 + I_1\Psi_2)\mathbf{1} - \Psi_2\,\mathbf{C} + I_3\Psi_3\,\mathbf{C}^{-1} + \Psi_4\,\mathbf{N}_0 + \Psi_5\,\mathbf{N}_{0C}\right] \qquad [V.76]$$

This constitutive formulation was successfully used by Weiss *et al.* (1996) to describe the mechanical behaviour of fascia lata tendons and the collateral ligaments of the knee and was implemented into an implicit finite element code. This work brought a significant contribution to finite element modelling of ligaments and tendons by taking into account, for the first time in a three-dimensional continuum model, the directional properties of ligaments. The experimental validation of the mechanical formulation demonstrated the relevance of using the continuum theory of fibre-reinforced composites at finite strain.

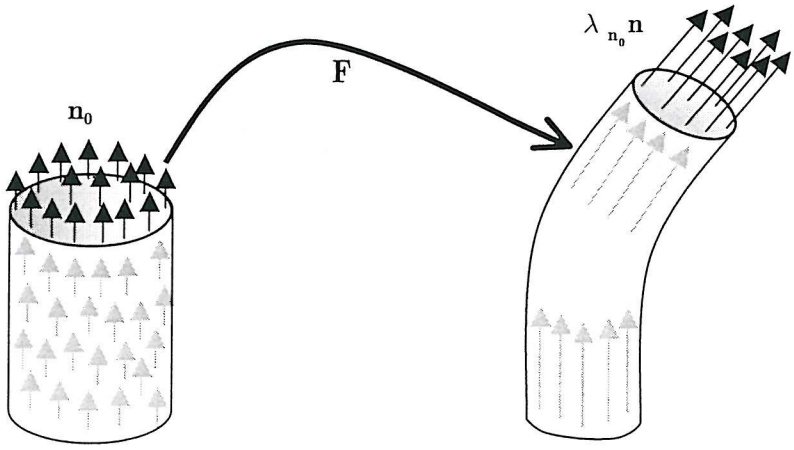

Figure V.3 - Unit vector field carrying the preferred fibre direction, before ($\mathbf{n}_0$) and after deformation ($\mathbf{n}$). Upon deformation $\mathbf{n}_0$ is mapped into $\lambda_{\mathbf{n}_0}\mathbf{n}$ according to Equation [V.29].

V.6.3 Isotropic symmetry

The material is a solid isotropic matrix which is not reinforced by any family of fibres. The constitutive equations merely degenerate from the ones given for transversely isotropy by suppressing the terms involving I_4 and I_5. In this case, only two scalar coefficients are necessary to define the constitutive law and the elasticity and stress tensors takes the following form:

$$\mathbf{A}^m := \bar{\mathbf{A}}^m_m + \tilde{\mathbf{A}}^m_m \qquad [V.77]$$

$$\mathbf{S} = 2\Big[(\Psi_1 + I_1\Psi_2)\mathbf{1} - \Psi_2\,\mathbf{C} + I_3\Psi_3\,\mathbf{C}^{-1}\Big] \qquad [V.78]$$

Isotropic constitutive law are widely used in rubber elasticity and the most popular constitutive laws are: the neo-Hookean model, the Mooney-Rivlin model, the Ogden power law or the Blatz-Ko model (Ogden, 1984). In the context of ligament modelling, Pioletti (1997) and Pioletti *et al.* (1998b) used an isotropic law based on the strain energy function proposed by Veronda and Westmann (1970) for skin modelling. However, isotropic models were shown to lead to unrealistic results (Limbert and Taylor, 2001a).

V.7 Kinematics constraints

In addition of being well justified for certain classes of problems, kinematics constraints can significantly simplify the formulation of the constitutive equations. Incompressibility and inextensibility in the fibre directions are presented. For sake of illustration, the expression of the Cauchy stress tensor is given.

V.7.1 Incompressibility

The assumption of incompressibility is often made in finite elasticity because of the satisfactory results it gives and the simplification it brings in experimental measurements (allows to compute out-of-plane deformations for example). Moreover, from a physiological point of view, this assumption can be justified by the fact that soft tissues have a very high water content. It is worthy to note that this assumption increases considerably the difficulty in finite element analyses because of various numerical singularities generated. As mentioned earlier, in this case, $I_3 = 1$, all the derivatives of Ψ with respect to I_3 are zero and an arbitrary pressure p, determined only by the equations of equilibrium or motion and the boundary conditions (not the constitutive equations), enters the stress under the form of a Lagrange multiplier as a reaction to the kinematics constraint of incompressibility.

The stress $p\mathbf{1}$ does not work in any deformation compatible with the condition $I_3 = 1$. The expression of the Cauchy stress tensor takes the following form:

$$\boldsymbol{\sigma} = \frac{2}{J}\left[(\Psi_1 + I_1\Psi_2)\mathbf{b} - \Psi_2\,\mathbf{b}^2 + I_4\Psi_4\,\mathbf{N} + I_4\Psi_5\,\mathbf{N}_\mathbf{b} + I_6\Psi_6\,\mathbf{M} + I_6\Psi_7\,\mathbf{M}_\mathbf{b} + \sqrt{I_4 I_6}\Psi_8\mathbf{T}_{\mathrm{nm}}\right] + p\mathbf{1} \quad [V.79]$$

V.7.2 Inextensibility

In fibre-reinforced composite materials, the stiffness of the fibres is generally much higher than that of the matrix. This implies that the extension moduli of the material in the fibre directions are much more larger that their shear moduli. The material will be therefore more likely to deform in a deformation mode other than extension in the fibre directions. For some applications it can be convenient to consider that the material is inextensible in the fibre directions and this corresponds to one or two kinematics constraints, respectively for one and two families of fibres reinforced-composites. This is a very relevant and interesting issue in soft tissue modelling as numerous studies have suggested and shown experimentally that a stressed fibre aligns to avoid a mechanical stimulus in the fibre direction under cyclic deformation (Yamada *et al.*, 2000). In the particular case when the material is inextensible in the two fibre directions $\mathbf{n}_0$ and $\mathbf{m}_0$, the inextensibility condition means that $I_4 = 1$ and $I_6 = 1$. In a similar manner as for the incompressible case, fibre reaction stresses q and r enter the stresses as reactions to the kinematics constraints of inextensibility. The expression of the Cauchy stress tensor takes the following form:

$$\boldsymbol{\sigma} = \frac{2}{J}\left[(\Psi_1 + I_1\Psi_2)\mathbf{b} - \Psi_2\,\mathbf{b}^2 + I_3\Psi_3\,\mathbf{1} + \Psi_8\mathbf{T}_{\mathrm{nm}}\right] + q\,\mathbf{N} + r\,\mathbf{M} \quad [V.80]$$

Obviously, incompressibility and inextensibility can coexist in the same constitutive law. Incompressibility is broadly used in finite element modelling of ligaments and tendons but inextensibility is only used in mathematical models describing ligaments as a collection of extensible and isometric fibres (O'Connor and Zavatsky, 1993). The hypothesis of inextensibility is probably relevant for finite element analyses of ligaments for particular fibre bundles within a ligament and for particular ranges of motion. Its influence should be assessed in order to allow for possible simplification of constitutive laws but the drawback is that if such constraints have to be enforced in a finite element context, they lead to extra computational cost and possible ill-conditioniong of matrices in implicit methods based finite element codes when associated with penalty methods.

V.8 Constitutive restrictions

Constitutive restrictions guiding the choice of the strain energy function have been largely investigated, especially for isotropic solids at finite strain (Ciarlet, 1988; Mardsen and Hughes, 1994; Oden and Reddy, 1978; Ogden, 1984; Truesdell and Noll, 1992). These restrictions can be divided into *mathematical* and *physical* restrictions. Mathematical restrictions are established in order to insure the existence and/or uniqueness of the solution of the initial/boundary value problem whilst physical restrictions impose constraints such that the material behaves in a physically acceptable manner, at least in the accessible experimental domain. It is worth emphasising that objectivity and material symmetry discussed previously are also mathematical restrictions put on the strain energy function. The consideration of these restrictive conditions can prevent introduction of non-physical behaviour or can put particular limits on the domain of validity of a constitutive law, at the formulation level. In the context of nonlinear finite element analyses, the restrictions imposed on the strain energy function can give confidence in the existence of a solution, or can explain particular results when, for example, the solution of a particular initial/boundary value problem is not unique. As there does not exist a general constitutive inequality encompassing all the required physical and mathematical properties, this leaves an open field for investigation. For further details about the notions of constitutive restrictions see Zee and Sternberg (1983) for the specific case of incompressible hyperelastic solids. For the question of existence and uniqueness in finite elasticity see Ball (1977, 1980), Gurtin (1980), Le Dret (1985), Valent (1980) and references given therein. For further details concerning some popular constitutive inequalities please see Appendix B.

V.9 A particular strain energy function for incompressible transversely isotropic hyperelasticity

Simple modelling considerations can be used to define a strain energy function that encompasses the principal features observed in biological connective soft tissues. The elastic response of the tissue is dictated by the resistance of the collagen fibre family, the ground substance matrix and their interaction. However, determining the exact nature of such interactions is intractable from an experimental point of view. This is the reason why, in the absence of relevant experimental material data, in the present study the mechanical behaviour of biological soft tissue is assumed to be governed by a function F_{12} representing the contribution of the matrix (dependent on I_1 and I_2) and by a function representing the mechanical contribution of the fibre (dependent on I_4). These two functions are not coupled but, with appropriate experimental protocols, it can be imagined to perform tests in order to characterise this coupling. Shear coupling is a good candidate for such an interaction. When the material is assumed to be incompressible, I_3 equals 1 and the strain energy function Ψ is independent of this third invariant. The strain energy function characterising the mechanical behaviour of ligaments can therefore be assumed to be the sum of two strain energy functions: one representing the matrix contribution and the other one representing the fibre contribution. The dependence of Ψ on I_4 can be replaced by an equivalent dependence on the stretch along the fibre direction, λ. This simplifies the identification process with experimental data.

$$\Psi = F_{12}(I_1, I_2) + f(\lambda) \qquad \text{[V.81]}$$

The preferred orientation of the collagen fibres induces the transversely isotropic symmetry of the ligament whereas the matrix (ground substance) is assumed to be isotropic.

This leads to the following form of the strain energy function if the matrix is assumed to be a Mooney-Rivlin material that degenerates into a neo-Hookean material if $C_2 = 0$:

$$\Psi = C_1(I_1 - 3) + C_2(I_2 - 3) + f(\lambda) \qquad \text{[V.82]}$$

The collagen does not support a significant compressive load and structures that are composed of mostly collagen will tend to buckle under very small compressive forces.

The tensile stress-stretch relation for collagenous tissues such as ligaments and tendons can be well approximated by an exponential toe region followed by a linear region. The transition is made when $\lambda = \lambda^*$. These observations guide the choice of the following function $f(\lambda)$ (Weiss *et al.*, 1996):

$$f(\lambda) = \int \frac{\partial f}{\partial \lambda}\, d\lambda \qquad \text{such that} \qquad \begin{cases} \dfrac{\partial f}{\partial \lambda} = 0, & \lambda < 1 \quad \text{a)} \\ \dfrac{\partial f}{\partial \lambda} = \dfrac{C_3\left(e^{C_4(\lambda-1)} - 1\right)}{\lambda}, & \lambda < \lambda^* \quad \text{b)} \\ \dfrac{\partial f}{\partial \lambda} = \dfrac{C_5\lambda + C_6}{\lambda}, & \lambda \geq \lambda^* \quad \text{c)} \end{cases} \qquad \text{[V.83]}$$

- λ^* represents the stretch in the fibre direction at which the collagen fibres are straightened.
- C_3 scales the stresses in the toe region.
- C_4 is the rate of uncrimping of the collagen fibres.
- C_5 is the linear modulus of the straightened collagen.
- C_6 is determined by assuming that $f(\lambda)$ is C^0-continuous at $\lambda = \lambda^*$.

V.9.1 Stress tensors

From Equations [V.39], [V.44], [V.82] and [V.83], one can derive the stress tensors in the material and spatial descriptions.

V.9.1.1 Second Piola-Kirchhoff stress tensor

$$\mathbf{S} = 2\left[(C_1 + I_1 C_2)\mathbf{1} - C_2\,\mathbf{C} + \frac{\partial f(\lambda)}{\partial \lambda}\mathbf{n}_0 \otimes \mathbf{n}_0\right] + p\,\mathbf{C}^{-1} \qquad \text{[V.84]}$$

V.9.1.2 Cauchy stress tensor

$$\boldsymbol{\sigma} = 2\left[(C_1 + I_1 C_2)\mathbf{b} - C_2\mathbf{b}^2 + \lambda\frac{\partial f(\lambda)}{\partial \lambda}\mathbf{n} \otimes \mathbf{n}\right] + p\,\mathbf{1} \qquad \text{[V.85]}$$

V.10 Concluding remarks

The theory of fibre-reinforced composites developed by Spencer (1992) has been presented and extended in the context of the constitutive modelling of biological soft connective tissues. New closed-form expressions of the material and the spatial versions of the elasticity tensors have been derived for continuum fibre-reinforced composite material containing up to two families of fibres. The derivations have been performed without restricting the way the strain energy function depends on its arguments. The coupling terms appearing by successive differentiation of the strain energy function have been isolated and discussed in connection with the modelling of ligaments and tendons. It was described how particular mechanical effects observed in biological structures can be accounted for by choosing appropriate functional forms of the strain energy function with respect to its arguments, that is tensorial invariants of the strain and structural tensor agencies.

The development of the expressions for the elasticity tensors in the material and spatial descriptions is of interest because, in addition of their relevance to predict and explore the mechanical behaviour of a given material, elasticity tensors hold fundamental mathematical properties of the constitutive law. Stability studies and constitutive restrictions generally rely on arguments based on these properties. The general expressions of the stress and elasticity tensors are also essential in the finite element implementation of constitutive laws for fibre-reinforced composites and it is hoped that they will be useful in this regard.

In implicit scheme based finite element methods, the elasticity tensor is used to calculate the tangent matrix which governs the convergence of the system of nonlinear equations whereas, in explicit analyses, the various coefficients of the elasticity tensors are used to calculate the largest stable time step by the mean of the equivalent Lamé's moduli.

The present phenomenological formulation is fairly simple but its drawback lies in the fact that the tensorial invariants of the right Cauchy-Green deformation tensor and agencies of structural tensors considered do not have all an easy physical interpretation like I_5 and I_7. This constitutes a possible limitation in the general applicability of the continuum theory of fibre-reinforced composites at finite strain. A particular research effort should be directed towards this important aspect of the constitutive formulation and especially for biological materials.

The presentation of the spatial elasticity tensor, in full generality, has allowed us to isolate terms which are representative of the mutual micromechanical interactions between the matrix and the two families of fibres. Phenomenological models such as the present one are macroscopic but can be motivated by structural or microstructural considerations and some invariants and suitable associated strain energy functions may characterise particular microstructural features of the material. For example, the fact that biological soft tissues made of collagen fibres buckle under very small compressive forces in the fibre direction can be integrated into the mathematical form of the strain energy function by assuming a zero mechanical contribution from the fibres when they are submitted to compression along their long axis (I_4 or $I_6 < 1$), in addition to their higher stiffness compared to the matrix. When a connective tissue undergoes a tensile load in the direction of the collagen fibres, the gradual uncrimping of the fibres produces a typical nonlinear response which is followed by a more or less linear response. This aspect can be put in equations by specifying appropriate functional forms in the expression of the strain energy function. The response arising from the tension of a particular family of fibres can be expressed by an exponential function of the stretch in the fibre direction followed by a linear function of the same argument like in the approach used by Weiss (1994) and Weiss *et al.* (1996). Instead of using a nonlinear and a linear function it can be advantageous to use a single multi-linear function (Hirokawa and Tsuruno, 2000).

The terms of the elasticity tensors (and the stress tensors) involving the volume ratio are often removed from the constitutive equations by assuming incompressibility of the material. It is believed that their contributions are probably not negligible as deformations of ligaments and tendons involve fluid displacement and exudation.

Experimental measurements performed on biological soft tissues are extremely delicate processes and the current experimental methods need to evolve in order to capture specific mechanical responses which may be missed otherwise. Applicability of the general fibre-reinforced composite model remains to be explored on experimental grounds but with suitable experimental material characterisation one can envisage to integrate complex interactions between elemental constituents within a constitutive law.

An important issue in ligament modelling is the fact these structures are naturally in a state of residual stress, even at rest. Residual stress can be incorporated at the formulation level (Hoger, 1996) but the applicability of such constitutive laws remains a difficult task given the difficulty of experimental testing on soft tissues, especially for initial stress measurements. The state of pre-stress within a ligament is probably highly inhomogeneous because ligaments are made of various fibre bundles that do not possess all the same lengths or the same mechanical properties (Butler *et al.*, 1992). In a three-dimensional finite element analysis of the anterior cruciate ligament, recently performed by Limbert and Taylor (2001b), it was demonstrated the necessity, not only to model the anterior cruciate ligament as an anisotropic hyperelastic material but, as importantly, to include pre-stress in order to obtain realistic results which agree with experimental observations.

In conclusion, it seems essential to have a deep knowledge of the microstructural properties of a biological soft tissue when formulating macroscopic constitutive laws. Particular features of the microstructure or the structure of the material can be taken into account by using appropriate functions for the definition of the strain energy function. Special attention should be taken in the choice of the mathematical expression of the strain energy function by assuring that it complies with essential constitutive inequalities. The identification of material parameters from experimental data must be conducted with constitutive inequalities in mind because particular states of stretch and deformations can lead to violation of constitutive inequalities and then discard a particular choice of a strain energy function. Although the developments presented in this chapter are aimed at the constitutive modelling of biological soft connective tissues, there is no restriction in using them for the formulation of constitutive laws for other biological structures. Indeed, skin, intervertebral discs, arteries, among others, due to their fibrous structures and strong anisotropy are well suited candidates for the application of a continuum theory of fibre-reinforced composites. There is therefore plenty of room for investigative research work in the field of (continuum) fibre-reinforced composite materials would it be experimental, analytical or computational.

Chapter VI

Finite element implementation of incompressible transversely isotropic hyperelasticity

Equation Section 6Equation Section 6

In this chapter, the finite element implementation of a transversely isotropic hyperelastic constitutive law for modelling soft tissues is described and validated. The formulation of the elastodynamic boundary value problem is presented in the general case. Solving techniques for explicit dynamic problems are described. Prior to this, a quick survey of the treatment of the constraint of incompressibility in finite element analysis is presented. Given the importance of the incompressibility hypothesis in finite element analyses of soft tissues, the description of its numerical enforcement is made by paying special attention to the particular penalty function which was used, in the frame of explicit finite element analyses. Finally, the validity of the finite element model for transversely isotropic hyperelasticity is checked against analytical solutions for homogeneous states of deformation.

VI.1 Incompressible behaviour and numerical singularities

Total incompressibility literally means that the material exhibits zero volumetric change (isochoric behavior) under hydrostatic pressure. The pressure in the material is not related to the strain in the material: it is an indeterminate quantity as far as the stress-strain relationship is concerned. The Poisson's ratio is exactly 0.5, while the bulk modulus is infinite. Incompressibility was first considered in finite element analysis by Hermann (1965). Analytical difficulties arise when it is combined with nonlinearities such as large displacements, large strains and contact. In finite element elasticity, when the material response is almost incompressible, the pure displacement formulation, in which the strain invariants are computed from the kinematic variables of the finite element model, is not appropriate and generally prevents convergence to a solution. One difficulty is that, from a numerical point of view, the stiffness matrix is almost singular because the effective bulk modulus of the material is so large compared to its effective shear modulus, thus causing difficulties with the solution of the discretised equilibrium equations. Another pathological numerical behaviour known as *mesh locking* may also appear during an analysis of incompressible or nearly incompressible analysis. Mesh locking refers to the inability of an element to perform accurately in an incompressible analysis, regardless of how refined the mesh is, due to an over-constrained condition and insufficient active degrees of freedom. Specifically, if a standard element is distorted into an hourglass mode, it will lock as the bulk modulus becomes infinite. It must be noted that the element locks despite the fact that its area has remained constant, resulting in the prediction of too small a displacement and too large a stress. Hence the locking is a peculiarity of the finite element discretisation, and special techniques have been used to improve the behaviour of elements. Unless reduced integration techniques are used, the stresses calculated at the numerical integration points show large oscillations in the pressure stress values, because, in general, the element cannot respond accurately and still has small volume changes at all numerical points.

Modern analytical techniques used in treating incompressibility effects in finite element codes are based on the *Hellinger-Reissner* (Valid, 1981) and *Hu-Washizu Variational Principles* (Washizu, 1974). Well known applications of these principles include *assumed strain methods*, such as the *mixed method* of Hermann (1965), the *constant dilatational method* of Nagtegaal *et al.* (1974), the related *B-bar method* of Hughes (1980) and Simo *et al.* (1985), the Hu-Washizu methods of Simo and Taylor (1991), the mixed assumed strain methods used with incompatible modes by Simo and Rifai (1990) and *selective-reduced integration methods* (Hughes, 1980).

Mixed methods usually have the stresses, strains, dilatation, or a combination of variables, as unknown. The earliest mixed method is the so-called *Hermann formulation.* A modified form of the *Hellinger-Reissner Variational Principle* is used to derive the stiffness equations. A pressure variable (energetically conjugate to the volume strain) is introduced in the form of a Lagrange multiplier. Hermann's approach has been used since the mid 1960s and 1970s in commercial finite element codes, and various in-house codes developed by leading solid rocket propellant manufacturers. *The constant dilatation method* of Nagtegaal *et al.* (1974) decouples the dilatational (volumetric) and distorsional (isochoric) deformations and interpolates them independently. Appropriate chosen functions will preclude mesh locking. *The B-bar method* of Hughes (1980) is a generalisation of this method for linearised kinematics. *Selective-reduced integration* under integrates the volumetric terms. However, all these methods can be shown to be equivalent under certain conditions (Malkus and Hughes, 1978). The separation of the volumetric and deviatoric deformations was first suggested in Flory (1961) and systematically exploited by Simo *et al.* (1985) among others. The uncoupling of the deviatoric and the dilatational response permits the formulation of the discrete problem in the variational form furnished by a three-field variational principle of the *Hu-Washizu type.* For alternative approaches see Glowinski and Le Tallec (1984).

VI.2 Implementation of the constitutive material model

The implementation of the incompressible transversely isotropic hyperelastic material model described in section V.9 was first done into the commercial FE code ABAQUS Standard 5.8 (® Hibbit, Karlsson & Sorensen Inc., Pawtucket, RI, USA) using a customised internal subroutine (UMAT) programmed in Fortran 77. The Standard version of ABAQUS 5.8 is based on an implicit nonlinear solver (full Newton-Raphson method). The optional user subroutine UMAT allows the definition of customised material models by providing explicit definition of the stress and the tangent stiffness matrix. However, UMAT does not permit to control with enough flexibility the state variables during the solving of the nonlinear FE equations. This is particularly problematic when a well conditioned tangent matrix is needed. In fact, the only way to enforce the incompressibility constraint within UMAT, is to use a penalty method. This method was not found to be sufficiently robust and too sensitive to the penalty parameter chosen to enforce the incompressibility constraint. When the penalty parameter is too high (in the order of 10^4), some terms of the tangent matrix are too large compared to others (bulk modulus several order of magnitude bigger than shear moduli), and this matrix controls the convergence of the nonlinear algebraic equations. In the context of large deformation, an augmented Lagrangean method is preferable (Simo and Taylor, 1991).

The model was tested with several types of 8-noded hexahedral elements. Finally, the first-order hybrid element (C3D8H) was the one that gave the best results in terms of convergence to a solution. In the formulation of this element, the pressure is treated as an independently interpolated basic solution variable, coupled to the displacement through the constitutive theory and the compatibility conditions. For further details concerning the formulation considered, please refer to "ABAQUS Theory Manual" (1997). The convergence of the model implemented was extremely difficult to achieve for very large deformations and, given its lack of robustness, it was decided to implement the constitutive material model into an explicit FE code which does not require the formation of a tangent stiffness matrix. The drawback of this, is that, when the material tends to be incompressible, in an explicit analysis, the stable time step tends to get closer to zero.

The explicit FE code chosen was PAM-CRASH^{TM} (PAM Systems International S.A., Rungis, France). The implicit codes (like ABAQUS Standard) and explicit codes (like PAM-CRASH) are named from the operator used for integration of the (nonlinear) FE equations in the time domain.

VI.3 Formulation of the elastodynamic initial boundary value problem

VI.3.1 Strong form of the equations

Let B be a three-dimensional continuum body occupying $\mathcal{B}$ with boundary $\partial\mathcal{B}$ at time t. The strong form of the initial boundary value problem consists of finding the displacement field:

$\mathbf{u}$: $\mathcal{B}$ x [0,T] $\rightarrow \Re$ such that the set of following relationships is satisfied:

Equation of motion:

$$\nabla.\boldsymbol{\sigma} + \mathbf{b} = \rho\ddot{\mathbf{u}} \quad \forall \mathbf{u} \text{ on } \mathcal{B} \times]0,T[\qquad \text{[VI.1]}$$

Conservation of mass:

$$\rho_0 = \rho J \qquad \text{[V.2]}$$

Constitutive equation:

$$\overset{\nabla}{\boldsymbol{\sigma}} = \mathbf{A}^{\sigma} : \dot{\boldsymbol{\epsilon}} \quad \text{or} \quad \boldsymbol{\sigma} = \mathbf{A}^{\sigma} : \epsilon \qquad \text{[VI.3]}$$

Strain rate-velocity equation:

$$\dot{\boldsymbol{\epsilon}} = \frac{1}{2}(\nabla\dot{\mathbf{u}} + \nabla^{T}\dot{\mathbf{u}} + \nabla^{T}\dot{\mathbf{u}}.\nabla\dot{\mathbf{u}}) \qquad \text{[VI.4]}$$

Prescribed displacement and traction on the boundary:

$$\mathbf{u} = \overline{\mathbf{u}} \quad \text{on } \partial\mathcal{B}_u \times]0,T[\qquad \text{[VI.5]}$$

$$\boldsymbol{\sigma}.\mathbf{n} = \overline{\mathbf{t}} \quad \text{on } \partial\mathcal{B}_t \times]0,T[\qquad \text{[VI.6]}$$

Initials conditions (time = 0):

$$\mathbf{u}(\mathbf{x},0) = \mathbf{u}^0 \quad \text{and} \quad \dot{\mathbf{u}}(\mathbf{x},0) = \dot{\mathbf{u}}^0(\mathbf{x}) \quad \forall \mathbf{x} \text{ on } \mathcal{B}, \text{ or} \qquad \text{[VI.7]}$$

$$\boldsymbol{\sigma}(\mathbf{x},0) = \boldsymbol{\sigma}^0 \quad \text{and} \quad \dot{\mathbf{u}}(\mathbf{x},0) = \dot{\mathbf{u}}^0(\mathbf{x}) \quad \forall \mathbf{x} \text{ on } \mathcal{B} \qquad \text{[VI.8]}$$

- ∇ is the divergence operator with respect to the current coordinates.
- $\boldsymbol{\sigma}$ is the Cauchy stress tensor.
- $\mathbf{b}$ represents the body forces (gravitational forces, electromagnetic forces, etc...).
- ρ_0 and ρ are the initial and current material densities. J is the Jacobian of the deformation.
- $\overline{\mathbf{u}}$ and $\overline{\mathbf{t}}$ are the prescribed displacements tractions on $\partial\mathcal{B}_u$ and on $\partial\mathcal{B}_t$, respectively.
- $\mathbf{u}^0, \dot{\mathbf{u}}^0(\mathbf{x}), \boldsymbol{\sigma}^0$ are, respectively, the initial displacement, velocity and stress fields.
- $\mathbf{A}^{\sigma}$ is the spatial elasticity tensor.
- $\overset{\nabla}{\boldsymbol{\sigma}}$ is an objective rate of Cauchy stress.

Examples of objective rates of Cauchy stress are the Jaumann (Equation [VI.9]) or the Green-Naghdi (Equation [VI.10]) stress rates (Bonet and Wood, 1997):

$$\overset{\nabla}{\boldsymbol{\sigma}} = \dot{\boldsymbol{\sigma}} - \boldsymbol{\omega}.\boldsymbol{\sigma} + \boldsymbol{\sigma}.\boldsymbol{\omega} \qquad [VI.9]$$

$$\overset{\nabla}{\boldsymbol{\sigma}} = \dot{\boldsymbol{\sigma}} + \boldsymbol{\sigma}.\dot{\mathbf{R}}.\mathbf{R}^{T} - \dot{\mathbf{R}}.\mathbf{R}^{T}.\boldsymbol{\sigma} \qquad [VI.10]$$

where $\boldsymbol{\omega}$ is the spin tensor (Bonet and Wood, 1997), given by:

$$\boldsymbol{\omega} = \frac{1}{2}(\dot{\mathbf{F}}.\mathbf{F}^{-1} - \mathbf{F}^{-T}.\dot{\mathbf{F}}^{T}) \qquad [VI.11]$$

where $\mathbf{R}$ is the rotational part in the polar decomposition of the deformation gradient $\mathbf{F}$.
The use of an objective stress rate in the constitutive equation is justified by the requirement of objectivity (see section V.4.2) with respect to rigid body motion, i.e., a rigid body rotation or translation should not result in any material stress or strain rate.

VI.3.2 Weak form of the equations and matrix form

Complete derivation of the weak form of the initial elastodynamic boundary value problem and the finite element discretised equations are largely treated in literature (Bonet and Wood, 1997; Oden and Reddy, 1978; Reddy, 1984; Zienkiewicz and Taylor, 1989) and this aspect will not be developed in the present thesis. However, basic important results like the matrix form of the discretised equations, are presented here for illustrating the explicit central difference solving method. After substituting the approximations (Galerkin's method) for the various quantities developed in the weak form, integrating the analytical expressions of the shape functions and using the constitutive material equations, the following familiar form of the equations of motion (in absence of damping) is obtained as:

$$\mathbf{M}\ddot{\mathbf{u}} + \mathbf{K}(\mathbf{u})\mathbf{u} = \mathbf{F}(\mathbf{u}) \qquad [VI.12]$$

$$\mathbf{u}(0) = \mathbf{u}_0 \text{ and } \dot{\mathbf{u}}(0) = \dot{\mathbf{u}}_0 \qquad [VI.13]$$

where $\mathbf{M}$ is the assembled mass matrix, $\mathbf{K}$ the assembled stiffness matrix and $\mathbf{F}$ the assembled force vector on the nodes. The superscript " e " refers to the matrix at the element level.

$$\mathbf{M} = \prod_{e=1}^{n^e} \mathbf{M}^e, \quad \mathbf{K} = \prod_{e=1}^{n^e} \mathbf{K}^e, \quad \mathbf{F} = \prod_{e=1}^{n^e} \mathbf{F}^e \qquad [VI.14]$$

VI.4 The solution method for explicit time integration

In explicit FE methods, the central difference method is among the most popular methods used. This method is named from the central difference operator used in the integration of the velocity and acceleration. The following developments will be presented in the context of rate-independent materials and Lagrangean meshes. The time of the simulation t ($0 \le t \le T$) is subdivided into time intervals or time steps, Δt^n (n=1 to n_{TS}, where n_{TS} is the number of time steps). T is the time at the end of the simulation. Let $\mathbf{u}^n$ be the matrix of nodal displacements at time step n. In general, the time step needs to be adjusted during the analysis. Let us define time increments n and $n+\frac{1}{2}$ by the following relationships:

$$\Delta t^{n+\frac{1}{2}} = t^{n+1} - t^n,\ \Delta t^n = t^{n+\frac{1}{2}} - t^{n-\frac{1}{2}} \text{ and } t^{n+\frac{1}{2}} = \frac{1}{2}(t^n + t^{n+1}) \qquad [VI.15]$$

The velocity is then expressed as:

$$\dot{\mathbf{u}}^{n+\frac{1}{2}} = \frac{1}{\Delta t^{n+\frac{1}{2}}}(\mathbf{u}^{n+1}-\mathbf{u}^n) \text{ or } \mathbf{u}^{n+1} = \mathbf{u}^n + \Delta t^{n+\frac{1}{2}}\dot{\mathbf{u}}^{n+\frac{1}{2}} \qquad [VI.16]$$

and the acceleration as:

$$\ddot{\mathbf{u}}^n = \frac{1}{\Delta t^n}(\dot{\mathbf{u}}^{n+\frac{1}{2}}-\dot{\mathbf{u}}^{n-\frac{1}{2}}) \text{ or } \dot{\mathbf{u}}^{n+\frac{1}{2}} = \dot{\mathbf{u}}^{n-\frac{1}{2}} + \Delta t^n\ddot{\mathbf{u}}^n \qquad [VI.17]$$

The explicit solution process advances along the time axis, t, along which the velocities are discretised at half time intervals, $t^{n-1/2}$, $t^{n+1/2}$ and the displacements and accelerations are discretised at full time intervals t^{n-1}, t^{n+1} (Bathe, 1982). By combining Equations [VI.16] and [VI.17], the acceleration can be written in terms of displacement:

$$\ddot{\mathbf{u}}^n = \frac{\Delta t^{n-\frac{1}{2}}(\mathbf{u}^{n+1}-\mathbf{u}^n) - \Delta t^{n+\frac{1}{2}}(\mathbf{u}^n-\mathbf{u}^{n-1})}{\Delta t^n \Delta t^{n-\frac{1}{2}} \Delta t^{n+\frac{1}{2}}} \qquad [VI.18]$$

If equation [VI.12] is now considered at the time step n, and written in terms of internal $\mathbf{f}^{int}(\mathbf{u}^n)$ and external forces $\mathbf{f}^{ext}(\mathbf{u}^n)$, the following expression is obtained:

$$\mathbf{M}\ddot{\mathbf{u}}^n = \mathbf{f}^n = \mathbf{f}^{ext}(\mathbf{u}^n, t^n) - \mathbf{f}^{int}(\mathbf{u}^n) \qquad [VI.19]$$

subject to

$$\mathbf{g}_i(\mathbf{u}^n) = 0,\ i = 1 \text{ to } n_c \qquad [VI.20]$$

where [VI.20] is a generalised representation of the n_c displacement boundary conditions and other constraints (linear and nonlinear algebraic functions of the nodal displacements) on the model. If the contraint involves integral or differential relationships, such as dependence on the velocities, it can be put in the above form by using difference equations or a numerical approximation of the integral. The nodal displacements determine the strains, which in turn determine the stresses and hence the nodal internal forces. Substituting equation [VI.19] into [VI.17] leads to:

$$\dot{\mathbf{u}}^{n+\frac{1}{2}} = \Delta t^n \mathbf{M}^{-1}\mathbf{f}^n + \dot{\mathbf{u}}^{n-\frac{1}{2}} \qquad [VI.21]$$

which gives the updating expression for the velocity. At any time step n, the displacements are known. The inversion of the mass matrix $\mathbf{M}$ (time independent in the context of a Lagrangean mesh) is trivial if $\mathbf{M}$ is diagonal. Combining the second expresion of [VI.16] and equation [VI.21] allows the dermination of the displacement at the time step n+1, $\mathbf{u}^{n+1}$. If $\mathbf{M}$ is diagonal (general case) the update of the nodal velocities and nodal displacements can be accomplished without solving any system of equations. This important characteristic constitutes a considerable advantage of explicit solution methods over implicit methods. However, the price to pay for the simplicity of the explicit method is the conditional requirement put on the size of the time step. In fact, if the time step exceeds a critical value Δt_c , the solution may propagate unboundedly and will make the analysis diverge. Δt_c, often called the " *stable time step* ", depends on the dimension of the elements and the mechanical properties assigned to these elements. For low order elements the critical time step for linear response is given by:

$$\Delta t_c = \min \frac{l_e}{c_e} \qquad [VI.22]$$

where l_e is a characteristic length of element e and c_e is the sound wave speed within element e. Thus the critical time step decreases with mesh refinement and increasing stiffness of the material. For nonlinear analyses, the calculation of the wave speed is based on the values of the maximum tangent moduli. When a material is fully incompressible, the sound wave speed is infinite and the critical time step is theoretically equals to zero. This is the reason why full incompressibility ($\nu = 0.5$) is never enforced exactly.

If the explicit computation is pursued to the point when steady-state conditions are reached, i.e. until: $\ddot{\mathbf{u}} = \dot{\mathbf{u}} = 0$, the solution to a nonlinear static problem is obtained. This type of technique is frequently efficient and has been applied successfully in the context of finite differences under the name of *dynamic relaxation* (Zienkiewicz and Lhöner, 1985).

VI.5 Enforcement of the incompressibility constraint

A penalty function $g(I_3)$ is used to enforce the kinematic condition $J = I_3 = 1$. g is defined such that $g(I_3) = 0$ when I_3 is equal to 1:

$$g(I_3) = A\left(\frac{1}{I_3^2} - 1\right) + B\left(I_3 - 1\right)^2 \qquad \text{[VI.23]}$$

where A and B are scalar coefficients to be determined. A provides equilibrium at zero strain and coefficient B is a penalty factor. If the material tends to be incompressible, the value of I_3 tends towards 1, and the penalty factor, B, tends towards infinity. Investigating equation [V.84] for a state of vanishing strains, reveals an explicit dependency of A on C_1 and C_2 as follows:

$$A = \frac{1}{2}C_1 + C_2 \qquad \text{[VI.24]}$$

VI.5.1 Equivalent isotropic elastic constants

For small strains the material can be considered isotropic linear elastic with equivalent Hooke's matrix coefficients. Expanding equation [V.75] for A^{m}_{1111} and A^{m}_{1122} of zero strain leads to the equivalent Poisson's ratio:

$$\nu = \frac{2C_1 + 5C_2 + 2B}{5C_1 + 11C_2 + 4B} = \frac{A^{m}_{1122}}{A^{m}_{1111}} \qquad \text{[VI.25]}$$

The value of the equivalent Poisson's ratio tends towards ½ (incompressibility limit) as the value of the penalty factor, B, tends towards infinity. At zero strain, Equation [V.75] allows the determination of B:

$$B = \frac{C_1(5\nu - 2) + C_2(11\nu - 5)}{2(1 - 2\nu)} \qquad \text{[VI.26]}$$

The corresponding equivalent Young's modulus, E and bulk modulus, κ at zero strain become:

$$E = 4(1+\nu)(C_1 + C_2) \quad \text{and} \quad E = 6\left(C_1 + C_2\right) \quad \text{for } \nu = \frac{1}{2} \qquad \text{[VI.27]}$$

$$\kappa = \frac{4}{3}\left(\frac{1+\nu}{1-2\nu}\right)\left(C_1 + C_2\right) \quad \text{and} \quad \kappa = \infty \quad \text{for } \nu = \frac{1}{2} \qquad \text{[VI.28]}$$

The corresponding equivalent Lamé's modulus, $\lambda + 2G$, becomes at zero strain:

$$A^{m}_{1111} = \lambda + 2G = \frac{4(1-\nu)}{1-2\nu}\left(C_1 + C_2\right) \quad \text{and} \quad A^{m}_{1111} = \infty \quad \text{for } \nu = \frac{1}{2} \qquad \text{[VI.29]}$$

and the equivalent shear modulus G at zero strain is:

$$G = 2\left(C_1 + C_2\right) \qquad \text{[VI.30]}$$

VI.6 Numerical tests and analytical solutions

Numerical tests were performed to ensure a proper finite element implementation of the incompressible transversely isotropic hyperelastic material model (described in section V.9) into PAM-CRASH^{TM}. An extension of the Mooney-Rivlin model was used under the form of the following strain energy function:

$$\Psi = C_1\left(I_1 - 3\right) + C_2\left(I_2 - 3\right) + C_3\left(e^{(I_4-1)} - I_4\right) \qquad \text{[VI.31]}$$

This form has an exponential behaviour in the fibre direction, one of the characteristics seen in most soft tissues (Weiss *et al.*, 1996). The FE model was validated by comparing the results of one-element tests for uniaxial, strip biaxial, equibiaxial and shear tests to the analytical solutions obtained for homogeneous deformations. In each of these cases, the computations were performed with two types of 8-noded hexahedral element: *reduced integration with hourglass control* and *selective reduced integration* formulations but as no difference was found in the results, a single graph is presented for each loading case. The same arbitrary material properties were used for the four analyses: C_1 = 10 MPa, C_2 = 10 MPa, C_3 = 100 MPa and ρ = 1000 kg/m3. The finite element was a unit-edge cube aligned with the global coordinate system where the unit vector was coincident with the director vector of the direction z. The element was stretched to 75 % strain for uniaxial and biaxial tests whereas it underwent shear loading to 50 % shear strain in the case of pure shear test. In all the tests the assumption of nearly incompressibility was made: i.e. $I_3 \simeq 1$. The Poisson's ratio chosen was ν = 0.49999: "nearly incompressible".

VI.6.1 Uniaxial extension in the fibre direction

The deformation gradient is:

$$\mathbf{F} = \begin{bmatrix} \frac{1}{\sqrt{\lambda}} & 0 & 0 \\ 0 & \frac{1}{\sqrt{\lambda}} & 0 \\ 0 & 0 & \lambda \end{bmatrix} \qquad \text{[VI.32]}$$

VI.6.1.1 Cauchy stresses

The Cauchy stresses versus the stretch in the fibre direction are plotted on Figure VI.1. The analytical solutions are given by:

$$\sigma_{xx} = \sigma_{yy} = 0 \qquad \text{[VI.33]}$$

$$\sigma_{zz} = 2\left\{\left[C_1 + C_2\left(\lambda^2 + \frac{2}{\lambda}\right)\right]\left[\lambda^2 - \frac{1}{\lambda}\right] - C_2\left(\lambda^4 + \frac{2}{\lambda^2}\right) + \lambda^2 C_3\left[e^{(\lambda^2-1)} - 1\right]\right\} \qquad \text{[VI.34]}$$

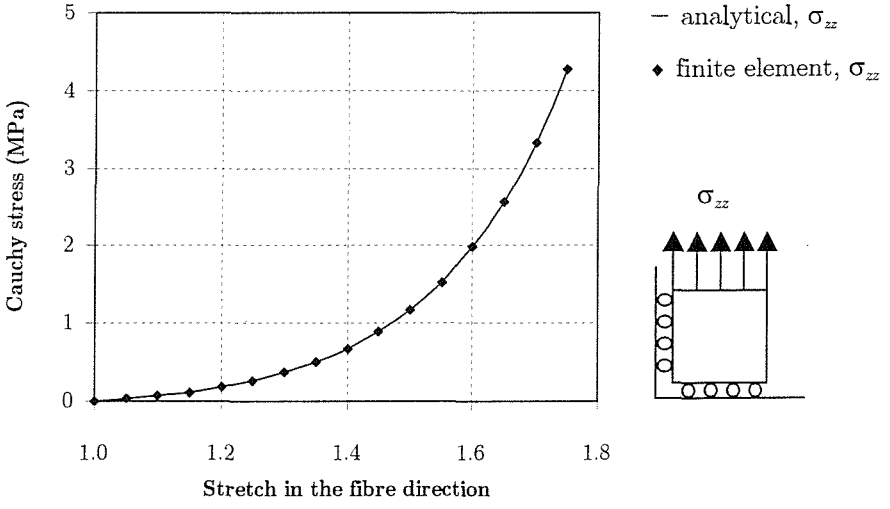

Figure VI.1 – Uniaxial extension test in the fibre direction. Comparison between analytical and finite element solutions for stress in the fibre direction.

VI.6.2 Strip biaxial extension

The deformation gradient is:

$$\mathbf{F} = \begin{bmatrix} \frac{1}{\lambda} & 0 & 0 \\ 0 & 1 & 0 \\ 0 & 0 & \lambda \end{bmatrix} \qquad [VI.35]$$

VI.6.2.1 Cauchy stresses

The Cauchy stresses versus the stretch in the fibre direction are plotted on Figure VI.2. The analytical solutions are given by:

$$\sigma_{xx} = 0 \qquad [VI.36]$$

$$\sigma_{yy} = 2\left\{\left[C_1 + C_2\left(\lambda^2 + \frac{1}{\lambda} + 1\right)\right]\left[1 - \frac{1}{\lambda^2}\right] - C_2\left(1 - \frac{1}{\lambda^4}\right)\right\} \qquad [VI.37]$$

$$\sigma_{zz} = 2\left\{\left[C_1 + C_2\left(\lambda^2 + \frac{1}{\lambda} + 1\right)\right]\left[\lambda^2 - \frac{1}{\lambda^2}\right] - C_2\left(\lambda^4 + \frac{2}{\lambda^4}\right) + \lambda^2 C_3\left[e^{(\lambda^2 - 1)} - 1\right]\right\} \qquad [VI.38]$$

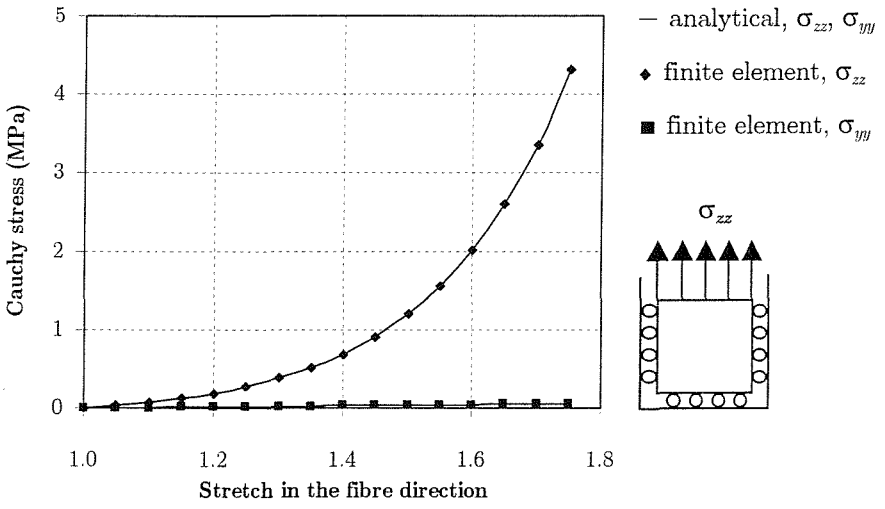

Figure VI.2 – Strip biaxial extension test in the fibre direction. Comparison between analytical and finite element solutions for stress in the fibre direction and in the the direction transverse to the fibre.

VI.6.3 Equibiaxial extension

The deformation gradient is:

$$\mathbf{F} = \begin{bmatrix} \frac{1}{\lambda^2} & 0 & 0 \\ 0 & \lambda & 0 \\ 0 & 0 & \lambda \end{bmatrix} \qquad [VI.39]$$

VI.6.3.1 Cauchy stresses

The Cauchy stresses versus the stretch in the fibre direction are plotted on Figure VI.3. The analytical solutions are given by:

$$\sigma_{xx} = 0 \qquad [VI.40]$$

$$\sigma_{yy} = 2\left\{\left[C_1 + C_2\left(2\lambda^2 + \frac{1}{\lambda^4}\right)\right]\left[\lambda^2 - \frac{1}{\lambda^2}\right] - C_2\left(\lambda^4 + \frac{2}{\lambda^4}\right)\right\} \qquad [VI.41]$$

$$\sigma_{zz} = 2\left\{\left[C_1 + C_2\left(2\lambda^2 + \frac{1}{\lambda^4}\right)\right]\left[\lambda^2 - \frac{1}{\lambda^2}\right] - C_2\left(\lambda^4 + \frac{2}{\lambda^4}\right) + \lambda^2 C_3\left[e^{(\lambda^2-1)} - 1\right]\right\} \qquad [VI.42]$$

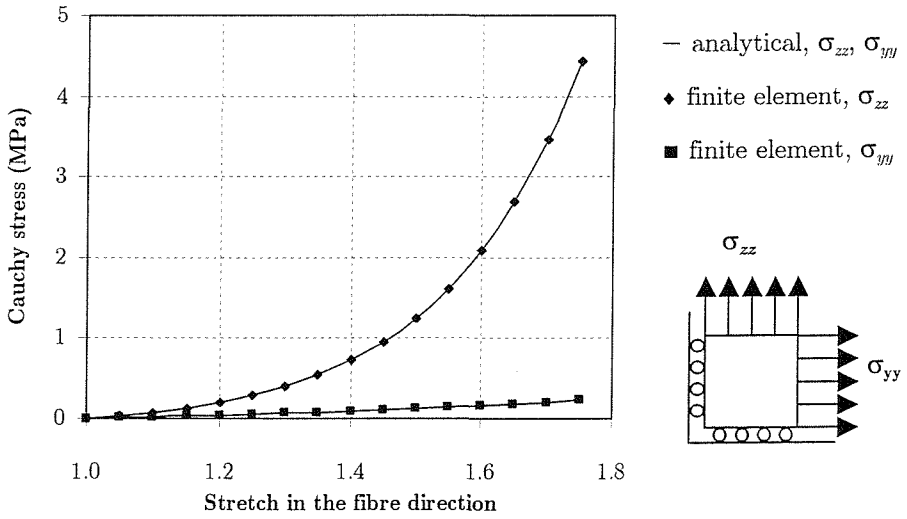

Figure VI.3– Equibiaxial extension test in the fibre direction. Comparison between analytical and finite element solutions for stress in the fibre direction and in the direction transverse to the fibre.

VI.6.4 Pure shear deformation γ in the plane of isotropy

The deformation gradient is:

$$\mathbf{F} = \begin{bmatrix} 1 & \gamma & 0 \\ 0 & 1 & 0 \\ 0 & 0 & 1 \end{bmatrix} \qquad \text{[VI.43]}$$

VI.6.4.1 Second Piola-Kirchhoff stresses

The analytical solutions are calculated as below:

$$S_{zz} = 0 \qquad \text{[VI.44]}$$

$$S_{xx} = -2\gamma^2\left[C_1 + C_2\left(\gamma^2 + 2\right)\right] \qquad \text{[VI.45]}$$

$$S_{yy} = -2C_2\gamma^2 \qquad \text{[VI.46]}$$

$$S_{xy} = 2\gamma\left[C_1 + C_2\left(\gamma^2 + 1\right)\right] \qquad \text{[VI.47]}$$

VI.6.4.2 Cauchy stresses

The expressions of the Cauchy stresses are obtained from the second Piola-Kirchhoff stresses.

$$\sigma_{xx} = S_{xx} + 2\gamma S_{xy} + \gamma^2 S_{yy} \qquad \text{[VI.48]}$$

$$\sigma_{yy} = S_{yy} \qquad \text{[VI.49]}$$

$$\sigma_{xy} = S_{xy} + \gamma S_{yy} \qquad \text{[VI.50]}$$

Finally, one obtains the following expressions for the Cauchy stresses (Figure VI.4):

$$\sigma_{xx} = 2\gamma^2\left(C_1 - C_2\gamma^2\right) \qquad \text{[VI.51]}$$

$$\sigma_{yy} = -2C_1\gamma^2 \qquad \text{[VI.52]}$$

$$\sigma_{xy} = 2\left(C_1 + C_2\right)\gamma \qquad \text{[VI.53]}$$

It is worth outlining that, despite the fact that the material behaviour is nonlinear, the shear stress is a linear function of the shear strain.

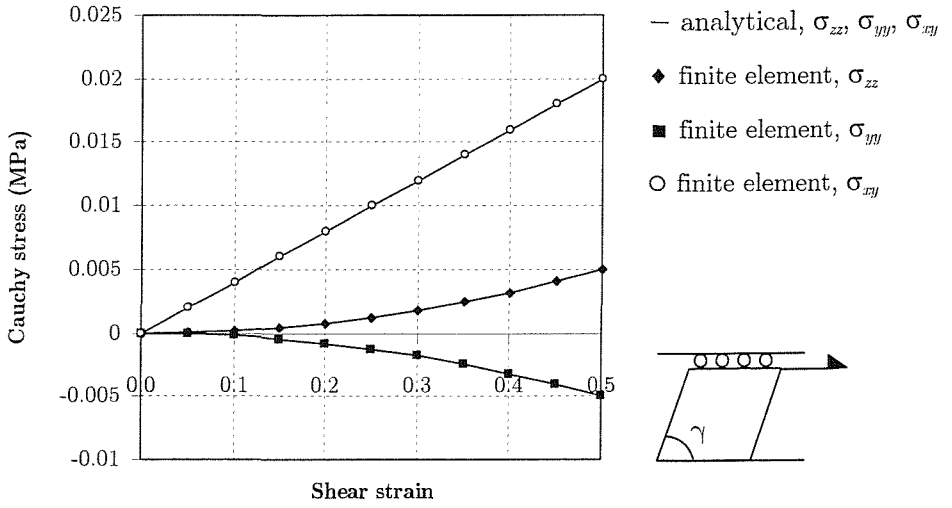

Figure VI.4 – Pure shear test in the XY plane. Comparison between analytical and finite element solutions for nonzero stresses.

VI.7 Concluding remarks

In this chapter, the finite element implementation of an incompressible transversely isotropic hyperelastic constitutive law for soft connective tissues was presented. The material model was tested for a simple finite element model under four different loading conditions: uniaxial stretch in the direction of the fibres, strip biaxial extension, equibiaxial extension and pure shear. The excellent agreement between finite element and analytical solutions for homogeneous states of deformation demonstrated the proper implementation of the finite element biological material model into the explicit code PAM-CRASH™ and the accurate enforcement of the constraint of incompressibility. This programming and numerical testing phase has provided a robust and efficient numerical tool to study the biomechanics of soft tissues.

Nota Bene

The programming of the new material model into PAM-CRASH™ (in Fortran 77) has required, in addition to the development of a dedicated material subroutine, substantial modifications of other subroutines within the general code in order to accommodate specific state variables and especially those related to the definition of the fibre direction at the element level.

Chapter VII

Sensitivity analyses of the incompressible transversely isotropic finite element material model

Equation Section 7

Chapter VI discussed the FE implementation of an incompressible transversely isotropic hyperelastic constitutive law into an explicit FE code. An excellent match between results of the FE analyses and analytical solutions for homogeneous deformation modes demonstrated the correct FE implementation of the material model. Although an essential prerequisite, this aspect is not sufficient to have confidence in the validity of the results obtained from FE analyses performed under other conditions. Other parameters may have a significant influence on the results: this includes the choice of element formulation, the density of the mesh and the type of boundary conditions. In this chapter, a series of finite element analyses was performed in order to test the accuracy of implemented material model in terms of the choice of the hourglass mode stabilisation methods for 8-noded hexahedral solid elements (reduced integration scheme with stiffness or viscosity hourglass control), validity of the quasi-static process hypothesis which is made when a physical process is simulated for a time scale much lower than its natural time scale, mesh density and boundary conditions. Computational time is an important aspect to consider in any FE computation. Indeed, in explicit FE analyses, there is conditional stability put on the size of the time step which is itself directly related to the characteristic dimension of the smallest element of the mesh. Refining the mesh and keeping the same number of elements has the effect of reducing element sizes and so the time step. This aspect is also investigated in this chapter. As is relevant for the analysis of biological soft tissues, influence of an initial stress field on stress and strain patterns is also studied for various loading conditions. Prior to this, a description of the methodology used for the FE implementation of the pre-stressing capability is presented.

VII.1 Objectives and structure of Chapter VII

The main objective of this chapter is to examine the major sources of error that can arise in the explicit FE computations involving the incompressible transversely isotropic FE material model. The choice of the preferred hourglass stabilisation method is made and discussed in section VII.2. Section VII.3 briefly discusses the conditions necessary to obtain a quasi-static solution of a mechanical problem simulated dynamically through an explicit FE code and presents numerical results regarding the convergence of a dynamic solution towards a quasi-static one. In section VII.4, influence of mesh density on the calculated displacements, stresses and resultant forces is evaluated for four different loading conditions. As residual stresses are an important issue in soft tissue modelling, influence of this factor on displacements, stresses and resultant forces is determined for three sets of boundary conditions (section VII.5). Finally, conclusions and recommendations to this chapter are drawn in section VII.6.

VII.2 Uniform reduced integration (URI) and hourglass mode stabilisation

The incompressible transversely isotropic hyperelastic material model discussed in Chapters V and VI, has been implemented into the explicit finite element code PAM-CRASH^{TM} for 8-noded hexahedral solid elements, often called "brick elements". For this element, two integration formulations are available: *uniform reduced integration* and *generalised selective reduced integration.*

In the URI formulation, the various integral quantities of the finite element equations are integrated using a single Gauss point within the element. This is advantageous as a single integration point reduces considerably the computational cost when compared to a selective reduced integration scheme (one-point integration for volumetric stresses and two-point quadrature in each direction for the deviatoric stresses) because it involves a single evaluation of the equation of state instead of eight (for three-dimensional problems). In incompressible finite element analyses, the use of uniform reduced integrated solid elements prevents, in the general case, the appearance of the so-called "locking" resulting for overconstrained conditions (see Chapter VI). However, the drawback of the URI is that it can lead to spurious deformation modes which can be stressless and then produce zero energy modes. If uncontrolled, these *hourglass modes* can propagate unboundedly within the solution process, leading to failure of convergence or pollution of the displacement field.

Flanagan and Belytschko (Belytschko, 1983; Flanagan and Belytschko, 1981) proposed two different methods to control hourglass modes. The first one is based on a *viscous control scheme* and the other one is based on a *stiffness control scheme.*

The hourglass effect is controlled by adding artificial stiffness (stiffness method) or damping (viscous method) along the hourglass modes which, in return, produce anti-hourglass forces that resist hourglass modes. The implementation of either of the two methods leads to orthogonality of the hourglass modes to the linear velocity field for arbitrary solid element shapes. Characteristics of the two methods are compared in Table VII.1.

Several tests were performed in order to assess the two methods of hourglass control. As outlined by Flanagan and Belystchko (Belytschko, 1983; Flanagan and Belytschko, 1981), the stiffness method leads to better results in terms of mesh stability and accuracy of the solution, provided that a small stiffness parameter is used (typically $\kappa = 0.01$). The sensitivity of the stiffness parameter κ on the mesh stability was also evaluated and small values of κ were found sufficient to preserve the solution accuracy whilst achieving mesh stability. For the sake of brevity and to concentrate on the essential aspects of the present research work, these sensitivity analyses are not reported in the present thesis.

VISCOUS Control	
Advantages	▪ Heavy damping affects slightly low frequency modes. ▪ No history variables need to be stored (i.e.: less memory per element).
Disadvantages	▪ Stability is not guaranteed by damping a stress-free global mode. Anti-hourglass viscosity slows down distortion but does not stabilize the solution. ▪ Mesh distortion is permanent in the absence of restoring forces. ▪ The explicit time step staility is lowered substantially by damping.
STIFFNESS Control	
Advantages	▪ Mesh distortion is controlled by restoring forces. Stability of the mesh is controlled. ▪ The explicit stable time step is not affected if κ (stiffness) remains lower than 1.
Disadvantages	▪ Large ratio κ affects the solution ("element locking"). ▪ History variables are required (i.e.: more memory per element).

Table VII.1 – Comparison of the principal features of the viscosity and stifness based hourglass control methods.

Theoretically, for a hyperelastic material, the work done during a closed path must be zero. However, it is not the case when using URI elements with hourglass control because this numerical procedure introduces residual forces at each time step that can accumulate significantly in the most severe cases of explicit analyses (excessive number of time steps). This is the reason why it is important to ensure that the hourglass energy (work produced by antihourglass mode forces) remains small when compared to the internal energy of the system.

VII.3 Quasi-static processes simulated by dynamics analyses. Practical considerations

The explicit base FE method was originally designed to simulate high-speed impact events where highly nonlinear transient phenomena occur (crash analysis, high-speed impact on aerospace structures to name a few). The method solves equations for a state of dynamic equilibrium and out-of-balance forces are propagated as stress waves between neighbouring elements. In general, time steps required for a stable analysis are quite small (order of the μs). Using explicit dynamic analyses to model quasi-static or low frequency events requires special considerations. Modelling a quasi-static process in its whole temporal period would require generally millions of cycles and so, is computationally expensive. Artificially increasing the speed of the process for an explicit simulation is necessary in order to obtain a computationally viable solution. As the speed of the process is increased, a state of static equilibrium evolves into a state of dynamic equilibrium and inertia forces become more dominant. The objective is therefore to obtain a solution in the shortest time possible with inertial forces remaining negligible. To obtain a quasi-static solution it is important to apply loads as gradually as possible in order to avoid undesirable effects, such as propagation of stress waves. The energy balance of the modelled system gives information about the accuracy of the quasi-static hypothesis. As a general rule, the kinetic energy of the body considered should not exceed a small fraction of its internal energy throughout the majority of the quasi-static event, typically in the order of 5 - 10 %. Moreover, in a quasi-static non-dissipative simulation involving a hyperelastic material, the work applied by the external forces to deform the hyperelastic body equals its internal energy. Special care should be taken if the material is rate-sensitive (not the case of the incompressible transversely isotropic hypereleastic material described in Chapters V-VI). In fact, as the speed of the event simulated increases, the material strain rates are artificially higher by the same factor as that applied to increase the loading rate. This can lead to erroneous solutions.

In order to verify the quasi-static hypothesis that was made for the explicit FE computations, a series of seven FE analyses was devised. All the characteristics of the computations (model, mesh, mechanical properties, boundary conditions are defined later in section VII.4.2) were identical with the exception of the physical time scale of the analysis. The physical time scales chosen were 1 s, 500 ms, 100 ms, 50 ms, 10 ms, 5 ms and 1 ms. The loading case consisted of a 15 % extension in the fibre direction. The first analysis (1 s) was assumed to have a quasi-static mechanical response and chosen as a reference to compare the other ones. In addition to a global inspection concerning the deformed shape and the stress distribution in order to perform a qualitative check of the solutions, quantitative data were output.

Figure VII.1 presents the relative errors in the three calculated maximum principal stresses when the solutions are compared to those of the 1 s analysis. The mesh chosen was that of model 5 defined in Table VII.3. Figure VII.1 shows clearly that a physical time of 10 ms (adopted for the FE analyses described in the next sections) for the explicit FE analyses provides results of a quasi-static solution with an accuracy greater than 99.5 %. It is worthy to note that a 5ms analysis still provides acceptable results with an error lower than 3 %.

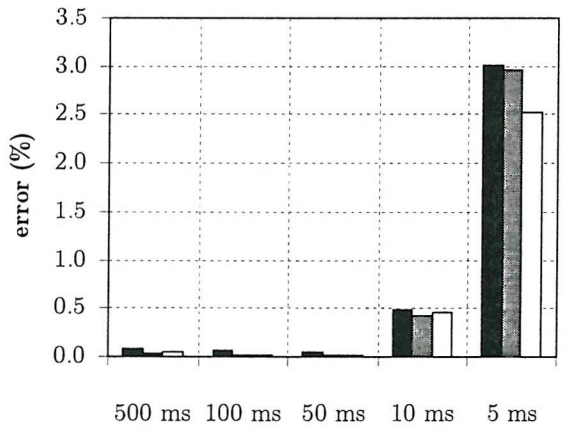

Figure VII.1 – The bar chart reprsents the relative error made in the FE calculations of the three maximum principal stresses by varying the time of the analysis. The reference values for stresses correspond to those obtained for a total analysis time of 1000 ms when the model undergoes 15 % extension. For the 1 ms analysis the relative errors for the three maximum principal stresses were respectively 23.75, 23.41 and 31.29 %.

VII.4 Influence of the mesh density

VII.4.1 Effects of mesh refinement in explicit FE analyses

For a three-dimensional problem, refining the mesh by a factor of two in each direction, increases the run time by a factor of 16 (explicit analysis). In fact, the refinement generates eight times the number of elements whilst the stable time step is approximately halved (decreasing the element dimension reduces the stable time step). It is worthwhile to note that in the case of an implicit analysis, the implicit run time is increased by a factor of 128 which corresponds to the degrees of freedom ratio (2^3) times the square of the wavefront ratio [$(2^2)^2$]. Explicit FE analyses have significant economic advantages as the model size grows. Refining the mesh whilst keeping the same number of elements typically occurs when it is needed to analyse localised mechanical responses (stress states around a hole or a notch, contact...). In this case, the cost of an implicit analysis is exactly the same as prior to refinement whereas the run time of an explicit analysis is increased due to a decrease in time step size.

VII.4.2 Geometric model and finite element meshes

A series of finite element tests was designed in order to assess the convergence of a particular solid model when meshed with different sized elements. The solid model was assumed to represent an idealised geometry which could correspond to a long and flat human ligament (eg a collateral ligament) (Figure VII.2). The dimension of the model and its mechanical properties are given in Table VII.2. The constitutive law chosen for the material model was derived from a strain energy function Ψ of the following form (Equation [V.82]):

$$\Psi = C_1\left(I_1 - 3\right) + C_2\left(I_2 - 3\right) + f(\lambda) \qquad \text{[VII.1]}$$

such that:

$$\frac{\partial f}{\partial \lambda} = 0 \quad \text{if } \lambda < 1; \quad \frac{\partial f}{\partial \lambda} = \frac{C_3\left(e^{(\lambda-1)} - 1\right)}{\lambda} \quad \text{if } \lambda \geq 1 \qquad \text{[VII.2]}$$

Dimensions	**length**: 40 mm	**width**: 8 mm	**depth**: 2 mm	
Mechanical properties	$C_1 = 1$ MPa	$C_2 = 1$ MPa	$C_3 = 100$ MPa	*density:* 900 kg/m^3

Table VII.2 – Dimensions and mechanical properties of the finite element model.

The mechanical properties were chosen to represent the typical stiffer mechanical response of soft connective tissues when loaded along their fibre directions. As C_3 scales the stress for the nonlinear response of the fibres and C_1 and C_2 characterise the stiffness of the matrix, an arbitrary factor of 100 (C_3/C_α, $\alpha = 1, 2$) was thought to be appropriate. Please note that the material coefficients are arbitrary and that, in order to restrict possible numerical singularities, the linear response of the fibre (Equation V.83.c) after a certain value of stretch (λ^*) has been removed. Eight mesh densities were chosen and created by varying the size of the elements. Characteristics of the various meshes are listed in Table VII.3.

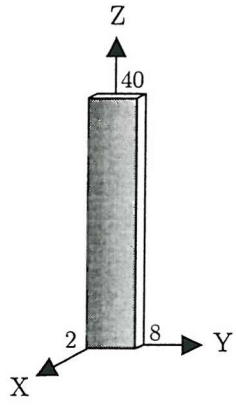

Figure VII.2 – Geometrical model used for the FE analyses. The principal directions of the model are aligned with the orthonormal axes (X, Y, Z) of the reference coordinate frame. The unit vector defining the fibre orientation is the one defining the third Cartesian direction (Z). Dimensions are given in mm.

MESH	(l x w x d) [mm]	NE	NN
model 1	10 x 8 x 2	4	20
model 2	5 x 4 x 1	32	81
model 3	5 x 2 x 1	128	225
model 4	2.5 x 2 x 1	256	425
model 5	2.5 x 1 x 1	512	765
model 6	1.25 x 1 x 1	928	1350
model 7	1.25 x 0.5 x 1	1856	2550
model 8	1.053 x 0.5 x 1	2368	3230

Table VII.3 – Characteristics of the eight meshes used in the mesh density analyses. [l, w, d stand respectively for the length, the width and the depth of the element while NE and NN represent respectively the number of elements and the number of nodes].

VII.4.3 Loading conditions

For each of the eight FE models built, four loading conditions were considered. Before going further, it is convenient to introduce additional notations to make easier the characterisation of the boundary conditions. Five faces have been defined on the model by specifying a fixed coordinate (X, Y or Z) as shown in Figure VII.2. All the nodes belonging to a face will be submitted to a particular set of boundary conditions. Here are the definitions of the faces:

Face **T** (Z = 40) Face **B** (Z = 0) Face **L** (Y = 0) Face **R** (Y = 8) Face **F** (X = 0)

Stretching, compression in the fibre directions, shearing in the plane of isotropy of the material are conditions that are likely to be found in the natural physiological conditions a knee ligament can be subjected to. An additional equibiaxial test is performed in order to assess the response of the material in its plane of isotropy and along its preferred mechanical direction (fibre direction). In the subsequent paragraphs, the expressions " face i " and " nodes belonging to face i " will be used synonymously. For each of the analyses corresponding to the four loading cases the time of the analysis was fixed at t = 10 ms (see section VII.3). This duration was used because it generates negligible inertial effects in the model and offers a good compromise in terms of computational time and accuracy of the quasi-static solution. This was also verified by checking ratio of kinetic energy over internal energy which was found to be extremely low (lower than 1 %).

VII.4.3.1 Extension in the fibre directions (Case 1)

Face B is restrained in the three directions whilst face T is restrained in the X and Y directions and undergoes a displacement corresponding to a stretch of 15 % along the Z direction. The nodes in both faces were restrained in the X and Y directions because it corresponds to the physical case of a ligament inserted into bone, where no significant deformation is allowed at the insertion site.

VII.4.3.2 Compression in the fibre directions (Case 2)

Face B is restrained in the three directions whilst face T is restrained in the X and Y directions and undergoes a displacement corresponding to a compression of 15 % along the Z direction. This condition is likely to occur when the two insertions sites of a ligament get closer in, for example, a flexion of the knee. As a simple analogy one can consider a piece of string held tight at its two extremities. When the two extremities are moved towards each other, buckling of the piece of string will be produced.

VII.4.3.3 Pure shear in the plane of isotropy of the material (Case 3)

Face L is restrained in the three directions whilst face R is restrained in the Y direction. Faces B and T are not allowed to displace in the Z direction. Pure shear is produced when face R undergoes a positive displacement of 4 mm in the X direction. Shearing forces within a ligament can be produced when the insertion areas of the ligament undergo a relative rotational motion or when a ligament warps around a bony structure and slides over it.

VII.4.3.4 Equibiaxial extension in the fibre and Y directions (Case 4)

Face L is restrained in the Y directions whilst face B is restrained in the Z direction and face F is fixed in the X direction. Face T and R undergo a displacement corresponding, respectively, to a stretch of 15 % along the Z direction and Y directions. A pure equibiaxial extension of a ligamentous structure is not very likely to occur in normal conditions but could be produced in severe injury cases (particularly motor vehicle accidents).

VII.4.4 Finite element analyses and results

Finite element analyses were performed on a PC built around a Pentium® III (600 MHz) processor and 512 Megabytes of RAM. A series of tests was performed for the eight meshes by using URI solid elements with stiffness hourglass control ($\kappa = 0.01$). As it is often the case in FE analyses, a large amount of data was produced from the computations and it is the task of the analyst to choose the most relevant for the problems considered. Resultant forces within ligaments are very important when considering clinical aspects. A surgeon generally needs to apply a specific tension when performing ligament reconstruction. Moreover, and more importantly, the knee joint is essentially a force-driven mechanical system where the motions of bony structures are primarily constrained by the ligamentous tissues. The knowledge of the forces present within the knee ligaments is essential for understanding the general kinematics of joints. Maximum stresses give an idea concerning the tolerance of a ligament to specific loading conditions. As the FE analyses were performed with using URI solid elements with hourglass control, hourglass energy is an important parameter to assess. However, given that this quantity was negligible in all cases it was decided not to present it in the results. Duration of explicit analyses is conditioned by the biggest stable time step, which is directly linked to the size of the smallest element of the mesh. The stable time step is therefore affected by mesh refinement and its variation during an analysis is important to consider.

VII.4.4.1 Time related aspects of the FE analysis

These basic aspects of the FE analyses, namely the range of variation of the stable time step, the number of time iterations and the total duration of the computation are given in Appendix C. These quantities are obviously of particular importance because they dictate the applicability of an explicit FE model with regards to the computational cost. Associated relevant ratios between these quantities also give an immediate overview of the characteristics of the FE analyses. As mentioned earlier in section VII.2, for all the FE analyses the hourglass energy was monitored in order to ensure that its proportion with respect to the total energy was sufficiently low (in the order of 0.5 %). Otherwise, an important error (of the same magnitude as the ratio discussed above) affects directly the results. The ratios of the CPU time used for the analysis of Model 2 to Model 8 as compared to Model 1 were comparable in the four different loading conditions. The variations of the total time of the analyses are easily explained by the fluctuations of the stable time step along the computations, themselves dictated by the deformations of the elements of the mesh.

VII.4.4.2 Results of interest

For each of the loading conditions and meshes tested, it was decided to record the maximum values of the components of the stress tensor at equilibrium. The locations of these extrema were appropriately checked to insure reliable comparisons between the different mesh densities. A result of interest is also the amount of contraction appearing at the middle section of the model (Z = 20) when it is stretched at its both ends. It is worth emphasising that the contraction in the X and Y planes is linked to the extension in the Z direction by the incompressibility constraint (the mutual product of the principal stretches, $\lambda_1 \lambda_2 \lambda_3$, is equal to one). Reaction forces were assessed for each case at the nodes where displacements are constrained in one direction (X, Y or Z). For case 1 and 2 , the reaction force is evaluated on face B (Z = 0) and face L for case 3. For equibiaxial extension conditions, two reaction forces were considered: the one on face B generated by stretch along Z and the other one on face L, produced by extension in the Y direction.

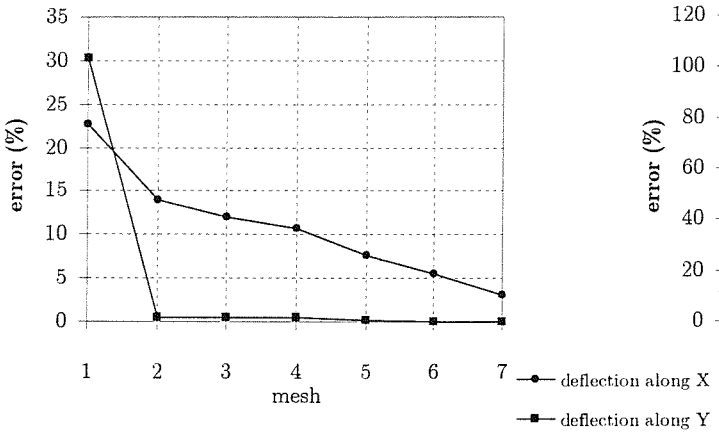

Figure VII.3 – Percentage error variation for the maximum deflection obtained at the central section (Z = 20) of the model in the X and Y directions in CASE 1 (15 % extension along the fibre direction). For mesh 8, maximum deflection along X = 0.17 mm, along Y = 0.27mm.

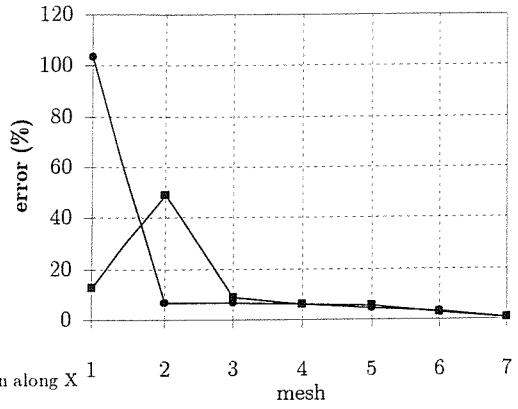

Figure VII.4 – Percentage error for the maximum deflection obtained at the central section (Z = 20) of the model in the X and Y directions in CASE 2 (15 % compression along the fibre direction). For mesh 8, maximum deflection along X = 8.22 mm, along Y = 0.25mm.

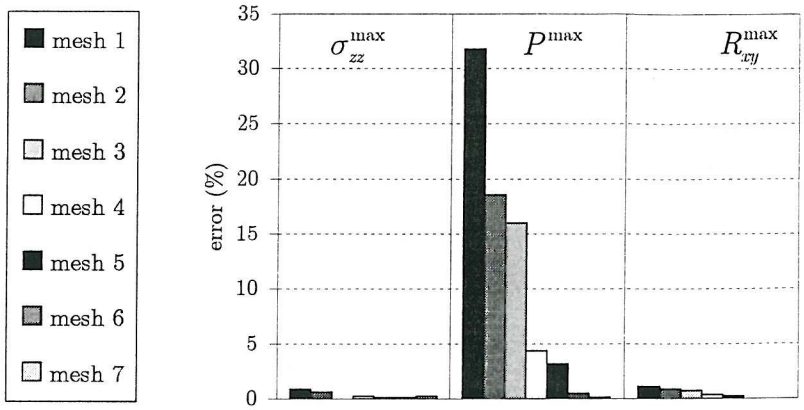

Figure VII.5 - Extension test in the fibre direction (15%). Error variations for maximum values of σ_{zz}, the pressure P and the reaction force R_{xy} to the face B (Z = 0), according to the mesh. For mesh 8 : $\sigma_{zz}^{max} = 36.06\,\text{MPa}$, $P^{max} = -9.94\,\text{MPa}$ and $R_{xy}^{max} = 548.59\,\text{N}$.

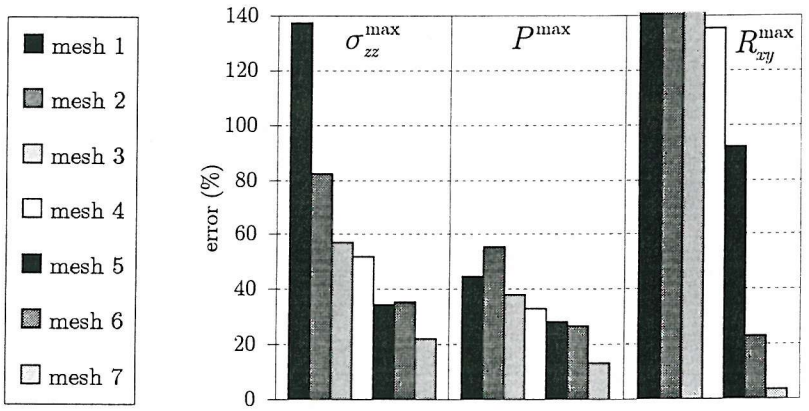

Figure VII.6 - Compression test in the fibre direction (15%). Error variations for maximum values of σ_{zz}, the pressure P and the reaction force R_{xy} to the face B (Z = 0), according to the mesh. For mesh 8 : $\sigma_{zz}^{max} = 6.59\,\text{MPa}$, $P^{max} = 2.97\,\text{MPa}$ and $R_{xy}^{max} = 4.03\,\text{N}$. NB: In comparison with tensile tests, the values are significantly lower.

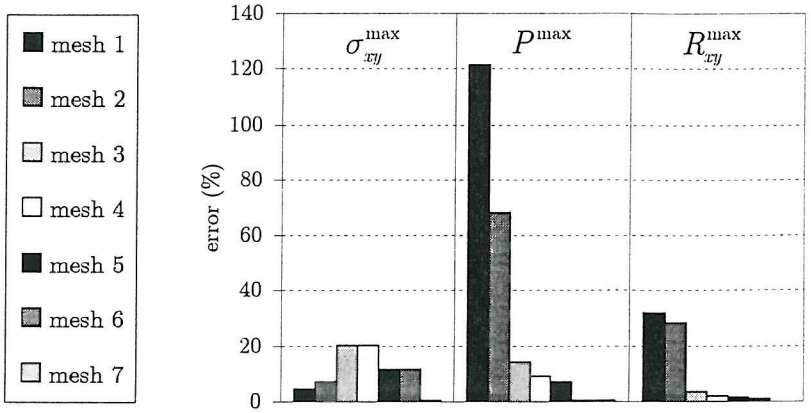

Figure VII.7 - Shear test in the XY plane (50%). Error variations for maximum values of σ_{xy}, the pressure P and the reaction force R_{xy} to the face B (Z = 0), according to the mesh. For mesh 8 : $\sigma_{xy}^{max} = 3.10\,\text{MPa}$, $P^{max} = 2.30\,\text{MPa}$ and $R_{xy}^{max} = 120.94\,\text{N}$.

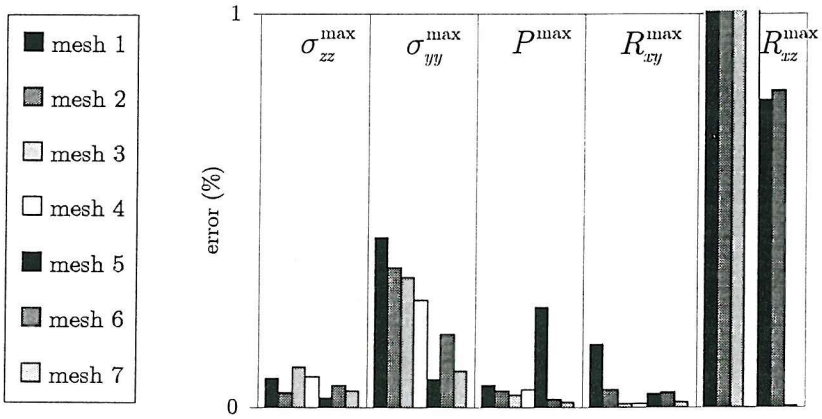

Figure VII.8 - Equibiaxial extension test in the fibre and Y direction (15%). Error variations for maximum values of σ_{zz}, σ_{yy}, the pressure P and the reaction forces R_{xy} and R_{xz} to the face B (Z = 0), according to the mesh. For mesh 8 : $\sigma_{zz}^{max} = 40.72\,\text{MPa}$, $\sigma_{yy}^{max} = 3.49\,\text{MPa}$, $P^{max} = -14.70\,\text{MPa}$, $R_{xy}^{max} = 566.03\,\text{N}$ and $R_{xz}^{max} = 242.81\,\text{N}$.

VII.4.5 Analysis of results

VII.4.5.1 Case 1

When applying a 15 % extension in the fibre direction to the model, convergence of the mesh was quickly obtained for the deflection along the Y axis but the rate of convergence is smaller for the deflection along X (Figure VII.3). This can be easily explained by the fact that the first mesh density possesses only one element in the X direction and two elements thereafter. However, error between mesh 7 and mesh 8 is only 3 % when considering the deflection along the Y axis (Figure VII.3). For the eight mesh densities comparison was made for maximum uniaxial stresses σ_{zz}, maximum pressures P and the reaction force R_{xy} at face B. Convergence was quickly obtained for maximum values of stress in the fibre direction and resultant force (error lower than 1 % from mesh 1) whereas for $P^{\max}$ the error started at around 32 % from mesh 1 and decreased to 0.16 % for mesh 7. One can explained this result by the fact that the constraints put on the nodes of faces B and T produce artificially higher stress at these locations and that a reasonable number of elements (in the XY plane) must be used to capture the high stress gradients. This is directly reflected in the maximum value of pressure by the way of the two principal stresses in the XY plane. Maximum stresses are located at the middle section of the model (Z = 20).

VII.4.5.2 Case 2

Compression of the model along the fibre direction produced buckling as soon as compression has reached a certain magnitude. This magnitude varies according to the mesh density and appearance of buckling is likely to occur earlier for the finest mesh densities. For mesh 2 and 8, the critical magnitudes of compression are respectively 6.3 % and 3 % of compressive strain. Obviously a large error is produced for the deflection along the Y axis for the first two meshes (1 and 2) because of the very large displacement of the structure compared to the size of element (Figure VII.4). From mesh 3 to 7, similar rates of convergence are observed for deflections along both directions X and Y (Figure VII.4) as the buckling process is rather uniform. The minimal error reaches 3.13 % for the deflection along the X axis and disappears (0 %) for the deflection along the Y axis. Errors for the maximum stresses σ_{zz}, pressure P and resultant force R_{xy} begins quite high from mesh 1 (respectively, 137.43 %, 45 % and 1093.23 %) and decrease monotonically (at the exception of P for mesh 2) till 22.29 %, 13.23 % and 3.63 % respectively. These significant errors can be accounted for the small magnitude of these three quantities considered, particularly with respect to the tensile load case.

Due to the characteristics of the material law, as soon as compression is developed in the fibre direction the mechanical response from the material is provided only by the matrix where small compressive stresses are generated. Buckling of the modelled structure is a highly nonlinear phenomenon and the mathematical properties of the equations describing the behaviour of the structure can lead to bifurcations of the solutions. It is therefore important to ensure that the mesh is dense enough in the directions of the fibres when compression is likely to occur along them.

VII.4.5.3 Case 3

A very good rate of convergence is obtained for the maximum pressure and resultant forces (error lower than 1% for mesh 7) whereas the convergence for the maximum shear strain is not perfectly monotonic. This is probably due to the small number of elements along the depth that can easily produce instabilities which in turn affect the possible non unique solution.

VII.4.5.4 Case4

Equibiaxial extension in the fibre and Y directions was performed respecting loading conditions leading to a state of homogeneous deformation. For all the seven meshes, errors for the maximum uniaxial stresses σ_{zz}, pressure P and the resultant force R_{xy} at face B, were lower than 1 % (). To achieve the same level of accuracy for the resultant force at face L, a mesh density corresponding at least to mesh 5 was necessary. This shows clearly that the absence of highly constrained boundary conditions allows the achievement of a very high rate of convergence with an excellent accuracy. This is also confirmed by noting that the maximum and minimal stresses are identical (error lower than 0.8 %).

VII.4.6 Concluding remarks to section VII.4

In light of these results for the four cases, it appears that highly constrained boundary conditions at the extremities of the model affect significantly the results by introducing numerical artefacts. This is obvious since the maximum stress occur at these particular locations and, in vertu of what led to the formulation of the well-known *Saint-Venant's Principle* (Ogden, 1984), edges effects pollute the solution of the boundary value problem expected for a state of homogeneous deformation. The characteristics of the stress field must be considered at a reasonable distance from the edges. However, it was shown that a good convergence of results could be achieved, in various types of loading conditions, by selecting a proper element density. It is essential to have a sufficient number of elements in the regions where the maximum strain gradients are likely to be found in order to capture accurately stress and strain variations. In a structure having approximately the same aspect ratio as the FE model tested (rectangular long and flat shape), it is very important to insure that enough elements are disposed across the thickness (referred as d: *depth*, in Table VII.2), especially for compressive loading along the fibre direction. This is obvious when one considers that when buckling occurs (accompanied by small flexural stresses within the matrix of the fibre-reinforced composite), one face of the structure is under tension whereas the opposite face is under a compressive state. A reasonable number of elements is required along the major characteristic length of the model (referred as l: *length*, in Table VII.2) for the deformation modes that solicit the structure in directions not parallel to the longitudinal principal direction of the model (Z direction). Moreover, the constraint of incompressibility puts high constraints on the nodes of the model that are not allowed to move. In fact, the elements formed by these nodes must simultaneously maintain a constant volume while deforming and while maintaining one of their faces as rigid. Increasing the number of elements at the extremity faces of the structure has the effect to diminish the constraints on each nodes belonging to these rigid faces and by doing so, reducing the local stress values.

VII.5 Influence of an initial stress field

An important issue in ligament modelling is the fact that these structures are naturally in a state of residual stress, even at rest. This can be simply demonstrated by cutting a ligament belonging, for example, to the knee joint. The shape of the ligament after sectioning demonstrates a reduction in the length, establishing the existence of a pre-stretched state. In a three-dimensional finite element analysis of the anterior cruciate ligament, recently performed by Limbert and Taylor (2001a) – Appendix D, it was demonstrated the necessity to include pre-stress in order to obtain realistic results which agree with experimental observations (Roberts *et al.*, 1994; Wascher *et al.*, 1993). In a FE context, application of an initial stretch to a mesh corresponding to a ligament in its already pre-stretched state is a challenging task. In fact, this amounts to generating stretch, and therefore stress without displacing the nodes of the ligament that is already in its initial pre-stressed configuration. At the insertion sites where the meshes corresponding respectively to bone and ligaments connect, the nodes representing the insertion surfaces of the ligament are rigidly fixed to the mesh of the bony structures.

A simple way to implement the capacity to apply initial stretch to a FE model consists in applying a multiplicative decomposition of the deformation gradient based on three different states (Weiss *et al.*, 1995). It is assumed the existence of a configuration, χ_0 at which the ligament is stress free, a state, χ_I at which the ligament is pre stressed but in the reference configuration (point of departure of the FE analysis) and the current state, or deformed state, χ_c. The total deformation gradient, $\mathbf{F}_{c0}$, from the stress-free to the current configuration is expressed as follows:

$$\mathbf{F}_{c0} = \mathbf{F}_{cI}\mathbf{F}_{I0} \qquad \text{[VII.3]}$$

where $\mathbf{F}_{cI}$ and $\mathbf{F}_{I0}$, are respectively the deformation gradients from the initial configuration to the current configuration and from the stress free configuration to the initial configuration.
By assuming a special form of $\mathbf{F}_{I0}$, it is possible to calculate the total deformation at any time of the FE analysis. It is noteworthy to emphasise that $\mathbf{F}_{I0}$ is defined as an input material parameter and is constant throughout the whole computation.
If we assume that an incompressible ligament has a initial pre-stretch λ_I in the direction Z (its fibre direction) and that the two other principal directions of the ligament lie in a plane perpendicular to the direction Z, then the deformation gradient, $\hat{\mathbf{F}}_{I0}$, in the material (or local) reference frame, takes the following form:

$$\hat{\mathbf{F}}_{I0} = \begin{bmatrix} \frac{1}{\sqrt{\lambda_I}} & 0 & 0 \\ 0 & \frac{1}{\sqrt{\lambda_I}} & 0 \\ 0 & 0 & \lambda_I \end{bmatrix} \qquad [VII.4]$$

If $\mathbf{R}$ represents the rotation matrix from the local coordinate frame to the global coordinate frame, $\mathbf{F}_{I0}$ is calculated as:

$$\mathbf{F}_{I0} = \mathbf{R}\hat{\mathbf{F}}_{I0}\mathbf{R}^T \qquad [VII.5]$$

Based on these considerations, the capacity to apply initial stretch, and by consequence, initial stress, was implemented into PAM-CRASH™.

A series of FE tests was designed in order to study the influence of an initial stress field on the deformation patterns of a geometrically idealised ligament (same model as used in section VII.4), the stress distributions and the reaction forces present in the ligament. To assess the influence of the initial stress field present in a ligament-like model, three different loading conditions cases were considered: 15 % extension and 15 % compression in the fibre direction and an additional case which encompasses a combination of compression, shear and extension. Within each of these three cases, ten FE analyses were run with a different value of initial stretch λ_I ranging from 0 till 1.10, in increments of 1% of stretch. The same geometric model as described in section VII.4 was used but with a different FE mesh. The mesh was constituted of 1846 nodes and 1280 elements (Figure VII.9). The initial stretch was assumed to be uniform within the ligament and within each element of the mesh.

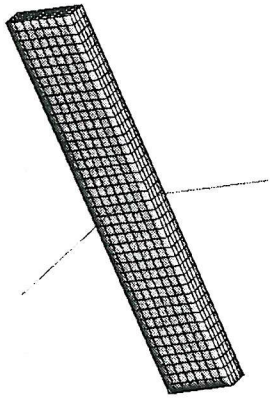

Figure VII.9 – Finite element mesh used to study the influence of the initial stress field on the mechanical behaviour of a ligament-like solid body. The two axis represented define the plane of mechanical isotropy of the material. The fibre direction is perpendicular to it.

Mechanical properties of the FE model were derived from literature (Pioletti *et al.*, 1998a). In his study of the human ACL, Pioletti *et al.* (1998a), identified experimental uniaxial testing data with an isotropic hyperelastic strain potential (Veronda and Westmann, 1970) (see paragraphs IV.2.2 and IV.4.2). In the present study, the uniaxial tensile values were identified with the nominal stresses in the fibre direction corresponding to a transversely isotropic hyperelastic material. This was steadily performed using a nonlinear regression computation. For the anisotropic hyperelastic material, the strain energy function Ψ was defined by Equations [VII.1] and [VII.2]. The following mechanical properties were used: $C_1 = 1.698$ MPa, $C_2 = 0$, $C_3 = 0.299$ MPa, $C_4 = 1$, $C_5 = 0$ MPa, $\lambda^* = 2$, density = 900 kg/m3. An analysis time of 10 ms was found to provide an excellent compromise between computational cost and quasi-static hypotheses (see section VII.3).

As the initial stretch increases and the later buckling of the model is likely to appear during the course of the compression in the fibre direction. This shows that initial stress affects significantly the pattern of deformation for the incompressible transversely isotropic hyperelastic model considered.

Figure VII.10 shows the fringe plotting of the mean volumetric deformation developed in the model during a compression of the structure along its axis of anisotropy. Maximum deformations occur in the regions were the buckling is initiated and this is clearly visible on the concave parts of the structure. Convex parts are essentially loaded in tension.

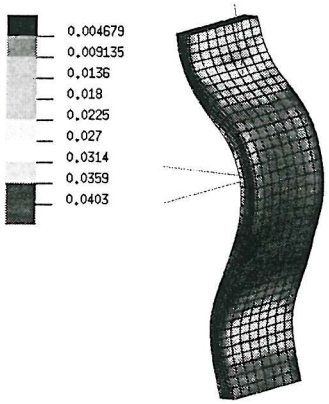

Figure VII.10 – Deformed shape of the ligament model when no initial stretch is taken into account. The fringe plot corresponds to the mean volumetric strain contours at the end of the FE analysis.

VII.5.1 Analysis of results

To assess the influence of an initial stress over the FE model considered, several quantities were defined (Equations [VII.6]). As mentioned earlier, maximum principal stresses and resultant forces within ligaments are essential in the understanding of the mechanics of the knee joint and its physiological loading conditions.

$$\alpha_1 = \frac{\sigma_1^{max}}{\overline{\sigma}_1^{max}},\ \alpha_2 = \frac{\sigma_2^{max}}{\overline{\sigma}_2^{max}},\ \alpha_3 = \frac{\sigma_3^{max}}{\overline{\sigma}_3^{max}},\ \alpha_4 = \frac{P^{max}}{\overline{P}^{max}},\ \alpha_5 = \frac{R}{\overline{R}} \qquad \text{[VII.6]}$$

σ_1, σ_2, σ_3 and P are the principal stresses and the pressure respectively. R is the resultant force in the structure at the end of the analysis. Quantities covered with a bar symbol represent values obtained (at the end of the analysis) when *no initial stretch* is applied to the FE model (λ_I = 1.00).

The deformation of the structure is affected by the pre-stretch and hence it was decided to define the following parameter χ that relate deflections of the structure to its original characteristics dimension (length):

$$\chi = 100\frac{|\Delta u_x|^{max}}{40} \qquad \text{[VII.7]}$$

The value 40 corresponds to the length (in mm) of the solid model whilst $|\Delta u_x|^{max}$ is the maximum absolute deflection of the mesh along the X axis. The volumetric strain is a combination of the principal strains and therefore provides a global mean to assess the strains in the model. The parameter δ, defined in Equation [VII.8], is an indicator of the effects of an initial stretch on the volumetric strain in the deformed configuration.

$$\delta = \frac{\varepsilon_V^{max}}{\overline{\varepsilon}_V^{max}},\ \text{where } \varepsilon_V^{max} \text{ represents the maximal volumetric strain} \qquad \text{[VII.8]}$$

VII.5.1.1 Extension in the fibre direction

As expected, increasing the value of the initial stretch in the case of a 15 % extension in the fibre direction increases the principal stress σ_1 (and so the pressure) according to the nonlinear elastic constitutive law chosen for the mechanical contribution of the fibre (Figure VII.11). There is a slight shift between the ratio of the maximum principal stresses σ_1 (parameter α_1) and the ratio of the resultant forces (parameter α_5) that, theoretically, should be identical. This could be explained by the errors made in the numerical assessment of nodal forces when compared to stress calculated by Gauss integration). The two other ratios α_2 and α_3, corresponding respectively to the principal stresses in the plane of material isotropy σ_2 and σ_3 increase mostly linearly (Figure VII.11). In a state of homogeneous deformations (uniaxial extension along the fibre direction), these two principal stresses should be zero. In the present case they are not because of the boundary conditions that constrain the extreme faces of the structure (Z = 0 and Z = 40). The consequence of these observations mean that an initial tensile pre-stress in a ligament loaded in tension is likely to affect its stress state mainly along the directions of it collagen fibres as compared to the stress state in the plane of material isotropy where the initial stretch has a more moderate (linear variation of α_2 and α_3) effect on σ_2 and σ_3.

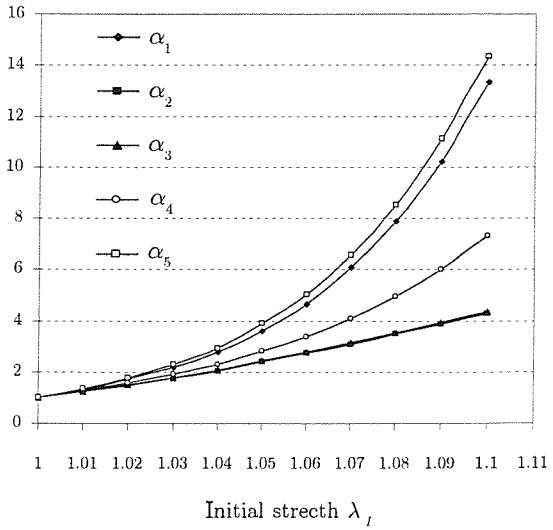

Figure VII.11 - Evolution of the stress based ratios α_i (Equation [VII.6]) according to the value of the initial stretch λ_I for the case of an extension of 15 % in the fibre direction.

The influence of an initial stretch is obvious: having an initial strain of around 3 % is sufficient to produce an increase of 100 % in the principal stress whereas this can reach up to 1350 % for an initial strain of 10 %. This is worth mentioning as knee ligaments can bear this kind of pre-strain in vivo (3 %) according to the particular configuration of the joint (Bach *et al.*, 1997).

As α_4 represents the ratios of the maximum pressure and as the pressure is a linear combination of the principal stresses, the nonlinear variation of α_1 induces a nonlinear variation of α_4. A residual stress in a ligament loaded in tension along its fibres therefore affects the global hydrostatic state of stress. The fact that a ligament loaded in tension is fixed at its extremities produces forces reacting to these displacement constraints, generating hydrostatic stresses within the ligament. This effect is amplified as the intensity of the residual tensile stress increases.

VII.5.1.2 Compression in the fibre direction

The amplitude of variations of α_1 (order of magnitude: 1.5) is much larger than that of the others α_i along the variation of the initial stretch λ_I. However, similar trends of evolution are observed for the five parameters α_i, especially when λ_I goes beyond 1.07. It appears that pre-stretching the body has a moderate influence on the resultant force and the principal stresses σ_2 and σ_3 (maximum variation of 100 %) whilst this is more significant on the first principal stress. When compressed, the body buckles according to the value of the initial stretch. This highly nonlinear behaviour induces deformations that are very sensitive to any perturbation (peak in α_i for $\lambda_I = 1.01$, see Figure VII.12). At the very beginning of the buckling, the compressive load is carried by the extremely compliant matrix (fibres do not provide any contribution) and progressively redistributed in the fibres as the buckling develops and produces very large displacements in addition to the very large deformations.

The ratio χ is an indicator of the model characteristics related to the large displacements regime. It means that when χ increases the deflection along the X axis becomes significant with respect to the initial major characteristic length of the structure (L = 40 mm). This is directly related to the way the soft tissue structure buckles under compressive load along the fibre directions. When there is no initial stretch within the model the maximum defelection along the X axis represents about 10.5 % of the initial length of the structure (Figure VII.14). At 1.01 of initial stretch this value reaches 22.5 % (maximum for λ_I varying between 1.0 and 1.10) and then decreases to less than 1 % from λ_I=1.07.

The correlation between residual stretch and deflection/buckling is quite clear but it is as well believced to be intrinsincally linked to the loading conditions, the geometrical and the mechanical properties of the structure.

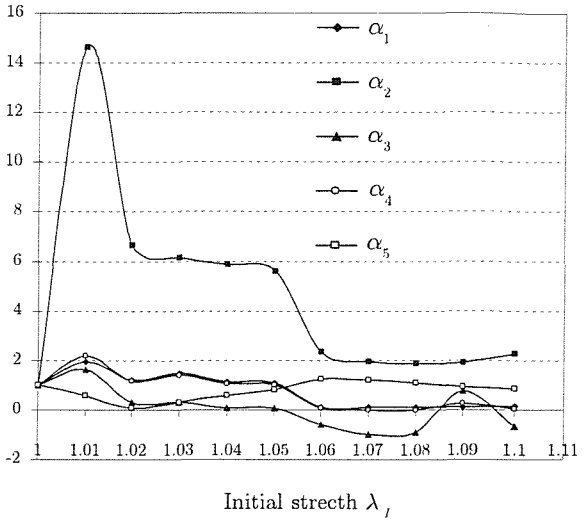

Figure VII.12 - Evolution of the stress based ratios α_i (Equation [VII.6]) according to the value of the initial stretch λ_I for the case of a 15 % compression in the fibre direction.

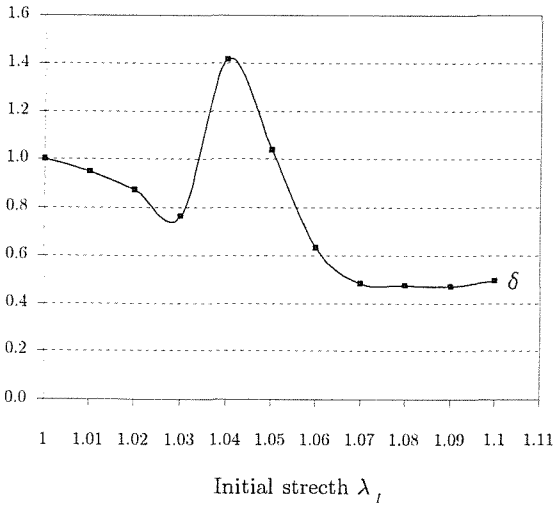

Figure VII.13 - Evolution of the strain based ratios δ (Equation [VII.8]) according to the value of the initial stretch λ_I for the case of a 15 % compression in the fibre direction.

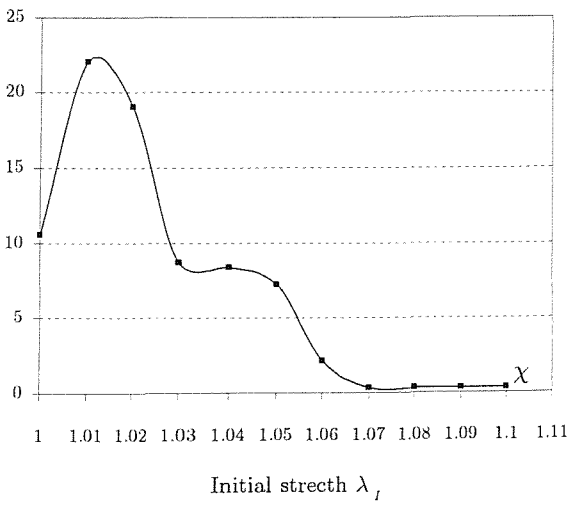

Figure VII.14 - Evolution of the percentage deformation based ratios χ (Equation [VII.7]) according to the value of the initial stretch λ_I for the case of a 15 % compression in the fibre direction.

Final deformed shapes of the mesh are presented for the compressive load when making varying the initial stretch from 1 to 1.1 (Figure VII.15-a-h). In Figure VII.15, it is clearly demonstrated the influence of an existing pre-stress on the deformation history of the FE model of an incompressible transversely isotropic hyperelastic material. Buckling of the solid structure appears at different steps of the analysis according to the initial stress field (Figure VII.15). Higher the initial stretch and later bucking is likely to occur for a compressive displacement during the FE analysis. Deformed shapes for the analyses with an initial stretch value of 1.08, 1.09 and 1.10 are not represented as the model is in a state of pure axial compression with no buckling produced, and therefore the distorted mesh are similar to that of the mesh corresponding to an initial stretch value of 1.07. Additional FE analyses (not presented here) have shown that by relieving rotational degrees of freedom of the top surface of the mesh (defined as a rigid surface) perturbs the solution in a way such that buckling is produced even for values of initial stretch over going 1.07.

Given that, in a FE model of a complete joint (bones and ligaments), ligaments are unlikely to be loaded in pure compression (with degrees of freedom of the extremities only free in the translational direction of compression) along the fibre directions, buckling is likely to occur.

λ_I	1.00	1.01	1.02	1.03	1.04	1.05	1.06	1.07	1.08	1.09	1.10
%	8.40	9.15	10.5	11.40	12.00	12.90	13.80	14.25	_	_	_
Δu_z	3.36	3.66	4.20	4.56	4.80	5.16	5.52	5.70	_	_	_

Table VII.4 – Table relating the initial stretch and the displacement of the top nodes (face T) of the FE model, Δu_z, at which buckling of the structure is initiated. Percentage of compressive strain (" % " in the table) is also given in order to relate more explicitly initial stretch to the boundary conditions (15 % of compressive strain).

Figure VII.15 shows clearly that the structure undergoing pure compression in the fibre direction will behave in a particular way according to the value of the pre-stretch and the magnitude of compression. Characteristic quantities associated with this phenomenon are gathered in Table VII.4. Figure VII.15-b-d illustrate buckling instabilities. Indeed, the deformed shapes of the mesh point towards opposite directions as for the other cases (Figure VII.15-a-b-e-f). A small perturbation (sensitive to the mesh density) caused for example by the motion of a single or several nodes is sufficient to alter significantly the deformation history of the structure.

This gives rise to very large deflections that modify the stress distribution and thus some parts of the body are loaded in tension and some others are loaded in compression (in the direction of the fibres) (Figure VII.15). As the fibres loaded in tension provide much more larger stiffness that the matrix loaded in compression, a large deflection of the body means a greater volume of the body loaded in tension and thus a greater value of principal stress. This is clearly shown by comparing the variations of α_1 (Figure VII.12) with the variation of χ (Figure VII.14) which have approximately identical shapes.

The evolution of the ratio δ shows that the maximum volumetric strains (representing the weighted sum of the principal strains) at the end of the analysis increases and decreases respectively to up to 40 % ($\lambda_I = 1.04$) and 55 % ($\lambda_I = 1.07 - 1.09$) by comparison with the case when there is no initial stretch, with respect to the initial stretch. Volumetric stress characterises the bulk response of the material when submitted to volumetric load (pressure). The nonlinear variation of δ becomes linear after $\lambda_I = 1.07$ where δ keeps almost constant as the initial stretch increases. This means that after locking of the structure in compression there is no significant volumetric change. However, it is believed that this (pure compression in the initial direction of the collagen fibres) is a situation unlikely to occur in a ligament *in vivo*.

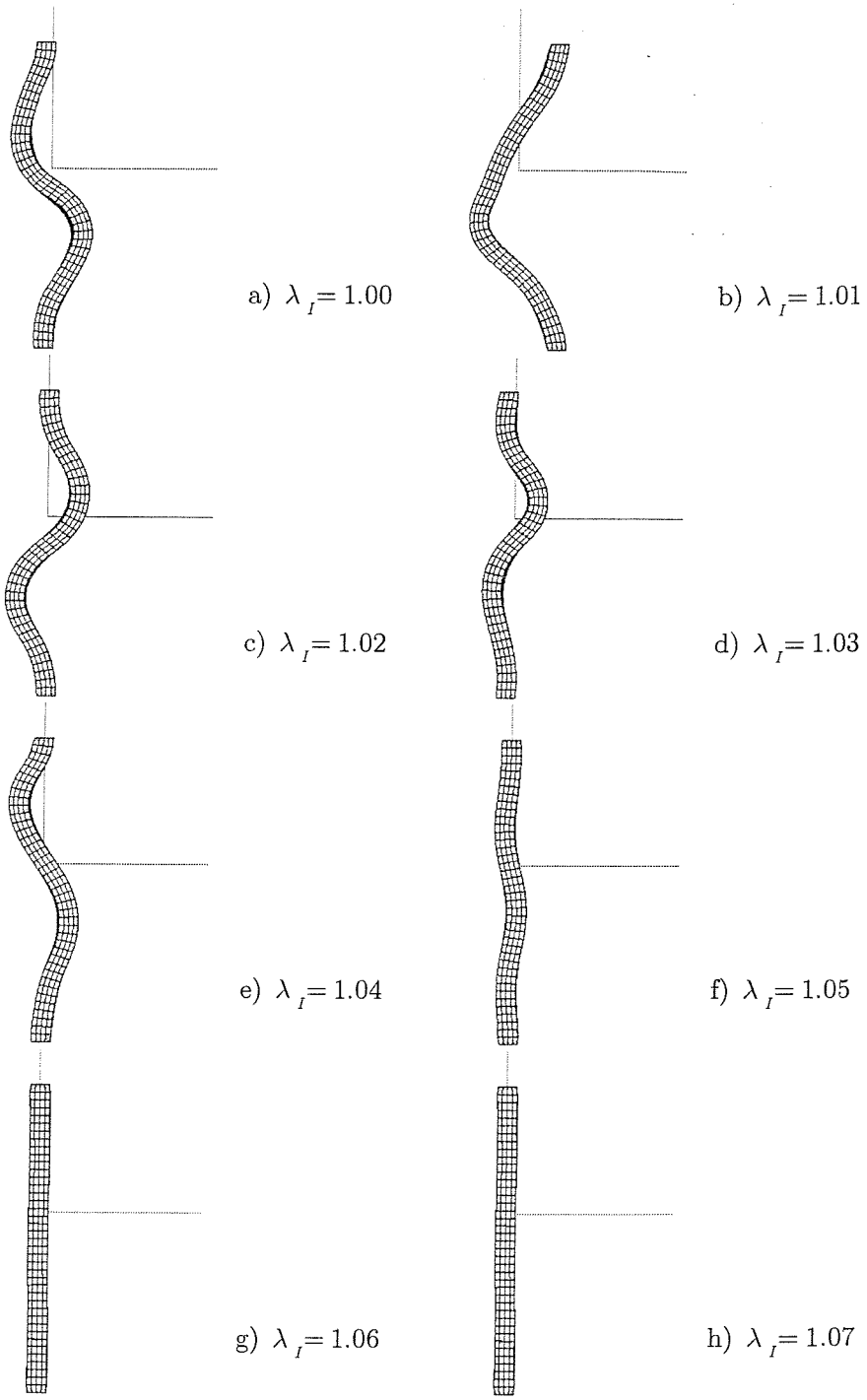

Figure VII.15 - (a-h) Deformed shapes of the mesh at the end of the FE analysis (lateral view) for various initial stretches λ_I. Plot a) corresponds to the deformed model subjected to no initial tension. Compressive load was applied at the top nodes of the model.

VII.5.1.3 Mixed boundary conditions

The maximum first principal stress σ_1 (and the pressure) increases monotonically by up to 140 % as the value of the initial stretch increases (Figure VII.16). The principal stresses σ_2 and σ_3 decrease monotonically by up to 50 % when the initial stretch is lower than 1.04 and then have an almost monotonic linear increase as σ_1 and the pressure. The ratio α_1 has a nonlinear variation and the final resultant force when $\lambda_I = 1.10$ was 260 % greater than when $\lambda_I = 1.00$.

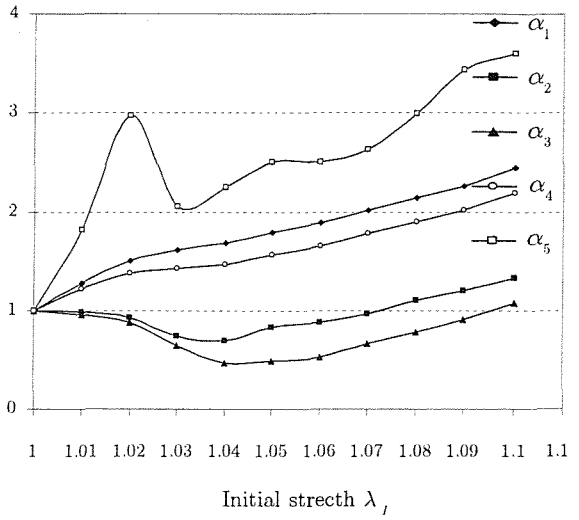

Figure VII.16 - Evolution of the stress based ratios α_i (defined by equation [VII.6]) according to the value of the initial stretch λ_I for the case of mixed boundary conditions.

From $\lambda_I = 1.04$ till $\lambda_I = 1.10$, the slopes of the linear curves representing the variations of $\alpha_1 - \alpha_5$ are almost identical meaning that an initial pre-stretch affects the three principal stresses in the same way (proportionality).

Overall, it seems that the influence of a residual stress on the stresses and resultant force is more moderate for the case of mixed boundary conditions than for the cases of uniaxial tensile and compressive loads.

At this stage it is convenient to introduce a stress invariant, the von Mises stress, because it is a quadratic combination of the principal stresses and so represents a scalar stress state at a given location. If we define $\boldsymbol{\sigma}_{dev}$, the deviatoric stress by:

$$\boldsymbol{\sigma}_{dev} = \boldsymbol{\sigma} - p\mathbf{1} \qquad \text{[VII.9]}$$

the von Mises stress, σ_{vM}, is given by:

$$\sigma_{vM} = \sqrt{\frac{3}{2}(\boldsymbol{\sigma}_{dev} : \boldsymbol{\sigma}_{dev})} \qquad \text{[VII.10]}$$

Figure VII.17 shows the deformed shapes of the model for the mixed boundary conditions ($\lambda_I = 1.0$) at various stages of the FE analyses in combination with a fringe plot representation of the von Mises stresses.

The typical buckling of the structure is clearly visible under the large deformations and displacements conditions. As expected, maximum von Mises stresses are located at the edge of the model that undergoes the biggest displacement and this effect is amplified by the rigid nature of the top face of the model (the one that is applied the displacement boundary condition).

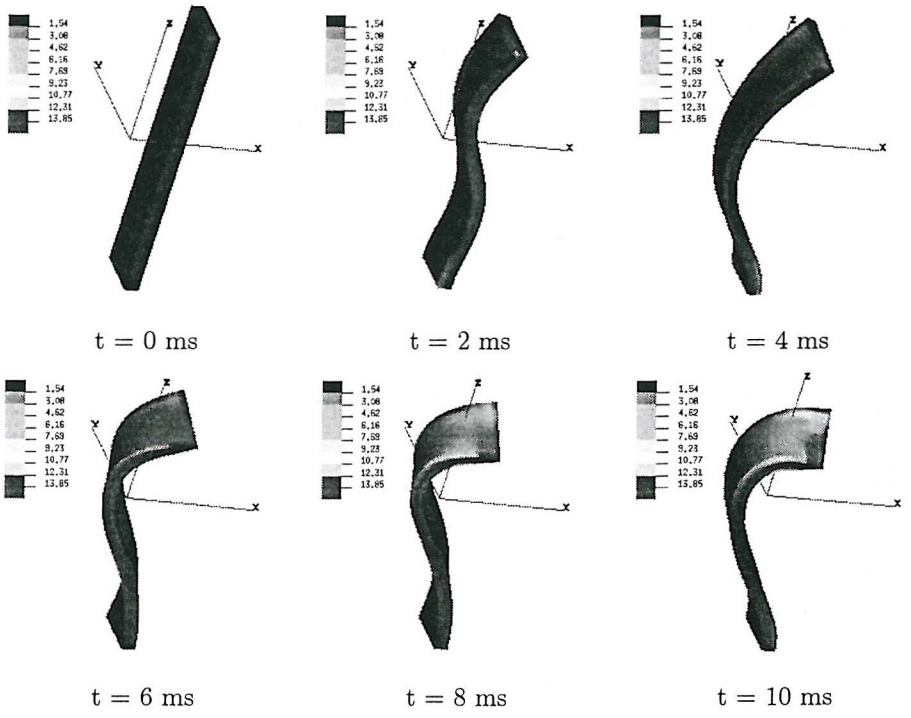

Figure VII.17 – Multistate representation of the ligament model for the third loading case (mixed boundary conditions) when no residual stress exists in the structure at the begining of the analysis. Fringe plots correspond to the von Mises stresses.

VII.5.2 Concluding remarks to section VII.5

The influence of a residual stress on the stress and strain history of an incompressible transversely isotropic hyperelastic body has been shown to be significant when considering particular sensitivity quantities. For the tensile load case, the stresses and the resultant force increase uniformly with the initial stretch whilst, in the case of compression, non uniform and smaller variations are observed. The major result for this particular loading case is that initial tensile pre-stress in the undeformed configuration will condition the deformation history and so the stress history of the soft tissue structure. Appearance of buckling will be conditioned by this factor and the constraining conditions at the extremities of the structure.

The third case encompassing a mixture of finite shear, compression and extension, seems very sensitive to the value of the initial stretch (up to 240 % of increase in the maximum first principal stress). For the compression case there exists a value of initial stretch (1.07) beyond which the ratios α_i become constant. This is certainly directly related to the particular enforced boundary conditions in association with mechanical properties used for the simulations. As ligaments are structures that are likely to be loaded non uniformly, the third case is probably the one that reflects the most real physiological conditions (perhaps at the difference that the magnitudes of displacement may be lower) and thus, pre-stretch, if identified from biological data, is highly relevant to include in FE analysis of soft connective tissues.

VII.6 Conclusions and recommendations

In this chapter, sensitivity analyses were performed in order to test the incompressible transversely isotropic hyperelastic finite element material model by looking at the influence of various parameters characterising the finite element analyses: hourglass control methods for uniform reduced integration eight-noded hexahedral elements, physical time chosen for the finite element simulations, mesh density and residual stress. All these tests were performed for different cases of boundary conditions as the loading conditions were thought to be crucial in the type of solutions to be found.

It appears that the stiffness method to control and stabilise the hourglass modes is the one that gave the best results in terms of accuracy of the results and shape stability of the mesh providing that a small stiffness parameter κ is used, typically $\kappa = 0.01$. It is important to ensure that the ration of the hourglass energy over the internal energy of the system is small (lower than few percents).

In order to simulate a particular mechanical phenomenon in a physical time scale much smaller than its natural time scale, it proved essential to take particular precautions. Indeed, the objectives are to diminish the physical time of a finite element analysis, for obvious computational efficiency reasons, while preserving the quasi-static nature of the solution. This was achieved by increasing the loading rate in a way such that inertia forces remain negligible and that stress waves do not pollute the solution. Within an explicit code, this is possible by defining very smooth loading curves such that their first and second derivatives are zero at the initial and final times of the analysis. Using this strategy, negligible or no stress waves are produced. For further details please see section VIII.3.3. Sometimes, it is necessary to run several analyses of the same problem by varying the physical time of the finite element computation. A global inspection of the deformed shape of the structure and values of strains and stresses gave a good indication of the nature of the solution. By reducing progressively the loading rate, the solution tends towards a quasi-static solution. The idea was to find the highest loading rate that achieves this sort of convergence. It was also important to make sure that the kinetic energy does not exceed a small fraction of the internal energy of the system throughout the majority of the quasi-static event, typically in the order of 5 - 10 %.

Mesh density sensitivity analyses have shown that a special care should be taken when designing the mesh for a particular problem. The key is to appreciate the nature of the problem and build the mesh accordingly, especially when large deformations and displacements are involved. Highly nonlinear phenomena such as buckling requires a sufficient mesh density to capture them properly. It is difficult to give a particular optimal mesh density as it is very problem-dependent. Regions of high stress gradients, such as the zones departing from the end of the structure where the load is applied or where the structure is embedded, should be descretised finely, i.e. having a fine mesh density, to allow for good tracking of the stress and strain variations. In the highly constrained regions (embedding of nodes + incompressibility constraints) this will have the effect of significantly reducing the peak stresses that are artificially created in these particular locations.

In the light of results from section VII.5, its is evident that residual stresses present in an incompressible transversely isotropic hyperelastic soft tissue structure made of a highly compliant matrix reinforced by stiff fibres have a major influence on the deformed shape and the continuous mechanical response of the whole structure. As residual stresses are present in ligaments *in vivo*, their inclusion in a finite element model are believed to be crucial. The influence of tensile residual stresses may be particularly important in soft tissue structures loaded in compression along their fibre directions. This affects the particular resulting deformation modes but this is largely dictated by the magnitude of the loads.

To finally conclude this chapter, the implemented finite element material model has been extensively tested under various boundary conditions and the influence of several relevant parameters of the finite element analyses was also extensively investigated. The outcome of these studies has provided indications for the best modelling strategy in order to perform accurate finite element analyses of ligamentous structures. This stage was absolutely essential for having confidence in the results of the finite element analyses that will be described and carried out in Chapters VIII and IX.

Chapter VIII

Application 1:
FE simulations of the mechanical behaviour of the human ACL

Equation Section 8

In the present chapter, as in the next chapter, it is proposed to demonstrate the relevance and usefulness of the numerical implementation of the anisotropic constitutive law for biological soft connective tissues. The capacity to apply a residual stress to a FE model of a soft tissue structure will also be shown to be essential. The incompressible transversely isotropic hyperelastic FE model is used to model the mechanical behaviour of the human ACL when the knee is subjected to a passive flexion.

VIII.1 Objectives and structure of Chapter VIII

Before going further, a brief description of the core aims of the present chapter is presented:

- The first objective is to prove that the implemented FE constitutive model (described in Chapters V and VI) is capable of reproducing the key mechanical features of the ACL in simulated physiological conditions and particular emphasis is put on the necessity to use a constitutive law of an *anisotropic* material. It is hypothesized that a transversely isotropic model, accounting for the structural features of the collagen fibres, will provide a much better mechanical model to represent the physiology of the ACL.
- The second objective is to assess the influence of a residual stress field within the ACL on the resultant force, strain and stress patterns within the ligament for a simulated passive knee flexion.
- Finally, the third aim is to provide a validation of the FE model of the ACL by comparing numerical and experimental results obtained for specific conditions, i.e., passive flexion of the knee.

The background to this research is first given in section VIII.2 where the importance of ACL injury is presented and provides a solid justification for studying the biomechanics of the ACL. Following standard usage in scientific publishing, there are separate sections for material and methods, results, discussion and conclusion.

VIII.2 The anterior cruciate ligament: generalities

The ACL is the most commonly injured ligament of the body (Fetto and Marshall, 1980; Johnson, 1982), especially during sport (Speer *et al.*, 1995) and motor vehicle accidents because of excessive loading and/or high strain rates (up to 500 %.s-1) (Crowninshield and Pope, 1976). According to Hirsham *et al.* (1990), in a study following five hundred patients over a three-year period, it was found that ACL ligament only injuries accounted for 48 % of the total number of knee-ligament injuries. MCL injuries were the next most frequent at 29 % of the total. ACL tears most often occur during football and basketball in younger patients, and occur most often from skiing injuries in older patients. Approximately 75% of ACL injuries are non-contact in origin.

ACL tears frequently occur when an athlete plants one foot and attempts a sudden change in direction (Simmons, 1998). Internal torque of the tibia was found to be an injury mechanism for the ACL (Ryder *et al.*, 1997). The pattern of reciprocal tension between the AMB and the PLB is such that the PLB checks and, therefore, tends to be injured with excessive knee hyperextension, while the AMB would tend to be injured with trauma to the flexed knee (Cabaud, 1983).

From this brief review, it is evident that the biomechanics of the ACL is of high interest. Although numerous clinical and mathematical modelling studies have focused on the mechanical characteristics of the ACL, very few full three-dimensional FE models of the ACL were developed (Daniel, 1999; Hirokawa and Tsuruno, 2000; Pioletti, 1997). Moreover, in these numerical studies, the authors only looked at the strain and stress distribution patterns obtained for simulated passive knee flexion or drawer tests. They did not consider the total resultant force present in the ACL during the various stages of the motion simulated. This quantity is essential in ACL reconstruction when the knowledge of the ideal initial pretension of the graft is required (Amis, 1989). This mechanical characteristic will condition not only the laxity of the repaired knee but also, in the case of a graft made of a biological material (generally, the patellar tendon), the healing and remodelling process (Beynnon *et al.*, 1993b; Hayashi *et al.*, 1996). Knowing the biomechanics of the ACL for particular physiological motion of the knee is another crucial aspect in knee rehabilitation after occurrence of an ACL disruption (Beynnon and Fleming, 1998; Beynnon *et al.*, 1995). In fact, in order to design efficient and harmless rehabilitation protocols for the disrupted knee after ACL injury, one must ensure that the ACL is not strained in unreasonable proportions during these exercises. Failure to protect the ACL from excessive mechanical loading would inexorably lead to a delayed healing and, in the worst case, to a complete failure of the surgical repair. Also, results concerning the force in the ACL are easily related to experimental studies (Roberts *et al.*, 1994; Wascher *et al.*, 1993) unlike stress and strain that are much more sensitive to the location and type of the measurement. A more accurate knowledge of the biomechanics of the ACL is fundamental in understanding the complexity of the knee joint global stability.

Prior to the present research work, no study has assessed the influence of a residual stress in the ACL at full extension on its mechanical behaviour. A preliminary FE study by Limbert and Taylor (2001a) (see Appendix D), was performed in order to circumvent this lack in the relevant literature. It was the occasion to call in to question the validity of the assumption of mechanical isotropy of the ACL. In the next sections, several three-dimensional FE analyses of the ACL are conducted with the new implemented transversely isotropic constitutive model described in Chapters V and VI.

VIII.3 FE analysis of a human ACL under passive flexion of the knee

VIII.3.1 Geometrical model of the ACL

The three-dimensional geometry of the insertion sites of an ACL was obtained from an experiment performed on a non pathological intact cadaveric right knee specimen from a male donor of unknown age. Using a direct measurement technique (Martelli *et al.*, 2000), it was possible to record the three-dimensional motions of the tibia relative to the femur (rigidly fixed in a horizontal position) during kinematic acquisitions made by a trained orthopaedic surgeon. After completion of repeated acquisitions of the knee kinematics, the knee was dismantled and cleared from its surrounding soft tissue structures (flesh, muscle, capsular structures) in order to allow easy access to the ACL and its insertion sites. Using an electrogoniometer, discrete points defining the contours of the ACL at its femoral and tibial insertions were acquired by the surgeon. In order to account for the orientation of the fibres composing the ACL, the same number of points (22) was used for defining the tibial and femoral contours of the ACL. The first point acquired on the tibia was put into correspondence with the first point acquired on the femur, the imaginary direct line joining them defined the local fibre orientation. Two additional points were acquired after sectioning the ACL at its top ends. These points corresponded to the approximate centre of the insertion areas of the tibia and of the femur respectively. A file containing the point numbers and their three-dimensional coordinates was then imported into the FE pre and post-processor Patran v8.0 (® The MacNeal Schwendler Corporation, Los Angeles, CA, USA). Prior to this, the ccordinates of the points defining the tibial insertion area were transformed (Martelli *et al.*, 2000) in order to obtain their position when the knee is at full extension and not at the position where the anatomical acquisition was made.

For each set of points (one for the tibial insertion, one for the femoral insertion), a surface interpolation was performed in the pre-processor software. The geometrical model includes the non planar insertion areas and respects the natural orientation of the fibres. Given that the full three-dimensional shape of the ACL was not available and that a "reasonable" ACL shape does not affect significantly the results of the finite element analysis (Pioletti, 1997), the ligament was reconstructed by connecting the two insertion surfaces. The solid volume reconstructed was that of the ACL when the knee is at full extension (as shown in Figure VIII.2).

VIII.3.2 Finite element model of the ACL

The solid volume representing the ACL was meshed with 8-noded hexahedron elements using Patran v8.0. Special care was taken in order to optimise the performance of the mesh for the large displacement and large strain analysis. In fact, due to its initial distorted shape, the ACL mesh can undergo severe distortions during the early stages of the analysis and can lead to premature convergence failure in the computation. The mesh consisted of 3297 elements and 3784 nodes. Reduced integration was used for the element formulation.

VIII.3.3 Boundary conditions

The passive flexion-extension kinematics tests, described in VIII.3.1, were performed with the knee in the neutral position (no internal or external rotation) for flexion angles of 0, 10, 30, 45, 90, 110 and 125 degrees that corresponds to full flexion of the knee. Although in the physical kinematic tests, the femur was rigidly embedded while the tibia was free to move in the flexion plane, these conditions were reversed in the FE analyses. The successive discrete positions of the femoral insertion of the ligament were used as displacement boundary conditions and the nodes of the tibial insertion area were considered as rigidly fixed. The displacement amplitude curves were smoothed by the way of a fifth-order polynomial (using a customised Fortran program) in order to avoid singularities associated with linear ramp displacement curves where velocity is piecewise constant and acceleration may be infinite (represented by a Dirac distribution). These phenomena pollute the solution by generating stress waves that prevent a quasi-static solution to be obtained. Smoothing of the amplitude curve ensures that the velocity varies continuously during the time period of the amplitude definition and that the acceleration no longer has singularities points. When the velocity time history is defined by a piecewise linear amplitude variation, the acceleration is piecewise constant.

VIII.3.4 Computational aspects

The FE analyses were performed for a total physical time of 14 ms. Inertial effects were found negligible at this loading rate. The computations were ran on a bi-processor Pentium® III PC clocked at 933 MHz (equipped with 1024 Mbytes of RAM) and the CPU time required for each FE analysis was about one hour and twenty seven minutes. This is extremely economic compared to implicit FE analyses which have a higher cost per time step and no mention is even made about the stronger robustness of explicit analyses involving finite deformations.

VIII.3.5 Constitutive law and mechanical properties

Pioletti (1997) performed uniaxial tensile tests on human ACL specimens and identified the material data to fit an incompressible isotropic hyperelastic law Ψ_I (Equation [VIII.1]) firstly proposed by Veronda and Westmann (1970).

$$\Psi_I = \alpha e^{\beta(I_1-3)} - \frac{\alpha\beta}{2}(I_2 - 3) \qquad \text{[VIII.1]}$$

It is now proposed to use the experimental data of Pioletti in order to identify the experimental curves with an incompressible transversely isotropic hyperelastic strain energy function. It was assumed that the strain energy function characterising the mechanical behaviour of the ACL. Ψ_{TI} can be split into the sum of a strain energy function representing the mechanical response of the ground substance Ψ_m and a strain energy function encompassing the anisotropic behaviour introduced by the collagen fibres Ψ_λ (Spencer, 1992):

$$\Psi_{TI} = \Psi_m + \Psi_\lambda \qquad \text{[VIII.2]}$$

Ψ_m is chosen as being a neo-Hookean isotropic hyperelastic potential which is a simple extension of the classical linear isotropic elasticity for the finite strain regime:

$$\Psi_m = C_1(I_1 - 3) \qquad \text{[VIII.3]}$$

In order to reproduce the stiffening features of the tissue constituting the ACL and its mechanical behaviour during large deformation, a transversely isotropic hyperelastic potential with an exponential law was used for representing the mechanical contribution of the collagen fibres. The inability of the collagen fibres to sustain compressive load in along their axis was taken into account:

$$\Psi_{\lambda} = \int \frac{\partial \Psi_{\lambda}}{\partial \lambda} d\lambda \quad \text{such that} \begin{cases} \dfrac{\partial \Psi_{\lambda}}{\partial \lambda} = 0 & \text{if } \lambda \leq 1 \\ \dfrac{\partial \Psi_{\lambda}}{\partial \lambda} = C_2 \left[e^{C_3(\lambda-1)} - 1 \right] & \text{if } \lambda > 1 \end{cases} \qquad \text{[VIII.4]}$$

As described in Chapter V, λ is a tensorial invariant representing the stretch in the fibre direction. The material parameters of the constitutive law Ψ_{TI} were identified with the mean stress-strain curve obtained by Pioletti (1997) for human ACLs by mean of a nonlinear regression analysis (Bates and Watts, 1998) producing then a first set of material parametsrs S0. The coefficient C_1 governs the isotropic mechanical response of the ground substance and was assumed to be 1 MPa as obtained experimentally by Ault and Hoffman (1992a).

From the mean experimental stress-strain curve obtained by Pioletti (1997), two other stress-strain curves were generated by adding an offset of ± 10 % of the initial curve. Then, the material coefficients of the incompressible transversely isotropic hyperelastic law described by equation [VIII.4], were identified with these two curves producing two additional sets of mechanical properties S+ and S- (Table VIII.1). These two sets of mechanical properties will be used in the study described in section VIII.4.6.

Mechanical formulation	*Isotropic*		*Transversely isotropic*		
Mechanical properties	α (MPa)	β	C_1 (MPa)	C_2 (MPa)	C_3
S0 - (Pioletti, 1997)	0.33	14.19	1	0.4247	22.2548
S+ - (Pioletti, 1997) * 1.1	-	-	1	0.3236	22.6696
S- - (Pioletti, 1997) * 0.9	-	-	1	0.3750	22.4199

Table VIII.1 – Mechanical properties used for the finite element analyses of the ACL when the knee is submitted to a passive flexion.
[- : not computed]. (S+) = (S0) + 10 % (S0), (S-) = (S0) - 10 % (S0).

The three stress-stretch curves obtained by identification of the incompressible transversely isotropic hyperelastic potential are represented on Figure VIII.1.

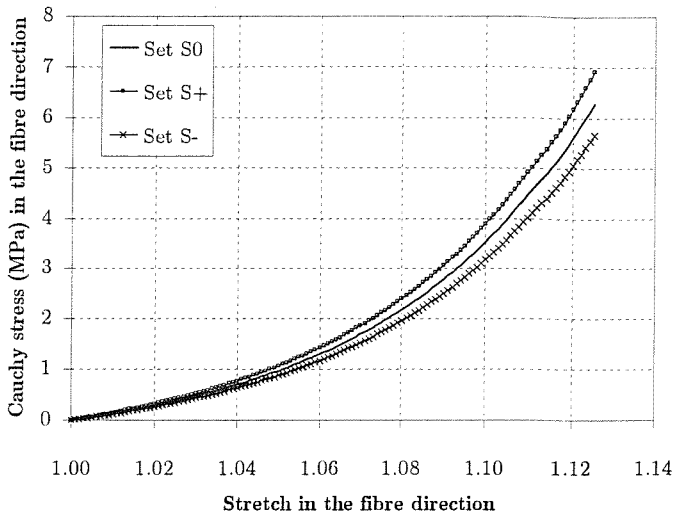

Figure VIII.1 – Analytical stress-stetch curves deriving from the potential Ψ_{TI} after identification with the three material sets S0, S+ and S-.

VIII.3.6 Initial stress field within the ACL at full extension

The ACL has no stress-free state at any of the knee flexion angles (Dürselen *et al.*, 1996). The stress distribution within the ACL when the knee is at full extension is unknown and has yet to be experimentally characterised. Concerning the resultant force generated by the ACL, there appears to be a large variability in the values reported in the literature. Wascher et al. (1993) performed an in-vitro study and reported a resultant force at full extension varying from 10 to 135 N. Roberts (1994) performed an in-vivo study and reported a resultant force at full extension of 104 N ($\pm$ 14). Using a direct measurement technique (strain gages), Bach *et al.* (1997) measured in vitro the strains in the anteromedial and posterolateral bands of the ACL from 10 degrees of hyperextension to full flexion. On a sample of ten cadaveric knee specimens, the range of strains at full knee extension was: 3.2-5.2 % for the AMB and 6-8.8 % for the PLB.

This shows that an initial stretch of 1.043 (about 4.4 % of strain) fits in this range of strain values even though the ranges considered concern only separate fibre bundles and not a complete ACL.

In a preliminary FE study related to the present research report (presented in Appendix D), Limbert and Taylor (2001a) examined the influence of the initial stress field on the stress distribution within the ACL. This parameter was shown to have non negligible effects. However, the constitutive model adopted for the ACL in this earlier work was that of an incompressible isotropic hyperelastic material.

As the incompressible transversely isotropic model (described in sections V.9 and VIII.3.5) is promising in avoiding appearance of excessive compressive stresses and in matching more closely the natural mechanical behaviour of the ACL, the hypothesis that the influence of the initial stress field at full knee extension is significant, need to be tested again. A residual force in the ACL at 0 degree of flexion can affect not only the behaviour of the ACL, but also the general stability of the knee joint. However, this latter feature could not be captured in an isolated FE analysis of a single ACL but Chapter IX will explore this in more detail.

VIII.3.7 FE analyses of the mechanical behaviour of the human ACL during a passive knee flexion

Here, it is proposed to simulate the mechanical behaviour of the ACL during a passive knee flexion. Using the boundary conditions described in the section VIII.3.3 and the mechanical properties (set S0) described in section VIII.3.5, two series of analyses were performed.

1. A first FE analysis was carried out with a stress-free ACL at full extension.

2. A second FE analysis, using exactly the same material properties and boundary conditions with the exception of an additional initial stress field within the ACL. The application of a uniform initial stretch was performed by using the numerical technique described in section VII.5. The value of the uniform initial stretch (λ_I = 1.043) was chosen such that the initial resultant force was equal to 135 N [upper value obtained experimentally by Wascher *et al.* (1993)] (see Figure VIII.2).

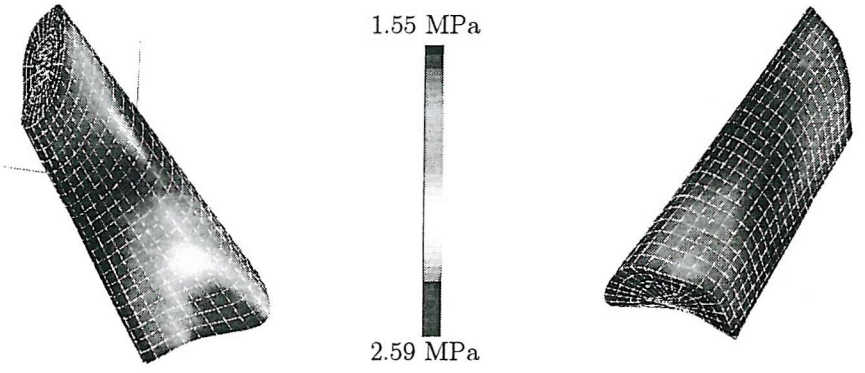

Figure VIII.2 – von Mises stresses within the ACL after application of an initial stretch λ_I = 1.043. This corresponds to the state of the ACL at full extension.

Figure VIII.2 shows the pattern of von Mises stresses at the surface of the ACL (at full extension) and highlights the fact that the maximum values are found at the anterior part of the tibial insertion whilst the minimal values occur in the middle section of the ACL. It is worthy to note that this does not contradict the fact that the posterior part of the ACL is taut at full extension (Jeffreys, 1963).

VIII.4 Results of the two FE analyses

Fringe plot of the von Mises stresses in the ACL throughout the flexion for the first FE analysis are reported in Figure VIII.3.

VIII.4.1 First FE analysis (no initial stretch)

In the first 10 degrees of flexion the maximum stresses are located in the anterolateral portion of the ACL near the femoral insertion zone. As flexion progresses, the anteromedial part of the ACL becomes the most stressed part with the maximum stress region migrating from the lateral side towards the medial side of the ACL (Table VIII.2). At 30 degrees of flexion the stresses are maximum in the midsubstance of the anteromedial band of the ACL.

VIII.4.2 Second FE analysis (initial stretch $\lambda_I = 1.043$)

At full extension of the knee, the maximum von Mises stresses are found at the anterior part of the tibial insertion of the ACL and clearly shows that the anterolateral band of the ACL is the most stretched part of the ligament. Between 0 and 10 degrees of flexion the zone of maximum stresses displaces quickly towards the femoral insertion of the ACL. At 30 degrees of flexion the stresses are still maximum in this location unlike for the first FE analysis.

VIII.4.3 Common results to the two FE analyses

The general results show that the stress distribution within the ACL is highly inhomogeneous throughout the knee flexion. From 30° of flexion, no significant difference in the general stress distribution is found between the pre-stressed ACL and the non pre-stressed one. However, this not the case for the magnitude of stress which can vary between 9 and 97 % (Table VIII.2). Despite the fact that the posterior part of the ACL at the femoral insertion site undergoes the largest displacement from full extension to full flexion, the maximum stresses are not located in this region. High stress values were found at full flexion, essentially due to the large sagittal plane rotation of the femoral insertion area. After 30° of flexion, the maximum stresses are found at the femoral insertion site of the antero-medial band of the ACL but it is worthy to note that this does not contradict the fact that the anteromedial band tightens along the flexion. If the ACL is loaded in cross-fibre directions, strains are higher at the insertion sites than in the midsubstance. This was also observed experimentally by Yamamoto *et al.* (1998) in a study using a photoelasticity methodology to track strain at the surface of the ACL.

As aimed in the formulation of the constitutive model, buckling of the ligament occurs as soon as compression or bending is developed with respect to the fibre orientation in the ACL. After 90 degrees of flexion, as reported experimentally (Girgis *et al.*, 1975), the typical necking/buckling of the ACL in the region close to the femoral insertion is also observed on both the FE analyses.

Angle of knee flexion (degrees)	$\lambda_I = 1.00$	Location	$\lambda_I = 1.043$	Location	Relative difference (%)
0	0	AM M	2.59	AM M	-
10	1.90	AM M	3.75	AM M	97.37
30	2.24	AM M	3.97	AM M	77.23
45	3.23	AM FI	4.83	AM FI	49.54
60	3.45	AM FI	4.23	AM FI	22.61
90	5.04	AM FI	5.49	AM FI	8.93
110	11.43	AM FI	10.34	AM FI	9.54
125	21.08	AM FI	34.46	AM FI	63.47

Table VIII.2 - Maximum von Mises stresses in the ACL recorded at various angles of knee flexion for the two FE analyses performed: $\lambda_I = 1.00$: the ACL is stress free at full knee extension; $\lambda_I = 1.043$: a 135 N residual force is present in the ACL at full knee extension. [AM M: Anteromedial part in the mid-substance; AM FI: Anteromedial part at the femoral insertion site].

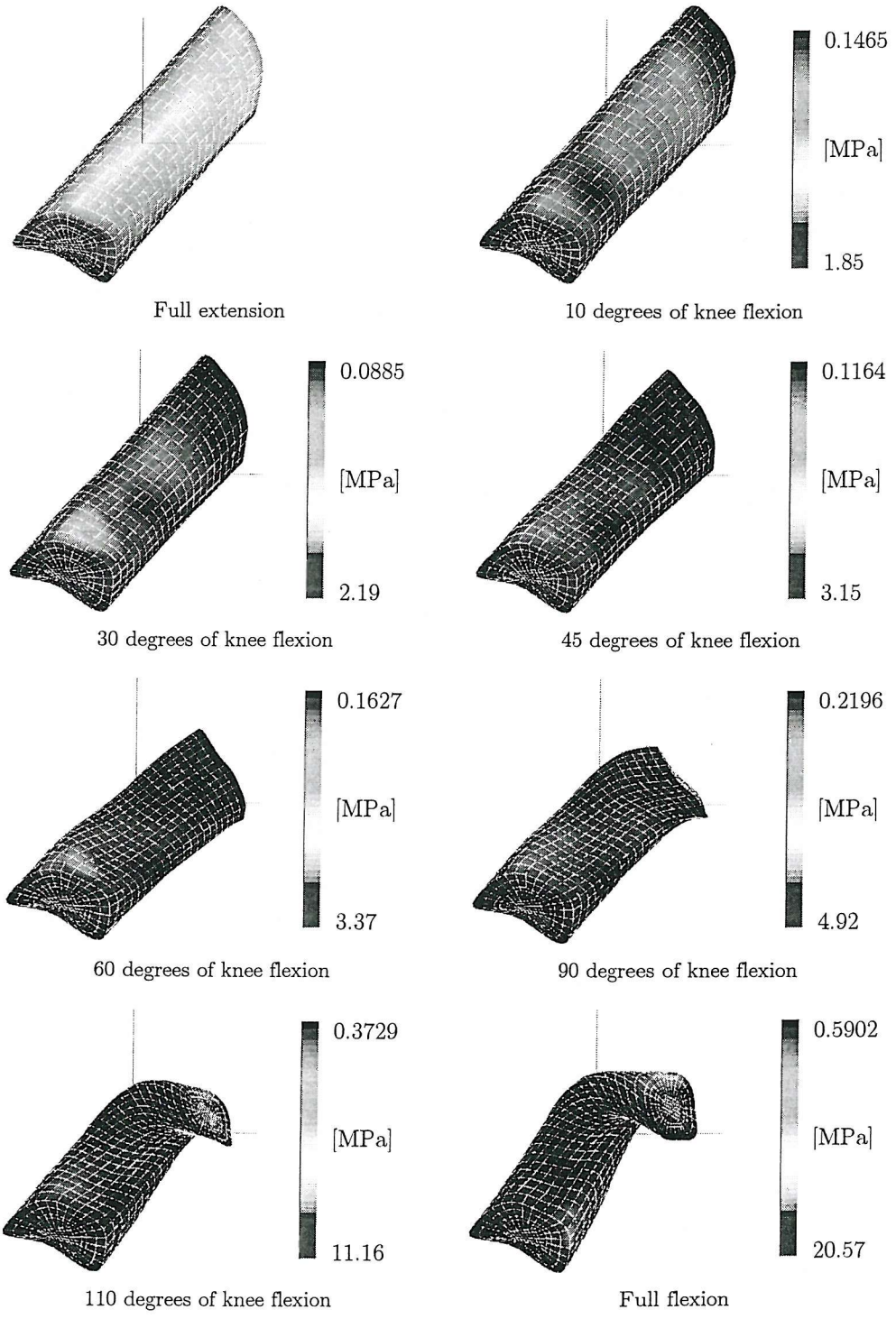

Figure VIII.3 – Contour plot of the von Mises stresses developed in the ACL during the various stages of the passive knee flexion. Results are presented in a posterior view of the ligament. In order to visualise more clearly the zones of maximum stress, the scale of the coloured fringe plots were kept different for each view of the ACL throughout the flexion.

VIII.4.4 Influence of a residual stress in the ACL at full extension of the knee

VIII.4.4.1 Evolution of α and β

In order to track the evolution of the resultant force within the ACL throughout the flexion and to compare the values obtained for the two FE analyses, a parameter α was defined as follows:

$$\alpha = \frac{R(\lambda_I = 1.0)}{R(\lambda_I = 1.043)} \qquad \text{[VIII.5]}$$

$R(\lambda_I = 1.0)$ and $R(\lambda_I = 1.043)$ represent respectively the current values of the resultant force in the ACL for the FE analysis with no pre-stretch at full knee extension and for the FE analysis accounting for a pre-stretch $\lambda_I = 1.043$ at full extension.

Similarly, an additional coefficient β (Equation [VIII.6]) was defined to follow the relative evolution of the maximum von Mises stresses for the two different FE analyses.

$$\beta = \frac{\sigma_{vMises}^{MAX}(\lambda_I = 1.0)}{\sigma_{vMises}^{MAX}(\lambda_I = 1.043)} \qquad \text{[VIII.6]}$$

The evolution of α and β is graphically represented on Figure VIII.4.

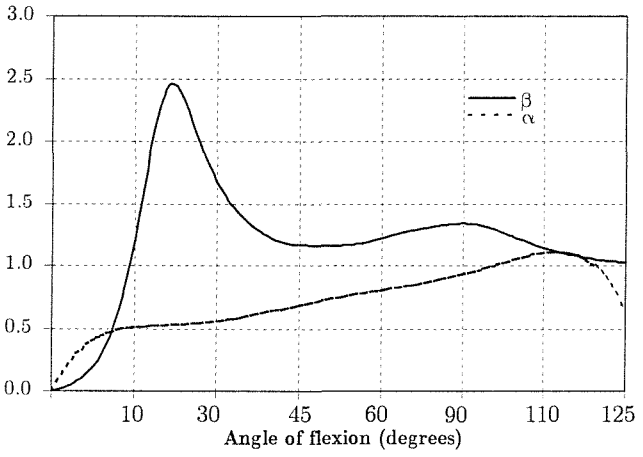

Figure VIII.4 – Evolution of the ratios α and β according to the angle of knee flexion (degrees). These dimensionless quantities are defined by Equations [VIII.5] and [VIII.6].

From full extension to 10 degrees of flexion, α increases nonlinearly to reach a value of 0.5 which means that the existence of a resultant force in the ACL at full extension generates a force at 10 degrees twice as much bigger in comparison with the case of an ACL stress-free at zero degree of flexion (first FE analysis). The variation of α is positively monotonic, mostly linear, from 10 degrees till 110 degrees of knee flexion. This is a very interesting point because it could suggest that what affects the value of the resultant force for this range of flexion considered, is a linear phenomenon.

The transversely isotropic hyperelastic model has a nonlinear behaviour in tension but, the particularity of the neo-Hookean constitutive law chosen for the matrix, is that the shear modulus is a constant and does not depend on strain. Therefore it could be hypothesized that shear behaviour at the insertion sites of the ACL is what differentiate the mechanical response of the ACL in the two FE analyses and that shear could be a dominant loading mode at these particular locations.

At 100 degrees, the resultant force is identical in the two FE models ($\alpha = 1$). Beyond 110 degrees of flexion the effect of a pre-stretched state at full extension is significant because it has a negative variation of approximately 42 % (from 1.2 to 0.7).

The amplitude of variation of β is more important than that of α (about 96 % bigger) and β evolves nonlinearly. One can distinguish four major phases in the evolution of β: 1/ from 0 to 20 degrees of flexion the increase is very steep (from 0 to 2.45), 2/ between 2 and 45 degrees, β drops from 51 %, 3/ from 45 to 90 degrees of flexion, a slight increase of 8 % is observed, 4/ between 90 degrees and full flexion β decreases by around 48 % (from 1.35 to 0.7). von Mises stresses are a positive definite combination of the principal stresses (see Chapter VII for a definition of von Mises stresses) and thus encompass the global state of stress in a material. The important nonlinear variation of β throughout the flexion shows that applying a pre-stretch to the FE model of the ACL at the beginning of the analysis has a significant effect on the magnitude of the maximum von Mises calculated. Interestingly, the four evolution stages observed for β are also found from the upper bound curves obtained experimentally for the resultant force within the ACL by Wascher *et al.* (1993). Again, this would tend to prove that our FE models is able to reproduce particular types of behaviour observed experimentally.

VIII.4.4.2 Resultant force within the ACL along a passive knee flexion

For sake of comparison, in addition to the results in resultant force obtained from the two FE analyses, three other sets of data were reported and combined in to a single graph (Figure VIII.5). An initial study performed by Limbert and Taylor (2001a) was performed using the implicit FE code ABAQUS/Standard. The FE model of the ACL and the boundary conditions were identical to those used in the two present FE analyses. However, the constitutive law was defined by an incompressible isotropic hyperelastic potential as desribed in equation [VIII.6]. The material parameters used were the same as in the study of Pioletti (1997). The analysis was run from 0 to 60 degrees of knee flexion.

The second and third sets of data represent the upper and lower bounds of the envelop of the resultant force curves obtained experimentally by Wascher et al. (1993). A significant variability was found among the eighteen cadaveric knee specimens tested.

As shown in Figure VIII.5, the qualitative and quantitative results for the resultant force in Limbert and Taylor (2001a) were not following the trend recorded experimentally by Wascher et al. (1993). In this isotropic FE model, very high compressive and flexural stresses were generated at the posterior side of the insertion zone of the ACL into the tibia, accounting for the high non physiological values for the total force in the ligament. This highlights the severe limitation of a phenomenological isotropic model when subject to bending and compressive loading.

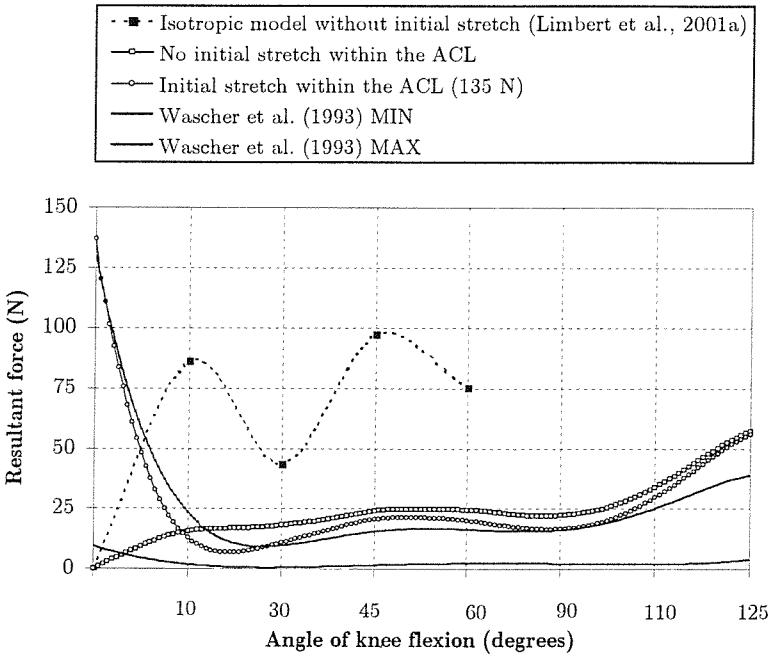

Figure VIII.5 – Graph comparing the resultant force within the ACL for three FE analyses and one experimental study performed by Wascher *et al.* (1993) on 18 cadaveric specimens. The resultant force (N) is given as a function of the angle of knee flexion.

The new constitutive model of the ACL proposed in the present work exhibits clearly a much better mechanical response when the knee is subjected to a passive flexion as the resultant force curves can testify on Figure VIII.5.

Indeed, for the first FE analysis (no initial pre-stretch at 0 degrees of flexion), after around 15 degrees of flexion, the trend of the curve follows closely that of the experimental upper bound curve of Wascher et al. (1993); the calculated force for the FE model is however slightly greater than that of the experimental curve.

Similar remarks apply for the second FE model curve (initial stretch $\lambda_I = 1.043$ at full extension) with the additional significant characteristic that between 0 and 20 degrees the calculated curve follows very well the trend of the upper bound of the experimental data. In this range of flexion, the typical steep drop in the value of the resultant force within the ACL (Wascher *et al.*, 1993) is also exhibited by the predicted reaction force of the pre-stressed ACL model. Calculated values of the resultant force are underestimated by comparison with the experimental curve from full extension towards 25 degrees of knee flexion.
From 8 degrees the resultant force of the un-pre-stressed ACL model bounds superiorly the force calculated in the pre-stressed ACL model. Beyond 110 degrees of flexion the two FE curves (with/without initial stretch) merge together as already observed through Figure VIII.4 ($\alpha \rightarrow 1$) and this is observed simultaneously with an upper shift from the upper bound experimental curve.

In light of these results concerning the resultant force within the ACL during a passive flexion of the knee, it is clear that the incompressible transversely isotropic hyperelastic constitutive law proposed for the ACL provides an excellent answer to the shortcomings of the existing three-dimensional FE isotropic models of the ACL found in literature (Limbert and Taylor, 2001a; Pioletti, 1997). Our initial hypothesis is therefore verified.

Moreover, our FE models not only reproduce qualitative mechanical behaviour of the ACL (buckling under very small compressive or flexural stresses, zone of maximum stress...) but also generate quantitative data comparable and in good agreement with experimental data obtained from physical cadaveric specimens. This latter issue is particularly important as no previous FE studies concerning the ACL has even reported the value of the resultant force in the ligament throughout the flexion cycle. Here, not only the values are reported but also, in the second FE model (initial stretch $\lambda_I = 1.043$ at full knee extension), they match closely the experimental data. By an inverse approach point of view, the FE results confirm that the ACL is in a pre-stressed state at full extension of the knee.

VIII.4.5 Comparisons of results with existing data

Given the small amount of three-dimensional FE studies of the ACL reported in literature (Hirokawa and Tsuruno, 2000; Limbert and Taylor, 2001a; Pioletti, 1997), comparisons with the new transversely isotropic hyperelastic FE model is rather quick to perform. Quantitative numerical results from Hirokawa and Tsuruno (2000) are difficult to compare with our results because these authors report results in terms of second Piola-Kirchhoff stresses and this measure of stress is radically different from the Cauchy stress at the finite strain regime (for further details please see section V.5.1). However, the general mechanical behaviour of their ACL model is very similar to that of our model: necking/buckling of the ACL appearing in the region near the femoral insertion, high stress values observed in the regions close to the femoral insertion. At 0 degree of knee flexion maximum stresses are found in the same zone but more specifically on the medial side. This conflicts with our findings for the pre-stressed ligament analysis (existence of a residual stress field at full extension of the knee) (see Figure VIII.2) and this could be explained by several factors: the initial geometry of the ACL is rather different between the two models, the boundary conditions are different and the way the FE analyses are performed is not the same. In this analysis, the simulation is started by assuming the existence of a residual stress within the ACL at full extension of the knee (enforced by the procedure described in section VII.5). The boundary conditions enforcing the flexion motions are then applied till full flexion. Hirokawa and Tsuruno (2000) deduced the geometry of the ACL from measurements made on an isolated ACL (not connected to bones and thus in a stress free state). The geometry was then idealised and deformations corresponding to an ACL attached to the bones at full extension were applied giving thus the state of stress and strain in this configuration (0 degree of flexion). It is believed that the sensitivity of the results to this procedure is quite high. Although the pre-stretch applied in our model is larger (resultant force = 135 N) than that of the model in Pioletti (1997) and Limbert and Taylor (2001a) (resultant force = 100 N), our results exhibit much lower values for the stress: 3.75, 3.97, 4.83, 4.23 MPa against 4.8, 8.1, 11.4 and 13.1 MPa found by Limbert and Taylor (2001a) for the following values of flexion angle: 10, 30, 45 and 60 degrees. The results of the two present FE analyses have shown that the maximum von Mises stresses were never located at the posterior part of the tibial insertion site as reported for isotropic models (Pioletti et al., 1998a; Limbert and Taylor, 2001a). This is easily explained by the fact that the new proposed anisotropic constitutive model of the ACL does not generate high non physiological compressive stresses when the ligament is loaded in compression or flexion along its fibre directions.

This is an important issue as it proves the advantage and the relevance of using a transversely isotropic constitutive law which accounts for the structural properties of the collagen fibres embedded in the solid matrix made of hydrophilic proteoglycans.

Since flexion-extension motions can produce different lengths and hence tension patterns in the ACL, it was found experimentally that the anteromedial band was taut throughout the entire flexion-extension cycle (Brantigan and Voshell, 1941; Fick, 1904), or at least to lengthen as the knee is extended (Arms *et al.*, 1984; Beynnon *et al.*, 1989). However, various studies have shown that the posterior band was slack in flexion and became taut only as the knee was brought to full extension (Amis and Dawkins, 1991; Bach *et al.*, 1997; Brantigan and Voshell, 1941; Fick, 1904; Girgis et al., 1975). As reported in these studies, it was found in the present numerical simulation that the posterolateral part of the ACL slackens during flexion whilst the anteromedial part tightens. For the first FE analysis, between 0 and 5 degrees of flexion the highest stress gradients are found near the femoral insertion zone; after 10 degrees, the maximum strains are located in the middle part of the anteromedial band of the ACL and from around 38 degrees, the highest strain gradients are found at the femoral insertion site to reach their maxima for deep flexion angles (>110 degrees). Generally in our model, the highest strain gradients are produced at the insertion sites of the ligament into the bone and this is also supported by the statements of Beynnon *et al.'s* (1993b). Our model also corroborates the experimental observations of Butler *et al.* (1992) i.e., the anteromedial band of the ACL carries the maximum load during the passive flexion. In another study, Butler *et al.* (1990) demonstrated experimentally that the strains in the longitudinal direction, near the insertion sites are larger than those of the mid-portion of the ACL. The present FE model also reproduces these characteristics.

The methodology adopted to apply a pre-stretch to the FE mesh is based on the assumption that the initial stretch is uniform (i.e. identical for each element of the mesh) within the ACL. It is now widely accepted that the ACL is made of two main fibre bundles having different lengths and mechanical properties (Amis and Dawkins, 1991). From a modelling point of view, it would be a very complex mechanical system to describe. Indeed, a reasonably accurate geometry of the two fibre bundles would be necessary, with relevant mechanical properties for each bundle, and maybe, more difficult, contact interaction zones should be defined between the AMB and PLB of the ACL. The nature of these contact interactions would be equally challenging to describe. In a real ACL, at full knee extension, the strain and hence the stress distribution is unlikely to be uniform but rather heterogeneous according to the fibre bundle considered and the location within the bundle.

In the FE model, the direction of the initial stretch in each element is given by the local element geometry and a state of homogeneous deformation is assumed for the pre-stressed state. A local strain at a particular location of the ACL does not influence necessarily the strain pattern at another location. So, the resultant force within the ACL at full extension found experimentally (Roberts *et al.*, 1994; Wascher *et al.*, 1993) may be the result of a pre-stretched state existing only in few fibre bundles of the ACL. This aspect is not captured by the present model.

Muscle activity increases the level of stress in the ACL (Beynnon *et al.*, 1995; Dürselen *et al.*, 1996). There is strong evidence that a passive flexion of the knee does not strain the ACL in great proportions, except for high values of knee flexion (> 110 degrees). It would therefore be certainly relevant to study the influence of a residual stress within the ACL during other kinds of physiological motion such as active flexion, squatting (with the important aspect of weight-bearing introduced) rotational motions of the knee joint, especially for extreme conditions (during sporting activities or injury scenarii), combined or not with anterior-posterior motions of the tibia relative to the femur.

In addition to the relevance in a better understanding of the biomechanics of the knee joint, there is a special interest of knowing the stress and strain states within an ACL graft as it is an important issue in rehabilitation after ACL reconstruction (Beynnon and Fleming, 1998). It seems essential to appreciate what effects particular rehabilitations exercises can have on the biomechanics of the ACL graft (which is indeed a controversial issue). Some exercises may be found inappropriate or even dangerous if they produce excessive strain in the ACL graft.

The three-dimensional geometry of the non planar insertion areas of the ACL in to the bone are subject to various errors: first, when the points are acquired on the cadaveric knee specimen by using an electrogoniometer. This introduces an error (the precision of the apparatus is in the order of 0.1 mm) which may be amplified by the action of the human operator. A second error is introduced during the geometrical reconstruction when performing an interpolation in order to define a surface from a cloud of points. These errors are difficult to quantify and, although this quantitative estimation was not developed in the present work, their existence was always kept in mind in order to have a cautious interpretation of the numerical results.

This chapter has concentrated on an isolated ACL and that implies that no possible interaction between tha ACL and the bony structures (tibia, femur) or between the ACL and the PCL (Hefzy and Grood, 1983) was taken into account. However, this effect is believed to be negligible for the particular motion analysed (passive knee flexion).

It is relevant to note that the hypothesis of incompressibility put high constraints on the nodes defining the insertion areas and therefore is likely to introduce numerical artefacts at these locations under the form of overestimated stress concentration. This effect is reinforced by the fact that nodes defining the tibial insertions are rigidly fixed and this introduces additional constraint relationships. This would recommend to be cautious when interpreting quantitative values of stress in these zones of high constraints.

VIII.4.6 Influence of the mechanical properties of the ACL on its mechanical behaviour during a passive knee flexion

In order to assess the influence of the mechanical properties of the ACL on its behaviour during a passive knee flexion, the pre-stressed ligament analysis presented in section VIII.3.7 was replicated for two different sets of material coefficients (S+ and S- defined in section VIII.3.5).

The pattern of deformation, stress and strain values were carefully compared between these two models and the model studied in section VIII.3.6 (model with mechanical properties S0) but no significant difference was found. The resultant force within the ACL along the passive knee flexion was also calculated and the relative errors between the values for extremal properties and for the reference mechanical properties were checked. The result are summarised in Table VIII.3.

	No initial stress		Initial stress	
Mechanical Properties set	S+	S-	S+	S-
Maximum relative error (%)	1.04	0.77	2.75	2.52

Table VIII.3 – Absolute relative difference in the resultant force within the ACL when considering two different sets of mechanical properties (for the whole flexion range). The reference values are those obtained for the mechanical properties belonging to the set S0. For each set of mechanical properties, the relative errors are calculated in two cases : 1/ when the ACL is stress-free at full knee extension. 2/ when the ACL is submitted to a uniform pre-stretch ($\lambda_I = 1.043$ for S+ / $\lambda_I = 1.046$ for S- model).

A difference of 10 % in the mechanical properties could be considered as an important one. However, at the light of the two last series of FE simulations, it appears that for the particular simulated motion (passive knee flexion), the influence of the mechanical properties is not particularly significant. This has two possible explanations. The first one is that, although the two sets of mechanical properties S+ and S- correspond to different stress-strain curves (see Figure VIII.1), it was assumed in both cases that the neo-Hookean coefficient C_1 was the same (i.e. 1 MPa as for the set S0). That means that the mechanical properties were modified only for the mechanical contribution of the collagen fibres. In this formulation, the fibres do not provide any stiffness to the ligament structure when they are loaded in compression along their long axis. This shows that during a passive flexion of the knee (at least for the range of flexion studied, i.e. 0-125 degrees), the mechanical load on the ACL is mainly carried by the ground substance. The second explanation could be that a passive flexion of the knee does not produce a significant load on the ACL no matter if one looks at the ground substance or at the collagen fibres mechanical response.

The kinematic tests were performed on a single cadaveric knee specimen whose mechanical properties for the ACL are probably distinct from the ones measured by Pioletti (1997). However, as it was found that their influence on the resultant force within the ACL and on the magnitude and distribution of stress and strain, were negligible this gives us confidence on the present FE results and legitimates the choice made for the mechanical properties

The importance of the inter-subject variability in mechanical properties, kinematic characteristics remain to be determined for the particular FE analyses performed.

At this stage an important remark must be made regarding the influence of the mechanical properties. In the current study these properties were varied but the kinematic conditions were kept identical. It could be hypothesized that the mechanical properties of the ACL affect the global response of the knee joint and thus its kinematics. However, in the author's opinion this effect can be considered as negligible for the particular conditions simulated.

VIII.5 Concluding remarks

VIII.5.1 Summary of findings

In this chapter, a three-dimensional finite element model of the human ACL was built and tested for a simulated passive knee flexion. For the first time, a transversely isotropic hyperelastic constitutive law was used to represent the anisotropic mechanical behaviour of this ligament. It was discovered later on that similar work had been conducted independently by two other groups (Daniel, 1999; Hirokawa and Tsuruno, 2000). However, these authors implemented phenomenological anisotropic constitutive equations in to FE codes but did not take into account any residual stress (Daniel, 1999) or used a highly idealised geometry for the ACL (Hirokawa and Tsuruno, 2000). In the present study, it was shown that a residual stress field affects significantly the magnitude of stress and the resultant force within the ACL. Moreover, the authors mentioned above did not verify that their model produced resultant force values in agreement with experimental observations and did not perform sensitivity analyses in order to assess the influence of the mesh density. In addition, in this study, the influence of the mechanical properties was also assessed. The relative simplicity of our phenomenological model describing the constitutive law for the ACL has been proven successful in the finite analyses of this ligament. The model exhibited the key characteristics of connective soft tissues: anisotropy, nonlinear behaviour, large strains, very high compliance for compressive or bending loading along the collagen fibres and incompressibility. The collagen fibre interactions, inexistent in isotropic models, were accounted for and their role was particularly significant when the ACL is twisted and flexed around its insertion sites.

The geometry of the FE model was based on anatomical measurements performed on an intact normal cadaveric knee joint specimen whilst the boundary conditions were obtained from physical kinematic tests performed on the same specimen. The mechanical properties used for the anisotropic constitutive model were derived from experimental data obtained independently by Pioletti (1997).

It was shown that the new constitutive model offers the significant advantage over the previous existing isotropic FE models (Limbert and Taylor, 2001a; Pioletti, 1997) to mimic more closely the natural behaviour of the ACL. Like other ligaments, the ACL is a mechanical structure that can carry an important load in extension along its fibres but offers a very small resistance in flexion or compression along its preferred mechanical direction.

In the present FE model, these features were integrated in the mechanical formulation (as discussed in VIII.3.5). As expected for a real ACL, the FE mesh of the ACL model deformed in a way such that buckling was produced as soon as compressive stresses developed in the direction of its axis of anisotropy. This qualitative behaviour was completed by very good quantitative results: no excessive compressive stresses appeared at the posterior side of the ACL where it inserts into the tibia. Globally, during the whole flexion cycle the posterior part of the ACL was the least stressed region in comparison with the anteromedial band. The developed FE model was able to reproduce typical stress distribution observed experimentally. This is a good qualitative indication of the relevance and usefulness of the numerical model.

An experimental validation of the FE model was obtained by comparison between the experimental and numerical results for the resultant force generated within the ACL during a passive knee flexion.

Qualitative results obtained for the FE model (stress and strain distribution, resultant force in the ligament, general mechanical behaviour) that correlate well with experimental observations bring a certain amount of confidence in the results gathered from numerical analyses.

VIII.5.2 Conclusions

To conclude this application chapter, the following conclusions are drawn:

- The new incompressible transversely isotropic constitutive law developed for the ACL and implemented numerically into an explicit FE code has been shown to be successful in representing the natural mechanical behaviour of the ACL in simulated physiological conditions. Severe limitations of previously reported three-dimensional incompressible isotropic hyperelastic models have thus been overcome.

- Numerical results from the FE simulations have shown good agreement with qualitative experimental observations in terms of stress and strain locations.

- The influence of an initial stress existing at full extension of the knee has been found significant on the magnitude of the maximum stresses but not on their distribution beyond 30 degrees of knee flexion.
- Accounting for the residual stress in the FE model simulating the mechanical behaviour of the ACL during a passive knee flexion has allowed for a close match between numerical results and experimental data in terms of the total force developed in the ACL. This can be considered as a validation of our numerical model, at least for the simulated physiological range of motions considered, i.e., a passive knee flexion. This presents a real novelty among the very few FE models of the ACL available as it provides quantitative information easily related to experimental data.
- The explicit FE implementation has been proven extremely robust to track accurately the highly nonlinear behaviour of soft tissue in the finite strains domain. The computational cost efficiency is another strong point of the explicit implementation.

Chapter IX

Application 2:
FE simulation of the mechanical behaviour of the human knee joint subjected to anterior-posterior forces

The previous chapter dealt with finite element simulations of the mechanical behaviour of an isolated ACL subjected to various loading conditions. In Chapter IX, it is proposed to study the mechanical response of a simplified human knee joint subjected to anterior-posterior drawer tests. The chapter describes the development of an idealised model that represents the complex mechanical system of the knee. The three bony structures are modelled as rigid bodies interacting with each other by the way of highly deformable three-dimensional links of different variable stiffness, i.e., the ligaments (ACL, PCL, LCL, MCL). Contact interactions are allowed to occur between articular cartilage of the femur and the tibia, ligament and bone and ligament and ligament during the FE analyses. The influence of residual stress within the ACL was also assessed in order to highlight its effects on the global mechanical response of the knee joint. The developed FE model provides new (in FE literature) information regarding the resultant forces developed in the ligaments during drawer tests as well as insight into the complexity of the mechanical response of the knee joint even for simple boundary conditions.

IX.1 Background

Extensive experimental work has been performed to study the knee biomechanics, particularly related to drawer tests (Brantigan and Voshell, 1941; Butler *et al.*, 1980; Fukubayashi *et al.*, 1982; Girgis *et al.*, 1975; Gollehon *et al.*, 1987; Levy *et al.*, 1982; Markolf *et al.*, 1976, 1984, 1995, 1990, 1993; Nielsen and Helming, 1985; Piziali *et al.*, 1980a, 1980b; Sullivan *et al.*, 1984). A drawer test is a clinical examination protocol used to assess the existence and the degree of severity of either an ACL or a PCL injury. It consists of applying a translational load to the tibia while maintaining the femur fixed, either at full knee extension or 90 degreees of flexion with respect to the tibia. While stabilising the femur with one hand, the examiner alternately draws the tibia forward and backward with the other hand. The amplitude of displacement recorded represents what is called the laxity of the joint. A positive anterior drawer test occurs when there is abnormal translation of the tibia anteriorly on the femur and no firm endpoint of an intact ACL is felt and is indicative of ACL injury. Similar findings for PCL in posterior drawer test apply. In the present study the strict definition of a drawer test (knee flexed at 90 degrees of flexion) is extended to define similar tests with the knee fully extended (0 degree of flexion) or at other angles of flexion of the knee. Although mainly focused on the biomechanical response of the knee joint subjected to drawer tests, all of the studies mentioned above are different in terms of the experimental methodology adopted and the boundary conditions applied. For example, Butler *et al.* (1980) and Race and Amis (1996) considered that accurate qualitative and quantitative evaluation of knee motions could only be provided by applying a fixed displacement and measuring the resistive load. On the other hand, other authors like Fukubayashi *et al.* (1982), Markolf *et al.* (1976, 1978) and Torzilli *et al.* (1981) have examined ligament function by measuring the joint displacement resulting from application of a known load. This relates to the usual clinical practice in which the surgeon assesses the degree and type of injury from the observed laxities (drawer and Lachman tests). A Lachman test is a clinical test performed to assess the anterior-posterior stability of the knee in the same way as a drawer test except that the knee should be in 30 degrees of flexion. Nevertheless, its is essential to keep in mind that the observed laxity depends on the magnitude of the applied load and that it is conditioned by the complex force interactions developed by the ligaments of the joint.

When a ligament is cut or damaged, these interactions are modified and lead to an increase in the laxity not only because of the missing action of the cut ligament but also because of the redistributed pattern of forces within the remaining ligaments (Fukubayashi *et al.*, 1982; Gollehon *et al.*, 1987; Piziali *et al.*, 1980a; Piziali *et al.*, 1980b).

It is now widely accepted that the ACL is the primary restraint to anterior tibial translation (Bendjaballah *et al.*, 1998; Butler *et al.*, 1980; Gollehon *et al.*, 1987; Markolf *et al.*, 1995, 1990, 1993; Piziali *et al.*, 1980a, 1980b). This was demonstrated by the isolated resection of the ACL. However, the role of the PCL in posterior tibial translation is not well defined and is a controversial issue. For example Gollehon *et al.* (1987) and Bendjaballah *et al.* (1998) found that the PCL is the primary restraint to posterior displacement while Markolf *et al.* (1976) and Race and Amis (1996) found its restraining action moderate. In another study, Markolf *et al.* (1996) reported a minor contribution of the PCL in resisting posterior drawer forces. It was shown by Gollehon *et al.* (1987) and Fukubayashi *et al.* (1982), among others, that when an anterior force was applied to the tibia of an intact knee, an internal rotation of the tibia was produced whereas external rotation occurred in the case of a posterior force. Cutting the ACL had the effect of eliminating these coupled rotations. Mathematical models of the knee have also been helpful in investigating the stiffness characteristics of the knee joint (Andriacchi *et al.*, 1983). The references given above are cited for sake of illustration but the list is far from being exhaustive.

FE models are useful in studying complex mechanical systems because they can provide deep insights into mechanical characteristics (e.g. resultant force, contact force and the stress distribution within the ligaments) which are very difficult or impossible to assess experimentally. To the best of my knowledge, no FE model of the knee joint with ligaments modelled as three-dimensional transversely isotropic hyperelastic structures, has been built in order to carry out these particular studies. Pioletti (1997) performed a three-dimensional FE analysis of the ACL when the knee is subjected to drawer tests. As this study did not include the PCL, LCL and MCL, no attempt was made to quantify the relative restraining functions of the ligaments when the knee undergoes anterior-posterior drawer forces. Knowing how each ligament contributes to the resisting forces to a particular motion of the knee joint is a key issue in the general understanding of knee biomechanics. Moreover, drawer tests are essential in clinical practice to assess the existence/severity of a ligament-injured knee (Torg *et al.*, 1976). In a FE study, Bendjaballah *et al.* (1998) assessed the passive mechanical response of the knee subjected to anterior-posterior forces. Although their three-dimensional knee model included the menisci, the modelling of the cruciate and collateral ligaments was simplified.

Each ligament was represented by five bundles, modelled as 2-noded uniaxial elements and a one-dimensional constitutive law was used. This representation was unlikely to capture the complex interactions between the bony structures and the ligaments that lead to particular redistribution of the stress within the ligaments especially since the model did not include the full geometry of the femur and that of the tibia. This had the potential to prevent some contact interactions between ligaments and bones to occur and consequently to alter the resultant forces in ligaments. Recently, Li *et al.* (1999) developed a more bio-fidelic three-dimensional finite model of the knee that was validated against experimental measurements (anterior-posterior loads at 0 and 30 degrees of knee flexion) by means of a parametric optimisation procedure. Ligaments were modelled as elastic springs obeying a piecewise function as used by Blankevoort and Huiskes (1991b). There was therefore no full three-dimensional modelling of the ligaments and their interactions with bony structures were not taken into account.

IX.2 Objectives of Chapter IX

In the light of the previous literature review concerning three-dimensional finite element models of the knee joint, it is clear that there is a definite space for investigative research. Indeed, no published finite element model of the knee joint represents the ligaments as three-dimensional continuum anisotropic hyperelastic structures and the bony structures as full three-dimensional solid bodies. The effect of the three-dimensional contact interactions between the bony and ligamentous structures on the mechanical response of the knee subjected to drawer forces has therefore never been captured. It appears that a mathematical model of the knee joint which does not account for the menisci is capable of reproducing "reasonably well" the laxity of the knee joint in anterior-posterior translations performed on a comparable experimental model (i.e, knee without menisci) (Mommersteeg *et al.*, 1996a). As the role of menisci was not believed to be essential in anterior-posterior drawer tests of the non-load bearing knee joint and because of the added complexity, these substructures of the knee were not accounted for in the present numerical model. This may restrict the validity of the model to *in-vitro* conditions. It has been hypothesized that the complex contact interactions between ligaments and bony structures of the knee may have a significant influence on the effective load-bearing characteristics of the ligaments by providing a mechanism partially responsible for the relative distribution of force within the ligaments of the knee.

The geometry of the insertion sites of ligaments into bones (relative angle between bone surface and line of action of the ligament) may also be an important factor because of the anisotropic characteristics of the ligaments. Modelling ligaments as three-dimensional transversely isotropic hyperelastic structures can therefore highlight particular behaviour missed by considering only isotropic mechanical properties.

Any computational biomechanical model requires experimental validation for obvious reasons. A first step towards achieving this goal is to make sure that the numerical model predicts the typical behaviour observed experimentally, firstly in the qualitative domain and secondly in the quantitative one. To this effect the main objectives of this chapter are:

- To confirm that the ACL is the primary restraint to anterior tibial translation.
- To assess the restraining function of the PCL to posterior tibial translation.
- To confirm that the LCL and MCL are secondary restraints to anterior-posterior motions of the knee joint.
- To demonstrate that the FE model of the knee joint is sensitive enough to pick up and simulate reliably an ACL-deficient knee.
- To investigate the influence of a residual stress present in the ACL with the knee at full extension on the anterior-posterior drawer motions when one applies drawer displacements to the tibia.

IX.3 Three-dimensional finite element modelling of the knee joint

IX.3.1 Geometrical and finite element model of the simplified knee joint

A solid model of an average human knee was built from a surface description (Viewpoint Digital, Draper, UT, USA). The geometry used to create this surface description was taken from a solid plastic model of a knee used for medical training. The original file format was DXF, widely used in CAD of consumer products and consisted of a collection of quadrilateral surfaces. Using a customised program, the file was converted into a format suitable to pass to a structured block mesh generator (TrueGrid™, XYZ Scientific Applications, Inc., Livermore, CA, USA).

Although the initial Viewpoint model included all the substructures within the knee (patella, patellar tendon, muscles, menisci...), it was decided to consider only the femur, the tibia, the fibula for the bones, the anterior and posterior cruciate ligaments (ACL, PCL) and the lateral and medial collateral ligaments (LCL, MCL). Bone surfaces were meshed with 4-noded shell elements and described as rigid surfaces whilst the four ligaments were meshed using 8-noded hexahedral elements. Each substructure was meshed independently from the others and a merge process was performed within TrueGrid™ for building the complete FE model. The FE model consisted of 15584 nodes, 2354 solid elements and 10589 shell elements (Figure IX.1, Figure IX.2).

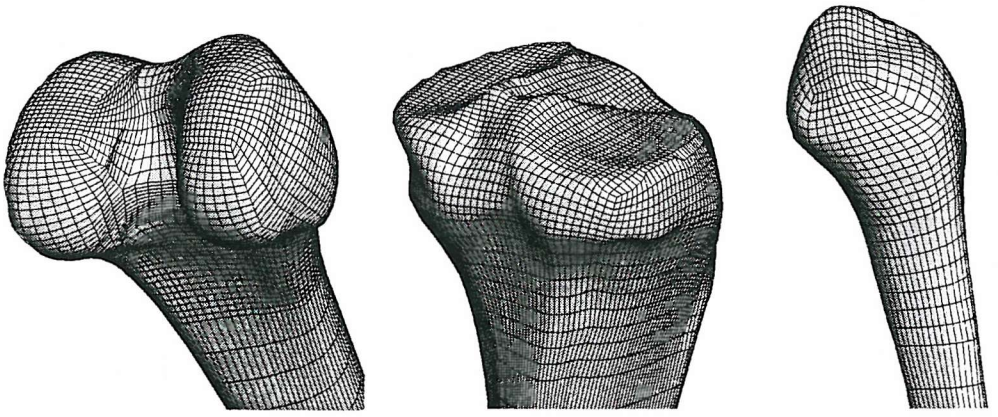

a) Femur b) Tibia c) Fibula

Figure IX.1 – Finite element meshes representing the bony structures of the knee joint model. The elements constituting the meshes are linear shell elements and are modelled as rigid structures. Characteristics of these three FE meshes : a) *femur* : 4704 nodes and 4663 elements. b) *tibia* : 4393 nodes and 4320 elements. c) *fibula* : 1608 nodes and 1606 elements.

As the FE meshes representing the three-dimensional ligament structures were meshed separately from the bony structures, it was necessary to use a special approach to connect these non congruent meshes together. The last rows of elements composing the ligaments (at the two extremities) were assumed to be made of the same rigid material as the bony structures to which they attach and also assumed to be part of the same rigid body. This also prevented singularities caused by the attachment of a soft deformable structure with sharp edges to a rigid structure. The fibula was rigidly attached to the tibia by making it part of the same rigid body as the tibia.

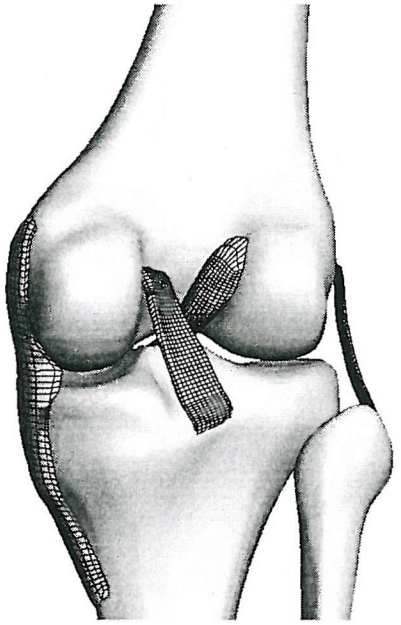

Figure IX.2 – Finite element model of the complete simplified knee joint. Bony structures (femur, tibia, fibula), represented with a Gouraud shading rendering, are modelled as rigid shell elements whilst the four ligaments (ACL, PCL, MCL, LCL) are meshed with 8-noded deformable hexahedral elements. The characteristics of the four solid meshes are the following :

ligament	*nodes*	*elements*
ACL	1406	640
PCL	1350	792
LCL	1232	550
MCL	882	372

A rigid body, defined as a collection of nodes, is a single body with global inertia properties. The distance between nodes belonging to the same rigid body are constant no matter what the loading conditions are. A rigid body is defined by a reference point (generally its centre of gravity) and its inertia properties that governs its global motions. A nonlinear FE analysis involving rigid bodies is computationally cost effective because internal forces of the nodes composing the rigid body are not computed although enforcement of kinematic constraints require additional computations.

In PAM-CRASH™, boundary conditions can only be applied to a rigid body at its centre of gravity. For this reason, in the various FE simulations performed, the prescribed translational conditions were applied to the centres of gravity of the tibia.

IX.3.2 Constitutive models and mechanical properties of knee ligaments

The incompressible transversely isotropic hyperelastic model described in Chapter V (Equations [V.82] and [V.83]) was adopted for the mechanical formulation of the behaviour of the two collateral ligaments of the knee. As no data was available for the tensile properties of the LCL, it was decided to use instead the data provided by Quapp and Weiss (1998) for the MCL as a first approximation. In their studies, Quapp and Weiss (1998) performed biaxial testing on MCL specimens and their experimental data were fitted to an incompressible transversely isotropic hyperelastic law. To describe the mechanical behaviour of the ACL and PCL, the constitutive formulation described in section VIII.3.5 was adopted. In this latter section the mechanical properties of the ACL were derived in order to fit the incompressible transversely isotropic hyperelastic law (Equations [VIII.2], [VIII.3] and [VIII.4]). In a similar manner, not presented here, the mechanical properties of the PCL (Pioletti, 1997) were derived to fit the same constitutive law as the ACL.

Ligament	Data source	C_1 (MPa)	C_2 (MPa)	C_3 (MPa)	C_4	C_5 (MPa)	λ^*
ACL	Pioletti (1997)	1	0	0.3750	22.4198	-	-
PCL	Pioletti (1997)	1	0	0.1177	40.6023	-	-
MCL	Quapp and Weiss (1998)	4.6	0	2.4	30.6	323.7	1.055

Table IX.1 – Material coefficients for the constitutive law defining the mechanical behaviour of the ACL and PCL (Equations [VIII.2], [VIII.3] and [VIII.4]) and for the constitutive law defining that of the MCL (Equations [V.82] and [V.83]).

IX.3.3 Contact conditions

The knee joint is a complex mechanical system where numerous structures interact between each other. Examples of these interactions are: direct contact between the femur and the tibia through the articular cartilage, sliding and warping of ligaments around bones and contact interactions between the two cruciate ligaments. In any FE simulation involving contact it is required to define, prior to the beginning of the analysis, all potential contact regions. Generally one defines a master and a slave zone, the latter being subjected to the action of the former. These two zones, forming a contact pair, can be a set of nodes, a set of element edges, a set of element faces or any combination of these according to the contact algorithm used.

Contact algorithms, according to their degree of sophistication, detect all contact zones in the predefined spaces where the contacts are assumed to occur. In the present FE model, the following contact pairs were considered:

- tibial plateau-femoral condyles: (algorithm: 33)
- ACL-PCL: (algorithm: 44)
- ACL-tibial plateau / ACL-intercondylar femoral groove: (algorithm: 44)
- PCL-tibial plateau / PCL-femoral condyle: (algorithm: 44)
- LCL-lateral femoral condyle: (algorithm: 33)
- MCL-medial femoral condyle / MCL-lateral side of the tibia: (algorithm: 44)

Contact algorithm 33 is a segment-to-segment contact: symmetric contact pairs are defined by faces of shell or solid elements. Contact algorithm 44 is a node-to-segment contact with smooth contact surface: the master surface is defined by faces of shell or solid elements while the slave surface is a set of nodes. In all the FE simulations performed, frictionless contact interactions were assumed. As the FE model of the knee joint did not include cartilage surfaces a simple trick was used to take into account cartilage thickness at the surfaces of the bones. Bony surfaces were defined by rigid shell elements which require the definition of a shell thickness. By playing with this parameter it was possible to adjust the uniform cartilage thickness to the desired value which was eventually chosen as 2 mm (Walker and Hajek, 1972).

IX.4 Simulations of drawer tests at full knee extension

The objective of this study is to assess the mechanical response of the knee joint when subjected to passive anterior-posterior drawer tests. The results of interest are the total resisting force developed by the tibia and the resultant forces within the four ligaments of the joint: ACL, PCL, LCL, MCL. In order to preserve the joint's natural function during the application of a drawer force, the constraints applied to the degrees of freedom characterising the rigid bodies were carefully chosen.

IX.4.1 Case 1a – Case1b: intact knee

It was shown by Andriacchi *et al.* (1983), using a three-dimensional model of the knee joint, that constraining coupled degrees of freedom strongly influenced the force-displacement relationship of the knee. An experimental study by Fukubayashi *et al.* (1982) also highlighted this characteristic. Two series of numerical analyses were performed: Case 1a and Case 1b (Figure IX.3). A posterior-anterior displacement of 16 mm (Case 1a) was applied to the tibia with the femur completely fixed whilst medial-lateral, proximal-distal coupled displacements, varus-valgus and internal-external coupled rotations were set free for the tibia. The test was performed again with an anterior-posterior displacement of 16 mm (Case 1b) applied to the tibia. Minimal constraining conditions were chosen in order to minimise the influence that the point of application of the applied displacement may have on the mechanical response of the knee joint.

IX.4.2 Case 2a – Case 2b: ACL resected knee

The analyses for Case 1a and Case 1b were repeated by simulating a total ACL resection. This was easily done by removing the ACL and all its associated contact pairs from the FE model. These tests were performed to confirm the primary role of the ACL in resisting anterior motion of the tibia relative to the femur and to assess its function in posterior motion of the tibia.

IX.4.3 Case 3a – Case 3b: influence of residual stress the ACL during simulated drawer tests of the knee at full extension

As suggested in the previous chapter concerning the ACL, it is relevant and certainly worthwhile to investigate the role of residual stress in knee ligaments when the knee is subjected to other motions than passive flexion, i.e., drawer tests at full extension.

A series of two numerical tests was designed in order to study the way residual stresses in the ACL (with the knee fully extended) can affect the displacement of the tibia relative to the femur and how the forces are redistributed within each of the four knee ligaments when the ACL is pre-stressed. Cases 3a and 3b are identical to cases 1a and 1b at the exception of an additional condition concerning pre-tension in the ACL at the beginning of the analysis. The equivalent force generated by this pre-tension was 135 N as described in the previous chapter (section VIII.3.6).

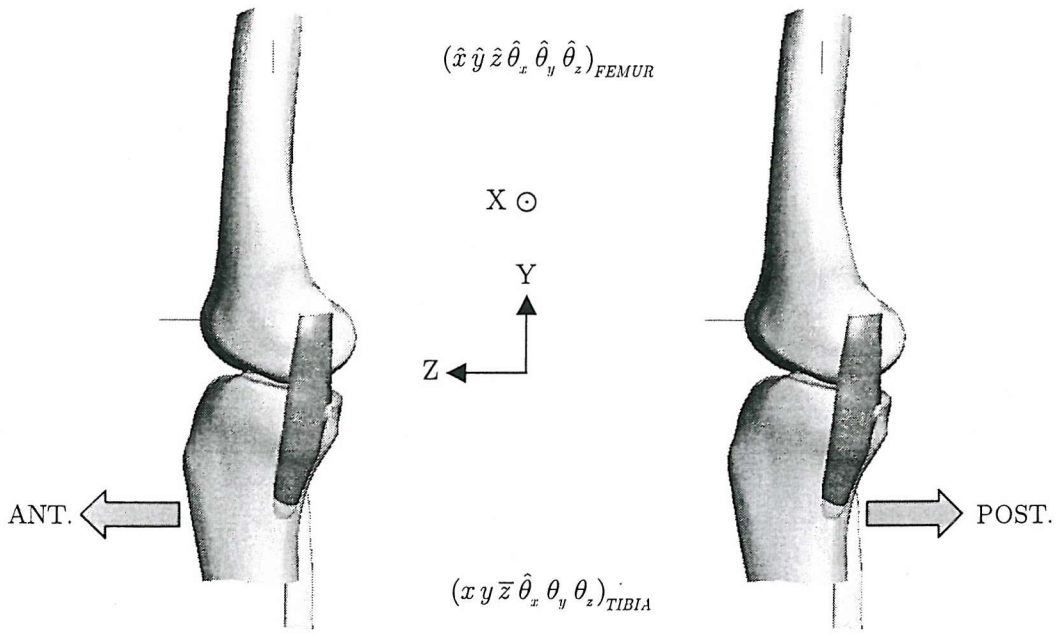

Figure IX.3 – Schematic representation of the two types of drawer tests performed on the FE model of the knee joint (viewed from the medial side). $x, y, z, \theta_x, \theta_y, \theta_z$ are respectively the translational and rotational degrees of freedom of the centres of gravity of either the tibia or either the femur. Convention for the degrees of freedom are: ^: *fixed* / a bar symbol: *prescribed* / no symbol: *free*. Each loading case is subdivided in to three subcases : 1 = intact knee; 2 = ACL-deficient knee and 3 = intact knee with an initial stress present within the ACL at full knee extension.

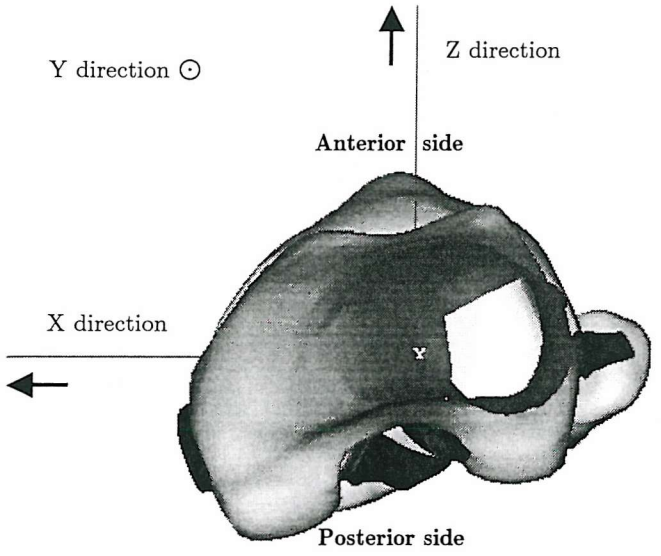

Figure IX.4 – Top view of the FE knee joint model. The first structure on the foreground is the femur. The X, Y and Z axis are respectively defined as the lateral-medial, distal-proximal and posterior-anterior axes. Rotations around X, Y, Z define respectively the flexion-extension, external-internal and varus-valgus rotation axes.

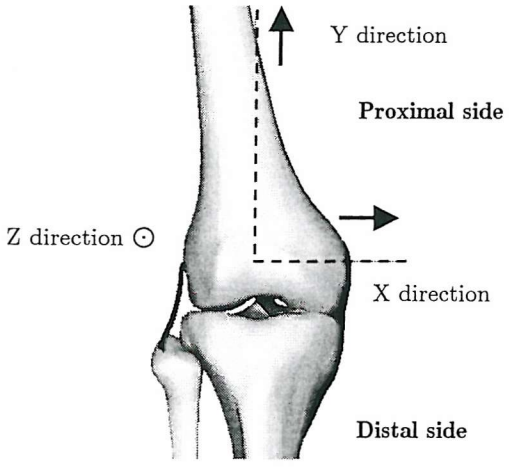

Figure IX.5 – Anterior view of the FE knee joint model. The X, Y and Z axis are respectively defined as the lateral-medial, distal-proximal and posterior-anterior axes. Rotations around X, Y, Z define respectively the flexion-extension, external-internal and varus-valgus rotation axes.

IX.4.4 Computational aspects

The FE simulations were performed over a total physical time of 100 ms. Displacement curves were smoothed by a fifth order polynomial form in order to obtain a quality quasi-static solution as discussed in section VIII.3.3. The simulations were ran on a dual-processor Pentium® III PC clocked at 933 MHz (equipped with 1024 Mbytes of RAM) and the CPU time required for each FE analysis was about six hours. This is extremely economic compared to implicit FE analyses which have a higher cost per time step. The explicit analyses involving finite deformations and complex contact interactions are also more robust than implicit solving techniques. The average time step for the FE analysis was in the order of 0.49 μs.

Table IX.2 presents a breakdown of the characteristics of a typical FE analysis simulating anterior-posterior motions of the knee joint at full extension.

	CPU(SEC)	SYS(SEC)	PCT
INITIALIZATION PHASE	5.156E-01	3.125E-02	0.00
INTERNAL FORCES	1.066E+04	3.547E+00	50.38
TIME INTEGR, FRAME UPD	7.313E+03	4.906E+00	34.56
I/O TO TAPES 2,4,5	7.908E+01	6.662E+01	0.69
CONTACT ALGORITHM	9.842E+02	3.078E+00	4.66
DISPLCT AND VELOCITY BC	3.919E+01	3.281E-01	0.19
NODAL CSTR, RB, RW	2.014E+03	2.828E+00	9.52
TOTALS	2.109E+04	8.134E+01	100.00
ELAPSED TIME	2.148E+04		
RATIO CPU/ELAPSED TIME	9.820E-01		

Table IX.2 – Computational aspects of a 100 ms (physical time) explicit finite element analysis simulating the mechanical behaviour of the knee joint under anterior-posterior forces. PCT means percentage of the total computational effort.

IX.5 Results and discussion

For each FE analysis anterior-posterior displacements of the tibia (defined by its centre of gravity) were plotted versus the variation of the reaction load: Figure IX.6 and Figure IX.10 for Cases 1-2 and 1-3. Resultant forces within each single ligament at special drawer displacements (4, 8, 12 and 16 mm) are represented on Figure IX.8, Figure IX.9 and
Figure **IX.11** respectively for Cases 1-a-b, 2-a-b and 3-a-b.
To ascertain the validity of the computations, equilibrium of forces and moments (ligament forces, contact forces and force applied) were checked and were found to be satisfactory.

IX.5.1 Results for Cases 1a, 1b, 2a and 2b. Effects of ACL resection

The forces show a general nonlinear response of the knee when subjected to anterior-posterior displacement as reported in other studies (Bendjaballah *et al.*, 1998; Fukubayashi *et al.*, 1982). This shows that there is a progressive recruitment of the ligamentous structures as the structure is drawn anteriorly and posteriorly. The nonlinear mechanical properties of ligaments are responsible for this but also the initial geometry of each of the ligaments in the FE model of the knee and the geometry of the femoral/tibial articular surfaces.

IX.5.1.1 Force-displacement results

The anterior and posterior forces acting on the tibia (intact and ACL-deficient knee) exhibit the typical nonlinear stiffening response of the knee subjected to anterior-posterior displacement (Figure IX.6). This is explained firstly by the initial geometry of the ligaments as they are not necessarily tense prior to the application of the drawer load and secondly by the nonlinear mechanical characteristic of ligaments whose stiffness increases with deformation. At the beginning of the application of the tibial displacement there is virtually no resistance (the current model does not include menisci or capsular structures) in the free motion of the tibia. As the displacement of the tibia increases and so the reaction load, the ligamentous structures get recruited and develop resisting forces which tend to increase with the stiffness of the joint.

It appears that the quantitative response of the tibia to drawer force is sensitive to the direction of the drawer force: applying the load in the anterior-posterior direction is different from applying in the posterior-anterior direction as reported in Bendjaballah *et al.* (1998) and implicitly implied by the experimental results from Fukubayashi *et al.* (1982). In this FE model, the mechanical response of the knee is much stiffer in the anterior direction than in the posterior direction. This is primarily due to the initial geometry of the PCL which, unlike the ACL, has its (collagen) fibres running in a direction less aligned with the orientation of the drawer load. This geometrical configuration is such that the PCL collagen fibres are not stretched along their natural axis and thus provide a low resisting force. Although the tibial insertion site of the PCL displaces significantly with the tibia, the PCL is not stretched sufficiently to produce a large resisting force.

At 50, 100, 150, 200, 300 and 400 N anterior tibial drawer load the displacement of the tibia are respectively 4.5, 7.65, 9.5, 10.98, 13 and 15 mm whilst a 16 mm posterior displacement of the tibia generates a resisting force of only 73 N.

Due to the numerous differences existing in the experimental or numerical protocols reported in literature, a large variability is found regarding the magnitude of the tibial displacements at a given load. It appears that constraining coupled motions during drawer tests leads to a much stiffer response of the knee joint (Butler *et al.*, 1980; Fukubayashi *et al.*, 1982; Markolf *et al.*, 1976; Piziali *et al.*, 1980b). Piziali *et al.* (1980b) reported anterior tibial displacements varying between 4.7 and 7.7 mm under forces ranging from 500 to 590 N. Fukubayashi *et al.* (1982) noted an increase of 30 % of tibial laxity when the tibia was free from rotational constraints along its principal axis.

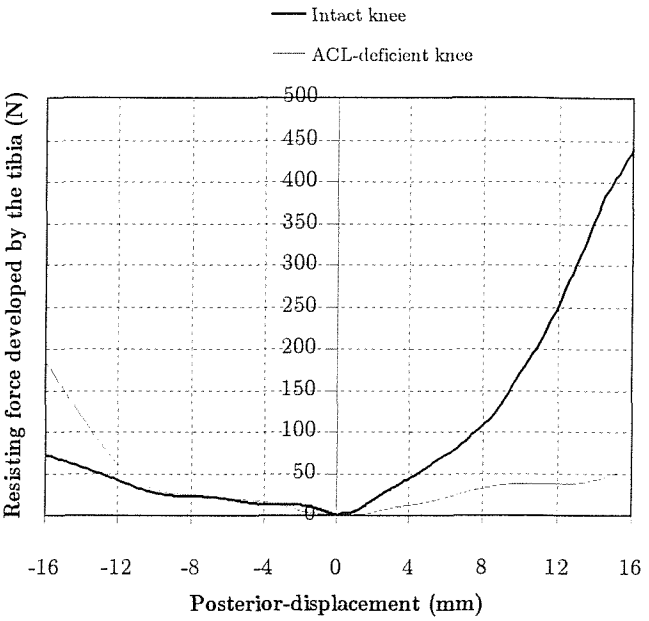

Figure IX.6 – Force-displacement curves for **Cases 1a**, **1b** (intact knee), **2a** and **2b** (ACL-deficient knee). A 16 mm displacement is applied to the tibia in the posterior-anterior direction (Case *i*a) and in the anterior-posterior direction (Case *i*b). The femur is constrained in all degrees of freedom whilst the tibia is constrained only in the rotational degree of freedom around the X axis (axis of flexion of the knee). The resisting force is the absolute magnitude of force measured at the centre of gravity of the tibia.

This was implicitly confirmed by Bendjaballah *et al.* (1998) who observed a 35 % decrease in tibial laxity when the tibia was prevented from rotating along the internal-external rotation axis. Using comparable boundary conditions to the present model, for the various drawer tests, Bendjaballah *et al.* (1998) found the following values respectively for an anterior and a posterior drawer test applied to the tibia (400 N force): approximately 5 and 4.2 mm for tibial displacements. When considering femoral drawer forces, these authors found displacements of approximately 4.1 and 5 mm, respectively for anterior and posterior forces. Results from an experimental study performed by Fukubayashi *et al.* (1982) showed that, at full extension, a 100 N force applied anteriorly to the tibia produces a 5 mm displacement while this displacement increased to 6 mm when the force is applied in the posterior direction. Butler *et al.* (1980) and Race and Amis (1996) applied drawer displacements to the tibia and measured the restraining forces generated. With the knee at 30 degrees of flexion, Butler *et al.* (1980) found that 5 mm displacements applied to the tibia in the anterior and posterior directions developed forces of respectively 333 and 331 N. It is worthy noting that the coupled motions were not allowed to occur.

Allowing for coupled motions of the tibia, Race and Amis (1996) reported displacements of about 2, 4 and 6 mm when the tibia is subjected to posterior drawer forces of respectively 40, 100 and 210 N with the knee at 0 degree of flexion. Bendjaballah *et al.* (1998), Fukubayashi *et al.* (1982), Gollehon *et al.* (1987) and Levy *et al.* (1982) reported tibial displacement values of about 2.1, 5, 4.5, 3.4 mm at 100 N tibial anterior drawer force and 1.7, 4, 5, 3.6 mm at 100 N tibial posterior force, respectively, with the knee at full extension. At 100 N of tibial drawer forces, the FE model produces much higher values, 7.65 (at 100 N of tibial drawer force) and 16 mm (at 73 N of tibial drawer force) respectively for anterior and posterior motions. For 200 and 300 N drawer forces, values of anterior tibial displacement were found to be 10.9 and 13 mm [3.1 and 4.1 mm in Bendjaballah *et al.* (1998)] for anterior motions. A 16 mm posterior displacement of the tibia in the model used in the present study produced a 73 N knee resisiting force and therefore it is not possible to compare our results with Bendjaballah *et al.* (1998) who found posterior displacement of 2.6 and 3.6 mm respectively at 200 and 300 N tibial loads. The high values of displacement found in our FE model are largely explained by the fact that the FE model did not include the postero-lateral capsules and the menisci. The geometry of the ligaments is essential as it conditions the laxity of ligaments and the orientation of the stiff collagen fibres. The mechanical response of a transversely isotropic structure whose anisotropic direction offers a much stiffer response that in the plane of isotropy, will vary significantly according to the direction of load. In consequence, it is essential to keep in mind all of these factors play an important role.

Cutting the ACL clearly decreases the stiffness of the joint in the anterior drawer test as demonstrated on Figure IX.6. For a given amount of anterior displacement, the resisting force developed by the tibia was much lower in the case of the ACL resected knee because the normal major resisting contribution from the ACL is no longer available. A clear illustration of this is given in Table IX.3 where one can see that resection of the ACL leads to an over three times bigger displacement for a given 50 N anterior drawer load (reaction load).

	Displacement (mm)		Variation (%)
50 N tibial load	Intact knee	ACL resected	-
PA force to the tibia	4.5	15.1	235.5
AP force to the tibia	13	11.4	-12.39

Table IX.3 – Anterior-posterior (AP) and posterior-anterior (PA) displacements of the tibia under a 50 N drawer load at full extension of the knee. Results are given for an intact and ACL-deficient knee. The percentage of variation of displacement between the two models is also presented.

In posterior motion, for the same reaction load (50 N), the tibial displacement decreases by 12.4 % when the ACL is resected. As a consequence of ACL resection, the stiffness of the knee joint increases in posterior drawer test. At 16 mm of posterior tibial displacement, the corresponding tibial force is 185 N whilst for the intact knee this value is only 73 N. This observation is explained by the fact that after ACL resection, the proximal-distal and medial-lateral motions of the tibia are altered as shown on Figure IX.7. From 0 to 2 mm and from 8 to 16 mm of posterior tibial displacement, the tibia is pulled apart from the femur in the vertical direction (Y axis) whilst from 2 to 8 mm displacement the trend is reversed. As the two bony structures are pulled away from each other, this has the effect of stretching the PCL and the LCL in greater proportions than for the case of the intact knee where the magnitudes of displacement are smaller and where the shifts of proximal-distal displacement directions appear at different values of posterior tibial displacement. From 0 to 8 mm of posterior tibial displacement, the tibia displaces laterally about 3 mm where it remains in this lateral position until 13 mm of posterior tibial displacement and then displaces back in the medial direction. For the intact knee, the maximum lateral displacement reached only 2.5 mm.

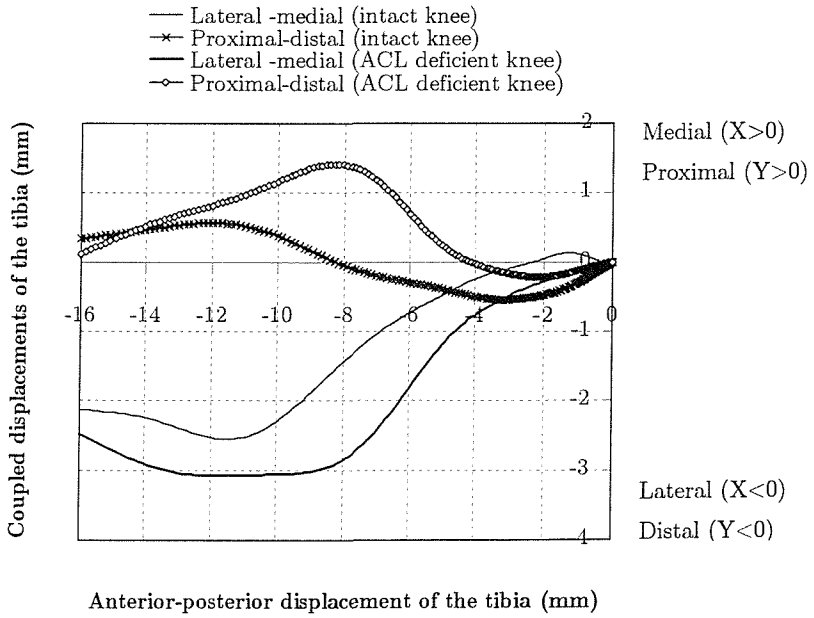

Figure IX.7 – Coupled displacements of the tibia with respect to the posterior tibial displacement for **Cases 1b** and **2b** (intact and ACL resected knee). The femur is constrained in all degrees of freedom whilst the tibia is constrained only in the rotational degree of freedom around the X axis (axis of flexion of the knee).

These observations clearly exhibit the fundamental mechanical interactions played by the ligaments within a knee joint. Removal of the ACL suffices to reorganize the force balance in the other ligaments and by doing so alter the coupled motions of the tibia. In the case of the intact knee subjected to posterior motion (Case 1b), the ACL buckles and is in a state of compression along its collagen fibre directions as will be discussed later in section IX.5.1.2. This particular mechanical configuration appears to restrict the range of proximal-distal displacement of the tibia during the posterior drawer test. From these results it is clear that complex interactions occur and produce some non intuitive phenomena. This is a good example of the advantage offered by a three-dimensional finite element model of the knee joint over, for example, a two-dimensional finite element model. In fact, it can capture some particular effects that would be missed otherwise.

IX.5.1.2 Results for Cases 1a, 1b, 2a and 2b. Forces in ligaments

Figure IX.8 presents the resultant force within each of the knee ligaments for Cases 1a and 1b (intact knee) while Figure IX.9 presents the resultant forces within the PCL, LCL and MCL for Cases 2a and 2b (ACL resected knee).

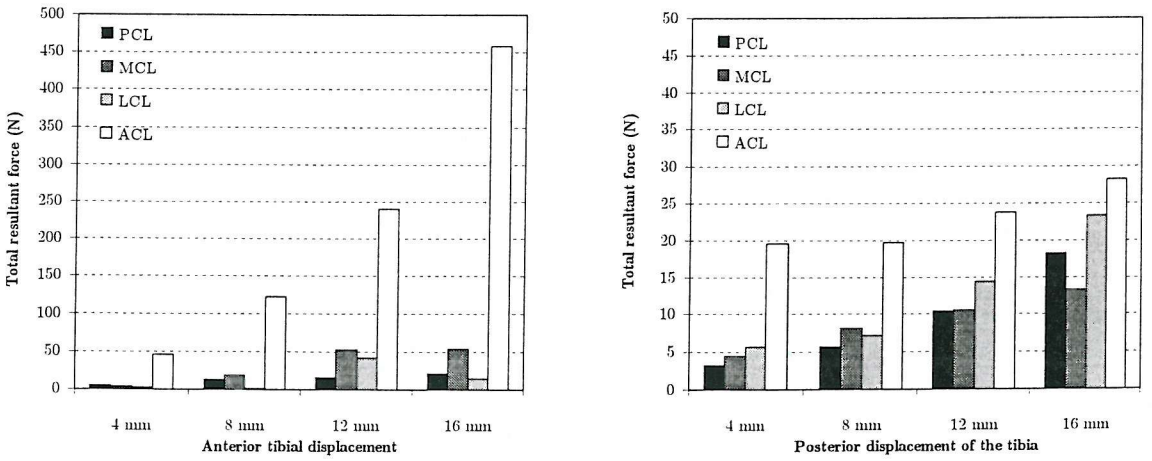

a) Anterior drawer

b) Posterior drawer

Figure IX.8 – Total resultant forces within the four ligaments of the knee (PCL, MCL, LCL, ACL) with respect to the drawer displacement applied to the tibia (Cases 1-a-b).

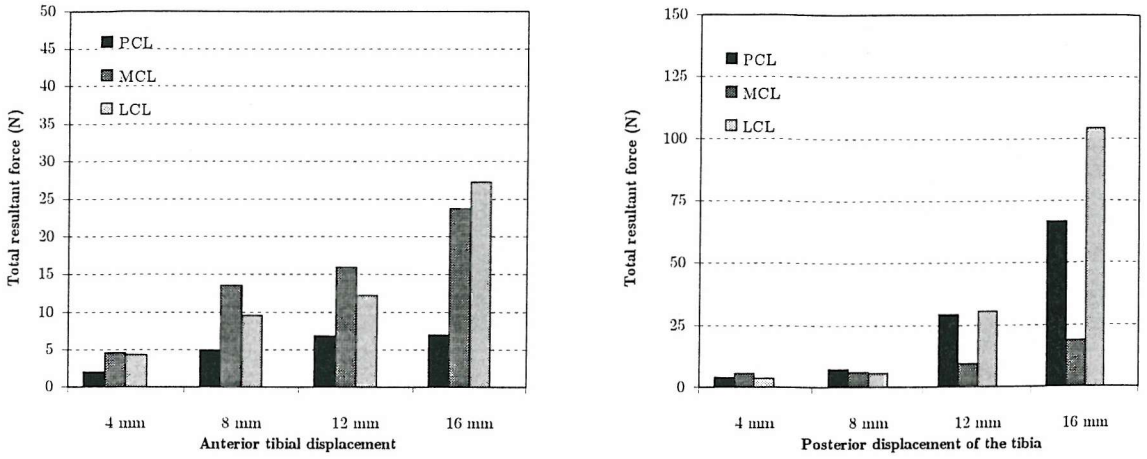

a) Anterior drawer

b) Posterior drawer

Figure IX.9 – Total resultant forces within the three ligaments of the knee (PCL, MCL, LCL) with respect to the drawer displacement applied to the tibia when the ACL has been resected (Cases 2-a-b).

Figure IX.8 and Figure IX.9 show a large disparity for the values of resultant force in the ligaments according to the type of drawer motions performed and the magnitude of displacement applied. As expected, applying an anterior displacement to the tibia develops forces in the ACL such that this ligament carries the largest force (respectively 458, 241, 123 and 46 N at respectively 4, 8, 12 and 16 mm of anterior tibial drawer displacement). The MCL appears to be the major restraining ligament after the ACL, carrying up to 53 N of the drawer load at 12 and 16 mm of tibial anterior displacement. The distinct mechanical properties of the ligaments probably play an important role in this fact and it is believed that this is amplified by size effects: the MCL is the largest ligament. For the range of displacement considered it is interesting to note that the resisting forces in the MCL, LCL and PCL are bounded superiorly (about 53 N) after a certain degree of tibial displacement has been reached (12 mm). The ACL is then the only ligamentous structure that has its total force increasing. It is worthy to note that the total resultant force in a ligament accounts for its stretch, shear and compression and its contact interactions with the other substructures of the knee. During the anterior tibial drawer test, the ACL bears the maximum force compared to the other knee ligaments. At 16 mm displacement the ACL provides 84 % of the resisting action. This confirms the largely accepted view of the primary restraining function of the ACL (Bendjaballah *et al.*, 1998; Butler *et al.*, 1980; Gollehon *et al.*, 1987; Markolf *et al.*, 1995, 1990, 1984, 1976, 1993; Nielsen *et al.*, 1984; Piziali *et al.*, 1980a, 1980b).

At 100 and 200 N anterior tibial forces, the total resultant force in the ACL was found to be respectively 162 and 293 N by Bendjaballah *et al.* (1998) in their FE model, 150 and 210 N in experimental studies by Markolf *et al.* (1995, 1990). These values contrast with the ones obtained in the present FE model (respectively 109 and 200 N) that could be explained by the initial configuration of the knee joint, the initial geometry and mechanical properties of the ligaments as well as the contact interactions between ligamentous and bony structures. Although lower, these values are of a similar order of magnitude as those reported in the literature. Moreover, the FE analyses were carried out by assuming no residual stresses in ligaments. As shown and discussed in Chapter VII and Chapter VIII, this could affect the results. As expected, the action of the PCL was minor in anterior drawer of the tibia and the action of the LCL was also minor compared to that the MCL at 8 and 16 mm displacement.

However, the expected effect for the primary action of the PCL in resisting anterior-posterior tibial force was observed only in the case of a posterior tibial displacement exceeding 20 mm. This was conducted on another analysis not reported here. The initial geometrical configuration of the ligaments and that of the bony structures can offer a valid explanation for the high laxity of the joint in the posterior direction as discussed in the previous section. This means that the tibia is relatively free to move in the posterior direction before significant forces are generated within the knee ligaments. The maximum resultant force was found in the ACL. Although counterintuitive, this result may be explained by the fact that as the posterior drawer load progresses the ACL buckles in a way that the collagen fibres undergo compression along their axis, becoming lax, and thus do not contribute to the stiffness of this ligament. The load taken by the ACL is therefore generated only by the deformation of the highly compliant solid matrix and not by stretch of the collagen fibres as would happen during anterior motion of the tibia. This was verified by running another FE analysis and considering the material of the ACL was made only of the matrix without the anisotropic characteristics introduced by a fibre contribution. The results of the analysis were virtually identical to those of the first FE analysis and thus confirmed this finding. The high values observed for the force in the ACL are simply due to the particular mechanical properties assumed for the matrix combined with the geometry of the model. The ratio of the size (volume) of the two cruciate ligaments probably plays a significant role in the observations.

For the posterior tibial motions, the MCL and LCL appear to offer comparable restraint of up to 23 N for a total tibial load of 73 N. The minor action of the PCL (9.8 % of the total resisting force at 4 mm tibial displacement) steadily increases as compared to the action of the other ligaments and represent about 22 % of the resisting action at 16 mm. If the displacement is increased (as performed in another FE analysis not reported here) the action of the PCL becomes the major restraint as would be intuitively expected. However, this magnitude of displacement is unphysiological and the response to this finding is again a question of initial geometry and mechanical properties assigned to the current FE model. The 17 N resultant force within the PCL under 73 N drawer force in posterior tibial motion is in line with the results of Markolf *et al.* (1996) who measured a 16 N force within the PCL under a 100 N drawer tibial load.

In the ACL-deficient knee, as described in the previous section, the resisting tibial force developed in anterior motion is significantly lower than for the intact knee for the same given amount of displacement. The absence of the ACL redistributes the load in the remaining ligaments while also increasing the knee laxity. These two phenomena are interrelated. For example, during anterior drawer tests the LCL bears the maximum force (28 N) at 16 mm drawer displacement that contrasts with the same boundary conditions in the case of the intact knee (Figure IX.8-a) where the maximum load (after the ACL) is taken by the MCL (53 N) while the LCL bears a force of only 14 N. The general results of the FE computations highlight again the complex mutual interactions operating between ligaments and bones within a knee joint.

It is worthy to note that the magnitude of force in any single ligament does not exceed 28 N for the whole displacement range (0-16 mm). Although much less bulky than the MCL (MCL and LCL were also assigned identical mechanical properties in the FE model), the LCL bears similar loads as the MCL. The natural initial configuration of the knee joint at full extension (see Figure IX.4) and the particular orientation of the LCL where it inserts into bone make it prone to produce high shear forces at these locations.

When compared to Case 1b (intact knee), the resection of the ACL for posterior motion of the tibia (Case 2b) significantly altered the resultant force in the collateral ligaments and in the PCL. At 16 mm posterior tibial displacement the forces in the MCL, LCL and PCL have increased respectively from 13 to 19, from 23 to 104 and from 18 to 67 N.

The mechanism observed is probably due to the way the missing ligament affects the natural balance of forces in the remaining ligaments. Prior to 10 mm of posterior tibial displacement, the force in the PCL, MCL and LCL are not significantly different when one compares the intact and ACL-deficient knee but beyond this value the ACL-deficient knee seems to have a stiffer response in the posterior direction as the forces in the PCL and LCL increase significantly. The absence of the buckling (compressive) force of the ACL relieves significantly the constraint put on the femur and the tibia, leaving room to the PCL to extend in larger proportions.

IX.5.2 Results concerning the influence of initial stress within the ACL.

IX.5.2.1 Force-displacement results

The significant influence of a residual stress in the ACL at full knee extension is clearly exhibited on Figure IX.10 when the developed forces are compared with Cases 1-a-b (no initial stress at full knee extension). As the pre-stretch of the ACL is performed along its fibre directions at full knee extension, the component of the force (135 N) along the anterior-posterior axis is not equal to 135 and has indeed a lower value. The contribution of the initial force within the ACL to the global stiffness of the joint in anterior-posterior motion is therefore reduced. For a given anterior displacement of the tibia, the resisting force developed by the tibia is greater when the ACL is pre-stressed. This is of no real surprise along with a comparable shape of the curves means that the stiffness of the joint are not significantly different in both cases.

As a result of the existence of a pre-stressed state within the ACL the posterior motion of the tibia is altered in a such way that the restraint force of the knee initially decreases until 4 mm of displacement where the resisting force starts to increase again. As described in sections IX.5.1.1 and IX.5.1.2, during posterior motion, the ACL buckles and no mechanical contribution is provided by its fibres. As shown in section VII.5.1.2, the behaviour of the soft tissue structure in these particular conditions is a highly nonlinear phenomenon that may affect erratically the deformed shape of the structure and so its stress field and ultimately the forces it transmits to the bony structures. This provides an explanation for the irregular variations of the reaction forced developed by the tibia in posterior motion.

The existence of a residual stress within the ACL induces smaller anterior displacements. For example at 100 N anterior drawer load the tibia displaces of 5.32 mm whereas this value reaches 7.65 mm when the knee is completely stress-free at full extension (see Table IX.4).

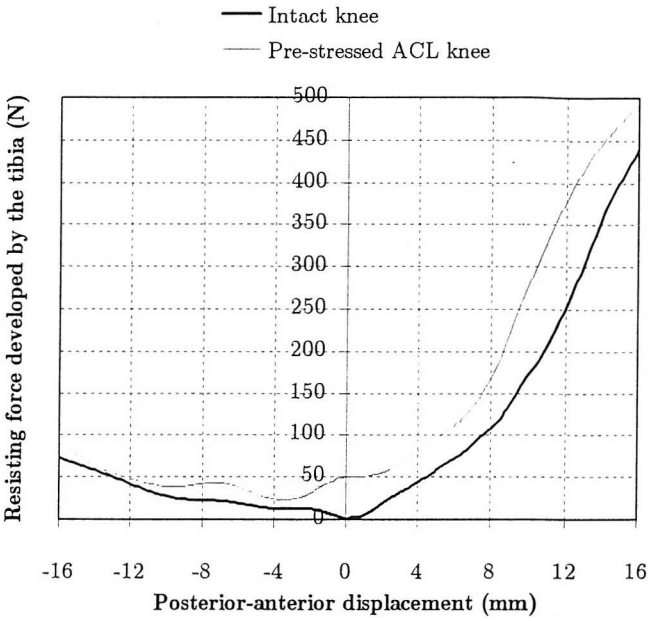

Figure IX.10 – Force-displacement curves for **Cases 1a**, **1b**, **3a** and **3b**. A 400 N force is applied to the tibia in the posterior-anterior direction (Case *i*a) and in the anterior-posterior direction (Case *i*b). The femur is constrained in all degrees of freedom whilst the tibia is constrained only in the rotational degree of freeom around the X axis (axis of flexion of the knee). Cases 3a and 3b correpsond to a knee where there is 135 N force present in the ACL at full knee extension The resisting force is the absolute magnitude of force measured at the centre of gravity of the tibia.

This compares well with the results obtained by Fukubayashi *et al.* (1982) who found an anterior displacement of 5 mm when the tibia is subjected to a 100 N load. Once again, this highlights the relevance of including the initial stress in ligament models. As explained above, the effect of the pre-stretch in the ACL for posterior motion is not as straightforward as that on the anterior motion. At the particular value of 50 N posterior drawer load the stress-free ACL knee displaces of 13 mm while it only displaces of 12.4 mm for the other case (Case 3b).

	Displacement (mm)		Variation (%)
	Case 1	Case 3	-
100 N PA force to the tibia	7.65	5.32	-30.5
50 N AP force to the tibia	-13	-12.4	4.6

Table IX.4 – Anterior-posterior (AP) and posterior-anterior (PA) displacements of the tibia under 400 N drawer loads at full extension of the knee. Results are given for Cases 1-a-b and Case 3-a-b as well as their relative variations.

Pre-stressing the PCL would probably have a particular effect on the mechanical response of the knee subjected to posterior motion, not only by redistributing the load in the other ligaments but also by stiffening the PCL. Similarly, considering pre-stress in the collateral ligaments would be likely to alter their behaviour.

IX.5.2.2 Results for Cases 3a and 3b. Forces in ligaments

Resultant forces developed in the four knee ligaments are represented on
Figure **IX.11**. Although the initial force in the ACL equals 135 N at the beginning of the FE analysis, several iterations are required to make the whole mechanical system (bony and ligamentous structures) reach a state of equilibrium. This has the effect of rebalancing the forces in the other ligaments. Moreover, the direction of the pre-stress force within the ACL is not directed along the anterior-posterior direction and this explains why the resisting force to drawer displacement does not equal 135 N at the origin of the tibial drawer displacements (Figure IX.10).

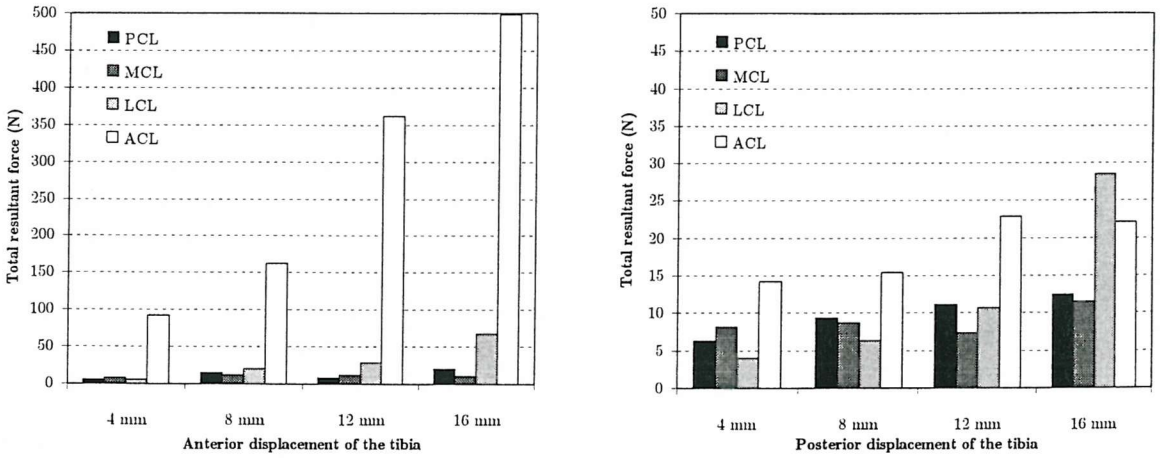

a) Anterior drawer

b) Posterior drawer

Figure IX.11 – Total resultant forces within the four ligaments of the kne (PCL, MCL, LCL, ACL) with respect to the drawer displacement applied to the tibia when a residual stress field (equivalent to a force of 135 N) is present within the ACL at full knee extension

The existence of a residual stress in the ACL at full extension clearly increases the total force in this ligament for anterior tibial drawer test. When, for Case 1a, the forces in the ACL were 45, 123, 241 and 458 N, respectively at 4, 8, 12 and 16mm tibial displacement (Figure IX.8-a), these values are 92, 163, 361 and 498 N for Case 3a.

The difference in force magnitude between the two cases appear to reduce as the tibial displacement progresses because the load borne by the ACL is progressively "shared" with the other ligaments. The particular geometrical characteristics of the ACL at its femoral insertion combined with the application of an initial pre-stretch at full extension place specific restraining constraints on the femur and modify consequently the load balance within the knee joint. In the posterior tibial drawer simulations the forces developed in the ACL are lower than Case 1b (no residual stress in the ACL) as well as the force within the PCL. This effect has again to be considered in the light of multi-body coupled mechanical system where force in one ligament may affect significantly load in another and so the global response of the system. Application of a pre-stretch to the ACL has the effect to close the joint leading to a slackening of the collateral.

IX.6 Discussion

A three-dimensional nonlinear FE model of the knee joint including a full three-dimensional representation of the ligaments has been proposed. The novelty of the model lies in a more accurate and realistic geometry of the ligaments and the bony structures (femur, tibia and fibula) coupled with a realistic three-dimensional constitutive law for soft connective tissue structures based on an incompressible transversely isotropic hyperelastic strain energy density and the capability to enforce all potential three-dimensional contact interactions. No similar model has been previously reported in literature. The FE model has allowed for the examination of the restraining functions of each of the ligaments when the knee is submitted to anterior-posterior drawer displacements.

The influence of residual stresses existing in the ACL on the biomechanical response of the joint was also assessed. The simulation of an ACL resection was helpful in identifying its effects on the global stability of the knee joint and thus in assessing the functional role of the ACL as a substructure of the knee in anterior-posterior drawer displacements. The FE model presented is therefore a very promising tool that grants access to some data unavailable by other methods.

Among numerous authors, Cabaud (1983) established that the ACL is the predominant restraint to anterior tibial displacement and reported 75 % of anterior force at full extension and approximately 85 % at 30 and 90 degrees of flexion. Piziali *et al.* (1980a, 1980b) performed cadaveric studies and showed that the ACL carried 87% of the total load when an anterior translational force was applied to an extended knee. In the present FE study, this percentage is variable, tending to increase as the magnitude of the anterior displacement increases.

In this study, it was found that at 400 N and 440 N applied anterior tibial force the ACL carried respectively 73 and 84 % of the applied load. In general, the results agree with the observations of these authors.

Given the much higher stiffness of bony structures over ligamentous tissues, the femur, tibia and fibula have been modelled as rigid bodies, thus speeding up the FE computations. Articular cartilage layers were intrinsically defined by specifying an appropriate shell thickness for the rigid bodies surfaces. However, due to this modelling strategy, these layers were assumed to be undeformable. It is believed that for non load-bearing motions of the knee joint, deformations of the cartilage are negligible with regards to their influence on the kinematics of the knee joint and therefore the cartilage layers can be considered as rigid for the present study.

The menisci have not been included in the FE model because it was thought that their influence was negligible in relation to the anterior-posterior motions of the passive knee. This is indeed a controversial issue as, for example, the work of Levy *et al.* (1982) and Markolf *et al.* (1976) testify. The former authors have found no effect on the primary laxity of a knee having undergone a medial meniscectomy while the latter authors observed a 43 % increase in anterior-posterior laxity of the knee. However some studies have hypothesized that menisci become a significant resisting factor in posterior-anterior drawer of the tibia in ACL-deficient knee (Levy *et al.*, 1982; Schoemaker and Markolf, 1986). The assumed negligible role of the menisci in the FE model was consistent as long as the forces in ligament remained small because the action of the ligaments would have generated minimal compressive loading of the femur relative to the tibia. However, as shown in the results concerning the resultant force within the ligaments, the high values found have invalidated the initial assumption putting therefore a limitation to the present model.

Capsular structures were not modelled due to the lack of geometrical and material data. Limitations of the multi-contact capability of PAM-CRASH^{TM} associated with numerous kinematic constraints (rigid body) would have also been an issue in modelling these structures. The inclusion of menisci and capsular structures would have most probably rendered the FE model of the knee joint much stiffer in the anterior-posterior direction.

The general results of the different FE analyses (Cases 1, 2, 3) have shown that the multi-parts nature of the knee joint makes it prone to very complex mechanical interactions the interpretation of which is sometimes difficult to appreciate.

The results of the FE analyses are very dependent on the boundary conditions and the mechanical properties of each substructure of the model. This may explain the difference of some of the results with data available in the experimental or mathematical modelling literature such as the fact that the PCL is not found to be the primary restraint in posterior motions of the tibia as discussed in section IX.1. High buckling forces have been found in the ACL during posterior motion. This result could be explained by the fact that the mechanical properties of ligaments used were extracted from different studies and hence different specimens. In section IX.5.1.1, it was shown how the deformation of the ACL generated stresses only in the matrix part of the continuum. High stresses in the matrix were due to the particular possibly too high mechanical properties used (Ault and Hoffman, 1992a) combined to a possible too large geometry of the ACL. The high stress values in the matrix were responsible for the high resultant force within the ACL.

The mechanical properties used for the ACL may have created a mismatch with the geometry of the ACL used in the FE analyses where size effects could result in the observations described above. In the model used in the present study, the definition of the anterior-posterior axis (Z axis) corresponds to the true anterior-posterior axis of the tibia but is not perpendicular to the transepicondylar axis of the femur. The orientation of this axis and the length and tensile properties of ligaments is the mechanism primarily conditioning the rotation of the tibia. A slight shift in this direction may have significant impact on the resultant rotations and so the anterior-posterior displacements. More importantly, the FE model of the knee joint has accounted for the arbitrary complex interactions occurring between the ligaments and the bony structures, thus capturing mechanical features unavailable when using simplified models for the ligaments. Although not investigated in the present study, the extent of these mechanical features and the influence that the contact interactions may have on the kinematic characteristics of the knee can be readily studied within the framework of the developed FE model.

The mix of mechanical properties for ligaments obtained from different experimental acquisitions performed on different specimens may not reflect the natural balance of the properties of each ligament within the same knee joint. It could be hypothesized that, for a given knee joint, there exists a relationship between the relative mechanical properties of the ACL, PCL, MCL and LCL. This is an issue worth investigating in the future. Interdependence of the ligaments is essential in knee stability and may be linked to remodelling phenomena (Hayashi *et al.*, 1996). However, a question remains: remodelling, cause or consequence?

Rigid bodies are only allowed to rotate around their centre of gravity and this could be the major factor influencing the results obtained from the FE analyses. Although not reported in detail in the present work, coupled rotations of the tibia were observed. For example, when an anterior force is applied to the tibia, by reaction to the kinematic constraints of the ligaments and those at the centre of gravity of the tibia, an internal rotation of the tibia is generated. Displacing the centre of gravity of the tibia will definitely modify the mechanical response and especially the rotational response of the knee joint. The relative positions of the centre of gravity of the tibia and that of the femur also dictate the characteristics of the coupled torques produced. In the FE model, the ACL inserts anteromedially in the tibia with respect to the axial tibial axis (collinear to the Y axis and passing by the centre of gravity of the tibia). Due to this configuration, the line of action of the force exerted by the ACL during an anterior motion of the tibia is likely to generate the observed internal rotation of the tibia.

Similarly, the PCL inserts posterolaterally with respect to the axial tibial axis leading to an external rotation of the tibia during a posterior displacement of the tibia.

It is also important to keep in mind that, in some circumstances, the motion of the knee joint may be driven more by surface constraints (articular surfaces) than by ligaments restraints.

Although realistic, the geometric model of the knee used for the FE analyses had some possible limitations such as the geometry of the ligaments at full knee extension. In fact, this configuration probably does not represent the natural anatomical state (shapes and so residual stresses, and orientation at the insertion sites) at full extension.

Moreover, the model has also been shown to be too lax in anterior-posterior drawer test, particularly for posterior displacements. The geometrical characteristics of the knee joint model are believed to be the major factor that explains these observations.

The present computational study has highlighted the sensitivity of the knee joint model to the boundary conditions applied and it is therefore important to interpret the various results obtained within a set of specific conditions. However, the FE model built was a first step toward more accurate models and was helpful in the development of a robust modelling tool that carries promising prospects for the future.

IX.7 Concluding remarks

The study presented in this chapter has shown that a simplified three-dimensional nonlinear finite element knee joint model can represent some essential mechanical characteristics of the joint subjected to anterior-posterior displacements. The inclusion of accurate three-dimensional constitutive modelling of ligaments has allowed us to integrate their physiological mechanical behaviour in combination with arbitrary complex contact boundary conditions developed with the bony structures. The objectives defined in section IX.2 were fulfilled. Results obtained in section IX.5.1 have led to the following conclusions:

- The ACL is effectively the primary restraint to anterior tibial translation.
- The PCL was not shown to be the primary restraint to posterior tibial translation except for extreme value of drawer displacement (over 16 mm) which unfortunately are not physiological. These findings are directly related to the geometry of the finite element model and the set of mechanical properties used.
- In all the drawer tests considered, the LCL and MCL provide secondary restraints to anterior-posterior motions of the knee joint.

The effects of ACL resection have been clearly exhibited in the finite element analyses and this has again highlighted the potential of computational methods to simulate orthopaedic pathologies.

Influence of residual stresses present in the ligaments of the knee at full extension on the anterior-posterior drawer motions when one applies drawer forces to the tibia or to the femur has been investigated in sections IX.5.2 and be proven to be significant.

The relative proportion of residual stress in each ligament is probably a major factor in the ligament balance of the knee in various configurations and is critical for the stability of the knee for specific motions. The present study has been done in the context of simple anterior-posterior drawer forces and it is imperative to be cautious and not to extrapolate the results when considering other types of motions when the various effects observed may be reduced or emphasised.

The FE model developed here is a first step towards more sophisticated models which will be more bio-fidelic (inclusion of capsular structures, non uniform thickness of cartilage layers...) and will be used to simulate other kinds of motions such as gait in normal, pathological and repaired (after partial or total knee replacement) conditions, stair-climbing, active or passive flexions. The numerical model would equally be a valuable tool in simulating various injury scenarios and surgical procedures like the ACL reconstruction. Also, FE models should be viewed not only as attractive and promising research tools but also appealing educational tools. The fact that the modelling methodology takes place within the framework of an explicit FE code is particularly relevant because this type of FE code is extremely well suited to simulate highly nonlinear dynamic events involving multi-body dynamics, complex impact-contact interactions, nonlinear materials, large displacements and rotations.

The next generation of three-dimensional FE models of ligaments should include multi-bundle representation with appropriate mechanical properties and recruitment parameters (residual stretch, zero force length) for each bundle (Mommersteeg *et al.*, 1996b). This will require a considerable effort not only in experimental acquisitions of the geometrical and mechanical features of each isolated bundle, but also in a robust and efficient way to build FE models from these data.

Chapter X

Synthesis, conclusions and recommendations

X.1 Synthesis of the outcome of the present research project

The objectives of this thesis have been to develop and improve current state of the art computational models of ligaments in order to provide the necessary modelling tools that will be used more and more in biomechanics research.

Firstly, the aim was to propose a rigorous general theoretical framework in which the formulation of three-dimensional constitutive laws could be developed. The main idea was to start from a continuum mechanics basis from which constitutive equations could be derived. The full generality of the formulation has allowed us to isolate particular terms of the constitutive equations and it was shown how particular structural mechanical interactions within the composite material could be taken into account by selecting the right coupling terms. Specific mechanical behaviour can then be described by selecting and degenerating the relevant equations. However, it is worth outlining that the inclusion of particular structural features is limited by the availability of experimental material data determined in corresponding characterising experimental protocols. The theory of continuum fibre-reinforced composite at finite strain developed by Spencer (1992) has been extended with regards to the elasticity tensors in the material and spatial configurations. Explicit first and second derivation of a general anisotropic hyperelastic strain energy function have been performed for the first time and it is hoped that these expressions will be useful to other researchers working in the field of nonlinear elasticity and finite element modelling. This constitutes one of the important scientific contributions of the present work.

An incompressible transversely isotropic hyperelastic constitutive law was identified and implemented into an explicit finite element code. The robust implementation was demonstrated in Chapters VI, VII, VIII and IX. To the best of our knowledge, it is the first successful finite element implementation of a transversely isotropic hyperelastic continuum material model into a commercial *explicit* FE code. The model was validated against analytical solutions for homogeneous states of deformation. The subroutine defining the strain energy function is easily modifiable to account for new transversely isotropic constitutive laws. The explicit model has been shown to be extremely efficient not only to track highly nonlinear phenomena much better than an implicit code but also in terms of computational cost. By taking special precautions (see section VII.3) a quasi-static response can be obtained in a physical time scale much lower than the natural time scale of the phenomenon considered. This proves very advantageous for computational efficiency as explicit finite element analyses do not have the demanding requirements of implicit codes in terms of temporary storage (on hard disk), memory (RAM) and mathematical operations. In implicit finite element analyses the computational effort is dominated by the inversion of the Jacobian matrix while in explicit finite element analyses the major effort is represented by the calculation of internal forces, requiring only basic algebraic operations. Explicit finite element codes are also very efficient at dealing with multibody contact interactions and rigid body handling.

Continuum three-dimensional isotropic finite element models of ligaments should not be used for simulating their mechanical behaviour in physiological conditions. Accounting of the anisotropy of ligaments was shown to be crucial in order to represent accurately the natural mechanical behaviour of ligaments under simulated physiological conditions. This was done by performing finite element analyses of an ACL model under a simulated passive flexion of the knee. The anisotropic model was successful in overcoming the significant limitations featured by three-dimensional isotropic finite element models of ligaments. Instead of producing unrealistically excessive compressive and flexural stresses when the ACL is loaded along the natural direction of the collagen fibres, the new finite element model behaves in a way such that buckling of the structure is produced as soon as compressive stresses are generated in the fibre direction. The finite element model of the ACL exhibited numerous qualitative characteristics observed experimentally on cadaveric ACL models (Wascher et al., 1993).

Moreover, the finite element model was validated by comparing the computed resultant force in the ligament during a passive flexion and the published one, recorded experimentally, which were in very close agreement. This was achieved by considering the existence of a residual stress present in the ACL at full knee extension. Its influence was significant on the resultant force in the first 30 degrees of knee flexion.

In Chapter X, a full three-dimensional model of the knee joint including the bones and the four main ligamentous structures (ACL, PCL, LCL and MCL) was built. Unlike previous published finite element models, the model presented here took into account all of the arbitary complex contact interactions between bone and ligaments of the knee. This presented a real novelty as contact interactions between bones and ligaments have been shown to be essential because a complex load redistribution occurred in each substructure of the knee during anterior-posterior translational motions. This contrasts with the previous studies that, by hypothesis, found that the sum of the total resultant force components in a particular direction (X, Y or Z) in each ligament is equal to the drawer load applied to the tibia or the femur in that particular direction. The inclusion of three-dimensional contact interactions and mechanical properties of ligaments in the finite element model of the knee joint has therefore highlighted specific effects that were not captured in the previous published mathematical and finite element models of the knee.

The finite element model has confirmed that the ACL is the primary restraint in resisting anterior tibial translation of the knee. The PCL has not been found to be the primary restraint of the joint in resisting posterior tibial motions except for extreme value of drawer displacement. The MCL and the LCL have been found to be secondary restraints in anterior-posterior translations of the knee. As shown experimentally, the finite element model of the joint exhibited the typical behaviour in which anterior-posterior translational motions of the tibia produce internal or external rotations.

Finite element analyses have also been proven to be successful in simulating reliably an ACL-deficient knee. Removal of the ACL leads to a significant increase in the tibia or femur displacement under anterior or posterior horizontal drawer forces as shown experimentally or routinely by clinicians. This has showed that the finite element model of the knee joint was sensitive enough to simulate particular pathological conditions. This a good example of the vast potential computational biomechanical models can offer in investigating consequences of injuries on the global knee joint or on each of its bony and ligamentous structures.

The inclusion of three-dimensional material and geometrical properties into the finite element model of the knee joint has highlighted the extreme complexity of this joint when subjected to even simple motions. Basic translational anterior-posterior motions suffice to produce very sophisticated mutual interaction between ligaments and bony structures. Ligaments put kinematic constraints on bones not only at their insertion sites but also by the way of direct contact interactions which redistribute the loads in the ligaments.

Residual tension in the ACL has also been shown to be important as it may condition the way particular displacements are produced. It affects the mechanical behaviour of ligaments (stress and deformation) which in turn alter the constraints put on the bony structures. This modifies the mutual kinematic constraints put by the bones on the other ligaments and modifies the balance existing between the ligaments and the whole knee structure by redistribution of loads within the ligaments. It appears highly relevant not only to consider three-dimensional geometrical and mechanical properties of all the substructures composing the knee joint but also the complex initial and general boundary conditions.

In Chapter X, the motions of the knee under anterior-posterior forces has been investigated. This type of passive motions is simple but, by relieving particular degrees of freedom of the tibia, coupled motions were produced. It would be certainly very interesting and useful to investigate the mechanical response of the knee under other type of motions such as varu-valgus, internal-external rotations, combined or not and active motions like walking, running, etc. This would probably highlight more complex three-dimensional mechanical behaviour where other knee substructures such as menisci, cartilage and capsula may play a major role. Influence of residula stresses could be magnified or diminished.

X.2 Concluding remarks - Contributions

Originality and novelty of the present research are represented by various aspects. Entirely new theoretical developments in the field of the nonlinear mechanics of fibre-reinforced composites were proposed (Chapter V). Their relevance to describe the constitutive behaviour of soft connective tissues has been emphasised despite the fact that the applicability of the theory is limited by the availability of experimental data. It is hoped that the analytical results reported will be used in the near future by the biomechanics research community in order to refine the existing constitutive models.

The three-dimensional incompressible transversely isotropic continuum finite element model of soft connective tissues has brought several significant improvements in comparison with the previous published models of ligaments or those of the knee joint. Concerning ligament modelling, it has been demonstrated that continuum isotropic models should not be used to simulate the natural complex mechanical behaviour of ligaments as proposed by (Pioletti, 1997; Pioletti *et al.*, 1998b) and (Limbert and Taylor, 2001a).

By integrating anisotropic properties, the new proposed finite element model of the ACL has been shown to offer a very promising answer for simulating realistically the behaviour of this ligament (and other ligaments) in physiological conditions. Very good quantitative agreement between the numerical results and experimental data concerning the resultant force within the ACL during a passive knee flexion supports the usefulness and the validation of the finite element model. Previous finite element studies did not consider this aspect at all (Daniel, 1999; Hirokawa and Tsuruno, 1997, 2000; Pioletti, 1997; Pioletti *et al.*, 1998b), reporting only values of stresses or strains and general qualitative behaviour. General precautions such as checking that during finite element analyses the ligament model does not go over its physiological range of stress and strain must be observed. It is a very essential first step in assessing whether a finite element model makes sense. The proposed model satisfied these basic requirements.

By comparison with mathematical models of the knee and ligaments (Abdel-Rahman and Hefzy, 1998; Andriacchi *et al.*, 1983; Blankevoort and Huiskes, 1991b; Chan and Seedhom, 1995; Imran and O'Connor, 1997; Loch *et al.*, 1992; Martelli *et al.*, 1998; O'Connor and Zavatsky, 1993; Shelburne and Pandy, 1997; Toutoungi *et al.*, 1997), in addition to the realistic constitutive model, the proposed finite element model of ligament integrated a three-dimensional knee joint model brought new features. Obvious benefits of finite element models are their capacity to output data (stress and strain distribution, energy density...) for arbitrary complex geometries and loading conditions that are unavailable from mathematical models, especially when they are two-dimensional. Realistic anatomical geometries (bones and ligaments) and the good performance of the explicit finite element code for multi-body contact analysis have allowed for the accounting of full three-dimensional contact interactions. This capacity has not been included and considered in previous published finite element models of the knee joint like those proposed by Bendjaballah *et al.* (1998) or Li *et al.* (1999). This novel approach has been proven to be relevant as discussed in the previous section. Validation is an essential stage in the development of any computational model. However, the finite element knee joint model has exhibited numerous qualitative features observed experimentally and the corresponding quantitative results have been found to lie in the same range of magnitude.

X.3 Recommendations for further research

This thesis work has only unravelled a few points in this vast research field that is the (finite element) constitutive modelling of biological soft connective tissues. During the course of this research, numerous difficulties have arisen. Worth mentioning is the fact that the highly nonlinear behaviour of ligamentous structures was challenging to simulate in an implicit FE code. The explicit code was found to be extremely robust and always achieved convergence where the implicit code failed. The formulation of a constitutive law was limited by the shortage of experimental material data necessary to characterise specific mechanical behaviours. Experimental measurements performed on biological soft tissues are extremely delicate processes and the current experimental methods need to evolve in order to capture specific mechanical responses that may be missed otherwise. Applicability of the general fibre-reinforced composite model (two families of fibres) remains to be explored on experimental grounds but with suitable experimental material characterisation, one can envisage the integration of complex interactions between elemental constituents within a constitutive law. Another major difficulty concerned the geometrical acquisition of the three-dimensional shape of ligaments. Perhaps medical imaging techniques such as MRI are the best way to go. Proper hexahedral elements meshing of biological structures was also a challenging and time-consuming task.

Improvements and developments of the techniques mentioned above are an obvious line for further research. However, other parts of the research effort should be directed towards investigating new issues. Some possible directions would be the following:

- An obvious extension of the present research would be to build a finite element model of the knee from anatomical measurements (MRI, direct 3D measurements). The ideal would be to acquire the geometry of all the knee structures (bones, ligaments, menisci...). Then (before, if the anatomical acquisition of the knee geometry was invasive) kinematic and kinetic tests would be performed. A robotic system capable of applying specific displacements, forces and moments under accurate control would probably be the best choice. At the end of these acquisitions, testing of ligaments and possibly other structures (cartilage, menisci, capsula...) would provide material data associated with the knee under study. All the information collected from the various tests (geometry, mechanical properties, displacements and forces) would then be used to build an accurate three-dimensional model of the knee joint.

- Specific boundary conditions in force or displacement would be used to test the model and hopefully validate it. Although the principle behind this further research is straightforward its practical implementation is not. This is a very ambitious project that is likely to be tractable only within a collaborative work group possessing all the various expertises required (medical imaging, image processing, experimental testing and computational techniques).

- Developing new constitutive models taking into account viscoelasticity, fluid motions, remodeling, fatigue, damage, and failure of ligaments. These developments would be limited by the availability of appropriate experimental procedures and relevant material data.

- Studying the interface problems between bone and ligaments. There is a gradation of mechanical properties of ligament where its inserts into bone. The integration of this characteristic will give more accurate information about the state of stress at these locations. The numerical artefact produced in finite element models (excessive stress) will then be reduced. There is a lot of research to be done in finding an optimal way to model the ligament-bone connection. It is believed that this aspect is somehow limiting in the existing finite element models of joints.

- The ultimate goal of the present research is to perform studies to assess the performance of total joint replacement, using advanced computational procedure to provide a scientific platform upon which risk analysis of implants could be based. The development of a three-dimensional virtual model of a knee will enable the production of virtual prototypes, realistically simulating the full-motion behaviour of complex biological systems and will allow to quickly analyse multiple design variations. This will reduce the number of costly physical prototypes and improve design quality, and will contribute to the improvement of implants with a longer useful life. An implant is intended to replace a living part of the human body. Therefore, it should be capable of performing the same functions as the living part.

It is strongly believed that the next trend in computational biomechanics research will be to use a dynamic approach and by doing so, more and more finite element analyses will be performed using explicit codes. At present, in 2001, explicit FE codes are mainly used by the automotive industry (and other transport industries) for crash and occupant safety simulations. However, the human body with all its complex joints, materials and physical phenomenon associated (flow, diffusion, heat exchange, electric conduction...), is essentially a complex dynamical system. Considering the never ending increase in computational power that has taken place over the last ten years, its seems not unreasonable to think that, in a near future, complex biomechanical systems with several millions of degrees of freedom could be simulated in their natural time scale.

Appendix A - Published models of soft connective tissues

Table A1 presents a description of the structural models of ligaments and tendons reported in literature.

Authors	(μ)-structural models	Results
(Viidik, 1968a)	Visoelastic parallel-fibered tissue consisting of a spring and dashpot combination. Kelvin elements in parallel with a nonlinear array of elastic springs (fibres) (sequential loading of structural elements).	Model able to describe qualitatively the mechanical behaviour of a rabbit's ACL. Good insight into the structural properties of collagenous tissues.
(Frisen *et al.*, 1969)	Viidik et al.'s model modified to account for the nonlinearity of the elastic response. Model consisting of springs, dashpots and friction elements.	Qualitative mechanical behaviour of rabbit's ACL reproduced. Complementary model of Viidik et al.'s.
(Diamant *et al.*, 1972)	Collagen fibres modelled as zig-zag shaped. Hinged rods with springs connecting adjacent rods. The crimped collagen fibres were modelled as having elastic segments joined by rigid hinges, producing a stress-strain curve with the appropriate shape.	Good prediction of experimental results (only for the older donors' specimens) and fibril character but there is no reproduction of the disappearance of crimp apices .
(Comninou and Yannas, 1976)	Collagen fibres modelled as planar sinusoid shape and represented as long elastic beams. Tendon represented as an aggregation of fibre and matrix layers.	This model qualitatively exhibited behaviour similar to rat tail tendon. Reproduction of the stiffening effect of the matrix in nonlinear part of the stress-strain curve. Stress too high at low strain level.
(Lanir, 1980)	The collagen fibres are assumed to be linearly viscoelastic with negligible bending strength and to be nonuniformly undulated. Two cases considered: high and low density of cross-links between collagen and elastin fibres.	The model predicted well the toe region. The nonuniformity of the collagen fibre structure is shown to account for the toe region as well as for the nonlinear viscoelastic behaviour of the tendon.
(Kastelic *et al.*, 1980)	Model based on sequential straightening and loading of the fibres. Crimp angles in the undeformed tendon are assumed to vary among fibrils.	Good agreement with experimental stress-strain curves for the rat tail tendon and good predictions for various ages of specimen.

(Decraemer *et al.*, 1980a)	Extension of the Frisen's and Viidik's models by incorporating internal friction between fibres and between fibres and the matrix Damping was introduced into the model by assuming that all fibres have identical linear viscoelastic properties	Model able to reproduce the mechanical behaviour of various soft tissues (human vein, fascia, tympanic membrane and rabbit papillary muscle).
(Lanir, 1983)	Extension of the Lanir's model (1980) to incorporate a full three-dimensional formulation. Strain energy method (energy of deformation due only to the fibril stetching) and kinematics taken into account. Matrix mechanical contribution under the form of a pressure term. Extension to viscoelasticity.	Complex mathematical formulation which gave similar results to those observed experimentally. The models offer a good insight into the tissue's function and response to mechanical loading.
(Stouffer *et al.*, 1985)	Kinematic chain of short elements connected by pins and torsional springs. This model takes into account the spatial variation in the crimp pattern. Model applied to simulation of the human patellar tendon bone units.	It was shown, analytically and experimentally that local strain in the proximity of the attachment site is significantly larger than the strain in the central region of the tendon
(Kwan and Woo, 1989)	Discrete model based on different group of bilinear collagen fibres each possessing a straightening strain or a failure strain.	Very good agreement was found between theoretical and experimental values (anteromedial part of the rabbit ACL and canine MCL) for uniaxial tensile tests
(Belkoff and Haut, 1991) (Belkoff and Haut, 1992)	Similar approach to Kwan and Woo. Linear elastic law and no kinematics taken into account. Collagen fibres straightening modelled by a Gaussian probability distribution function.	Good representation of the behaviour of the rat dorsal skin. Fibre stiffness increasing during maturation. Model not suitable for some flat, featureless heel region of the stress-strain curve.
(Ault and Hoffman, 1992a) (Ault and Hoffman, 1992b)	Composite-materials approach. The matrix and the fibril are supposed to be linearly elastic. Three-dimensional fibril orientation taken into account.	Good fit of experimental curves (rat tail tendon) with theoretical values but not as good for the cat's knee capsule (crimp pattern more complex). Restrictive assumptions concerning the uniformity of strain or stress.
(Hurschler *et al.*, 1997)	Strain energy formulation for the constitutive law of the collagen fibres. Three-dimensional orientation of collagen fibrils taken into account. The matrix is assumed to contribute to stress only by an hydrostatic pressure. Combination of structural (fibre) and microstructural (fibril) approach.	Model reproduces the nonlinear behaviour of ligaments well, including toe-in region, damage and eventual failure (healing rabbit medial collateral ligament).

Table A1 - Brief description of the various microstructural and structural models found in literature.

Table A2 presents a description of the phenomenological models of ligaments and tendons reported in literature.

Authors	Phenomenological Models	Main limitations
(Beskos and Jenkins, 1975)	A mammalian tendon is modelled as an incompressible fiber reinforced composite material. Collagen fibres modelled as helical shaped inextensible cords embedded in an incompressible hollow right circular cylinder. Formulation of a boundary-value problem. A form of the deformation is first assumed and then checked to see wether it satisfies the constraints (incompressibility, fibre inextensibility) and the equilibrium equations.	• Model valid for a particular geometry and a particular load. The cylinder need to be hollow. • assumed shape of the pattern of the fibres (helical). • Model developed independently of any real biological mechanical properties • when the fibres are straightened the modulus of elasticity is infinite
(Fung, 1968)	Quasi-Linear Viscoelasticity (QLV). Combination of elastic and time-dependent response using an integral formulation. Exponential form of the stress-strain relation for uniaxial tension.	• Material assumed to be isotropic
(Haut and Little, 1972)	Quasilinear viscoelasticity	• Material assumed to be isotropic
(Fung, 1972)	Quasilinear viscoelasticity	• Material assumed to be isotropic
(Barbenel et al., 1973)	Generalisation of the combination of spring and dashpot. The relaxation spectrum is assumed to have a logarithmic expansion.	• Material assumed to be isotropic
(Woo et al., 1981)	Quasilinear viscoelasticity	• Material assumed to be isotropic
(Woo et al., 1982)	Quasilinear viscoelasticity	• Material assumed to be isotropic
(Sanjeevi et al., 1982)	Viscoelasticity	• Material assumed to be isotropic
(Lyon et al., 1988)	Quasilinear viscoelasticity	• Material assumed to be isotropic
(Woo et al., 1993)	Quasilinear viscoelasticity	• Material assumed to be isotropic
(Johnson et al., 1996) *(Johnson et al., 1992)* *(Woo et al., 1993)*	Single integral finite strain viscoelasticity. Formulation offering a general framework for nonlinear and three-dimensional mechanical behaviour	• Material assumed to be isotropic

Table A2 – Sample of the various phenomenological models of soft connective tissues (tendons and ligaments) encountered in the literature.

Appendix B - Constitutive restrictions

This appendix is an extension of section V.8. and presents briefly some of the most popular constitutive restrictions. Please note that the terminology of Truesdell and Noll (1992) is adopted.

*Equation Section 10***Coerciveness condition**

(Ciarlet, 1988) describes this condition by stating that the strain energy function Ψ must approach $+\infty$ when any of the eigenvalues of $\mathbf{F}$ approach 0 or $+\infty$:

$$\lim_{J\to 0^+} \Psi(\mathbf{F}) = +\infty \quad \text{and} \quad \lim_{J\to +\infty} \Psi(\mathbf{F}) = +\infty \tag{B.1}$$

B2 Existence of a natural reference state

This condition assumes the existence of a reference state, in the undeformed configuration, at which the strain energy function vanishes and so the stress:

$$\exists \chi_0 \ / \ \Psi(\chi_0) = 0 \tag{B.2}$$

B3 Reduction to the linear elasticity theory at small strains

The free energy function must reduce to the quadratic function of strains of the linear theory when the body is considered at infinitesimal deformations:

$$\lim_{\mathbf{F}\to 1} \mathbf{A}^{\mathcal{M}}(\mathbf{F}) = \lim_{\mathbf{F}\to 1} \mathbf{A}^{\mathcal{S}}(\mathbf{F}) = \mathbf{A}^{\mathcal{L}} \quad \text{and} \quad \lim_{\mathbf{F}\to 1} \mathbf{S}(\mathbf{F}) = \lim_{\mathbf{F}\to 1} \boldsymbol{\sigma}(\mathbf{F}) = \boldsymbol{\sigma}^{\mathcal{L}} \tag{B.3}$$

B4 Tension-Extension condition

Lets consider a solid material given in two distinct reference states $\mathcal{B}_0$ and $\mathcal{B}_0^*$. Lets denote F_i, σ_i and λ_i respectively as the principal forces, stresses and stretches in the *i-th* direction of a Cartesian referential such that:

$$F_i = F_i\left(\lambda_1, \lambda_2, \lambda_3\right) \tag{B.4}$$

If two principal stretches are maintained fixed whilst one increases the third, the necessity of applying a tension is quite obvious. In the other hand, if we decrease the third stretch, one might expect to have to apply a pressure. The tension-extension condition is expressed as follows:

$$\left(F_i^* - F_i\right)\left(\lambda_i^* - \lambda_i\right) > 0, \quad \text{if} \quad \lambda_i^* \neq \lambda_i, \ \text{and} \ \lambda_j = 1, \ j \neq i \tag{B.5}$$

B5 Extension-Tension condition

If we hold two principal forces, increasing the third one should produce an increase in the corresponding stretch. This condition is expressed as follows:

$$\left(F_i^* - F_i\right)\left(\lambda_i^* - \lambda_i\right) > 0, \quad \text{if } F_j^* = F_j, \text{ when } j \neq i \qquad [B.6]$$

B6 Invertibillity of the force-stretch relationship

The force-stretch relationship given in equation [B.4] must be uniquely invertible.

B7 Pressure-compression inequality

The volume of a compressible material must decrease when the body is subjected to a hydrostatic compression and must increase when it is subjected to a hydrostatic tension.

B8 Baker-Ericksen inequality

For isotropic solids only, the maximum principal stress should occur in the direction of the maximum principal stretch (Baker and Ericksen, 1954) as expressed as follows:

$$(\sigma_i - \sigma_j)(\lambda_i - \lambda_j) > 0, \quad \text{if} \quad \lambda_i \neq \lambda_j \qquad [B.7]$$

B9 Ordered forces inequality

It is worth mentioning that this condition is not equivalent to the Baker-Ericksen inequality although it has a comparable structure given as follows:

$$\left(F_i - F_j\right)\left(\lambda_i - \lambda_j\right) > 0, \quad \text{if} \quad \lambda_i \neq \lambda_j \qquad [B.8]$$

B10 Generalized Colleman-Noll inequality

This inequality requires that the transformation from the deformation gradient **F** to the Piola stress **P** be monotonic:

$$(\mathbf{F}^* - \mathbf{F}) : (\mathbf{P}^* - \mathbf{P}) > 0 \quad \text{if } \mathbf{F}^* \neq \mathbf{F} \qquad [B.9]$$

This inequality violates the principle of material frame indifference in some cases, like for example a state of pure rotation. To overcome this, Colleman and Noll have weakened the condition by excluding rotational terms in **F**. Then **F** and **F*** must differ only by a state of pure stretch. This led them to formulate the Colleman-Noll inequality.

B11 Colleman-Noll inequality

This inequality apply to the free energy function Ψ and is given as:

$$\Psi(\mathbf{F}^*) - \Psi(\mathbf{F}) - (\mathbf{F}^* - \mathbf{F}) : \frac{\partial \Psi(\mathbf{F})}{\partial \mathbf{F}} > 0 \qquad \text{if } \mathbf{F}^* \neq \mathbf{F} \qquad \text{[B.10]}$$

In the case of isotropic solids, the conditions given by equations [B.9] and [B.10] imply strict convexity of the free energy function, condition discussed in the next paragraph.

B12 Convexity of the free energy function

$$\mathbf{T} : \frac{\partial^2 \Psi(\mathbf{F})}{\partial \mathbf{F} \partial \mathbf{F}} : \mathbf{T} > 0 \qquad \forall \mathbf{T} \text{ (second order tensor)} \neq \mathbf{0} \qquad \text{[B.11]}$$

Convexity is unacceptable because it implies uniqueness of the solution of the initial/boundary value problem and this is in disagreement with experimental observations (buckling, bifurcations of equilibrium). The convexity constraint conflicts with material frame indifference and prevents the strain energy to become infinite as the deformation gradient approaches zero.

B13 Polyconvexity

To weaken the convexity condition, Ball (1977) was the first to introduce the notion of polyconvexity. This concept was able to bring existence theorems in nonlinear elastostatics and is regarded as a very promising route in the constitutive modeling of nonlinear materials. Polyconvexity can be defined by stating that a function Ψ is polyconvex if there exists a convex function $\Psi^*(\mathbf{F}, \text{cofactors } (\mathbf{F}), J)$ such that:

$$\Psi(\mathbf{F}) = \Psi^*[\mathbf{F},\ \text{cofactors}(\mathbf{F}),\ J] \qquad \forall \mathbf{F} \qquad \text{[B.12]}$$

Polyconvexity implies strong ellipticity which is also considered as an attractive constitutive requirement (Mardsen and Hughes, 1994).

B14 Hadamard's condition

This condition is linked to the concept of strong ellipticity. A necessary condition for *material stability* is that the speeds of all plane waves, propagated in a body of the material filling three-dimensional space, be positive.

Appendix C - Temporal aspects of the FE analyses performed in Chapter VII

The times reported below are based on calculations performed in a PC built around a Pentium® III (600 MHz) processor with 512 Megabytes of RAM.

CASE1

MESH	Δt^{max} (ms)	Δt^{min} (ms)	N_c	TT (s)	$\Delta t_i^{min} / \Delta t_1^{min}$	N_c^i / N_c^1	TT_i / TT_1
MODEL 1	0.1112E-02	0.9703E-03	95600	6.200E+01	1.00	1.00	1.00
MODEL 2	0.5646E-03	0.4868E-03	190883	3.890E+02	0.50	2.00	6.27
MODEL 3	0.2823E-03	0.2430E-03	382176	2.511E+03	0.25	4.00	40.50
MODEL 4	0.2824E-03	0.2393E-03	384580	4.923E+03	0.25	4.02	79.40
MODEL 5	0.2823E-03	0.2399E-03	383829	9.747E+03	0.25	4.01	157.21
MODEL 6	0.2824E-03	0.2351E-03	387601	1.785E+04	0.24	4.05	287.90
MODEL 7	0.2737E-03	0.2281E-03	399627	3.643E+04	0.24	4.18	587.58
MODEL 8	0.2737E-03	0.2267E-03	400956	4.686E+04	0.23	4.19	755.81

Table C1 – Table summarizing the temporal aspects of the first serie of FE analyses for CASE 1. Δt^{max}, Δt^{min}, N_c, TT are respectively, the maximum and the minimal stable time step, the number of cycles performed during the analysis and the total time of the analysis. The super- or subscript "i" corresponds to a quantity attached to the i-th model.

CASE 2

MESH	Δt^{max} (ms)	Δt^{min} (ms)	N_c	TT (s)	$\Delta t_i^{min} / \Delta t_1^{min}$	N_c^i / N_c^1	TT_i / TT_1
MODEL 1	0.1358E-02	0.1129E-02	77276	5.200E+01	1.00	1.00	1.00
MODEL 2	0.5647E-03	0.5501E-03	166936	3.190E+02	0.49	2.16	6.13
MODEL 3	0.2593E-03	0.2556E-03	364852	2.342E+03	0.23	4.72	45.04
MODEL 4	0.2593E-03	0.2477E-03	382933	4.772E+03	0.22	4.96	91.77
MODEL 5	0.2824E-03	0.2630E-03	350353	8.682E+03	0.23	4.53	166.96
MODEL 6	0.2824E-03	0.2685E-03	357638	1.602E+04	0.24	4.63	308.08
MODEL 7	0.2737E-03	0.2607E-03	369486	3.807E+04	0.23	4.78	577.31
MODEL 8	0.2593E-03	0.2455E-03	388789	2.482E+04	0.22	5.03	732.12

Table C2 – Table summarizing the temporal aspects of the first serie of FE analyses for CASE 2. Δt^{max}, Δt^{min}, N_c, TT are respectively, the maximum and the minimal stable time step, the number of cycles performed during the analysis and the total time of the analysis. The super- or subscript "i" corresponds to a quantity attached to the i-th model.

CASE 3

MESH	Δt^{max} (ms)	Δt^{min} (ms)	N_c	TT (s)	$\Delta t_i^{min} / \Delta t_1^{min}$	N_c^i / N_c^1	TT_i / TT_1
MODEL 1	0.1129E-02	0.8079E-03	97007	6.600E+01	1.00	1.00	1.00
MODEL 2	0.6185E-03	0.4084E-03	187988	3.620E+02	0.51	1.94	5.48
MODEL 3	0.2824E-03	0.2243E-03	375387	2.714E+03	0.28	3.87	41.12
MODEL 4	0.2824E-03	0.2242E-03	375741	4.701E+03	0.28	3.87	71.23
MODEL 5	0.2824E-03	0.2099E-03	385452	9.502E+03	0.26	3.97	143.97
MODEL 6	0.2824E-03	0.2100E-03	385779	1.721E+04	0.26	3.98	260.76
MODEL 7	0.2824E-03	0.1911E-03	404815	3.605E+04	0.24	4.17	546.21
MODEL 8	0.2824E-03	0.1914E-03	404720	4.600E+04	0.24	4.17	696.97

Table C3 – Table summarizing the temporal aspects of the first serie of FE analyses for CASE 3. Δt^{max} , Δt^{min} , N_c, TT are respectively, the maximum and the minimal stable time step, the number of cycles performed during the analysis and the total time of the analysis. The super- or subscript "i" corresponds to a quantity attached to the i-th model.

CASE 4

MESH	Δt^{max} (ms)	Δt^{min} (ms)	N_c	TT (s)	$\Delta t_i^{min} / \Delta t_1^{min}$	N_c^i / N_c^1	TT_i / TT_1
MODEL 1	0.1129E-02	0.8183E-03	104682	7.300E+01	1.00	1.00	1.00
MODEL 2	0.5628E-03	0.4091E-03	209358	4.190E+02	0.50	2.00	5.74
MODEL 3	0.2824E-03	0.2046E-03	418783	2.769E+03	0.25	4.00	37.93
MODEL 4	0.2824E-03	0.2046E-03	418793	5.404E+03	0.25	4.00	74.03
MODEL 5	0.2824E-03	0.2046E-03	418796	1.249E+04	0.25	4.00	171.10
MODEL 6	0.2824E-03	0.2046E-03	418801	1.932E+04	0.25	4.00	264.66
MODEL 7	0.2737E-03	0.1983E-03	432078	4.052E+04	0.24	4.13	555.07
MODEL 8	0.2737E-03	0.1983E-03	432080	5.061E+04	0.24	4.13	693.29

Table C4 – Table summarizing the temporal aspects of the first serie of FE analyses for CASE 4. Δt^{max} , Δt^{min} , N_c, TT are respectively, the maximum and the minimal stable time step, the number of cycles performed during the analysis and the total time of the analysis. The super- or subscript "i" corresponds to a quantity attached to the i-th model.

Appendix D - Three-dimensional finite element modelling of the anterior cruciate ligament: influence of the initial stress field.

Georges Limbert and Mark Taylor

This research was published as a referred book section (see PREFACE) and was given as an oral presentation at the occasion of the *Fourth International Symposium in Computer Methods in Biomechanics and Biomedical Engineering, October 13-16, 1999, Lisbon, Portugal.*

1. ABSTRACT

This study was based on a three-dimensional finite element analysis of the human Anterior Cruciate Ligament (ACL). The objective was to assess the influence of the initial stress field within the ACL on the distribution and magnitudes of the stresses during flexion extension. The resultant force within the ACL was determined during various simulated kinematic conditions. The constitutive law was based on a incompressible isotropic hyperelastic strain energy function. The initial stress field within the ACL at full extension of the knee has a significant influence on the distribution and magnitude of the stresses at the various angles of flexion. Moreover it appears that this observation depends on which part of the ACL is considered. Increasing the initial stress field by 25 % leads to a reduction in the von Mises stresses of up to 80 % in the anterior and lateral part of the ACL. Also there is an increase in the von Mises stresses by up to 33 % in the posterior and lateral part of the ACL during a passive knee flexion ranging from 0° to 60°. However, significant compressive stresses were observed in the various models. Therefore, the results obtained concerning the resultant force and the principal stress directions call in question the validity of the isotropic hyperelastic formulation for anatomical models.

2. INTRODUCTION

The Anterior Cruciate Ligament (ACL) is essential for the stability of the knee by preventing anterior displacement of the tibia relative to the femur and hyperextension of the joint. Some authors also argue that the ACL, like other ligaments, has a proprioceptive function in addition to its mechanical role. The ACL is the most commonly injured ligament of the body [Fetto *et al.*, 1980] especially during sport [Speer *et al.*, 1995] and motor vehicle accidents because of excessive loading and/or high strain rate (up to 500 $\%.s^{-1}$) [Crowninshield *et al.*, 1976].

The ACL has no free stress state at any of the knee flexion angles [Dürselen *et al.*, 1996]. The stress distribution within the ACL when the knee is at full extension is unknown. Concerning the resultant force generated by the ACL, there appears to be a large variability in the values reported in the literature. Wascher [Wascher *et al.*, 1993] performed an *in-vitro* study and reported resultant forces at full extension of ranging between 5 and135 N. Roberts [Roberts et al., 1994] performed a *in-vivo* study and reported a resultant force at full extension of 104 N (± 14).

In order to gain a better understanding of the mechanisms of injury within the ACL it is necessary to assess the magnitude and the distribution of stresses within this ligament and therefore a three dimensional continuum model of the ACL is required. A literature survey showed that few authors have developed and implemented suitable constitutive laws for the ACL within three-dimensional finite element models. Recently, Pioletti (1997) developed a full thermodynamic formulation of a constitutive law, based on an incompressible isotropic hyperelastic formulation, for the ACL and derived material data from experiments and implemented it into the commercial code ABAQUS (® Hibbit, Karlsson & Sorensen Inc., Pawtucket, RI, USA). Weiss (1994) developed a general finite element framework for soft tissue modelling. Weiss formulated an incompressible transversely isotropic hyperelastic constitutive law and performed a parametric analysis to derive the material constants from experiments performed on fascia lata tendons. To the best of our knowledge, no study has examined the influence of the initial stress field on the stress distribution in the ACL. This study intends to assess the importance of this parameter during various ranges of motion.

3. MATERIALS AND METHODS

3.1 Geometrical model of the ACL

The three-dimensional geometry of the insertion sites of the ACL were obtained from an experiment performed on a cadaveric knee specimen. Several markers were placed along the contours of the ACL at the tibial and femoral insertion sites in order to track their three-dimensional location during the passive knee flexion tests. The geometrical model includes the non planar insertion areas and respects the natural orientation of the fibres. Given that the full three-dimensional shape of the ACL was not available and that a "reasonable" ACL shape does not affect significantly the results of the finite element analysis (Pioletti, 1997), the ligament was reconstructed by connecting the two insertion surfaces. This operation was performed in the pre and post-processor Patran v8.0 (® The MacNeal Schwendler Corporation, Los Angeles, CA, USA). The solid volume reconstructed was that of the ACL when the knee is at full extension.

3.2 Finite element model of the ACL

In order to carry out a finite element analysis it is necessary to discretize the domain of interest with finite elements. The solid volume was meshed with 8-noded hexahedron elements using Patran v8.0. Special care was taken in order to optimize the performance of the mesh for the large displacement and large strain analysis. In fact, due to its initial distorted shape, the ACL mesh can undergo severe distortions during the analysis and can lead to premature convergence failure in the computation. The mesh consisted of 3297 elements and 3784 nodes.

3.3 Constitutive law and material properties

In order to reproduce the stiffening features of the tissue constituting the ACL and its mechanical behaviour during large deformation, a hyperelastic potential with an exponential law was used. The strain energy function W proposed by Pioletti (1997) was used, which depends on the first and second invariants of the right Cauchy-Green deformation tensor **C**. The behaviour is isochoric (incompressible material) and therefore has no dependence on the third invariant which is the square of the Jacobian of the deformation. Therefore,

$$W = \alpha e^{\beta(I_1 - 3)} - \frac{\alpha\beta}{2}(I_2 - 3) \qquad [1]$$

Pioletti (1997) performed mechanical tests on cadaveric ACL in order to derive the material constants α and β. From this work we extracted: $\alpha = 0.74$ [MPa]; $\beta = 15.2$.
The material model was implemented within ABAQUS 5.8 via a customised subroutine.

3.4 Element formulation

Standard ABAQUS isoparametric hybrid incompressible elements, C3D8H, were used which are capable of sustaining large deformations. The formulation was based on a linear displacement field associated with an additional variable, the hydrostatic pressure. This independent interpolated basic variable was coupled to the displacement solution through the constitutive theory and the compatibility conditions. The pressure was assumed to be constant within the element. The formulation described above prevents the appearance of the "locking phenomenon" which is a degenerative behaviour appearing when the element is unable to distort while simultaneously meeting the incompressibility requirement at all the points of the element [Bonet *et al.*, 1997].

3.5 Boundary conditions

The passive flexion-extension kinematics tests, described in 3.1, were performed with the knee in the neutral position (no internal or external rotation) for flexion angles of 0, 10, 30, 45 and 60 degrees. The tibia was fixed and the femur was free to move in the flexion plane. The resulting positions of the femoral insertion of the ligament were used as displacement boundary conditions and the nodes of the tibial insertion area were rigidly fixed.

3.6 Initial stress field: methodology

The finite element analysis was performed in two steps.
STEP1: The FE model of the ACL was prestressed using the Abaqus subroutine SIGINI. During this procedure the equilibrium of the initial stress field with the applied forces and distributed loads was checked. No translation was allowed for the femoral nodes and a uniform stress was applied to the femoral insertion elements in the direction of the mean axis of the ACL. Four cases were considered: a uniform stress corresponding to a initial force at full extension of 50 N, 75 N and 100 N. These initial forces correspond to the upper and lower bounds reported in the literature [Wascher et al., 1993; Roberts et al., 1994]. The fourth case assumed no initial stress within the ACL at full extension (no STEP1).
STEP2: A finite deformation analysis was performed using the standard Abaqus nonlinear solver (iterative Newton-Raphson method) where boundary conditions were prescribed in displacement and corresponded to the flexion angle considered.

4. RESULTS

Results were postprocessed using Patran v8.0 and a customised Abaqus subroutine. The von Mises (VM) stresses and the resultant force within the ACL have been reported. The VM stresses at the anterior, posterior, medial and lateral aspects of a section mid way along the length of the ACL have been reported in detail.

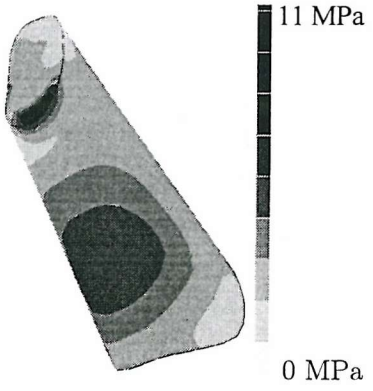

Figure 1a. von Mises stresses at 30° of neutral flexion(no initial stress field)

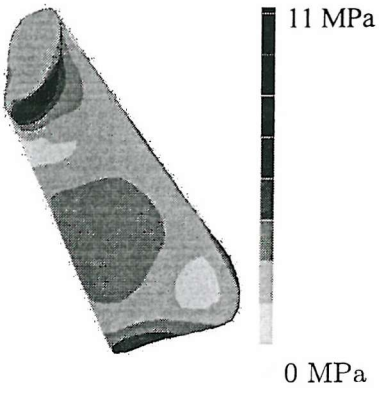

Figure 1b. von Mises stresses at 30° of neutral flexion (100N equivalent force)

The distribution and magnitude of VM stresses are in accordance with those found in literature (Pioletti, 1997) between 0 and 30° degrees of flexion. During knee flexion, in the anterior part of the ACL, there was an increase in the VM stresses. For sake of space VM contour plots (Figures 1a, b) were presented only in the case of no initial stress field and for a equivalent stress field of 100 N at full extension. Prestressing the ligament seems to reduce the VM stresses in the antero-middle part of the ACL and has a significant effect on the resulting stress distribution. Increasing the initial stress by 25 % leads to 80 % of increase in VM stresses when considering the anterior and the lateral side of a middle cross section of the ligament and up to 33 % increase for the medial and posterior sides (see Figures 2a, b, c, d). At 30° of flexion compressive stresses appears at the posterior side of the ACL at the tibial insertion site. This is clearly shown on Figures 2b, c through the peak in VM stresses which are a result of a dominant compressive principal stress.

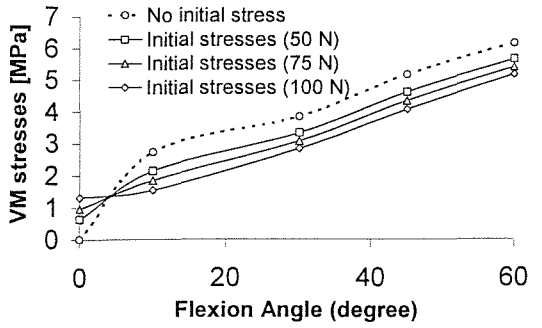

Figure 2a.

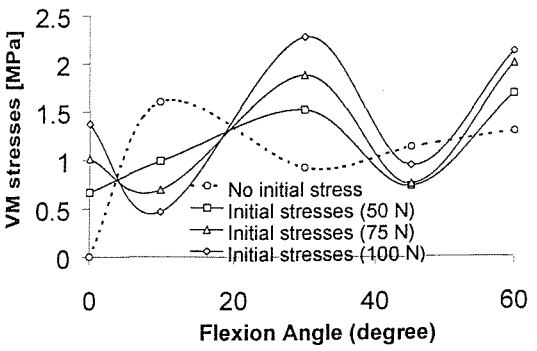

Figure 2b.

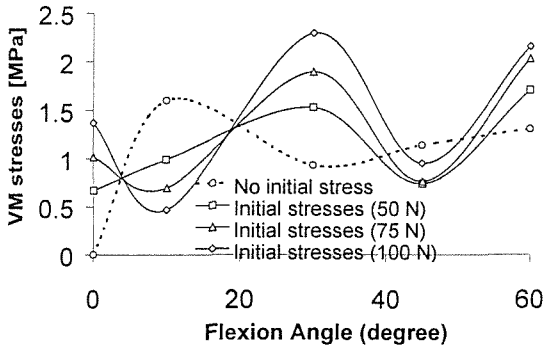

Figure 2c.

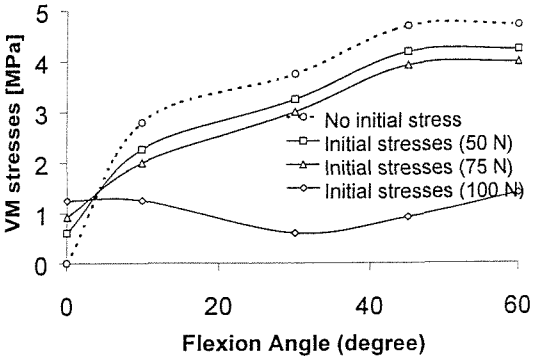

Figure 2d.

Figure 2. von Mises stresses within the ACL (a): anterior side; b): lateral side; c): posterior side; d): medial side.

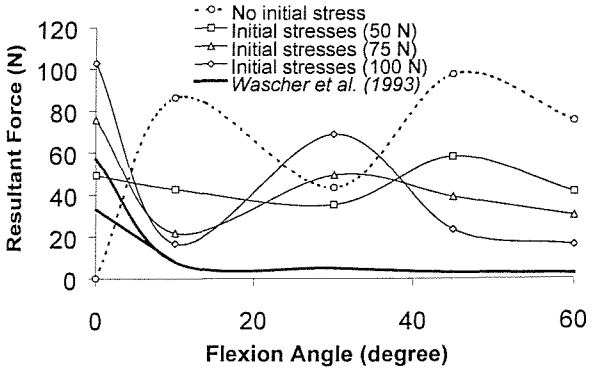

Figure 3. Resultant force in the ACL versus flexion angle for various initial conditions.

Wascher [Wascher *et al.*, 1993] showed that the resultant force within the ACL decreases monotonically from full extension till 60° degrees of flexion. The FE predictions of the resultant force do not follow the same trends as reported by Wascher *et al.* in their experiments. As the flexion angle increases, the predicted resultant force tends to fluctuate significantly, regardless of the magnitude of the initial stress field rather than decreasing to zero as observed in Wascher's experiments. This was due to the ligament taking compressive loads.

5. DISCUSSION

The initial stress field present within the ACL at full extension appears to have a significant effect on the stress distribution during the knee flexion. This raises the question of the care that has to be taken when pretensioning the graft in the ACL reconstruction even if the material is fundamentally different from that of a real ACL. Also, the ACL acts as a constraint for the movement of the tibia relative to the femur and therefore a realistic force/pre-stress must be used when performing global FE analyses of the knee.

However, this study has raised concerns regarding the validity of using an isotropic hyperelastic constitutive law when performing anatomical finite element modelling of the ACL. Pioletti (1997) developed an incompressible isotropic hyperelastic constitutive model of the ACL and implemented it within a FE code. The material parameters were derived from tensile tests and, in consequence, may not reflect the material behaviour of the ligament. Pioletti modelled the ACL subjected to physiological motions and reported a calculated resultant force in agreement with the experimental results of Wascher *et al.* [5] and Roberts *et al.* [6], only when considering the posterior part of the ACL. No mention of unrealistic compressive loads in the remaining portion of the ACL was made. Our study has shown that using the proposed constitutive law for physiological conditions, significant compressive stresses can be generated within the ligament which adversely affects the resultant forces (figure 3). These compressive stresses are not physiological and do not fit the mechanical behaviour of the ACL. The feasibility of implementing a "NO-COMPRESSION" option within the finite element model is currently under investigation. The other alternative would be to derive a transversely isotropic hyperelastic law where the energy function will avoid the compression in the fibre direction. However, the extreme difficulty to test the ACL in tension and in the transverse direction prevents us from using such an approach. The ACL is made of two major fibre bundles, an anteromedial band and a posterolateral bulk (Fick, 1904) that are probably loaded differently and this feature may affect significantly the results of the present work. The mechanical interaction between bundles need to be considered as well. The inclusion of these features is the next step of our investigation.

6. AKNOWLEDGEMENTS

The authors would like to thank Dr. V. Pinskerova, Dr. S. Martelli and Mr. M. A. R. Freeman for providing experimental data and Dr. D. Pioletti for his kind advice.

7. REFERENCES

Fetto, J. E. and Marshall, J. L., The natural history and diagnosis of anterior cruciate ligament insufficiently, Clin Orthop., 1980, Vol. 147, 29-38.

Speer, K. P., Warren, R. F., Wickiewicz, T. L., Horowitz, L. and Henderson, L., Observation on the injury mechanism of anterior cruciate ligament tears in skiers, Am J Sports Med., 1995, Vol. 23(1), 77-81.

Crowninshield, R. D. and Pope, M. H., The strength and failure characteristics of rat medial collateral ligament, J Trauma., 1976, Vol. 16, 99-105.

Dürselen, L., Claes, L. and Kiefer, H., The influence of muscle forces and external loads on cruciate ligament strain, Am J Sports Med., 1996, Vol. 23, 129-136.

Wascher, D. C., Markolf, K. T., Shapiro, M. S. and Finerman, G. A., Direct in vitro measurement of forces in the cruciate ligaments. Part I: the effect of multiplane loading in the intact knee, J Bone Joint Surg., 1993, Vol. 75-A, 377-386.

Roberts, C. S., Cumming, J. F., Grood, E. S. and Noyes, F. R., In-vivo measurement of human anterior cruciate ligament forces during knee extension exercises, *In* 40th ORS, New Orleans, 1994, 84-15.

Pioletti, D., Viscoelastic properties of soft tissues: Application to knee ligaments and tendons, Ph. D Thesis, EPF Lausanne, Switzerland, 1997.

Weiss, J. A., A constitutive model and finite element representation for transversely isotropic soft tissues, Ph D Thesis, University of Utah, USA, 1994.

Bonet, J. and Wood, R., Nonlinear continuum mechanics for finite element analysis, Cambridge University Press, 1997.

Fick, R., Anatomie und Mechanik der Gelenke. Part 1., Anatomie der Gelenke. Gustav Fischer, Jena, 1904.

LIST OF REFERENCES

[1] (1997). ABAQUS Theory Manual., Hibbitt, Karlsson & Sorensen, Inc.

[2] Abdel-Rahman, E. M. and Hefzy, M. S. (1998). Three-dimensional dynamic behaviour of the human knee joint under impact loading. *Medical Engineering & Physics* **20**(4): 276-290.

[3] Abrahams, M. (1967). Mechanical behavior of tendon in vitro. *Medical & Biological Engineering* **5**: 433.

[4] Amiel, D., Frank, C., Harwood, F., Fronek, J. and Akeson, W. (1984). Tendons and ligaments: A morphological and biochemical comparison. *Journal of Orthopaedic Research* **1**(3): 257-265.

[5] Amis, A. A. (1989). Anterior cruciate ligament replacement. Knee stability and the effects of implants. *Journal of Bone and Joint Surgery* **71B**(5): 819-824.

[6] Amis, A. A. and Dawkins, G. P. (1991). Functional anatomy of the anterior cruciate ligament. Fibre bundle actions related to ligament replacements and injuries. *Journal of Bone and Joint Surgery* **73B**(2): 260-267.

[7] Andriacchi, T. P., Mikosz, R. P., Hampton, S. J. and Galante, J. O. (1983). Model studies of the stiffness characteristics of the human knee joint. *Journal of Biomechanics* **16**(1): 23-29.

[8] Arms, S. W., Pope, M. H., Johnson, R. J., Fischer, R. A., Arvidsson, I. and Eriksson, E. (1984). The biomechanics of anterior cruciate ligament rehabilitation and reconstruction. *American Journal of Sports in Medicine* **14**: 8-18.

[9] Armstrong, C. G., Lai, W. M. and Mow, V. C. (1984). An analysis of the unconfined compression of articular cartilage. *Journal of Biomechanical Engineering* **106**: 165-173.

[10] Aubriot, J. H. (1998). Post-traumatic knee degeneration. *Revue du Praticien* **48**(16): 1799-804.

[11] Ault, H. K. and Hoffman, A. H. (1992a). A composite micromechanical model for connective tissues: Part I -- Theory. *Journal of Biomechanical Engineering* **114**: 137-141.

[12] Ault, H. K. and Hoffman, A. H. (1992b). A composite micro mechanical model for connective tissues: Part II -- Application to rat tail tendon and joint capsule. *Journal of Biomechanical Engineering* **114**: 142-146.

[13] Bach, J. M., Hull, M. L. and Patterson, H. A. (1997). Direct measurement odf strain in the posterolateral bundle of the anterior cruciate ligament. *Journal of Biomechanics* **30**(3): 281-283.

[14] Bailey, A. J. (1968). Comprehensive biochemistry. Amsterdam, Elsevier.

[15] Baker, M. and Ericksen, J. L. (1954). Inequalities restricting the form of the stress-deformation relations for isotropic elastic solids and Reiner-Rivlin fluids. *Journal of the Washington Academy of Sciences* **44**: 33-35.

[16] Ball, J. M. (1977). Convexity conditions and existence theorems in nonlinear elasticity. *Archive of Rational Mechanics and Analysis* **63**: 337-403.

[17] Ball, J. M. (1980). Existence of solutions in finite elasticity. *IUTAM Symposium on Finite Elasticity, Lehifh University, Bethlehem, PA, USA*, August 10-15, Nijhoff, Martinus, D. E. Carlson and R. T. Shield Ed., 1-12.

[18] Barbenel, J. C., Evans, J. H. and Finlay, J. B. (1973). Stress-strain-time relations for soft connective tissues. Perspectives in Biomedical Engineering. London, MacMillan: 165-172.

[19] Bates, D. M. and Watts, D. G. (1998). Nonlinear regression analysis and its applications., John Wiley and Sons.

[20] Bathe, K. J. (1982). Finite element procedures in engineering analysis. Englewood Cliffs, Prentice-Hall, Inc.

[21] Belkoff, S. M. and Haut, R. C. (1991). A structural model used to evaluate the changing microstructure of maturing rat skin. *Journal of Biomechanics* **24**(8): 711-720.

[22] Belkoff, S. M. and Haut, R. C. (1992). Microstructurally based model analysis of Gamma-irradiated tendon allografts. *Journal of Orthopaedic Research* **10**(3): 461-464.

[23] Belytschko, T. (1983). Correction of article by D. P. Flanagan and T. Belytschko. *International Journal for Numerical Methods in Engineering* **19**: 467-468.

[24] Bendjaballah, M. Z., Shirazi-Adl, A. and Zukor, D. J. (1998). Biomechanical response of the passive human knee under anterior-posterior forces. *Clinical Biomechanics* **13**: 625-633.

[25] Beskos, D. E. and Jenkins, J. T. (1975). A mechanical model for mammalian tendon. *Journal of Applied Mechanics* **42**: 755-758.

[26] Beynnon, B. D. and Fleming, B. C. (1998). Anterior cruciate ligament strain in-vivo: a review of previous work. *Journal of Biomechanics* **31**: 519-525.

[27] Beynnon, B. D., Fleming, B. C., Johnson, R. J., Nichols, C. E., Renström, P. A. and Pope, H. M. (1995). Anterior cuciate ligament strain behavior during rehabilitation exercises in vivo. *Americal Journal of Sports in Medicine* **23**(1): 24-34.

[28] Beynnon, B. D., Johnson, R. J. and Fleming, B. C. (1993b). The mechanics of anterior cruciate ligament reconstruction. The anterior cruciate ligament: current and future concepts. D. W. Jackson. New York, Raven Press: 269.

[29] Beynnon, B. D., Pope, M. H., Fleming, J. G., Howe, A. R., Johnson, R. J., Erickson, C. M., Wertheimer, C. and Nichols, C. E. (1989). An in vivo study of the ACL strain biomechanics in the normal knee. *Orthoapedic Research Society* Ed., 324.

[30] Blankevoort, L. and Huiskes, R. (1991b). Ligament-bone interaction in a three-dimensional model of the knee. *Journal of Biomechanical Engineering* **113**(3): 263-269.

[31] Blatz, P. J., Chu, B. M. and Wayland, H. (1969). *Transaction of the Society of Rheology* **13**: 83-102.

[32] Boehler (1978). Lois de comportement anisotrope des milieux continus. *Journal de Mécanique* **17**: 153-190.

[33] Bonet, J. and Wood, R. D. (1997). Nonlinear continuum mechanics for finite element analysis. Cambridge, Cambridge University Press.

[34] Brand, R. A. (1986). Knee ligaments: a new view. *Journal of Biomechanical Engineering* **108**: 106-110.

[35] Brantigan, O. C. and Voshell, A. C. (1941). The mechanics of the ligaments of the knee joint. *Journal of Bone and Joint Surgery* **23**: 44-66.

[36] Butler, D. L., Grood, E. S. and Noyes, F. R. (1978). Biomechanics of ligaments and tendons. *Exercise and Sport Sciences Reviews* **6**: 125.

[37] Butler, D. L., Guan, Y., Kay, M. D., Cummings, J., Feder, S. and Levy, M. (1992). Location-dependent variations in the material properties of the anterior cruciate ligament. *Journal of Biomechanics* **25**(5): 511-518.

[38] Butler, D. L., Kay, M. D. and Stouffer, D. C. (1986). Comparison of material properties in fascicle-bone units from human patellar tendon and knee ligaments. *Journal of Biomechanics* **19**(6): 425-32.

[39] Butler, D. L., Noyes, F. R. and Grood, E. S. (1980). Ligamentous restraints to anterior-posterior drawer in the human knee. *Journal of Bone and Joint Surgery* **62A**: 259-270.

[40] Butler, D. L., Sheh, M. Y., Stouffer, D. C., Samaranayake, V. A. and Levy, M. S. (1990). Surface strain variation in human patellar tendon and knee cruciate ligaments. *Journal of Biomechanical Engineering* **112**: 38-45.

[41] Cabaud, H. E. (1983). Biomechanics of the anterior cruciate ligament. *Clinical Orthopaedics* **172**: 26-31.

[42] Carlstedt, C. A. and Nordin, M. (1989). Biomechanics of tendons and ligaments. Basic biomechanics of the musculoskeletal system. M. Nordin and V. H. Frankel. Philadelphia, London, Lea & Febiger.

[43] Chan, S. C. N. and Seedhom, B. B. (1995). The effects of the geometry of the tibia on prediction of the cruciate ligament forces: a theoretical analysis. *Proceedings of the Institute of Mechanical Engineers [H]* **209**: 17-30.

[44] Chimich, D. D., Shrive, N. G., Marchuk, L. and Bray, R. C. (1992). Water content alters the viscoelastic behaviour of the normal adolescent rabbit medial collateral ligament. *Journal of Biomechanics* **25**(18): 831-837.

[45] Ciarlet, P. (1988). Mathematical foundations of elasticity. I. Amsterdam, North-Holland Publishing Company.

[46] Cohen, H. and Wang, C. C. (1987). On the response and symmetry of elastic materials with internal constraints. *Archive of Rational Mechanics and Analysis* **99**: 1.

[47] Coleman, B. D. and Noll, W. (1964). Material symmetry and thermostatic inequalities in finite elastic deformations. *Archive of Rational Mechanics and Analysis* **17**: 87-111.

[48] Comninou, M. and Yannas, I. V. (1976). Dependence of stress-strain nonlineraity of connective tissues on the geometry of collagen fibers. *Journal of Biomechanics* **9**: 427-433.

[49] Crowninshield, R. D. and Pope, M. H. (1976). The strength and failure characteristics of rat medial collateral ligament. *Journal of Trauma* **16**: 99-105.

[50] Cruise, A. J. (1958). The structural periodicity of microscopic collagen fibers. London, Pergamon Press.

[51] Daniel, W. J. T. (1999). Three-dimensional orthotropic viscoelastic finite element model of human ligament. *Fifth US National Congress on Computational Mechanics (USNCCM99), Boulder, Colorado, USA*, August 4-6, 1999,, Ed., 256.

[52] Decraemer, W. F., Maes, M. A. and Vanhuyse, V. J. (1980a). An elastic stress-strain relation for soft biological tissues based on a structural model. *Journal of Biomechanics* **13**: 463-468.

[53] Delp, S. L., Kocmond, J. H. and Stern, S. H. (1995). Tradeoffs between motion and stability in posterior substituting knee arthroplasty design. *Journal of Biomechanics* **28**(10): 1155-1166.

[54] Demiray, H. (1972). A note on the elasticity of soft biological tissues. *Journal of Biomechanics* **5**: 309-311.

[55] Diamant, J., Keller, A., Baer, E., Litt, M. and Arridge, R. G. C. (1972). Collagen: Ultrastructure and its relation to mechanical properties as a function of ageing. *Proceedings of the Royal Society of London [Biology]* **180B**: 293-315.

[56] Dürselen, L., Claes, L. and Kiefer, H. (1996). The influence of muscle forces and external loads on cruciate ligament strain. *Americal Journal of Sports in Medicine* **23**: 129-136.

[57] Ericksen, J. L. (1978). On the symmetry and stability of thermoelastic solids. *Journal of Applied Mechanics* **45**: 740.

[58] Ericksen, J. L. (1979). On the symmetry of deformable crystals. *Archive of Rational Mechanics and Analysis* **72**: 1-13.

[59] Ericksen, J. L. and Rivlin, R. S. (1954). Large elastic deformations of homogeneous anisotropic materials. *Journal of Rational Mechanics and Analysis* **3**: 281-301.

[60] Feagin, J. A., Jr. and Lambert, K. L. (1985). Mechanism of injury and pathology of anterior cruciate ligament injuries. *The Orthopedic Clinics of North America* **16**(1): 41-45.

[61] Fetto, J. E. and Marshall, J. L. (1980). The natural history and diagnosis of anterior cruciate ligament insufficiently. *Clinical Orthopaedics* **147**: 29-38.

[62] Fick, R. (1904). Anatomie und Mechanik der Gelenke. Part 1., Anatomie der Gelenke. Jena, Gustav Fischer.

[63] Flanagan, D. P. and Belytschko, T. (1981). A uniform strain hexahedron and quadrilateral with orthogonal hourglass control. *International Journal for Numerical Methods in Engineering* **17**: 679--706.

[64] Flory, P. J. (1961). Thermodynamic relations for high elastic materials. *Transactions of the Faraday Society* **57**: 829-838.

[65] France, E. P., Daniels, A. U., Goble, E. M. and Dunn, H. K. (1983). Simultaneous quantitation of knee ligament forces. *Journal of Biomechanics* **16**(8): 553-564.

[66] Frank, C., MacFarlane, B., Edwards, P., Rangayyan, R., Liu, Z.-Q., Walsh, S. and Bray, R. (1991). A quantitative analysis of matrix alignment in ligament scars: a comparison of movement versus immobilization in an immature rabbit model. *Journal of Orthopaedic Research* **9**: 219-227.

[67] Frank, C., McDonald, D., Bray, D., Bray, R., Rangayyan, R., Chimich, D. and Shrive, N. (1992). Collagen fibril diameters in the healing adult rabbit medial collateral ligament. *Connective Tissue Research* **27**: 251-263.

[68] Frank, C. B. and Shrive, N. G. (1999). Biological Materials - 2.5 LIGAMENT. Biomechanics of the musculo-skeletal system. B. M. N. a. W. Herzog. Chichester, New York, Weinheim, Brisbane, Toronto, Singapore: 107-126.

[69] Frisen, M., Magi, M., Sonnerup, L. and Viidik, A. (1969). Rheological analysis of soft collagenous tissue. Part II: Experimental evaluation and verification. *Journal of Biomechanics* **2**: 21-28.

[70] Fukubayashi, T., Torzilli, P. A., Sherman, M. F. and Warren, R. F. (1982). An in vitro biomechanical evaluation of anterior-posterior motion of the knee. Tibial displacement, rotation, and torque. *Journal of Bone and Joint Surgery* **64A**(2): 258-64.

[71] Fung, Y. C. (1967). Elasticity of soft tissues in simple elongation. *Americal Journal of Physiology* **213**: 1532-1544.

[72] Fung, Y. C. (1968). Biomechanics, its scope, history, and some problems of continuum mechanics in physiology. *Applied Mechanics Review* **21**: 1-20.

[73] Fung, Y. C. (1972). Stress-strain-history relations of soft tissues in simple elongation. Biomechanics: its foundations and objectives. Englewood Cliffs, NJ, Prentice-Hall.

[74] Fung, Y. C. (1973). Biorheology of soft tissues. *Biorheology* **10**: 139-155.

[75] Fung, Y. C. (1981). Biomechanics: mechanical properties of living tissues. New York, Springer-Verlag.

[76] Girgis, F. G., Marshall, J. L. and Al Monajem, A. R. S. (1975). The cruciate ligaments of the knee joint. Anatomical, functional and experimental analysis. *Clinical Orthopaedics and Related Research* **106**: 216-231.

[77] Glowinski, R. and Le Tallec, P. (1984). Finite element analysis in nonlinear incompressible elasticity. Finite Elements. O. J. T. and C. G. F. Englewood Cliffs, N.J, Prentice Hall. **V**.

[78] Gollehon, D. L., Torzilli, P. A. and Warren, R. F. (1987). The role of the postero-lateral and cruciate ligaments in the stability of the human knee. *Journal of Bone and Joint Surgery* **69A**: 233-242.

[79] Grassmann, R. M., Shrive, N. G. and Franck, C. B. (1998). A 2D finite element model of a medial collateral ligament reconstruction. Computer Methods in Biomechanics and Biomedical Engineering - 2. J. Middleton, M. L. Jones and G. N. Pande, Gordon and Breach Science Publishers: 553-560.

[80] Grood, E. S., Noyes, F. R., Butler, D. L. and Suntay, W. J. (1981). Ligamentous and capsular restraints preventing straight medial and lateral laxity in intact human cadaver knees. *Journal of Bone and Joint Surgery* **63A**(8): 1257-69.

[81] Gurtin, M. E. (1980). On uniqueness in finite elasticity. *IUTAM Symposium on Finite Elasticity, Lehifh University, Bethlehem, PA, USA*, August 10-15, Nijhoff, Martinus, D. E. Carlson and R. T. Shield Ed., 191-199.

[82] Hahn, T. (1987). Space-group symmetry. Vol. A. Dordrecht, Dreidel, D.

[83] Haines, R. W. (1941). Anatomical note: a note on the actions of cruciate ligaments of the knee joint. *Journal of Anatomy* **75**: 373-375.

[84] Harfe, D. T., Chuinard, C. R., Espinoza, L. M., Thomas, K. A. and Solomonow, M. (1998). Elongation patterns of the collateral ligaments of the human knee. *Clinical Biomechanics* **13**(3): 163-175.

[85] Haut, R. C. and Little, R. W. A. (1972). A constitutive equation for collagen fibers. *Journal of Biomechanics* **5**: 523.

[86] Hayashi, K., Kamiya, A. and Ono, K. (1996). Remodeling of tendon autograft in ligament reconstruction. Biomechanics-Functional adaptation and remodeling. Tokyo, Springer-Verlag**:** 213-250.

[87] Hayashi, K., Miyazaki, H. and Hasegawa, Y. (2000). Mechanical properties of cells and collagen fiber. *10th International Conference on Biomedical Engineering, Singapore*, December 6-9,, Ed., 55-56.

[88] Hefzy, M. S. and Grood, E. S. (1983). An analytical technique for modelling knee joint stiffness - part II: Ligamentous geometric nonlinearities. *Journal of Biomechanical Engineering* **105**: 145-153.

[89] Hermann, L. R. (1965). Elasticity equations for nearly incompressible material by a variational theorem. *J. AIAA* **3**: 1896-1900.

[90] Hirokawa, S. and Tsuruno, R. (1997). Hyper-elastic model analysis of anterior cruciate ligament. *Medical Engineering & Physics* **19**(7): 637-51.

[91] Hirokawa, S. and Tsuruno, R. (2000). Three-dimensional deformation and stress distribution in an analytical/computational model of the anterior cruciate ligament. *Journal of Biomechanics* **33**: 1069-1077.

[92] Hirsham, H. P., Daniel, D. M. and Myasaka, K. (1990). The fate of unoperated knee ligament injuries. Knee ligaments: structure, function, injury, and repair. D. M. Daniel, W. H. Akeson and J. J. O'Connor. New York, Raven Press**:** 481-503.

[93] Hoger, A. (1996). The elasticity tensor of a transversely isotropic hyperelastic material with residual stress. *Journal of Elasticity* **42**: 115-132.

[94] Hollinshead, W. H. (1982). Anatomy for Surgeons: The Back and Limbs. Anatomy for Surgeons: The Back and Limbs. Philadelphia, Harper and Row. **3:** 747, 754, 757-762, 767-768, 771-772.

[95] Hollis, J. M., Lyon, R. M., Marcin, J. P., Horibe, S., Lee, E. B. and Woo, S. Y. L. (1988). Effect of age and loading axis on the failure properties of the human ACL. *34 Ann. ORS* Ed., 81.

[96] Holzapfel, G. A., Eberlein, R., Wriggers, P. and Weizsäcker, H. W. (1996). Large strain analysis of soft biological membranes: Formulation and finite element analysis. *Computer Methods in Applied Mechanics and Engineering* **132**: 45-61.

[97] Hughes, T. J. R. (1980). Generalization of selective integration procedures to anisotropic and nonlinear media. *International Journal of Numerical Methods in Engineering* **15**(15): 1413-1418.

[98] Hughston, J. C., Andrews, J. R., Cross, M. J. and Moschi, A. (1976a). Classification of knee ligament instabilities. Part I. The medial compartment and cruciate ligaments. *Journal of Bone and Joint Surgery* **58A**(2): 159-72.

[99] Hughston, J. C., Andrews, J. R., Cross, M. J. and Moschi, A. (1976b). Classification of knee ligament instabilities. Part II. The lateral compartment. *Journal of Bone and Joint Surgery* **58A**(2): 173-9.

[100] Humphrey, J. D. (1990a). Determination of a constitutive relation for passive myocardium: I: "A new functional form". *Journal of Biomechanical Engineering* **112**: 333-339.

[101] Humphrey, J. D. (1990b). Determination of a constitutive relation for passive myocardium: II:"Parameter estimation". *Journal of Biomechanical Engineering* **112**: 340-346.

[102] Humphrey, J. D. and Yin, F. C. P. (1987). On constitutive relations and finite deformations of passive cardiac tissue: I: "A pseudostrain energy function". *Journal of Biomechanical Engineering* **109**: 298-304.

[103] Hurschler, C., Loitz-Ramage, B. and Vanderby, R. J. (1997). A structurally based stress-stretch relationship for tendon and ligament. *Journal of Biomechanical Engineering* **119**: 392-399.

[104] Imran, A. and O'Connor, J. J. (1997). Theoretical estimates of cruciate ligament forces: effects of tibial surface geometry and ligament orientations. *Proceedings of the Institute of Mechanical Engineers* **211**(Part H): 425-439.

[105] Inman, V. T., Ralston, H. J. and Todd, F. (1981). Human walking. Baltimore, Williams & Wilkins.

[106] Jeffreys, T. E. (1963). Recurrent dislocation of the patella due to abnormal attachment of ilio-tibial tract. *Journal of Bone and Joint Surgery* **45B**: 740-743.

[107] Jenkins, R. B. and Little, R. W. (1974). A constitutive equation for parallel-fibered elastic tissue. *Journal of Biomechanics* **7**: 397-402.

[108] Johnson, G. A., Livesay, G. A., Woo, S. L. Y. and Rajagopal, K. R. (1996). A single integral finite strain viscoelastic model of ligaments and tendons. *Journal of Biomechanical Engineering* **118**: 221-226.

[109] Johnson, G. A., Rajagopal, K. R. and Woo, S. L. Y. (1992). A single integral finite strain (SIFS) model of ligaments and tendons. *Advances in Bioengineering* **22**: 245-248.

[110] Johnson, G. A., Tramaglini, D. M., Levine, R. E., Ohno, K., Choi, N. Y. and Woo, S. L. Y. (1994). Age related changes in the tensile and viscoelastic properties of the human patellar tendon. *Journal of Orthopaedic Research* **12**: 796-803.

[111] Johnson, R. J. (1982). The anterior cruciate: a dilemma in sports medicine. *International Journal of Sports Medicine* **3**: 71-79.

[112] Kapandji, I. A. (1987). The Knee. The Physiology of the Joints. Edinburgh, London, Melbourne, New York, Churchill Livingstone. **Volume II - Lower Limb:** 64-147.

[113] Kastelic, J., Galeski, A. and Baer, E. (1978). The multicomposite structure of tendon. *Connective Tissue Research* **6**: 11-23.

[114] Kastelic, J., Palley, I. and Baer, E. (1980). A structural mechanical model for tendon crimping. *Journal of Biomechanics* **13**: 887-893.

[115] Kato, Y. P., Christiansen, D. L., Hahn, R. A., Shieh, S. J., Goldstein, J. D. and Silver, F. H. (1989). Mechanical properties of collagen fibres: a comparison of reconstituted and rat tail tendon fibres. *Biomaterials* **10**: 38-42.

[116] Kennedy, J. C., Hawkins, R. J., Willis, R. B. and Danylchuck, K. D. (1976). Tension studies of human knee ligaments. Yield point, ultimate failure, and disruption of the cruciate and tibial collateral ligaments. *Journal of Bone and Joint Surgery* **58A**(3): 350-355.

[117] Klisch, S. M. and Lotz, J. C. (1999). Application of a fiber-reinforced continuum theory to multiple deformations of the annulus fibrosus. *Journal of Biomechanics* **32**: 1027-1036.

[118] Kocmond, J. H., Delp, S. L. and Stern, S. H. (1995). Stability and range of motion of Insall-Burstein condylar prostheses. A computer simulation study. *Journal of Arthroplasty* **10**(3): 383-338.

[119] Kwan, M. K. and Woo, S. Y. L. (1989). A structural model to describe the nonlinear stress-strain behaviour for parallel-fibered collagenous tissues. *Journal of Biomechanical Engineering* **111**: 361-363.

[120] Lanir, Y. (1978). Structure-function relations in mammalian tendon: The effect of geometrical nonuniformity. *Journal of Bioengineering* **2**: 119-128.

[121] Lanir, Y. (1980). A microstructure model for the rheology of mammalian tendon. *Journal of Biomechanical Engineering* **102**: 332-339.

[122] Lanir, Y. (1983). Constitutive equations for fibrous connective tissues. *Journal of Biomechanics* **16**(1): 1-22.

[123] Le Dret, H. (1985). Constitutive laws and existence questions in incompressible nonlinear elasticity. *Journal of Elasticity* **15**: 369-387.

[124] Levy, I. M., Torzilli, P. A. and Warren, R. F. (1982). The effect of medial menisectomy on anterior-posterior motion of the knee. *Journal of Bone and Joint Surgery* **64**(A): 883-888.

[125] Li, G., Gil, J., Kanamori, A. and Woo, S. L. Y. (1999). A validated three-dimensional computational model of a human knee joint. *Journal of Biomechanical Engineering* **121**(6): 657-662.

[126] Limbert, G. and Taylor, M. (2001a). Three-dimensional finite element modelling of the human anterior cruciate ligament. Influence of the initial stress field. Computer Methods in Biomechanics and Biomedical Engineering - 3. J. Middleton, M. L. Jones and G. N. Pande, Gordon and Breach Science Publishers. **3:** 355-360.

[127] Limbert, G. and Taylor, M. (2001b). An explicit three-dimensional finite element model of an incompressible transversely isotropic hyperelastic material. Application to the study of the human anterior cruciate ligament. *First MIT Conference on Computational Fluid and Solid Mechanics, Cambridge, MA, USA*, June 12-15, Elsevier Science, K. J. Bathe Ed., 319-322.

[128] Lin, H. S., Liu, Y. K., Ray, G. and Nikravesh, P. (1978). System identification for material properties of the intervertebral joint. *Journal of Biomechanics* **11**: 1-14.

[129] Loch, D. A., Luo, Z. P., Lewis, J. L. and Stewart, N. J. (1992). A theoretical model of the knee and ACL: theory and experimental verification. *Journal of Biomechanics* **25**(1): 81-90.

[130] Lyon, R. M., Lin, H. C., Kwan, M. K. W., Hollis, J. M., Akeson, W. H. and Woo, S. Y. L. (1988). Stress relaxation of the anterior cruciate ligament (ACL) and the patellar tendon (PT). *Transactions of the ORS* Ed., 81.

[131] Malkus, D. S. and Hughes, T. J. R. (1978). Mixed finite element methods - Reduced and selective integration techniques: a unification of concepts. *Computer Methods in Applied Mechanics and Engineering* **15**: 63-81.

[132] Mardsen, J. E. and Hughes, T. J. R. (1994). Mathematical Foundations of Elasticity. New-York, Dover.

[133] Marinozzi, G., Pappalardo, S. and Steindler, R. (1983). Human knee ligaments: mechanical tests and ultrastructural observations. *Italian Journal of Orthopaedics and Traumatology* **9**: 231-240.

[134] Markolf, K. L., Burchfield, D. M., Shapiro, M. M., Shepard, M. F., Finerman, G. A. M. and Slauterbeck, J. L. (1995). Combined knee loading states that generate high anterior cruciate ligament forces. *Journal of Orthopaedic Research* **13**: 930-935.

[135] Markolf, K. L., Gorek, J. F., Kabo, J. M. and Shapiro, M. S. (1990). Direct measurement of resultant forces in the anterior cruciate ligament. An in vitro study performed with a new experimental technique. *Journal of Bone and Joint Surgery* **72A**(4): 557-567.

[136] Markolf, K. L., Graff-Radford, A. and Amstutz, H. C. (1978). *In-vivo* knee stability: a quantitative assessment using an instrumented clinical testing apparatus. *Journal of Bone and Joint Surgery* **60A**(5): 664-674.

[137] Markolf, K. L., Kochan, A. and Amstutz, H. C. (1984). Measurement of knee stiffness and laxity in patients with documented absence of the anterior cruciate ligament. *Journal of Bone and Joint Surgery* **66A**: 242-253.

[138] Markolf, K. L., Mensch, J. and Amstutz, H. (1976). Stiffness and laxity of the knee - The contributions of the supporting structures. *Journal of Bone and Joint Surgery* **58A**:583-594.

[139] Markolf, K. L., Slauterbeck, J. L., Armstrong, C. G., Shapiro, M. M. and Finerman, G. A. M. (1996). Effect of combined knee loadings on posterior cruciate ligament force generation. *Journal of Ortopaedic Research* **14**: 633-638.

[140] Markolf, K. L., Wascher, D. C. and Finerman, G. A. (1993). Direct in vitro measurement of forces in the cruciate ligaments. Part II: The effect of section of the posterolateral structures. *Journal of Bone and Joint Surgery* **75A**(3): 387-394.

[141] Martelli, S., Joukhadar, A., Marcacci, M., Lavallee, S. and Champleboux, G. (1998). Fiber-based anterior cruciate ligament model for biomechanical simulations. *Journal of Orthopaedic Research* **16**(3): 379-385.

[142] Martelli, S., Zaffagnini, S., Falcioni, B. and Marcacci, M. (2000). Intraoperative kinematic protocol for knee joint evaluation. *Computer Methods and Programs in Biomedicine* **62**: 77-86.

[143] Matyas, J. R., Anton, M. G., Shrive, N. G. and Frank, C. B. (1995). Stress governs tissue phenotype at the femoral insertion of the rabbit MCL [see comments]. *Journal of Biomechanics* **28**(2): 147-57.

[144] Mechanic, G. L. (1974). An automated scintillation counting system with high efficiency for continuous analysis: cross-links of [3H]NaBH4 reduced collagen. *Annals of Biochemistry* **61**: 349-354.

[145] Minns, R. J. and Soden, P. D. (1973). The role of the fibrous components and ground substance in the mechanical properties of biological tissues: A preliminary investigation. *Journal of Biomechanics* **6**: 153-155.

[146] Mommersteeg, T. J. A., Huiskes, R., Blankevoort, L., Kooloos, J. G. M., Kauer, J. M. G. and Maathuis, P. G. M. (1996a). A global verification study of a quasi-static knee model with multi-bundle ligaments. *Journal of Biomechanics* **29**(12): 1659-1664.

[147] Mommersteeg, T. J. A., Blankevoort, L., Huiskes, R., Kooloos, J. G. M. and Kauer, J. M. G. (1996b). Characterization of the mechanical behavior of human knee ligaments: a numerical-experimental approach. *Journal of Biomechanics* **29**(2): 151-160.

[148] Mommersteeg, T. J. A., Huiskes, R., Blankevoort, L., Kooloos, J. G. M. and Kauer, J. M. G. (1997). An inverse dynamic modeling approach to determine the restraining function of the human knee ligament bundle. *Journal of Biomechanics* **30**: 139-146.

[149] Morgan, F. R. (1960). The mechanical properties of collagen fibers: Stress-strain curves. *Journal of the Society Leath Trades Chemistry* **44**: 170-182.

[150] Müller, W. (1983). The Knee. Form, Function and Ligament Construction. New York, Springer-Verlag.

[151] Nagtegaal, J. C., Parks, D. M. and Rice, J. R. (1974). On numerically accurate finite element solution in the fully plastic range. *Computer Methods in Applied Mechanics and Engineering* **4**: 153-178.

[152] Negahban, M. and Wineman, A. S. (1989a). Material symmetry and the evolution of anisotropies in a simple material - I. Change of reference configuration. *International Journal of Nonlinear Mechanics* **24**: 521-536.

[153] Negahban, M. and Wineman, A. S. (1989b). Material symmetry and the evolution of anisotropies in a simple material - II. The evolution of material symmetry. *International Journal of Nonlinear Mechanics* **24**: 537-549.

[154] Nestler, F. H. M., Hvidt, S. and Ferry, J. D. (1983). Flexibility of collagen determined from dilute solution viscoelastic measurements. *Biopolymers* **22**: 1747-1758.

[155] Nicholas, J. A. and Hershman, E. B. (1986). The lower extremities and spine in sports medicine. St Louis, C. V. Mosby.

[156] Nielsen, S. (1987). Kinesiology of the knee joint. An experimental investigation of the ligamentous and capsular restraints preventing knee instability. *Danish Medical Bulletin* **34**(6): 297-309.

[157] Nielsen, S. and Helming, P. (1985). Instability of knee with ligament lesions. Cadaver studies of the anterior cruciate ligament. *Acta Orthopaedica Scandinavica* **56**: 426-429.

[158] Nielsen, S., Rasmussen, O., Ovesen, J. and Andersen, K. (1984). Rotatory instability of cadaver knees after transection of collateral ligaments and capsule. *Archives of Orthopaedic and Trauma Surgery* **103**(3): 165-9.

[159] Noyes, F. R., Butler, D. L., Grood, E. S., Zernicke, R. F. and Hefzy, M. S. (1984). Biomechanical analysis of human ligament grafts used in knee-ligament repairs and reconstructions. *Journal of Bone and Joint Surgery* **66A**(3): 344-352.

[160] Noyes, F. R. and Grood, E. S. (1976). The strength of the anterior cruciate ligament in humans and Rhesus monkeys. *Journal of Bone and Joint Surgery* **58A**(8): 1074-1082.

[161] Noyes, F. R., McGinniss, G. H. and Grood, E. S. (1985). The variable functional disability of the anterior cruciate ligament- deficient knee. *The Orthopedic Clinics of North America* **16**(1): 47-67.

[162] O'Connor, J. J. and Zavatsky, A. (1993). Anterior cruciate ligament forces in activity. The anterior cruciate ligament: current and future concepts. New York, Raven Press.

[163] Oden, J. T. and Reddy, J. N. (1978). An introduction to the mathematical theory of finite elements. New York, Academic Press.

[164] Ogden, R. W. (1984). Non-Linear Elastic Deformations. West Sussex, England, Ellis Horwood Ltd.

[165] Padgett, L. R. and Dahners, L. E. (1992). Rigid immobilization alters matrix organisation in the injured rat medial collateral ligament. *Journal of Orthopaedic Research* **10**: 895-900.

[166] Partington, F. R. and Wood, G. C. (1963). The role of non-collagen components in the mechanical behaviour of tendon fibers. *Biochemistry and Biophysics Acta* **69**: 485-495.

[167] Pioletti, D. P. (1997). Viscoelastic properties of soft tissues: Application to knee ligaments and tendons. Département de Physique. Lausanne, Switzerland, Ecole Polytechnique Fédérale de Lausanne.

[168] Pioletti, D. P., Heegaard, J. H., Rakotomanana, R. L., Leyvraz, P. F. and Blankevoort, L. (1995). Experimental and mathematical methods for representing relative surface elongation of the ACL. *Journal of Biomechanics* **28**(9): 1123-1126.

[169] Pioletti, D. P., Rakotomanana, L., Benvenuti, J. F. and Leyvraz, P. F. (1998b). Finite element model of the human anterior cruciate ligament. Computer Methods in

Biomechanics and Biomedical Engineering - 2. M. L. J. a. G. N. P. J. Middleton, Gordon and Breach Science Publishers: 561-568.

[170] Pioletti, D. P., Rakotomanana, L. R., Benvenuti, J. F. and Leyvraz, P. F. (1998a). Viscoelastic constitutive law in large deformations: application to human knee ligaments and tendons. *Journal of Biomechanics* **31**(8): 753-757.

[171] Pioletti, D. P., Rakotomanana, L. R., Gilliéron, C., Leyvraz, P. F. and Benvenuti, J. F., Eds. (1996). Nonlinear viscoelasticity of the ACL: experiments and theory. Computer Methods in Biomechanics and Biomedical Engineering, Gordon and Breach Pub.

[172] Piziali, R. L., Rastegar, J., Nagel, D. A. and Schurman, D. J. (1980a). The contribution of the cruciate ligaments to the load-displacement characteristics of the human knee joint. *Journal of Biomechanical Engineering* **102**(4): 330-337.

[173] Piziali, R. L., Seering, W. P., Nagel, D. A. and Schurman, D. J. (1980b). The function of the primary ligaments of the knee in anterior-posterior and medial-lateral motions. *Journal of Biomechanics* **13**(9): 777-84.

[174] Pope, T. L. J. (1996). MR Imaging of knee ligaments. *Journal of the Southern Orthopaedic Association* **Spring 1996**.

[175] Prietto, M. P., Bain, J. R., Stonebrook, S. N. and Settlage, R. (1988). Tensile strength of the human posterior cruciate ligament (PCL). *34th Orthopaedic Research Society* Ed., 195.

[176] Puso, M. A. and Weiss, J. A. (1998). Finite element implementation of anisotropic quasi-linear viscoelasticity using a discrete spectrum approximation. *Journal of Biomechanical Engineering* **120**(1): 62-70.

[177] Quapp, K. M. and Weiss, J. A. (1998). Material characterization of human medial collateral ligament. *Journal of Biomechanical Engineering* **120**(6): 757-763.

[178] Race, A. and Amis, A. A. (1994). The mechanical properties of the two bundles of the human posterior cruciate ligament. *Journal of Biomechanics* **27**(1): 13-24.

[179] Race, A. and Amis, A. A. (1996). Loading of the two bundles of the posterior cruciate ligament: An analysis of bundle function in A-P drawer. *Journal of Biomechanics* **29**: 873-879.

[180] Reddy, J. N. (1984). An introduction to the finite element method. New York, McGraw-Hill.

[181] Rich, A. and Crick, F. H. C. (1955). The structure of collagen. *Nature* **176**: 915.

[182] Rigby, B. J., Hirai, N. and Spikes, J. D. (1959). The mechanical properties of rat tail tendon. *The Journal of General Physiology* **43**: 265-289.

[183] Roberts, C. S., Cumming, J. F., Grood, E. S. and Noyes, F. R. (1994). In-vivo measurement of human anterior cruciate ligament forces during knee extension exercises. *40th Orthopaedic Research Society, New Orleans, USA* Ed., 84-15.

[184] Ryder, S. H., Johnson, R. J., Beynnon, B. D. and Ettlinger, C. F. (1997). Prevention of ACL injuries. *Journal of Sports Rehabilitation* **6**: 80-96.

[185] Sambatakakis, A., Attfield, S. F. and Newton, G. (1993). Quantification of soft-tissue imbalance in condylar knee arthroplasty. *Journal of Biomechanical Engineering* **15**(4): 339-343.

[186] Sanjeevi, R., Somanathan, N. and Ramaswamy, D. (1982). A viscoelastic model for collagen fibres. *Journal of Biomechanics* **15**: 181-183.

[187] Sasaki, N. and Odajima, S. (1996a). Stress-strain curve and Young's modulus of a collagen molecule as determined by the X-ray diffraction technique. *Journal of Biomechanics* **29**(5): 655-658.

[188] Sasaki, N. and Odajima, S. (1996b). Elongation mechanism of collagen fibrils and force-strain relations of tendon at each level of structural hierarchy. *Journal of Biomechanics* **29**(9): 1131-1136.

[189] Schoemaker, S. C. and Markolf, K. L. (1986). The role of the meniscus in the naterior-posterior stability of th eloaded anterior cruciate-defficient knee. Effects of partial versus total excision. *Journal of Bone and Joint Surgery* **68**(A): 71-79.

[190] Schreppers, G. J. M. A., Sauren, A. A. H. J. and Huson, A. (1990). A numerical model of the load transmission in the tibio-femoral contact area. *Journal of Engineering in Medicine* **204**: 53-59.

[191] Shelburne, K. B. and Pandy, M. G. (1997). A musculoskeletal model of the knee for evaluating ligament forces during isometric contractions. *Journal of Biomechanics* **30**(2): 163-176.

[192] Simbeya, K. W., Shrive, N. G. and Franck, C. B. (1996). Assessment with the FEM of the sensitivity of experimental results to experimental procedures in testing the rabbit medial collateral ligament. Computer Methods in Biomechanics and Biomedical Engineering - 1. J. Middleton, M. L. Jones and G. N. Pande, Gordon and Breach Science Publishers: 261-270.

[193] Simbeya, K. W., Shrive, N. G., Franck, C. B. and Matyas, J. R. (1992). A micromechanical finite element model of the rabbit medial collateral ligament. Computer Methods in Biomechanics and Biomedical Engineering - 1. J. Middleton, G. N. Pande and Williams, Gordon and Breach Science Publishers: 240-249.

[194] Simmons, P. (1998). Surgeons examine links between ACL injuries and arthritis. Mechanism of ACL injury may play a role in the development of arthritic changes. *Orthopaedics Today* **October**.

[195] Simo, J. C. and Rifai, M. S. (1990). A class of mixed assumed strain methods and incompatible modes. *International Journal of Numerical Methods in Engineering* **29**: 1595-1638.

[196] Simo, J. C. and Taylor, R. L. (1991). Quasi-incompressible finite elasticity in principal stretches. Continuum basis and numerical algorithms. *Computer Methods in Applied Mechanics and Engineering* **85**: 273-310.

[197] Simo, J. C., Taylor, R. L. and Pister, K. S. (1985). Variational and projection methods for the volume constraint in finite deformation plasticity. *Computer Methods in Applied Mechanics and Engineering* **51**: 177-208.

[198] Soong, Y. T. and Huang, W. H. (1973). A stochastic model for biological soft tissue elasticity in simple elongation. *Journal of Biomechanics* **6**: 451-458.

[199] Speer, K. P., Warren, R. F., Wickiewicz, T. L., Horowitz, L. and Henderson, L. (1995). Observation on the injury mechanism of anterior cruciate ligament tears in skiers. *Americal Journal of Sports in Medicine* **23**(1): 77-81.

[200] Spencer, A. J. M. (1992). Continuum theory of the mechanics of fibre-reinforced composites. New York, Springer-Verlag.

[201] Stouffer, D. C., Butler, D. L. and Hosny, D. (1985). The relationship between crimp pattern and mechanical response of human patellar tendon-bone units. *Journal of Biomechanical Engineering* **107**: 158-165.

[202] Sullivan, D., Levy, I. M., Sheskier, S., Torzilli, P. A. and Warren, R. F. (1984). Medial restraints to anterior-posterior motion of the knee. *Journal of Bone and Joint Surgery* **66A**: 930-936.

[203] Tamea, C. D., Jr. and Henning, C. E. (1981). Pathomechanics of the pivot shift maneuver. An instant center analysis. *Americal Journal of Sports in Medicine* **9**(1): 31-7.

[204] Tanzer, M. L. (1973). Cross-linking of collagen. *Science* **180**: 561-566.

[205] Thielke, R. J., Vanderby, R., Jr. and Grood, E. S. (1995). Volumetric changes in ligaments under tension. *Bioengineering Conference ASME BED* Ed., 197.

[206] Torg, J. S., Conrad, W. and Kalen, V. (1976). Clinical diagnosis of anterior cruciate ligament instability in the athlete. *Americal Journal of Sports in Medicine* **4**: 84-93.

[207] Torzilli, P. A., Greenberg, R. L. and Insall, J. (1981). An in vivo biomechanical evaluation of anterior-posterior motion of the knee. Roentgenographic measurement technique, stress machine, and stable population. *Journal of Bone and Joint Surgery* **63A**(6): 960-968.

[208] Toutoungi, D. E., Zavatsky, A. B. and O'Connor, J. J. (1997). Parameter sensitivity of a mathematical model of the anterior cruciate ligament. *Proceedings of the Institute of Mechanical Engineers* **211**(Part H): 235-246.

[209] Trent, P. S., Walker, P. S. and Wolf, B. (1976). Ligament length patterns, strength, and rotational axes of the knee joint. *Clinical Orthopaedics* **117**: 263-270.

[210] Truesdell, C. and Noll, W. (1992). The non-linear field theories of mechanics. Berlin ; New York, Springer-Verlag.

[211] Valanis, K. C. and Landel, R. I. (1967). *Journal of Applied Physics* **38**: 2997-3002.

[212] Valent, T. (1980). Local theorems of existence and uniqueness in finite elastostatics. *IUTAM Symposium on Finite Elasticity, Lehifh University, Bethlehem, PA, USA*, August 10-15, Nijhoff, Martinus, D. E. Carlson and R. T. Shield Ed., 401-421.

[213] Valid, R. (1981). Mechanics of continuous media and analysis of structures. 26, North Holland Publishing Company.

[214] Veronda, D. R. and Westmann, R. (1970). Mechanical characterization of skin - finite deformations. *Journal of Biomechanics* **3**: 111-124.

[215] Viidik, A. (1968a). A rheological model for uncalcified parallel-fibered collagenous tissue. *Journal of Biomechanics* **1**: 3-11.

[216] Viidik, A. (1973). Functional properties of collagenous tissues. *International Review of Connective Tissue Research* **6**: 127.

[217] Viidik, A. and Ekholm, R. (1968b). Light and electron microscopic studies of collagen fibers under strain. *Z. Anat. Entwick. Gesch.* **127**: 154-164.

[218] Walker, P. S. and Hajek, J. V. (1972). The load-bearing area in the knee joint. *Journal of Biomechanics* **5**: 581-589.

[219] Wascher, D. C., Markolf, K. L., Shapiro, M. S. and Finerman, G. A. (1993). Direct in vitro measurement of forces in the cruciate ligaments. Part I: The effect of multiplane loading in the intact knee. *Journal of Bone and Joint Surgery* **75A**(3): 377-86.

[220] Washizu, K. (1974). Variational methods in elasticity and plasticity. Oxford, England, Pergamon Press.

[221] Weiss, J. A. (1994). A constitutive model and finite element representation for transversely isotropic soft tissues, University of Utah, Utah, USA.

[222] Weiss, J. A., Maker, B. N. and Govindjee, S. (1996). Finite element implementation of incompressible transversely isotropic hyperelasticity. *Computer Methods in Applied Mechanics and Engineering* **135**: 107-128.

[223] Weiss, J. A., Maker, B. N. and Schauer, D. A. (1995). Treatment of initial stress in hyperelastic finite element models of soft tissues. *ASME Conference BED* Ed., 105-106.

[224] White, A., Handler, P. and Smith, E. L. (1964). Principles of Biochemistry. New York, McGraw-Hill.

[225] Williams, P. L. and Warwick, R. (1980). Gray's Anatomy. Philadelphia, W. B. Saunders: 395,397,400,403,404,406,489.

[226] Wilson, A. N., Shrive, N. G. and Franck, C. B. (1996). Verification of a three dimensional ligament model. Computer Methods in Biomechanics and Biomedical Engineering - 1. J. Middleton, M. L. Jones and G. N. Pande, Gordon and Breach Science Publishers: 281-294.

[227] Wineman, A. S. and Pipkin, A. C. (1964). Material symmetry restrictions on constitutive equations. *Archive of Rational Mechanics and Analysis* **17**: 184-214.

[228] Woo, S. L. Y., Debski, R. E., Withrow, J. D. and Janaushek, M. A. (1999). Biomechanics of knee ligaments. *Americal Journal of Sports in Medicine* **Jul / Aug**.

[229] Woo, S. L. Y., Gomez, M. A. and Akeson, W. H. (1981). The time and history-dependent viscoelastic properties of the canine medial collateral ligament. *Journal of Biomechanical Engineering* **103**: 293-298.

[230] Woo, S. L. Y., Gomez, M. A., Masahiro, I. and Akeson, W. H. (1987). New experimental procedures to evaluate the biomechanical properties of healing medial collateral ligaments. *Journal of Orthopaedic Research* **5**: 425-432.

[231] Woo, S. L. Y., Johnson, G. A. and Smith, B. A. (1993). Mathematical modeling of ligaments and tendons. *Journal of Biomechanical Engineering* **115**(4 pt B): 468-473.

[232] Woo, S. L. Y., Maynard, J., Butler, D. L., Lyon, R., Torzilli, P. A. and Akeson, W. H. (1988). Ligament, tendon and joint capsule insertions into bone. Injury and Repair of the Musculoskeletal Soft Tissues, Park Ridge. S. L. Y. Woo and J. A. Buckwalter. Park Ridge, IL, American Academy of Orthopaedic Surgeons: 133-166.

[233] Woo, S. L. Y., Orlando, C. A., Camp, J. F. and Akeson, W. H. (1986). Effects of postmortem storage by freezing on ligament tensile behavior. *Journal of Biomechanics* **19**(5): 399-404.

[234] Woo, S. Y. L., Gomez, M. A., Woo, Y. K. and Akeson, W. H. (1982). Mechanical properties of tendons and ligaments. I. Quasi-static and non-linear viscoelastic properties. *Biorheology* **19**: 385-396.

[235] Yamada, H., Takemasa, T. and Yamaguchi, T. (2000). Theoretical study of intracellular stress fiber orientation under cyclic deformation. *Journal of Biomechanics* **33**(11): 1501-1505.

[236] Yamamoto, K., Hirokawa, S. and Kawada, T. (1998). Strain distribution in the ligament using photoelasticity. A direct application to the human ACL. *Medical Engineering & Physics* **20**(3): 161-8.

[237] Yannas, I. (1972). Collagen and gelatin in the solid state. *Review of Macromolecular Chemistry* **C7**: 49.

[238] Zee, L. and Sternberg, E. (1983). Ordinary and strong ellipticity in the equilibrium theory of incompressible hyperelastic solids. *Archive of Rational Mechanics and Analysis* **83**: 53-90.

[239] Zheng, Q. S. and Boehler, J. P. (1994). The description, classification, and reality of material and physical symmetries. *Acta Mechanica* **102**: 73-89.

[240] Zienkiewicz, O. C. and Lhöner, R. (1985). Accelerated "relaxation" or direct solution? Future prospects for finite element methods. *International Journal of Numerical Methods in Engineering* **21**: 1-11.

[241] Zienkiewicz, O. C. and Taylor, R. L. (1989). The Finite element method. 1. London, McGraw-Hill.

[242] Zuppinger, H. (1904). Die aktive Flexion im unbelasteten Kniegelenk (translated from German by Paul Maquet). Wiesbaden, Bergmann.